Neurochemical mechanisms of cortical dynamics and decision making

Inaugural-Dissertation

Zur Erlangung des Doktorgrades
der Mathematisch-Naturwissenschaftlichen Fakultät
der Heinrich-Heine-Universität Düsseldorf

vorgelegt von

Ana Antonia Dias Maile
aus Köln

Düsseldorf, Juli 2026

aus dem Institut für Experimentelle Psychologie,
Biologische Psychologie des Entscheidungsverhaltens
der Heinrich-Heine-Universität Düsseldorf

Gedruckt mit der Genehmigung der
Mathematisch-Naturwissenschaftlichen Fakultät der
Heinrich-Heine-Universität Düsseldorf

Berichterstatter:

1. Prof. Dr. Gerhard Jocham

2. Prof. Dr. Susanne Becker

Tag der mündlichen Prüfung: 23.09.2026

Preface

This dissertation includes my work at the Institute of Experimental Psychology, Biological Psychology of Decision Making, at Heinrich Heine University Düsseldorf between October 2022 and July 2026. It builds on the following publications:

Dias Maile AA[*], Kohl O[*], Ort E, Froböse MI, Kurtenbach H, Butz M, Schreivogel E, Schnitzler A, Florin E[†], Jocham G[†] (2026). *Role of GABA and NMDA receptors in shaping cortical timescales and large-scale network dynamics*. bioRxiv. https://doi.org/10.64898/2026.05.11.723797

Dias Maile AA, Gruendler TOJ, Fischer AG, Kurtenbach H, Kaiser LF, Froböse MI, Jocham G (2025). *Bidirectional modulation of reward-guided decision making by dopamine.* Psychopharmacology, 242(11), 2547–2559. https://doi.org/10.1007/s00213-025-06816-9

Dias Maile AA, Andronova E, Ball F, Aravitska D, Dannenberg LK, Schnitzler A, O'Reilly JX, Jocham G (2026). *Cholinergic and noradrenergic modulation of perceptual decision making and learning.* bioRxiv. https://doi.org/10.64898/2026.06.22.732890

Kurzfassung

Von einfachen Wahrnehmungsurteilen bis hin zu komplexen zielgerichteten Handlungen beruht Verhalten auf einem kontinuierlichen Strom von Entscheidungen. Die Entscheidungsfindung bietet somit einen Einblick in die Kognition, indem sie die Ergebnisse von ansonsten verborgenen neuronalen Prozessen offenlegt. Unabhängig vom Kontext erfordert Entscheidungsfindung die Bewertung und Integration von Informationen, die relevant für das Verhalten sind. Solche Informationen können aus der Umgebung stammen, wo sich die Auswahlmöglichkeiten oft in mehreren Merkmalen unterscheiden. Darüber hinaus ermöglichen vergangene Erfahrungen die Bildung von Erwartungen und Präferenzen. Spezifische neuronale Mechanismen ermöglichen die Verarbeitung und Integration dieser großen Informationsmenge in Entscheidungen. Diese Dissertation trägt zu einem besseren Verständnis dieser für adaptives Verhalten zentralen Prozesse bei, indem sie die neurochemischen Mechanismen untersucht, die der Informationsverarbeitung während des Ruhezustands, der Entscheidungsfindung und des Lernens zugrunde liegen. Zunächst untersuchten wir die Rolle von $GABA_A$- und NMDA-Rezeptoraktivität in kortikalen Zeitskalen und Netzwerkdynamiken im Ruhezustand. Diese kortikalen Mechanismen bilden die zeitliche und räumliche Organisation des Gehirns und bestimmen, wie Informationen über die Zeit hinweg in verteilte kortikale Regionen integriert werden. Zweitens untersuchten wir die Rolle von Dopamin bei der Selektion von Entscheidungsstrategien, die bestimmen, wie die Merkmale verschiedener Wahloptionen zu einer einheitlichen Wertdarstellung integriert werden. Wir identifizierten eine spezifische Rolle von Dopamin bei der Nutzung von entscheidungsrelevanten Merkmalen während der Entscheidungsfindung. Dadurch moduliert Dopamin das Ausmaß, in dem Entscheidungen durch verfügbare

Informationen gesteuert werden. Schließlich untersuchten wir die Rolle von Acetylcholin und Noradrenalin bei der Integration von sensorischer Information mit erlernten Erfahrungen. Wir fanden heraus, dass beide Neurotransmittersysteme beim Lernen eine wichtige Rolle spielen, indem sie die Integration von bereits erlernten Erwartungen zusammen mit neuen Erkenntnissen bestimmen. Insgesamt trägt diese Dissertation zu einem ganzheitlicheren Verständnis dessen bei, wie neurochemische Systeme die neuronalen Dynamiken während der Ruhephasen und die Entscheidungsfindung während des Verhaltens beeinflussen. Unsere Ergebnisse weisen darauf hin, dass verschiedene Neurotransmittersysteme komplementäre Rollen bei der Gestaltung der Informationsverarbeitung und -gewichtung in unterschiedlichen kognitiven Kontexten spielen. Eine Herausforderung für zukünftige Forschungsarbeit besteht darin, zu zeigen, dass Kognition nicht auf unabhängigen Einflüssen beruht, sondern aus der koordinierten Aktivität mehrerer Neurotransmittersysteme entsteht, die über verschiedene Hirnregionen und zeitliche Skalen hinweg agieren.

Abstract

From simple perceptual judgments to complex goal-directed actions, behavior is shaped by a continuous stream of decisions. As such, decision making provides a window into cognition by revealing the outcomes of otherwise hidden neuronal processes. Across contexts, decisions require the evaluation and integration of information relevant for guiding behavior. Such information may originate from the environment, where choice options often differ across several attributes. In addition, past experiences enable the formation of expectations and preferences. Distinct neuronal mechanisms enable the processing and integration of this large volume of information into choices. This dissertation contributes to a better understanding of these processes central to adaptive behavior by investigating the neurochemical mechanisms underlying information processing during rest, decision making and learning. First, we investigated the role of $GABA_A$ and NMDA receptor activity in shaping cortical timescales and network dynamics at rest. These cortical mechanisms form the temporal and spatial organization of the brain and determine how information is integrated across time in distributed cortical regions. Second, we examined the role of dopamine in arbitrating between decision strategies that determine how attributes of different choice options are integrated to a unified value representation. We identified a specific role of dopamine in shaping the use of choice-relevant attributes during decision making, thereby modulating the extent to which choices were driven by available information. Finally, we investigated the role of acetylcholine and noradrenaline in the integration of bottom-up perceptual information with top-down learned beliefs. We found that both neurotransmitter systems play an important role during learning by determining the updating of prior expectations in response to new evidence. Together, this dissertation contributes to a

more integrated understanding of how neurochemical systems shape neuronal dynamics during rest and decision making during behavior. Our findings demonstrate that distinct neurotransmitter systems play complementary roles in shaping the processing and weighting of information across cognitive contexts. A challenge for future work is to characterize how cognition emerges from the coordinated activity of multiple neurotransmitter systems operating across different brain regions and temporal scales.

Content

1 Introduction

Imagine standing in the supermarket trying to decide which chocolate bar to buy. One option is cheaper, while another promises better taste or has a more appealing packaging. A third one you might have already tried and enjoyed. In order to arrive at a decision, these different sources of information must be weighed against each other.

Likewise, consider trying to cross a busy street. As a continuous stream of cars rushes past, you must decide when it is safe to step onto the road. This requires estimating the speed and distance of oncoming cars. However, the decision is not based on sensory information alone. Instead, prior experiences also play a crucial role by shaping expectations about how drivers are likely to behave. Especially in chaotic traffic situations, this learned knowledge becomes an increasingly important source of information, guiding decision making.

These everyday situations highlight the quantity and complexity of decisions faced in daily life. Still, decisions are often made quickly and with little effort. Within seconds, the brain combines the different sources of information, which shape choices. Understanding this process requires a closer look at the underlying mechanisms. It demands investigating how the brain learns from past experiences and uses this knowledge to guide future behavior. Further, it is necessary to examine the fast perception of new input as well as the more extended integration with other streams of information.

Importantly, information processing does not occur in isolated neurons, but emerges from the coordinated activity of different brain regions with distinct functional properties (Bressler, 1995). Neurotransmitters shape this coordination by mediating the excitatory and inhibitory synaptic communication between neurons. Neurotransmitters are defined as chemical substances that are synthesized within

neurons and stored in vesicles of the presynaptic terminal buttons (Figure 1.1). Upon depolarization of the presynaptic neuron, neurotransmitters are released into the synaptic gap. They bind to receptors in the postsynaptic membrane, where they activate signaling pathways in the postsynaptic neuron. Neurotransmitter actions are terminated either through metabolic degradation or reuptake (Birbaumer & Schmidt, 2010). Through synaptic transmission and receptor-mediated signaling, diverse neurotransmitter systems support communication between neurons as well as information processing across distant brain regions.

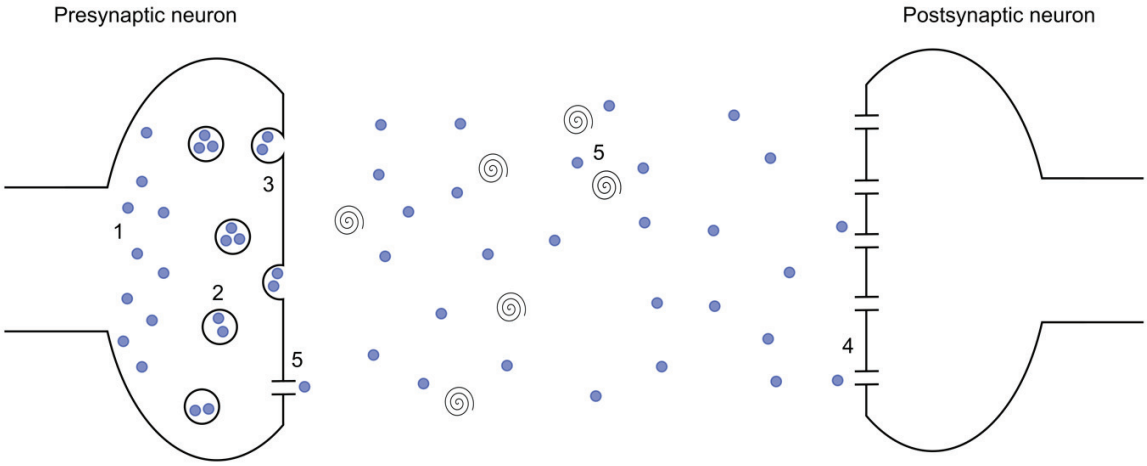

Figure 1.1: Schematic of neurotransmitter dynamics at the synapse. (1) Neurotransmitters (blue dots) are typically synthesized in the presynaptic terminal. **(2)** They are stored in synaptic vesicles (black circles), **(3)** which fuse with the presynaptic membrane to release neurotransmitters into the synaptic gap. **(4)** The released neurotransmitters bind to receptors on the postsynaptic membrane, triggering intracellular signaling cascades. **(5)** Neurotransmitter action is terminated through reuptake into the presynaptic terminal (channel in presynaptic neuron) or enzymatic degradation (spirals)

Most neuronal communication relies on two principal neurotransmitter systems: glutamate and γ-aminobutyric acid (GABA; Figure 1.2). These shape most synaptic excitation and inhibition, respectively, and form the foundation of neuronal information processing (Carlson, 2010). In contrast, other neurotransmitter systems play a more specialized functional role. Dopamine, for example, has been associated with reward-processing (e.g., Schultz et al., 1993) and action selection (e.g., Frank, 2005). Noradrenaline has been shown to modulate arousal and alertness (e.g., Aston-Jones & Bloom, 1981; Berridge, 2008). Together with acetylcholine, it also plays a crucial role in attention (e.g., Deco & Thiele, 2011; Devauges & Sara, 1990) and perception (e.g., Herrero et al., 2017; Manunta & Edeline, 1997). Serotonin, in turn, has been implicated in mood regulation and processing of negative outcomes (Dayan & Huys, 2009). Dysfunctions in these neurotransmitter systems are associated with a wide range of clinical conditions. For instance, Parkinson's disease is a neurodegenerative disorder

characterized by motor deficits such as tremor, bradykinesia and rigidity, which are caused by a dopaminergic depletion in the dorsal striatum (Kish et al., 1988). Symptoms are commonly treated with the dopamine precursor levodopa (L-DOPA; Connolly & Lang, 2014). In addition to motor impairments, patients often also suffer of cognitive deficits (e.g., impairments in learning), sleep disorders and depression, which have been linked to dopaminergic dysfunction but also alterations in other neurotransmitter systems, including the cholinergic system (Frank, 2005; Pasquini et al., 2025).

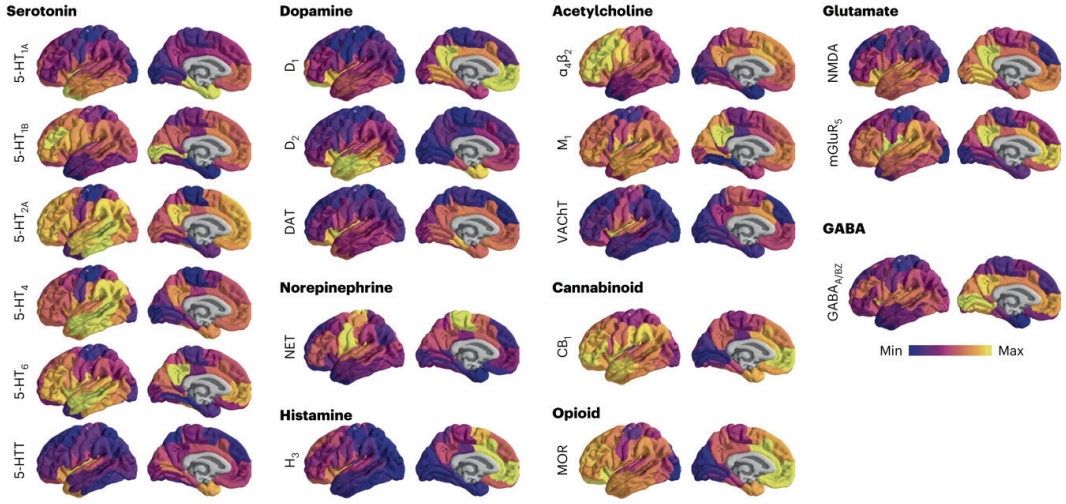

Figure 1.2: Neurotransmitter systems. Receptor and transporter distribution maps of nine different neurotransmitter systems based on positron emission tomography tracer images. Receptor maps indicate where neurons express receptors that respond to specific neurotransmitters. Transporter maps show the distribution of transporter proteins involved in neurotransmitter reuptake and vesicular storage. Together, these maps provide complementary information about neurotransmitter signaling and projection patterns across the cortex. Serotonin: Distribution of six serotonergic receptor subtypes (5-HT_{1A}, 5-HT_{1B}, 5-HT_{2A}, 5-HT_{4}, 5-HT_{6}) and the serotonin transporter (5-HTT), which is primarily involved in reuptake. Dopamine: Distribution of D_1 and D_2 dopamine receptors and the dopamine transporter (DAT) involved in reuptake. Noradrenaline: Distribution of the noradrenergic transporter (NET) involved in reuptake. Histamine: Distribution of the H_3 histamine receptor. Acetylcholine: Distribution of nicotinic ($\alpha_4\beta_2$) and muscarinic (M_1) receptor subtypes, as well as vesicular acetylcholine transporter (VAChT) involved in vesicular storage. Cannabinoid: Distribution of the cannabinoid receptor type 1 (CB_1). Opioid: Distribution of the μ-opioid receptor (MOR). Glutamate: Distribution of the NMDA receptor and the metabotropic glutamate receptor subtype 5 (mGluR5). Importantly, the NMDA receptor map reflects the distribution of open NMDA receptor channels. GABA: Distribution of the benzodiazepine binding sites of $GABA_A$ receptors. Reproduced from Hansen et al. (2022). CC-BY 4.0.

Hence, understanding how distinct neurotransmitters enable neuronal communication is crucial to uncover the mechanisms underlying cognition and behavior in both health and disease. The present dissertation aims to advance this understanding by investigating the role of neurotransmitter systems in decision making, with a particular focus on information integration. Specifically, across three studies, pharmacological interventions are implemented to investigate the causal contribution of specific

neurotransmitters in shaping cortical dynamics and various aspects of decision making in healthy adults.

1.1 Role of GABA and NMDA receptors in shaping cortical timescales and large-scale network dynamics (Study 1)

1.1.1 Synaptic excitation and inhibition

Synaptic communication relies on a tightly regulated balance between excitation and inhibition (E/I balance), governed by glutamatergic and GABAergic activity (Abeysuriya et al., 2018; Turrigiano & Nelson, 2004). In the healthy brain, neuronal homeostasis is characterized by inhibitory control which scales with the strength of excitation (Xue et al., 2014). Disruptions of this balance are associated with neurological disorders such as epilepsy, in which alterations in the E/I-balance lead to neuronal hyperexcitability and seizure generation (van van Hugte et al., 2023). A similar mechanism underlies symptoms of sudden alcohol withdrawal after an alcohol use disorder. Chronic alcohol consumption increases GABAergic inhibitory signaling, prompting compensatory neuronal adaptions that increase excitability. When alcohol intake is abruptly stopped, the enhanced GABAergic inhibition is removed while the hyperexcitability persists, resulting in withdrawal symptoms, including hallucinations and seizures (Ariwodola & Weiner, 2004; Basu & Suh, 2020; Littleton, 1998). Importantly, while these strong disruptions of the E/I-balance cause severe neurological symptoms such as seizures, even more subtle alterations can likewise have serious consequences. Schizophrenia and autism spectrum disorder, for example, are characterized by a dysregulation of the E/I-balance that correlates with symptom severity (Arazi et al., 2025; Gao & Penzes, 2015; Watanabe et al., 2019). In order to better understand these mechanisms, it is necessary to examine the E/I balance at the synaptic level, where it is governed by the neurotransmitters glutamate and GABA.

1.1.2 Glutamate

Glutamate (L-glutamate) is synthesized either from glucose via the Krebs cycle or from glutamine supplied by glia cells, which is locally converted by glutaminase. Glutamate is subsequently stored in synaptic vesicles by the vesicular glutamate transporters and released into the synaptic gap upon presynaptic depolarization. Termination of glutamatergic signaling occurs primarily through reuptake by the plasma membrane glutamate transporter (Iversen et al., 2009). Glutamatergic receptors, also referred to

as excitatory amino acid receptors, can be classified into at least five different subtypes: N-Methyl-D-aspartate (NMDA), α-amino-3-hydroxy-5-methyl-4-isoxazolepropionic acid (AMPA), kainate, 1,2-amino-4-phosphonobutyrate (AP-4; primarily inhibitory autoreceptors) and metabotropic glutamate receptors (Figure 1.2). NMDA, AMPA and kainate receptors are ionotropic receptors that generate depolarizing excitatory responses (Iversen et al., 2009; Willard & Koochekpour, 2013). Among these, AMPA receptors are the most prevalent and give rise to fast excitatory synaptic transmission. Their activation enables sodium (NA^+) and potassium (K^+) flow, resulting in postsynaptic depolarization (de Leon-Lopez et al., 2025; Reiner & Levitz, 2018). A similar activity profile applies to kainate receptors, which are distributed in a complementary pattern to AMPA receptors (Iversen et al., 2009; Pinheiro & Mulle, 2006). NMDA receptors show a largely parallel distribution to AMPA receptors (Figure 1.2). They enable calcium (CA^{2+}) and NA^+ influx through ion channels that are ligand- and voltage-dependent. Pharmacological studies have identified at least six binding sites on the NMDA receptor: the glutamate (transmitter) binding site, a glycine (or D-serine) co-agonist binding site, a voltage-dependent magnesium (Mg^{2+}) binding site, a site binding phencyclidine, an inhibitory divalent cation site and a polyamine regulatory site. For channel activation, glutamate (or a related agonist) must bind to the transmitter binding site, glycine (or a related co-agonist) must bind to the glycine site and the postsynaptic membrane must be partially depolarized to relieve the Mg^{2+}-block of the channel (Carlson, 2010; Iversen et al., 2009; Paoletti & Neyton, 2007).

1.1.3 GABA

GABA is synthesized by the enzyme glutamic acid decarboxylase, which converts the GABAergic precursor L-glutamic acid to GABA. Newly synthesized GABA is then packaged into synaptic vesicles by the vesicular GABA transporter. Upon neuronal depolarization, these vesicles fuse to the presynaptic membrane and release GABA into the synaptic gap. Termination of GABAergic signaling occurs primarily through reuptake mediated by GABA transporters (Iversen et al., 2009). Two major types of GABA receptors have been identified: $GABA_A$ and $GABA_B$ receptors. $GABA_A$ receptors are ionotropic ligand-gated chloride (Cl^-) channels located on the postsynaptic membrane. Multiple modulatory binding sites on the $GABA_A$ receptor have been identified by pharmacological studies: the GABA (transmitter) binding site, the benzodiazepine-binding site (Figure 1.2) and binding sites for barbiturates, steroids, picrotoxin and ethanol. Activation of $GABA_A$ receptors increases Cl^- conductance,

causing hyperpolarization and therefore inhibition of excitatory neuronal activity (Carlson, 2010; Iversen et al., 2009; Sigel & Steinmann, 2012). $GABA_B$ receptors are metabotropic G-protein-coupled receptors that are located both pre- and postsynaptically. They are coupled to CA^{2+} and K^+ channels via G-proteins and second messenger pathways. Their activation is associated with reduced neurotransmitter release or neuronal hyperpolarization (Bowery, 2006; Carlson, 2010; Iversen et al., 2009). Most GABAergic neurons function as inhibitory interneurons, meaning that they modulate the activity of nearby excitatory pyramidal neurons. Accordingly, GABAergic signaling can be further characterized by three different interneuron subtypes, which have been defined through their relative expression of parvalbumin (PV), somatostatin (SST) and vasoactive intestinal peptide (VIP). PV^+ interneurons control spiking output of pyramidal cells, whereas SST^+ interneurons regulate their synaptic input and VIP^+ interneurons modulate primarily SST^+ interneurons (Tremblay et al., 2016; Wang, 2020; Wang et al., 2004).

1.1.4 Neuronal timescales

Beyond these excitatory and inhibitory synaptic mechanisms, neuronal information processing relies on activity operating across multiple timescales (Murray et al., 2014). For example, when listening to a piece of music, primary sensory regions operate on short timescales, enabling the rapid detection of individual notes or shifts in volume, whereas higher-order association regions integrate this information over longer timescales to track the theme and emotional arc of the song (Baldassano et al., 2017; Çatal et al., 2023; Honey et al., 2012; Lerner et al., 2011). The temporal organization of neuronal activity thus follows a hierarchical gradient across the cortex characterized by short timescales in early sensory regions and increasingly longer timescales in higher-order association areas (Figure 1.3; Murray et al., 2014; Shafiei et al., 2023; Wang, 2020). This pattern is essential for information processing as it enables the fast perception of new information as well as a more extended integration with other sources (Baldassano et al., 2017; Çatal et al., 2023; Honey et al., 2012; Lerner et al., 2011; Zilio et al., 2021). The hierarchical organization has been consistently found across different tasks and species (Cusinato et al., 2023; Halgren et al., 2021). Beyond this, neuronal timescales of cortical regions have been shown to dynamically adapt according to cognitive demands (Bernacchia et al., 2011; Gao et al., 2020; Ito et al., 2020; Lendner et al., 2024; Manea et al., 2024; Zeraati et al., 2023).

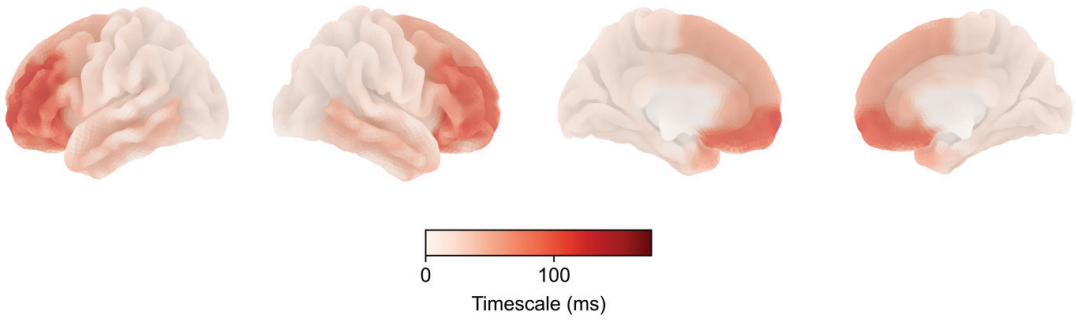

Figure 1.3: Hierarchical organization of neuronal timescales across the cortex. Neuronal timescales (in milliseconds) distributed across the cortical surface, with darker shades of red representing longer timescales. A hierarchical gradient is evident, whereby primary sensory regions are characterized by shorter timescales, which progressively increase towards frontal higher-order association regions. Adapted from Dias Maile, Kohl, et al. (2026). CC-BY 4.0.

Cortical regions do not process information in isolation but rather organize into short-lived transient network states. These are characterized by distinct spectral signatures and support cognitive functions across different time windows (Gohil, Kohl, et al., 2024; Quinn et al., 2018; Rossi et al., 2023; Rossi et al., 2024; Vidaurre et al., 2018).

The stability of network states as well as the length of neuronal timescales are proposed to be governed by the balance between glutamatergic excitation and GABAergic inhibition (Abeysuriya et al., 2018; Gao et al., 2017; Murray et al., 2014; Pascoa Dos Santos & Verschure, 2025; Wang, 2020). Cortical regions at the top of the hierarchy, including the prefrontal cortex, are rich in recurrent connections supported by NMDA glutamate receptors (Burt et al., 2018). NMDA receptor currents exhibit slow decay time constants of about 50-100 ms, resulting in a long persistent activity even without continuous external input (see methods; Angulo et al., 1999; Sah et al., 1990). NMDA receptor expression is less pronounces in early sensory areas (Burt et al., 2018), where neuronal activity fluctuates on shorter timescales and closely tracks perceptual input (Baldassano et al., 2017; Honey et al., 2012). Long NMDA-mediated excitation is controlled by shorter GABAergic feedback inhibition (~5-10 ms; Gupta et al., 2000), which displays a similar hierarchical gradient: The composition of GABAergic interneurons, controlling spiking output (PV^+) and synaptic input (SST^+), changes across cortical regions, creating an inhibitory hierarchy from sensory to association areas (Burt et al., 2018). The interplay between recurrent NMDA-mediated excitation and GABAergic feedback inhibition in higher-order cortical regions is proposed to enable complex cognitive functions, including working memory and decision making (Wang et al., 2008; Wang, 1999, 2002, 2008). Biophysically realistic cortical network models propose that during working memory slow recurrent NMDA-

mediated excitation enables cell populations to maintain persistent activity following brief inputs (Wang et al., 2013; Wang, 1999). Concurrently, during decision making, these cell populations compete through GABAergic feedback inhibition, leading to attractor state dynamics in which the winning population exhibits sustained activity while the competing populations are suppressed (Wang, 2002, 2008; Wong & Wang, 2006).

Despite these influential theoretical accounts, the extent to which NMDA and GABA receptor activity controls neuronal timescales across the cortex has not been investigated. In addition, it remains unknown whether different cortical network states are characterized by distinct neuronal timescales and how state transitions are influenced by GABA- and NMDA-mediated activity. This leaves a critical gap between synaptic-level mechanisms and cortical dynamics that support information processing.

1.2 Bidirectional modulation of reward-guided decision making by dopamine (Study 2)

1.2.1 Decision making

Decision making offers a window into cognition by revealing the outcomes of otherwise hidden neuronal processes (e.g., information integration), making it a valuable research subject in cognitive neuroscience (Shadlen & Kiani, 2013). At the same time, decision making extends far beyond neuroscience, representing an important field of research in a wide range of disciplines, including economics, philosophy, psychology and political science (Bizer et al., 2011; Thaler, 1980; Thomson, 1976). Decision making comes in many forms: Perceptual decisions rely on interpreting sensory information e.g., judging if a gap in traffic is large enough to safely cross a busy street (see Section 1.3.2; Hanks & Summerfield, 2017). Reward-guided decision making entails choosing between different alternatives based on their value e.g., choosing a chocolate bar by evaluating its qualities, including appearance, price and taste. In this process available options are identified and assigned a subjective value. The values are compared and the option with the highest subjective value is selected. Consistent with this value comparison, activity in the ventromedial prefrontal cortex has been shown to correlate with the value difference of chosen and unchosen option, independent of motor-related signals (Jocham et al., 2012; Wunderlich et al., 2009, 2010). In addition, by evaluating the choice outcome, subjective values can be

adjusted to improve future decisions (see Section 1.3.1 on learning; Rangel et al., 2008).

Most decisions however involve some degree of risk, since the relationship between an action and its reward is often probabilistic. In such cases, it is important to not only consider information on the magnitude of potential reward but also on the likelihood of receiving it. According to the Expected Utility Theory this is achieved by weighting the value of each option by its probability:

$$EV = M \cdot P \tag{1.1}$$

The expected value (EV) is defined as the product of the magnitude *M* and the probability *P* (Neumann & Morgenstern, 1944). The EV has been shown to guide decision making (Farashahi et al., 2019; Kaiser et al., 2021; Kurtenbach et al., 2026) and neuronal correlates of the EV have been found in several brain regions, including the ventromedial prefrontal cortex, posterior parietal cortex and orbitofrontal cortex (Jocham et al., 2014; Kaiser et al., 2021; Platt & Glimcher, 1999; Rolls et al., 2008; Wunderlich et al., 2009). While choosing based on the EV is statistically optimal, research indicates that humans often deviate from this and instead follow different decision strategies (Figner & Voelki, 2004; Tversky & Kahneman, 1979).

1.2.2 Decision strategies

Humans do not always behave statistically optimal. Instead, information on reward magnitudes and on probabilities are often subject to a biased interpretation, as captured by the non-linear distortions proposed by Prospect Theory (Tversky & Kahneman, 1979). This theorem suggests that magnitudes, here referred to as outcomes, are compared to a neutral reference point and thereby classified as either gains or losses. The corresponding value function is S-shaped: concave for gains above the reference point and convex for losses below it. As a result, the objectively same value difference is perceived as larger when occurring in the domain of low values (e.g., the difference between 10 € and 20 € is perceived as larger than the difference between 110 € and 120 €). Additionally, responses to losses are more pronounced than equivalent gains, a phenomenon known as loss aversion (e.g., loosing 50 € is perceived as more significant than winning 50 €). This leads to risk aversion in the context of losses and risk seeking in the context of gains. Hence, decisions are modulated by whether their outcomes are framed as gains or losses (Tversky & Kahneman, 1986). Additionally, probabilities are transformed into decision

weights, such that low probabilities tend to be overestimated and high probabilities underestimated. This leads to the certainty effect, where completely certain options are often preferred over high-probability options, even when the latter have a higher EV (e.g., guaranteed 50 € are preferred over a 95% chance of winning 60 € despite the higher EV of 57 €; Tversky & Kahneman, 1992). Value and decision weight are combined multiplicatively to form a subjective value for each option, similar to the EV. The decision behavior predicted by Prospect Theory has been shown to fit empirical data across a variety of experimental paradigms (Ruggeri et al., 2020). However, one limitation of this framework is that the multiplicative information integration treats probabilities and magnitudes proportionally, preventing one from being weighed higher than the other. Consequently, it does not allow for direct comparisons between reward magnitude and probability. In contrast, to account for a flexible weighting of reward magnitudes relative to reward probabilities, an additive integration strategy has been proposed:

$$sv = \omega_p \cdot P + \left(1 - \omega_p\right) \cdot M \tag{1.2}$$

where the subjective value *sv* is based on the relative weighting of probability *P* and magnitude *M* governed by the parameter ω_p. Due to this relative balance, higher weighting of reward magnitudes is associated with risk seeking choices, whereas higher weighting of reward probabilities is linked to risk aversion. Therefore, in this framework risk preferences are not fixed by the context (gains vs. losses) but can be flexibly adjusted. Recent evidence suggests that choices of both humans and non-human primates are best described by a mixture of additive and multiplicative integration strategies:

$$sv = \omega_{mult} \cdot P \cdot M + (1 - \omega_{mult}) \cdot (\omega_p \cdot P + \left(1 - \omega_p\right) \cdot M) \tag{1.3}$$

where the parameter ω_{mult} describes the relative allocation between the multiplicative and additive response strategy (Farashahi et al., 2019; Figner & Voelki, 2004; Scholl et al., 2014). The degree to which each strategy prevails varies as a function of uncertainty (i.e., variability of reward contingencies). Greater uncertainty shifts behavior toward additive integration, allowing a flexible weighting of the uncertain attribute (Farashahi et al., 2019; Kurtenbach et al., 2026). These computations are not purely theoretical, but are supported by neuronal mechanisms. In particular, midbrain

dopamine neurons have been shown to encode risk as well as expected reward (Schultz, 1998; Schultz et al., 1997; Tobler et al., 2005).

1.2.3 Dopamine

Dopamine is a key neurotransmitter in the central nervous system, critically involved in a range of neuronal processes, including action selection (Frank, 2005), attention (Seamans et al., 2001; Seamans & Yang, 2004), motivation (Cools, 2008), learning and reward-processing (Schultz et al., 1993). Dopamine belongs to the group of catecholamine, a class of organic compounds with a catechol nucleus and an amine group. Other catecholamines are noradrenaline (i.e., norepinephrine) and adrenaline (i.e., epinephrine). Together with the indolamine serotonin they belong to the broader group of monoamine neurotransmitters (Carlson, 2010). Catecholamine synthesis begins with the amino acid tyrosine. The enzyme tyrosine hydroxylase adds a hydroxyl group to L-tyrosine forming L-DOPA. L-DOPA is then decarboxylated by DOPA-decarboxylase to produce dopamine. Dopamine is subsequently converted to noradrenaline through the actions of dopamine-β-hydroxylase, which adds another hydroxyl group. At last, noradrenaline is synthesized to adrenaline by the enzyme phenylethanolamine-N-methyltransferase in the adrenal medulla (Carlson, 2010; Iversen et al., 2009; Klein et al., 2019; Latif et al., 2021). Vesicular monoamine transporters store dopamine in synaptic vesicles for subsequent release into the synaptic gap. Dopaminergic signaling is terminated primarily through reuptake by dopamine transporters. The primary enzymes responsible for dopamine metabolism (and that of other catecholamines) are monoamine oxidase (MAO) and catechol-o-methyltransferase (COMT). Metabolism of extracellular dopamine by COMT is thought to play an important role especially in regions with a relatively low dopamine transporter expression, such as the prefrontal cortex (Figure 1.2; Carlson, 2010; Cools & D'Esposito, 2011; Iversen et al., 2009; Latif et al., 2021; Tunbridge et al., 2004).

Dopaminergic pathways form four major systems, which differentiate in their location, connectivity and functional role. The diencephalon system (encompassing the tuberoinfundibular dopaminergic pathway) includes dopamine neurons that originate from the dorsal hypothalamus and periventricular grey of the central thalamus and extend to the spinal cord. These projections have been linked to perception, including pain. Dopaminergic dysregulations in the diencephalon system have been linked to restless leg syndrome, which is characterized by abnormal limb sensations (Carlson, 2010; Clemens et al., 2006; Fleetwood-Walker et al., 1988; Iversen et al., 2009; Klein

et al., 2019). Dopaminergic pathways of the nigrostriatal system project from the substantia nigra to the dorsal striatum (caudate nucleus and putamen), where dopamine activates the direct and indirect striatopallidal circuits. These modulate thalamocortical circuits, which are crucial for the control, initiation and selection of actions (Carlson, 2010; Frank, 2005; Iversen et al., 2009; Latif et al., 2021). As such, the neurodegenerative disorder Parkinson's Disease is characterized by a profound dopaminergic depletion in the dorsal striatum (Kish et al., 1988). Patients' dominant symptoms are motor deficits, including tremor, bradykinesia and rigidity, which are commonly reduced through the treatment with the dopamine precursor L-DOPA (Connolly & Lang, 2014). The mesolimbic system consists of dopaminergic neurons in the ventral tegmental area that project to the limbic system, including the ventral striatum (nucleus accumbens), amygdala and hippocampus. It is considered essential for reward processing and motivation and hence is associated with automatic and reflexive behavior (Carlson, 2010; Cools, 2008; Hamid et al., 2016; Iversen et al., 2009; Scholz et al., 2022). Lastly, dopaminergic projections of the mesocortical system also originate from the ventral tegmental area, but project to the prefrontal cortex. This system has been linked to complex cognitive abilities, such as working memory, attention and cognitive flexibility enabling goal-directed behavior (Carlson, 2010; Iversen et al., 2009; Miederer et al., 2025; Scholz et al., 2022; Seamans et al., 2001; Seamans & Yang, 2004; Williams & Goldman-Rakic, 1995). Dopaminergic dysregulations in the mesocortical and mesolimbic system have been linked to attention deficit hyperactivity disorder (ADHD). Patients show symptoms of increased distractibility, impulsiveness and hyperactivity, which are commonly alleviated through methylphenidate (i.e., Ritalin), a dopamine and noradrenaline reuptake inhibitor (Coghill et al., 2014; Cubillo et al., 2012).

Dopaminergic receptors are metabotropic and are broadly categorized into D_1 and D_2 receptors (Figure 1.2). D_1 receptors are mainly postsynaptic and are further divided into the subtypes D_1 and D_5. They are coupled to $G\alpha_{s,olf}$ proteins and stimulate adenylyl cyclase, thereby increasing cyclic adenosine monophosphate (cAMP) production (Carlson, 2010; Iversen et al., 2009; Klein et al., 2019). In the striatopallidal circuit, D_1 receptors are mostly expressed on the direct path, sending a "Go" signal to execute an action (Frank, 2005). D_2 receptors include three subtypes: D_2-D_4. They exist both in the pre- and postsynaptic neuron. D_2 receptors are coupled to $G\alpha_{i,o}$ proteins and decrease adenylyl cyclase, thereby reducing cAMP production (Carlson,

2010; Iversen et al., 2009; Klein et al., 2019). In the striatopallidal circuit, they are predominantly expressed in neurons of the indirect path, which sends a “No-Go” signal suppressing an action (Frank, 2005). Moreover, the gating function of the striatopallidal circuit has been proposed to extend beyond action selection and to modulate cognitive functions as well. As such, attention switching is associated with increased basal ganglia and prefrontal cortex activity (van Schouwenburg et al., 2010). Accordingly, the two-state model proposes that dopamine can switch attention networks in prefrontal cortex by activation of D_1 and D_2 receptors (Seamans et al., 2001). State 1 is dominated by D_2 receptor activation and enables multiple working memory representations to be held in prefrontal networks nearly simultaneously. However, these representations are vulnerable to disruption. Conversely, during state 2, only particularly strong inputs can access prefrontal networks, which are then relatively robust to disruption. This state is dominated by activation of D_1 receptors. (Seamans et al., 2001; Seamans & Yang, 2004).

1.2.4 Dopamine in reward-guided decision making

Decision making relies on dopaminergic signaling, which encodes the expected reward of available choice options. Presentation of a choice option elicits a dopaminergic response proportional to the expected reward (see Section 1.3.1 for the dopaminergic role in learning; Glimcher, 2011; Schultz, 1998; Schultz et al., 1993; Schultz et al., 1997). However, midbrain dopamine neurons have been shown to not only encode the expected reward size but also the probability of receiving it i.e., risk (Tobler et al., 2005). This evidence is reinforced by clinical dysfunctions in the dopaminergic system that cause altered risk preferences. As discussed in Section 1, Parkinson’s Disease is caused by a dorsal striatal dopamine depletion dominantly characterized by motor deficits. However, patients also experience cognitive deficits as well as an increased risk aversion (Cherkasova et al., 2019; Cools et al., 2001; Kobayashi et al., 2019). Treatment with L-DOPA alleviates motor symptoms but can increase risk seeking behavior, including impulsive control disorder and pathological gambling (Evans et al., 2009; Molina et al., 2000; Weintraub et al., 2006). Similar effects have been observed in healthy participants, where L-DOPA administration enhances risk seeking depending on participants’ impulsivity and reward sensitivity (Petzold et al., 2019; Rigoli et al., 2016; Rutledge et al., 2015; White et al., 2007). Conversely, D_2 receptor antagonism seems to produce comparable effects (Burke et al., 2018; Ojala et al., 2018). Thus, dopaminergic signaling is critically involved in encoding reward

magnitudes and probabilities. However, it remains unclear which neurochemical mechanisms enable the integration of these two sources of information. It is unknown what drives the allocation of different integration strategies (i.e., multiplicate versus additive value integration; Section 1.2.2) during decision making. This leaves a critical gap between neurochemical signaling and the cognitive computations inferred from behavior.

1.3 Cholinergic and noradrenergic modulation of perceptual decision making and learning (Study 3)

1.3.1 Learning

Optimal decision making requires learning from past experiences. Learning involves evaluating the outcomes of previous decisions and updating the values assigned to available options in order to guide future behavior. In reinforcement learning, this computation is captured by the prediction error, which quantifies the discrepancy between the estimated value and the actual outcome:

$$PE_t = r_t - Q_t \tag{1.4}$$

where the prediction error *PE* reflects the difference between actual outcome *r* and the estimated value *Q* in trial *t* (Sutton & Barto, 2018). Midbrain dopaminergic activity has been identified as a neuronal correlate of the prediction error. As discussed in Section 1.2.4, midbrain dopaminergic signals are thought to encode the expected reward of a choice option. Upon outcome presentation, deviations between the expected and actual outcome i.e., positive or negative prediction errors, are encoded in phasic increases or decreases in dopaminergic firing, respectively. When outcomes match expectations, no prediction error is generated and dopaminergic activity remains at baseline (Glimcher, 2011; Schultz, 1998; Schultz et al., 1993; Schultz et al., 1997).

In a next step, the prediction error is used to update the estimated value. In the Q-learning framework, this is implemented using a delta update rule governed by the learning rate (Rescorla & Wagner, 1972):

$$Q_{t+1} = Q_t + \lambda \cdot PE_t \tag{1.5}$$

Hence, the learning rate λ determines the extent to which the prediction error influences the updating of the estimated value from trial *t* to trial *t* + 1. A high learning

rate means that recent outcomes strongly influence value updating, leading to a rapid adaption to new information. This is advantageous in changing environments, where contingencies need to be updated. In contrast, a low learning rate means that less weight is assigned to recent prediction errors and instead information is integrated over a longer history of past outcomes. This strategy is advantageous in stochastic but stable environments, where individual outcomes may be noisy but the underlying contingencies remain constant. At the neuronal level, the learning rate has been associated with activity in the anterior cingulate cortex, which predicts the weighting of new information (Behrens et al., 2007).

1.3.2 Perceptual decision making

Perceptual decision making involves interpreting sensory information to guide choices. This process is prominently captured by sequential sampling models, such as the Drift Diffusion Model (Ratcliff, 1978). Evidence favoring different response options is gradually accumulated until it reaches a decision threshold, resulting in the commitment to one option. This evidence accumulation is inferred from observed choices and reaction times. The centroparietal positivity (CPP) has been suggested to reflect the neuronal signal of evidence accumulation (O'Connell et al., 2012). The CPP is recorded at the standard site CP_z of the electroencephalography (EEG). During decision making, it ramps up following stimulus onset until it reaches a decision threshold, which triggers response execution. Its slope is modulated by sensory evidence, with stronger evidence leading to a steeper ramping (O'Connell et al., 2012). The precise neuronal origin of the CPP remains unclear, however the middle temporal area has been identified as a neuronal correlate of the current sensory evidence. This is partly because most perceptual tasks are visual, often requiring discrimination of motion direction, such as the random dot motion task (RDM, Section 2.3.2). Middle temporal neurons are specifically tuned to the direction of visual motion (Baker et al., 1981; Maunsell & Van Essen, 1983). Stimulation of middle temporal neurons tuned to a specific direction, biases both choice and reaction times in favor of that direction (Ditterich et al., 2003; Salzman et al., 1990). This sensory evidence is then accumulated in other brain regions, as suggested by sequential sampling models and the CPP. Since many perceptual paradigms require an eye-movement response, research has focused on brain regions involved in saccade preparation and selection, including the lateral intraparietal area, superior colliculus, frontal eye field and dorsolateral prefrontal cortex (Gold & Shadlen, 2007). The lateral intraparietal area

receives input from the middle temporal area and projects to frontal eye field and superior colliculus (Blatt et al., 1990; Gold & Shadlen, 2007; Lynch et al., 1985; Pare & Wurtz, 1997). Moreover, activity in the lateral intraparietal area, closely matches the predictions of sequential sampling models: During decision making, lateral intraparietal activity ramps until a firing threshold is reached, triggering a choice. Stronger visual evidence leads to a faster ramping and shorter reaction times (Roitman & Shadlen, 2002). Moreover, activity in the lateral intraparietal area has been shown to be independent of the response modality (Liu & Pleskac, 2011). Hence, the lateral intraparietal area represents a strong candidate brain region for evidence accumulation in perceptual decision making.

1.3.3 Acetylcholine

Acetylcholine was long studied for its role outside the central nervous system, where cholinergic motor neurons drive muscle activation. However, in the 1920s, its crucial function as a neurotransmitter in the central nervous system was revealed (Iversen et al., 2009). Cholinergic activity in the brain has been shown to support essential cognitive processes, such as attention (Bauer et al., 2012; Deco & Thiele, 2011; Heishman et al., 2010; Herrero et al., 2008), memory (Hasselmo et al., 1996; Heishman et al., 2010; Wezenberg et al., 2005) and perception (Herrero et al., 2017; Jimenez-Martin et al., 2021; Mishra et al., 2024). Supporting this, cognitive deficits symptomatic for the early stages of Alzheimer's disease are likely to be caused by a cholinergic degeneration and are often treated by increasing acetylcholine availability (cholinesterase inhibitors; Ellis, 2005; Iversen et al., 2009; Perry et al., 1978).

Acetylcholine is synthesized in cholinergic neurons from acetyl coenzyme A and choline by the enzyme choline acetyltransferase. Acetylcholine is then transported into synaptic vesicles by the vesicular cholinergic transporter (Figure 1.2). Upon depolarization of the presynaptic terminal, the vesicles fuse to the presynaptic membrane, releasing acetylcholine into the synaptic gap. Its actions are terminated by cholinesterase, which breaks acetylcholine down into choline and acetate. The choline is then taken back up into the presynaptic neuron via the high affinity choline transporter where it can be used again for acetylcholine synthesis (Carlson, 2010; Iversen et al., 2009).

Cholinergic projections form two major systems: the pontomesencephalotegmental network and the basal forebrain network. The pontomesencephalotegmental network includes ascending pathways from the

pedunculopontine nuclei and laterodorsal tegmental nuclei to diencephalic structures such as the thalamus. It also includes descending pathways to brainstem nuclei, including cranial nerve nuclei and vestibular nuclei (Ballinger et al., 2016; Iversen et al., 2009). This system has been implicated in the regulation of rapid eye movement sleep (REM sleep; Carlson, 2010; Kroeger et al., 2017). The second major cholinergic system originates from nuclei in the basal forebrain, including the medial septal nucleus, diagonal band nuclei, substantia innominate, magnocellular preoptic field and nucleus basalis and projects to the nonstriatal telencephalon, including the hippocampus (Ballinger et al., 2016; Iversen et al., 2009). This system is critically involved in cognition, including memory (Ballinger et al., 2016; Carlson, 2010; Roland et al., 2014), learning (Carlson, 2010; Hangya et al., 2015; Mitsushima et al., 2013) and perception as well as perceptual learning (i.e., a training-based improvement in a perceptual task; Carlson, 2010; Pinto et al., 2013; Rokem & Silver, 2010, 2013). Additionally, cholinergic interneurons enable local circuits for example, in the striatum and cortex (Ananth et al., 2023; Dudai et al., 2021; Higley et al., 2011).

Cholinergic receptors can be broadly classified into nicotinic and muscarinic types. Muscarinic receptors are metabotropic and thus G-protein-coupled to second messenger systems, leading to a slower response time compared to ionotropic nicotinic receptors, which directly modulate ion channels (Carlson, 2010; Iversen et al., 2009). Nicotinic receptors are highly prevalent in muscle fibers, but are also expressed in the central nervous system. They are categorized into 17 subunits ($\alpha_{1\text{-}10}$, $\beta_{1\text{-}4}$, δ, ε, γ), with α_7, $\alpha_4\beta_2$ (Figure 1.2) and $\alpha_3\beta_4$ being the most commonly expressed receptor subtypes in the brain (Iversen et al., 2009). Nicotinic receptor activity has been associated with improvements in attention, memory and fine motor abilities (Heishman et al., 2010). Muscarinic receptors are divided into 5 subtypes: M_1-M_5. M_1, M_3 and M_5 receptors signal via $G_{q/11}$-proteins, activating phosphatidylinositol hydrolysis, while M_2 and M_4 receptors are coupled to $G_{i/o}$-proteins, reducing cAMP signaling (Iversen et al., 2009; Thiele, 2013). Among these, M_1 (Figure 1.2), M_2 and M_4 receptors are predominantly expressed in the cortex, striatum and hippocampus. M_3 receptors are also found in the hippocampus, whereas M_5 receptors are more widely distributed in the ventral tegmental area and substantia nigra, where they interact with dopaminergic neurons (Bubser et al., 2012; Levey et al., 1991; Thiele, 2013). Especially M_1 and M_4 receptors are considered essential for cognition, including memory, learning and

perception (Erskine et al., 2019; Iversen et al., 2009; Marshall et al., 2016; Wezenberg et al., 2005).

1.3.4 Noradrenaline

Similar to acetylcholine, noradrenaline has long been studied for its role outside the central nervous system, particularly in regulating sympathetic activation within the peripheral nervous system (Carlson, 2010; Iversen et al., 2009). As a neurotransmitter in the central nervous system, noradrenaline plays an essential role in arousal (Aston-Jones & Bloom, 1981; Berridge, 2008), attention (Bouret & Sara, 2005; Devauges & Sara, 1990), perception (Manunta & Edeline, 1997; Waterhouse & Woodward, 1980) and memory (Devauges & Sara, 1991; Sara et al., 1999). Accordingly, increased noradrenaline release during memory retrieval and consolidation has been linked to post-traumatic stress disorder, which is characterized by flashbacks and nightmares following a traumatic experience (Strawn & Geracioti, 2008).

Noradrenaline belongs to the class of catecholamines. For details on its synthesis, see Section 1.2.3. Reuptake of noradrenaline occurs via the plasma membrane transporter noradrenaline transporter (Figure 1.2). Similar to dopamine, noradrenaline is metabolized mainly by MAO and COMT (Carlson, 2010; Iversen et al., 2009).

The largest noradrenergic nucleus is the locus coeruleus located in the dorsal pons. It gives rise to three major ascending pathways that stay largely ipsilateral. The largest of these projects to the mesencephalic tegmentum and is referred to as the dorsal bundle. A second projection passes through the central grey and continues along the dorsal longitudinal fasciculus (central gray dorsa longitudinal tract). A third ascending pathway projects ventrally through the mesencephalic tegmental area to the medial forebrain bundle (ventral tegmental-medial forebrain bundle tract; Iversen et al., 2009; Moore & Bloom, 1979). Locus coeruleus projections to the ventral tegmental area modulate dopamine release, demonstrating a close functional interaction between dopamine and noradrenaline (reviewed in Sara, 2009; Weinshenker & Schroeder, 2007). These three pathways enable noradrenergic innervation of the thalamus, hypothalamus, olfactory bulb and cerebral cortex. Additional projections reach the cerebellar cortex via the superior cerebellar peduncle. The locus coeruleus also gives rise to descending pathways to the mesencephalon and spinal cord. Apart from the locus coeruleus, another noradrenergic system originates in the lateral

tegmental area and projects to the forebrain, including the nucleus accumbens, amygdala and hypothalamus (Iversen et al., 2009; Moore & Bloom, 1979).

Noradrenergic receptors (i.e., adrenoceptors) are metabotropic G-protein-coupled receptors that respond to both noradrenaline and adrenaline. Based on their associated G proteins, they are classified into α_1-, α_2- and β-adrenoceptor families. α_2 adrenoceptors (subtypes α_2A, $\alpha_2\beta$, α_2C) are coupled to G_i-proteins. Activation inhibits adenylyl cyclase, resulting in reduced cAMP production. α_2-adrenoceptors are expressed both pre- and postsynaptically (Carlson, 2010; Iversen et al., 2009). Postsynaptic α_2-adrenoceptor activation has been associated with working memory performance especially in non-stressful environments (Arnsten & Goldman-Rakic, 1985; Arnsten & Pliszka, 2011; Li & Mei, 1994). α_1-adrenoceptors (subtypes α_1A, α_1B, α_1C, α_1D) are coupled to G_q-proteins. Their activation stimulates phospholipase C and CA^{2+} mobilization. During perception, α_1-adrenoceptor activity has been shown to facilitate neuronal responses to weak sensory inputs (Ciombor et al., 1999; Manunta & Edeline, 1997). β-adrenoceptors (subtypes β_1, β_2, β_3) are coupled to G_s-proteins. Activation stimulates adenylyl cyclase, increasing intracellular cAMP levels. β-adrenoceptor activity modulates gene expression and synaptic plasticity (Iversen et al., 2009; Sara, 2009). It thus plays an important role in memory consolidation, which has been shown to be impaired under β-adrenoceptor blockade (Sara et al., 1999).

1.3.5 Neurochemistry of learning and perception

Noradrenaline and acetylcholine are proposed to play an important role during learning and perception. During learning, cholinergic activity in the basal forebrain signals reinforcement (reward and punishment), including its unexpectedness (Hangya et al., 2015). In line with this, muscarinic acetylcholine receptor antagonism disrupts error-related adjustments in cortical dynamics as well as in behavior (Danielmeier et al., 2015). Additionally, it causes a faster updating of value estimates, thereby reducing the stability of learned representations (Kurtenbach et al., 2026). Complementary to this, tonic noradrenergic activity facilitates shifts of attention toward contextual changes, thus promoting exploration of novel stimuli (Aston-Jones & Cohen, 2005; Devauges & Sara, 1990). During learning and memory formation, noradrenaline promotes synaptic plasticity (Jami et al., 2023; Larsen et al., 2023; Sara et al., 1999). Accordingly, β-adrenoceptor antagonism has been shown to slow down the updating of value estimates in volatile environments (Lawson et al., 2021).

During perception, acetylcholine reduces spontaneous activity in sensory cortices while enhancing responses to incoming signals (Eggermann et al., 2014; Herrero et al., 2017; Jimenez-Martin et al., 2021; Kuchibhotla et al., 2017; Meir et al., 2018). Noradrenergic signaling causes similar adjustments in sensory cortices, while additionally increasing response selectivity by sharpening neuronal tuning curves (Hasselmo et al., 1997; Kasamatsu & Heggelund, 1982; Kossl & Vater, 1989; Manunta & Edeline, 1997, 2004; McLean & Waterhouse, 1994; Waterhouse et al., 1998) Hence, acetylcholine and noradrenaline enhance the signal-to-noise ratio in sensory processing, thereby improving perceptual discrimination performance (Chaudhury et al., 2009; Gelbard-Sagiv et al., 2018; Leach et al., 2013; Mishra et al., 2024; Nuiten et al., 2023, 2024).

Taken together, noradrenaline and acetylcholine play a central role in both learning from past experiences and the processing of sensory information. During decision making, these streams of information must often be integrated to guide behavior (Figure 1.4). As such, decisions are rarely based solely on sensory input (i.e., bottom-up processing), but they are also shaped by top-down expectations learned from past experiences. These learned expectations enable anticipating outcomes, prioritizing relevant information and generating predictions that guide perception and action (de Lange et al., 2018). The weighting of sensory evidence relative to prior knowledge should be in accordance with the reliability of each stream of information: When sensory evidence is unreliable, greater weight is assigned to learned expectations, whereas when expectations are unclear, sensory input dominates (Hanks et al., 2011).

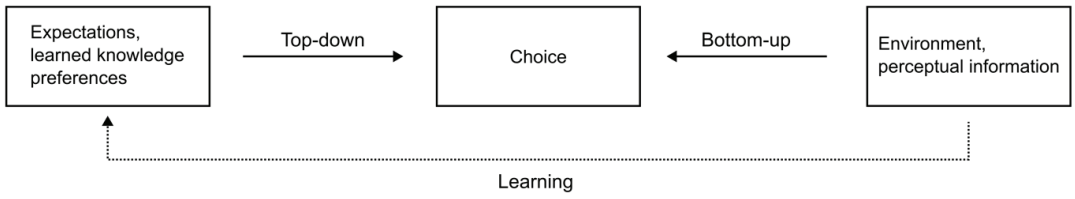

Figure 1.4: Decision making based on top-down and bottom-up information. Expectation, learned knowledge, and preferences exert a top-down influence on choices. The environment, including its perceptual input, provide a bottom-up information source. During decision making, these two streams need to be dynamically weighted by their reliability and integrated. In addition, the environment, including the outcomes of past choices, supports learning whereby top-down knowledge and expectations are continuously updated.

In the brain, representations of expectations are distributed across multiple levels of the perceptual hierarchy, ranging from early sensory areas to higher-order association regions (Findling et al., 2025; Kok et al., 2013; Schneider & Blank, 2026). This suggests that the integration of expectations with sensory evidence is not confined to a single

processing stage. However, the underlying neurochemical mechanisms that drive this integration remain poorly understood. Influential theoretical accounts propose roles for noradrenergic and cholinergic signaling, which have been shown to guide learning and perception individually (Yu & Dayan, 2005). However, direct experimental evidence for this is limited, leaving a critical gap in our understanding of how neuronal mechanisms give rise to the dynamic integration of bottom-up input with top-down learned expectations required for adaptive behavior.

1.4 Overview

My dissertation consists of three studies. The corresponding methods and key results are presented in Section 2 and 3. In Section 4, results are interpreted in regard to the hypotheses and discussed in light of previous research.

In **Study 1**, we investigate how NMDA and $GABA_A$ receptors influence neuronal timescales across cortical regions and the dynamical organization of large-scale cortical networks. Neuronal timescales are measured in the magnetoencephalography (MEG; Section 2.2) across three drug conditions (Section 2.1.1 and Section 2.1.2). Corresponding results are presented in Section 3.1.

In **Study 2**, we examine the role of dopamine in risk preferences and the selection of decision strategies in reward-guided decision making. For this purpose, we implemented a reward-guided decision-making task (Section 2.3.1), which participants performed across three drug conditions (Section 2.1.3). Key results are described in Section 3.2.

In **Study 3**, we investigate how acetylcholine and noradrenaline influence perception, learning and the integration of bottom-up sensory evidence with top-down learned expectations. We used a perceptual decision-making task (Section 2.3.2). Participants performed this task across three drug conditions (Section 2.1.4 and Section 2.1.5). Key results are presented in Section 3.3.

1.5 Hypotheses and objectives

The aim of my dissertation is to investigate neurochemical mechanisms that drive decision making with a particular focus on information integration. The present section describes our corresponding objectives and hypotheses.

Study 1: NMDA and $GABA_A$ receptors in neuronal timescales across cortical regions and cortical networks

1. *Neuronal timescales follow a hierarchical gradient across the cortex.* Extensive research has shown that neuronal timescales follow a hierarchical gradient across the cortex with shorter timescales in primary sensory regions and increasingly longer timescales in higher-order association areas (Murray et al., 2014; Shafiei et al., 2023; Wang, 2020)
2. *Increased activity at NMDA and $GABA_A$ receptors prolongs neuronal timescales.* Neuronal excitation during rest is dominated by AMPA receptor activity characterized by fast decay kinetics (~2 ms) relative to NMDA (~50-100ms) and GABA (~5-10 ms) receptors (Angulo et al., 1999; Gupta et al., 2000; Sah et al., 1990). Thus, increasing NMDA and $GABA_A$ receptor activity should prolong neuronal timescales.
3. *Explorative analysis of neuronal timescales across distinct cortical networks.* Large-scale cortical networks have distinct spectral signatures, which support cognitive processes on different timescales (Quinn et al., 2018; Rossi et al., 2023; Rossi et al., 2024). We therefore expect that cortical networks show distinct neuronal timescales.
4. *Explorative analysis of the influence of NMDA and $GABA_A$ receptor activity on neuronal timescales across cortical networks and on network dynamics.* Metastable resting-state dynamics emerge from the balance between glutamatergic excitation and GABAergic inhibition (Abeysuriya et al., 2018; Pascoa Dos Santos & Verschure, 2025). Therefore, modulation of NMDA and $GABA_A$ receptor activity should modulate large-scale cortical network dynamics. We further explore how region-wise modulations of neuronal timescales through NMDA and $GABA_A$ are mirrored in network-specific timescales.

Study 2: Dopamine in reward-guided decision making

5. *Reward-guided decision making is best described by a hybrid decision strategy that incorporates an additive and multiplicative value integration*. Recent evidence suggests that choices are best captures by a mixture of additive and multiplicative strategy (Farashahi et al., 2019; Figner & Voelki, 2004; Scholl et al., 2014).

6. *Dopamine guides the allocation of decision strategies.* Dopamine plays an important role in reward-guided decision making by signaling both the expected reward magnitude and the likelihood of receiving it, thereby shaping risk preferences (Burke et al., 2018; Glimcher, 2011; Kobayashi et al., 2019; Molina et al., 2000; Rutledge et al., 2015; Schultz, 1998; Schultz et al., 1993; Schultz et al., 1997; Tobler et al., 2005). We expect dopamine to also govern the integration of this reward information.

Study 3: Noradrenaline and acetylcholine in perceptual decision making. The hypotheses, objectives and planned analyses for Study 3 were preregistered (Dias Maile, Andronova, et al., 2025).

7. *Muscarinic acetylcholine receptor antagonism and β-adrenoceptor antagonism impair perceptual decision making*. Past studies have shown that acetylcholine and noradrenaline improve perceptual acuity (Chaudhury et al., 2009; Gelbard-Sagiv et al., 2018; Leach et al., 2013; Mishra et al., 2024; Nuiten et al., 2023).
8. *Muscarinic acetylcholine receptor antagonism increases the learning rate, causing a faster updating of learned beliefs. β-adrenoceptor antagonism decreases the learning rate, causing a slower updating of learned beliefs.* A recent study in our lab has shown increased learning rates under muscarinic acetylcholine receptor antagonism (Kurtenbach et al., 2026). Under β-adrenoceptor antagonism, previous research suggests a slower updating of reward-contingencies. This aligns with a decreased learning rate (Lawson et al., 2021).
9. *Muscarinic acetylcholine receptor antagonism and β-adrenoceptor antagonism modulate the integration of bottom-up perceptual information with top-down learned expectations*. Influential theoretical accounts propose a role of acetylcholine and noradrenaline in integrating bottom-up perceptual information with top-down learned expectations (Yu & Dayan, 2005).

2 Methods

This chapter presents an overview of the main methods used across the three studies. It describes the pharmacological interventions, MEG data analyses, experimental paradigms and computational modeling. For more detailed information, readers are referred to the original work (Dias Maile, Andronova, et al., 2026; Dias Maile, Gruendler, et al., 2025; Dias Maile, Kohl, et al., 2026).

2.1 Pharmacological interventions

The experiments described in this dissertation were conducted with healthy human participants and each of the three studies included a pharmacological intervention. Drugs were administered orally in a placebo-controlled, within-subject, crossover design. The inclusion of a placebo condition enabled attributing observed effects specifically to the drug by providing a baseline.

Drugs can modulate neurotransmission by either reducing or strengthening it. They can act at different sites, including the presynaptic neuron, synaptic gap and postsynaptic neuron (Carlson, 2010):

- Modulation of neurotransmitter synthesis by either serving as a precursor or inhibiting the synthetic enzyme
- Modulation of neurotransmitter storage by interfering with vesicular storage
- Modulation of neurotransmitter release by either inhibiting or facilitating it
- Modulation of autoreceptors by either blocking (leading to increased neurotransmitter release) or stimulating them (leading to decreased neurotransmitter release)

- Modulation of postsynaptic receptors by either stimulating (agonist) or blocking them (antagonist)
- Modulation of neurotransmitter inactivation by either blocking or inactivating the metabolic enzyme

Pharmacokinetics describe how a drug is absorbed, distributed and metabolized in the body (Carlson, 2010). The time to peak plasma concentration (also referred to as t_{max}) defines the time at which the highest concentration of the drug is reached in the bloodstream. The elimination half-life refers to the time required for the plasma concentration to decrease by 50 %.

2.1.1 Glutamatergic intervention

In Study 1, we used D-cycloserine, a partial NMDA receptor agonist, acting at the glycine-binding site (Section 1.1.2; Thomas et al., 1988), to investigate the role of NMDA receptor activity in shaping neuronal timescales across the cortex. In the clinical context, D-cycloserine is conventionally used in tuberculosis treatment due to its antibacterial effects. However, studies suggest that, through modulation of glutamatergic signaling, it is also effective in treating psychiatric and neurological disorder, such as anxiety and dementia (reviewed in Schade & Paulus, 2016). D-cycloserine reaches peak plasma concentration after about 2 h and has an elimination half-life of 12 h (Patel et al., 2011; van Berckel et al., 1998). Participants in our study received a dose of 250 mg.

2.1.2 GABAergic intervention

In Study 1, we used lorazepam, a benzodiazepine receptor agonist that binds allosterically at $GABA_A$ receptors (Section 1.1.3; Riss et al., 2008; Tallman et al., 1978), to investigate the role of $GABA_A$ receptor activity in shaping neuronal timescales across the cortex. In the clinical context, lorazepam is conventionally used to treat anxiety due to its sedative effect, but studies suggest it is also effective in the treatment of epilepsy by strengthening synaptic inhibition (reviewed in Riss et al., 2008). Lorazepam reaches peak plasma concentrations after 2-3 h and has an elimination half-life of about 12 h (Greenblatt et al., 1976; Riss et al., 2008). Participants in our study received a dose of 1.0 mg.

2.1.3 Dopaminergic intervention

In Study 2, participants received amisulpride and L-DOPA to investigate the role of dopamine in the recruitment of decision strategies. Amisulpride is a D_2/D_3 receptor

antagonist (Section 1.2.3; Schoemaker et al., 1997) that is used in the treatment of schizophrenia (reviewed in McKeage & Plosker, 2004). The dopamine precursor L-DOPA is used in the treatment of Parkinson's disease (reviewed in Nagatsua & Sawadab, 2009). Amisulpride reaches peak plasma concentration after about 3 h and has an elimination half-life of 12 h (Hamon-Vilcot et al., 1998). L-DOPA reaches peak plasma concentration after about 1 hour and has a short half-life of 1.5 h (Schneider et al., 2018). Participants in our study received the drugs using a dummy administration procedure due to their different pharmacokinetics. They received two pills separated by 2 h, of which at least one always contained a placebo. Amisulpride was given at a dose of 400 mg and L-DOPA at a dose of 100 mg plus 25 mg of carbidopa.

2.1.4 Cholinergic intervention

In Study 3, we used biperiden to investigate the role of acetylcholine in perception, learning and the integration of perceptual information with learned expectations. Biperiden is a M_1-preferring acetylcholine receptor antagonist (Section 1.3.3; Syvalahti et al., 1987). In the clinical context, it is commonly used in the treatment of Parkinson's disease (Brocks, 1999). Biperiden reaches peak plasma concentration after approximately 1 h and has an elimination half-life of about 21 h (Brocks, 1999; Grimaldi et al., 1986). Participants in our study received a dose of 4 mg.

2.1.5 Noradrenergic intervention

In Study 3, we used propranolol to investigate the role of noradrenaline in perception, learning and the integration of perceptual information with learned expectations. Propranolol is a β-adrenoceptor antagonist, which is used to treat cardiovascular diseases such as hypertension (Section 1.3.4; reviewed in Lowenthal, 1984). It reaches peak plasma concentration after 1-2 h and has an elimination half-life of approximately 5 h (Borgstrom et al., 1981; Kalam et al., 2020). Participants in our study received a dose of 40 mg.

2.2 Magnetoencephalography

In Study 1, we recorded five minutes of eyes-open resting state MEG to investigate the role of $GABA_A$ and NMDA receptor activity on neuronal timescales across the cortex. The MEG is a non-invasive neuroimaging technique that measures the magnetic fields generated by neuronal activity. Electrical currents give rise to orthogonal magnetic fields, which can be intuitively illustrated by the right-hand rule: If the thumb points in

the direction of the electrical flow, the curled fingers indicate the direction of the magnetic fields (Hari & Puce, 2017). In the brain, this electromagnetic pattern is observed in postsynaptic currents flowing along the dendrites of pyramidal neurons. A single postsynaptic potential generates a magnetic field that is too weak to be detected. However, the temporal and spatial summation of many synchronously active neurons produce signals that are measurable by the MEG (Luck, 2005). Therefore, the MEG can directly measure neuronal activity, enabling a high temporal resolution compared to indirect measures, such as functional magnetic resonance imaging (fMRI; Pfister et al., 2014).

Due to the folded structure of the cortex, pyramidal neurons generate currents with different orientations: Currents at the top of gyri are predominantly radial, whereas those along the walls of sulci are primarily tangential. MEG sensors, arranged in a helmet around the head, are mainly sensitive to tangential currents (Hari & Puce, 2017; Malmivuo et al., 1997). Consequently, MEG predominantly captures activity originating from sulci, which make up a large proportion of the cortical surface (Hillebrand & Barnes, 2002). In addition, the MEG is less sensitive to deeper brain structures (Hillebrand & Barnes, 2002). A key advantage of the MEG is that magnetic fields are less smeared by differences in tissue conductivity (e.g., skull and scalp) compared to electrical potentials. This enables a higher spatial resolution in the MEG compared to its electrical correlate, the EEG (Hari & Puce, 2017; Luck, 2005).

Since neuronal magnetic fields are extremely small relative to environmental magnetic noise, MEG recordings are conducted in a magnetically shielded room to attenuate external interference. The magnetic fields are detected by highly sensitive sensors know as superconducting quantum interference devices (SQUIDs). Their high sensitivity arises from superconductivity, a physical state characterized by no electrical resistance. This state is achieved by cooling the SQUIDs to temperatures below 9 Kelvin using liquid helium (Hari & Puce, 2017; Luck, 2005). SQUIDs are configured as either magnetometers or gradiometers. Magnetometers consist of a single loop and are highly sensitive to magnetic fields, but are more susceptible to external noise. In contrast, gradiometers consistent of multiple loops that measure spatial differences in the magnetic field, which reduces susceptibility to sources of noise. Depending on their geometry, gradiometers can be further classified as axial or planar (Hari & Puce, 2017).

In Study 1, MEG recordings were conducted in a 306-channels whole-head MEG system (Elekta Neuromag, Vectorview) consisting of 204 planar gradiometers and 102 magnetometers. Analyses focused on gradiometer recordings.

2.2.1 Preprocessing

MEG recordings were preprocessed prior to analyses to reduce artefacts. Preprocessing included applying a 0.1 Hz high-pass filter to reduce slow drifts in the data. Additionally, independent component analysis (ICA) was used to remove artefacts related to eye movements and heartbeat (Ablin et al., 2018). Noisy channels and time segments were excluded based on visual inspection.

2.2.2 Source reconstruction

The combination of MEG and magnetic resonance imaging (MRI) enabled source reconstruction, providing an estimate of the location of neuronal activity in the brain. Inferring the underlying sources from sensor-level data constitutes the inverse problem, which does not have a unique solution. To constrain this problem, the forward solution was constructed, which described how neuronal activity in the brain generated signals measured at the sensors (Hari & Puce, 2017; Westner et al., 2022). In addition, a noise covariance was estimated from empty-room recordings to capture signals unrelated to brain activity. Finally, the source reconstruction was performed using a linear-constraint minimum-variance (LCMV; Sekihara & Nagarajan, 2008) beamformer.

2.2.3 Estimating neuronal timescales

MEG time series were converted into the frequency domain. To this end, power spectral densities (PSDs) were estimated using a modified Welch's method (Cohen, 2014; Gao et al., 2020; Shafiei et al., 2023). A fast Fourier transform (FFT) decomposed the time series into its constituent frequencies and their power (Cohen, 2014). FFT was computed for 10 s segments with 50% overlap. For each segment, a Hann window was applied to reduce spectral leakage caused from edge artefacts (Cohen, 2014; Donoghue et al., 2020). Power spectra were then averaged across segments by applying the median instead of mean to reduce the effect of artefacts (Cohen, 2014; Gao et al., 2020; Shafiei et al., 2023). This procedure was repeated for time series of each neuronal source. Next, the spectral data was decomposed into its periodic and aperiodic components (Figure 2.1). The periodic component reflects oscillatory activity which manifests as peaks in the PSD. Aperiodic activity follows a $\frac{1}{f^x}$

shape whereby power decreases exponentially with increasing frequency (Donoghue et al., 2020). While the aperiodic activity was historically often ignored or treated as noise, recent studies have highlighted its functional relevance. For example, changes in aperiodic activity during REM sleep have been associated with insight and memory formation (Lendner et al., 2023; Lowe et al., 2025). Moreover, aperiodic activity has been studied as a marker for brain maturation (Chini et al., 2022; He et al., 2019; Schaworonkow & Voytek, 2021; Schmidt et al., 2023; Voytek et al., 2015). Alterations in aperiodic activity have also been reported in neurological disorders, including Parkinson's disease (Helson et al., 2023; Wiest et al., 2023). Periodic and aperiodic components were identified using a multistep fitting procedure (Donoghue et al., 2020). First, an initial fit of the aperiodic component was estimated and subtracted from the PSD. In an iterative process, peaks above the noise threshold were identified and removed from the PSD by applying a Gaussian fit. When no peaks above the threshold remained, a multi-Gaussian model was fit to all identified peaks and subtracted from the original PSD. The resulting spectrum was then used to re-estimate the aperiodic component.

Peaks of the periodic component were each characterized by a central frequency, power and bandwidth. The aperiodic component *L* was defined by a Lorentzian function (Donoghue et al., 2020):

$$L = b - \log(k + F^x) \tag{2.1}$$

with the broadband offset *b*, the exponent *x* and the knee parameter *k*. The knee parameter *k*, together with the exponent *x*, was used to compute the knee frequency f_k (Donoghue et al., 2020):

$$f_k = k^{\frac{1}{x}} \tag{2.2}$$

The knee frequency defines the transition point at which power is no longer constant across frequencies, but instead decreased exponentially with increasing frequencies (Donoghue et al., 2020). This Lorentzian shape of the aperiodic component has been shown to be particularly prominent in the cortex compared to deeper brain structures, such as the thalamus (Bush et al., 2024). Finally, the knee frequency was used to estimate the decay time constant τ of each neuronal source (Gao et al., 2020):

$$\tau = \frac{1}{2\pi f_k} \tag{2.3}$$

The decay time constant describes the rate of decay of the autocorrelation function of a neural signal. It thus defines the signal's decreasing self-similarity across time and was taken as an index of neuronal timescales. Using the Desikan-Killiany atlas, neuronal timescales were parcellated by averaging within each of the 34 cortical regions per hemisphere (Desikan et al., 2006; Shafiei et al., 2023).

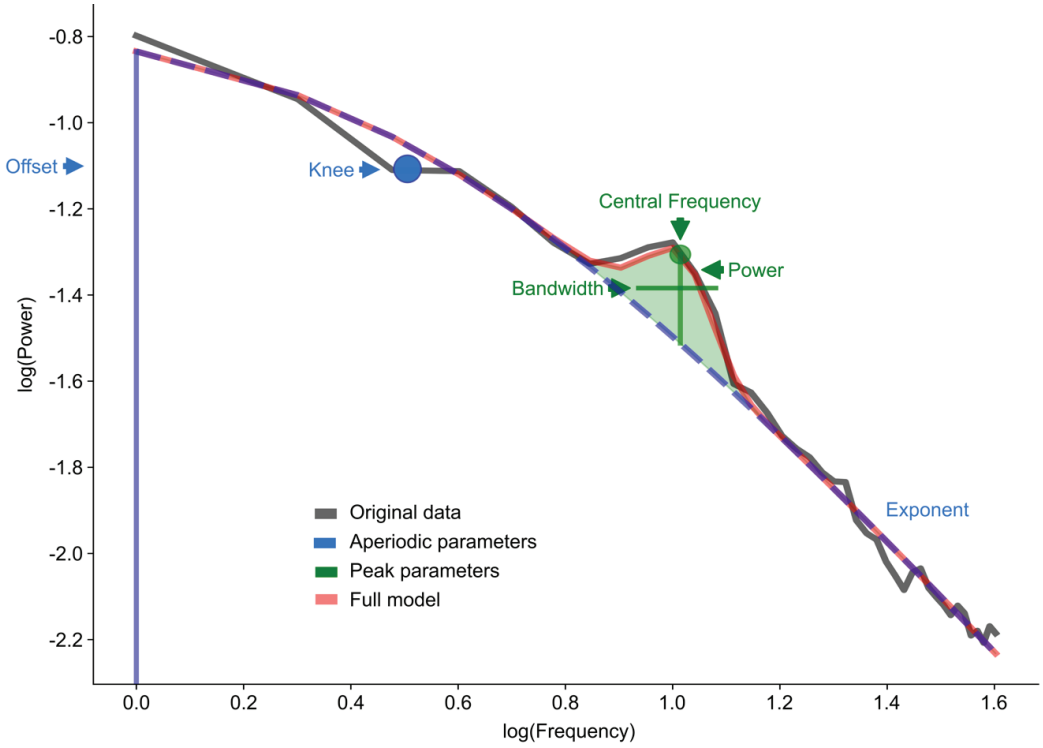

Figure 2.1: Schematic of periodic and aperiodic data fitting. The aperiodic and periodic components in the data were identified using a multistep fitting procedure. PSD of an example neuronal source, with logarithmic power plotted against logarithmic frequency. Periodic activity appears as peaks in the PSD. These are characterized by a central frequency, a bandwidth and power. The aperiodic component, is modeled using a Lorentzian function defined by an offset, exponent and knee parameter.

2.2.4 Time-Delay Embedded Hidden Markov Model

Distant brain regions spontaneously organize into short-lived, transient functional network states with distinct spectral signatures. Importantly, these states are latent and therefore not directly observable from the recorded data (Quinn et al., 2018). We applied Time-Delay Embedded Hidden Markov Models (TDE-HMMs) to the parcellated MEG time series in order to infer the dynamics of distinct large-scale cortical networks (Desikan et al., 2006; Vidaurre et al., 2018). In this data-driven approach, the time series data is represented as a sequence of mutually exclusive hidden states. Each of these states is defined by distinct multiregional covariance patterns that capture differences in spectral power and phase-locking across regions. After fitting the TDE-HMM, the a-posteriori probability time course of each state was used to estimate the

state-specific power spectra and connectivity patterns with a multitaper approach pooling across state visits (Vidaurre et al., 2016). Based on the resulting power spectra, state-specific neuronal timescales were estimated following the procedure described in Section 2.2.3. In addition, the a-posteriori probability time courses were hard-classified by assigning each time point to the state with the highest occurrence probability. These hard-classified time courses were used to quantify the temporal properties of the inferred network dynamics. The fractional occupancy described the overall proportion of time a specific state was active. The fractional occupancy depends on complementary metrics such as the state lifetime, the interval time and the state rate. State lifetime referred to the average duration of a continuous visit to a given state. The interval time defined the average duration between successive visits to that state. The state rate quantified how frequently a state was entered per second (Gohil, Huang, et al., 2024). Finally, state transition probabilities, describing the likelihood of transitioning from one state to another, were inferred to characterize the temporal structure of the state dynamics.

2.3 Experimental paradigms

While Study 1 analyzed resting-state data, Studies 2 and 3 used task-based paradigms. The tasks probed different forms of decision making to address respective research questions.

2.3.1 Reward-guided decision-making paradigm

In Study 2, we investigated the role of dopamine in risk preferences and the selection of decision strategies. To this end, we implemented a reward-guided decision-making paradigm (Figure 2.2). On each trial, participants chose between two options. Each option was defined by a reward magnitude and a probability of obtaining this reward. Reward magnitude was indicated by the width of a horizontal bar, whereas reward probability was presented as a percentage written underneath the corresponding bar. Because both choice attributes were explicitly presented, no learning was required during the task. In addition, reward probabilities were independent across options, such that either, both or neither option could be rewarded on a given trial. The two options were presented sequentially with the left option always presented first, followed by a short delayed and the subsequent presentation of the right option. After presentation of the second option, a question mark prompted participants to indicate

their choice with a button press. To make statistically optimal choices, participants needed to multiplicatively integrate the reward magnitude and probability into the EV and chose the option associated with a higher EV. Reward magnitudes and probabilities were never identical for the two choice options. If the chosen option was rewarded, the reward magnitude of that option was added to the participant's bonus. Although the outcome of the unchosen option did not affect the bonus, the outcomes of both choice options were displayed. This was intended to illustrate the occasional win of low reward probabilities and hence stimulate risk seeking.

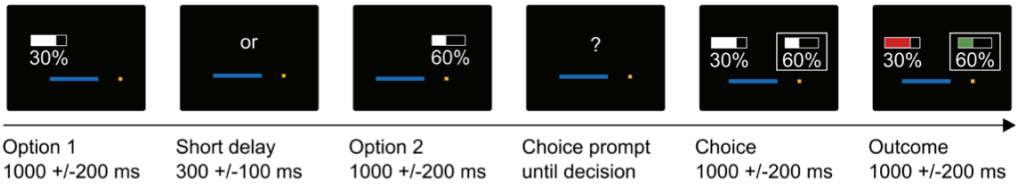

Figure 2.2: Task schematic and trial timeline of the reward-guided decision-making paradigm. Each option was defined by a reward probability (percentage) and a reward magnitude (width of the horizontal bar). Options were presented sequentially, with the left option always shown first for 800-1200 ms, followed by a short delay of 200-400 ms. The right option was then presented for the same duration. A question mark subsequently prompted participants to respond and remained on screen until a choice was made. This was indicated by a square surrounding the selected option. Participants then received feedback on the outcome (reward/no reward) for both the chosen and the unchosen option. The obtained reward was added to the progress bar displayed as a blue bar at the bottom of the screen throughout the entire task. This bar tracked earnings toward 2 € and reset itself after reaching this amount. Adapted from Dias Maile, Gruendler, et al. (2025). CC-BY 4.0.

2.3.2 Perceptual decision-making paradigm

In Study 3, we investigated how acetylcholine and noradrenaline influence perception, learning and the integration of bottom-up with top-down information. To this end, we implemented a perceptual decision-making paradigm based on the random dot motion task (Froböse & Ort, 2022; Marshall et al., 2024). On each trial, participants were presented a random dot kinematogram (Figure 2.3). Most dots moved randomly, while a subset moved coherently either left- or rightward. Participants were instructed to indicate the mean movement direction with a button press. Accordingly, perceptual task difficulty was determined by the proportion of coherently moving dots. This proportion was manipulated across four coherence levels (6%, 12%, 24% and 48%). In addition, a prior probability biasing motion direction was introduced across blocks of 44 or 84 trials. This prior specified the probability of rightward motion and took three possible values (0.2, 0.5 and 0.8). Importantly, the prior and its changes were not explicitly cued and therefore needed to be learned by participants across trials. Learning was based on veridical feedback and hence independent of the strength of sensory evidence. This allowed us to measure effects on learning, independently of perception and its integration. We further included 0% coherence trials, in which no perceptual evidence

was available and choices had to rely exclusively on the learned prior. A Bayesian optimal learner captured the prior estimates participants could ideally obtain, and was used to plot participants raw task behavior (Behrens et al., 2007).

Together, this paradigm required participants to integrate bottom-up sensory evidence and top-down prior expectations learned across past outcomes. Since each information source varied independently in its reliability, we expected the integration to adapt dynamically. Under lower levels of perceptual reliability (i.e., low motion coherence), participants were expected to rely more strongly on the learned prior probability. In contrast, when perceptual reliability was high (i.e., strong motion coherence), we expected a diminished influence of the prior probability.

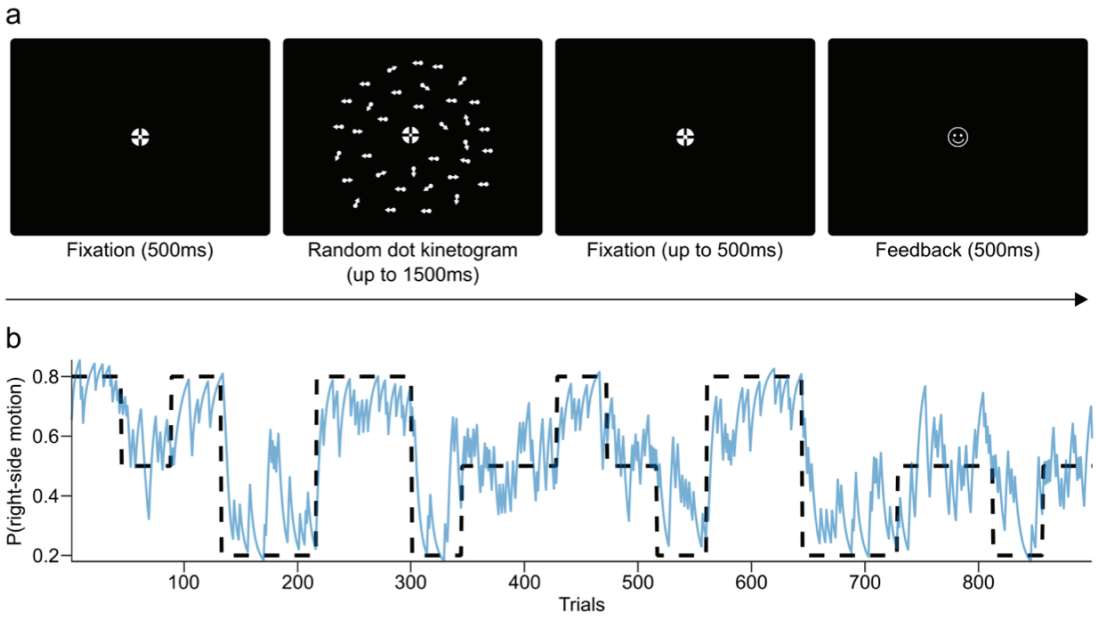

Figure 2.3: Example trial of the perceptual decision-making paradigm. (a) Each trial began with a fixation cross, presented for 500 ms. This was followed by a random dot kinematogram with the coherent motion displayed for up to 1500 ms or until the participant made a response. If no response was made within this window, the response window was extended by an additional 500 ms without the stimulus. Following the decision, feedback was provided via a smiley or frowny, indicating whether the response was correct. (b) Example time course of the task. The probability of rightward coherent motion varied across three levels (0.2, 0.5, 0.8) as indicated by the black dotted line. Since this probability and its switches were not signaled to the participant, they were estimated using a Bayesian optimal learner, which captured what participants could ideally know (blue line). Adapted from Dias Maile, Andronova, et al. (2026). CC-BY 4.0.

2.4 Mixed-effects modeling

In Study 1 and 2, we implemented mixed-effects modeling to examine the pharmacological modulations of cognitive processes. In contrast to analysis of variance (ANOVAs) and standard linear regressions, mixed-effects models account for both within- and between-subject variability in line with our within-subject pharmacological design. This reduces the risk of committing statistical Type I or Type

II errors. Moreover, mixed-effects models are more robust to missing data (Brown, 2021; Harrison et al., 2018; Jaeger, 2008). In Study 1, we were interested in the pharmacological modulation of neuronal timescales and how it related to the hierarchical cortical organization. We thus implemented a linear mixed-effects model with neuronal timescales as the outcome variable. In Study 2, we were interested in how task parameters influenced participants' decisions and how these effects were modulated by the pharmacological interventions. We hence implemented a general linear mixed-effects model with a binomial distribution, to analyze participants' choice behavior (left vs. right choice). Across both studies, we specified the random-effects structure to be as complex as supported by the data, in order to accurately disentangle within- and between-subject variability. The structure was determined using a principal component analysis, which required random components to explain at least 1% of variance (Bates et al., 2015).

2.5 Computational modeling

In Studies 2 and 3, we implemented mathematical models to disentangle behavioral choice data into the latent cognitive processes. This approach enabled investigating how neuronal computations were modulated by the pharmacological interventions. We compared multiple possible mathematical models, each representing different hypothesized cognitive computations, to determine which described best the observed behavioral data. Model comparison was based on the Bayesian Information Criterion (BIC), which penalizes the number of free parameters (Wilson & Collins, 2019):

$$BIC = -2log\widehat{LL} + k_m \log(T) \tag{2.4}$$

where $\widehat{LL}$ is the maximal log-likelihood of the model fit and *k* captures the number of free parameters of the model *m.* The model with the smallest BIC fits best to the data. Accordingly, since the BIC penalizes model complexity, it avoids overfitting and thus promotes models with a higher generalizability (Wilson & Collins, 2019). Based on the winning model, we then examined drug effects on the inferred neuronal computation.

2.5.1 Value-based model

In Study 2, we first identified the computational model and the associated cognitive process that best accounted for the observed choice behavior. To this end, we compared several candidate models, including a multiplicative, additive and hybrid

subjective value integration. The multiplicative model assumed that participants compute subjective values as the product of reward magnitude and probability (Farashahi et al., 2019):

$$sv_{i,t} = P_{i,t} \cdot M_{i,t} \tag{2.5}$$

where the subjective value $sv_{i,t}$ was based on the multiplication of the reward magnitude $M_{i,t}$ and the reward probability $P_{i,t}$ of option i in trial t.

In contrast, the additive model assumed that subjective value is computed as a weighted additive combination of reward probability and magnitude:

$$sv_{i,t} = \omega_p \cdot P_{i,t} + (1 - \omega_p) \cdot M_{i,t} \tag{2.6}$$

where ω_p determined the relative weight given to probability versus magnitude. Values of $\omega_p > 0.5$ indicated a stronger influence of probabilities consistent with more risk aversive behavior. Conversely, values of $\omega_p < 0.5$ reflected a stronger influence of magnitudes consistent with risk-seeking behavior (Scholl et al., 2014). The hybrid model combined both integration strategies:

$$sv_{i,t} = \omega_{mult} \cdot P_{i,t} \cdot M_{i,t} + (1 - \omega_{mult}) \cdot (\omega_p \cdot P_{i,t} + \left(1 - \omega_p\right) \cdot M_{i,t}) \tag{2.7}$$

where the parameter ω_{mult} governed the relative contribution of multiplicative versus additive value integration. Values $\omega_{mult} > 0.5$ indicated a dominance of the multiplicative processing.

In addition, we implemented three Prospect Theory models to relate our findings to previous work and compare model fits. These models allowed for non-linear distortions of reward probability (Eq. XY), reward magnitude (Eq. XY), or both (Eq. XY):

$$sv_{i,t} = \frac{P_{i,t}^{\gamma}}{(P_{i,t}^{\gamma} + (1 - P_{i,t})^{\gamma})^{\frac{1}{\gamma}}} \cdot M_{i,t} \tag{2.8}$$

$$sv_{i,t} = P_{i,t} \cdot M_{i,t}^{\alpha} \tag{2.9}$$

$$sv_{i,t} = \frac{P_{i,t}^{\gamma}}{(P_{i,t}^{\gamma} + (1 - P_{i,t})^{\gamma})^{\frac{1}{\gamma}}} \cdot M_{i,t}^{\alpha} \tag{2.10}$$

where parameters γ and α captured non-linear distortion of probability and magnitude, respectively.

Additionally, we observed a switching bias in the behavioral data, which was incorporated into the best-fitting model as an additional parameter. Across all models, choices were generated using a softmax choice rule:

$$p_{A,t} = \frac{1}{1+ e^{-(\Delta sv_t \cdot \tau)}} \quad (2.11)$$

where the probability *p* to choose action *A* in trial *t* was generated by the subjective value difference Δsv and the inverse temperature τ, which governed choice stochasticity.

Based on the BIC, we selected the winning model and implemented it within a Bayesian hierarchical framework to examine the dopaminergic modulation. In this approach, group-level parameters serve as priors for the individual-level parameters. Hence, complex data structures can be captured by modeling group- and individual-level effects simultaneously (Baribault & Collins, 2023). Accordingly, the pharmacological intervention was modeled as within-subject parameter shifts for each free parameter. Parameters were estimated as posterior distributions and credible effects were defined as those for which the 95% highest density interval did not include zero. Posterior predictive checks confirmed the reliability of the fitting procedure (Baribault & Collins, 2023).

2.5.2 Perceptual model

In Study 3, we identified the best-fitting model based on the BIC in an independent dataset using the same perceptual decision-making task. We compared a basic model defined by a relative weighting of the perceptual information and the learned prior to several other implementations of this integration process. In a coherence-dependent weighting model, the influence of the learned prior decreased with increasing motion coherence. In a further variant, this coherence-dependent weighting was exponentially scaled. We further implemented a model characterized by coherence-dependent modulation of the learning rate. In addition, we implemented all models with an additional side bias, due its strong influence on choice behavior. Since the basic model with an additional side bias had the lowest BIC, we preregistered this model for use in the pharmacological dataset (Dias Maile, Andronova, et al., 2025).

Specifically, the model assumed a weighted additive integration of motion coherence and learned prior:

$$sv_{D,t} = \theta \cdot c_{D,t} + (1 - \theta) \cdot v_{D,t} + b \quad (2.12)$$

where $sv_{D,t}$ is the subjective value of direction D presented in trial t, $c_{D,t}$ the motion coherence, $v_{D,t}$ the learned prior and b the side bias. The parameter θ determined the relative weighting of sensory evidence versus prior expectations, with values $\theta > 0.5$ indicating a stronger influence of perceptual information. The learned prior was modelled using a Q-learning rule:

$$v_{D,t+1} = v_{D,t} + \lambda \cdot (r_{D,t} - v_{D,t}) \tag{2.13}$$

where the prediction error, defined as the difference between the actual outcome $r_{D,t}$ and the current prior $v_{D,t}$, was used to update the prior for the next trial $v_{D,t+1}$. The learning rate λ governed how strongly the prediction error influenced this update. We additionally implemented a model with separate learning rates for rewarded and unrewarded choices to account for potential asymmetries in learning from positive and negative outcomes:

$$v_{D,t+1} = v_{D,t} + \lambda_{r,u} \cdot (r_{D,t} - v_{D,t}) \tag{2.14}$$

where λ_r and λ_u are the learning rates for rewarded and unrewarded trials, respectively. Similar to the approach in Study 2, choices were generated using a softmax choice rule:

$$p_{D,t} = \frac{1}{1+e^{-(\Delta sv_t \cdot \tau)}} \tag{2.15}$$

where $p_{D,t}$ is the probability to choose direction D in trial t, Δsv is the subjective value difference between options and τ is the inverse temperature capturing choice stochasticity. The model complexity did not allow the planned Bayesian hierarchical implementation. Model integrity was confirmed by a successful parameter recovery and model validation.

3 Results

The following chapter, describes the key results of the three studies. For more detailed information, readers are referred to the original work (Dias Maile, Andronova, et al., 2026; Dias Maile, Gruendler, et al., 2025; Dias Maile, Kohl, et al., 2026).

3.1 Role of GABA and NMDA receptors in shaping cortical timescales and large-scale network dynamics (Study 1)

The following section is based on our preprint, which is currently under review at eLife (see Research articles):

Dias Maile AA*, Kohl O*, Ort E, Froböse MI, Kurtenbach H, Butz M, Schreivogel E, Schnitzler A, Florin E†, Jocham G† (2026). Role of GABA and NMDA receptors in shaping cortical timescales and large-scale network dynamics. bioRxiv. https://doi.org/10.64898/2026.05.11.723797

Study 1 investigated the organization of neuronal timescales and large-scale network dynamics across the cortex, focusing on their modulation by $GABA_A$ and NMDA receptor activity. Accordingly, results are reported based on a region-wise (Section 3.1.1) and a network-level analysis (Section 3.1.2) of neuronal timescales.

3.1.1 Timescales follow a hierarchical cortical gradient and are prolonged by GABAergic activity

Neuronal timescales were estimated from open-eyed resting-state MEG recordings and parcellated into 34 cortical regions per hemisphere based on the Desikan-Killiany atlas (Section 2.2.3; Desikan et al., 2006). Recordings were acquired across three pharmacological sessions, during which participants received the benzodiazepine

receptor agonist lorazepam that binds allosterically at $GABA_A$ receptors (Section 2.1.2), the glutamatergic partial NMDA agonist D-cycloserine, which acts at the glycine-binding site (Section 2.1.1), or a placebo. We hypothesized that neuronal timescales follow a hierarchical gradient across the cortex, with shorter timescales in primary sensory regions and progressively longer timescales in higher-order association areas (Murray et al., 2014; Shafiei et al., 2023; Wang, 2020). As a proxy for a region's position within this hierarchy, we used an MRI-based index of myelinization, the T1w/T2w ratio. Lower values indicated a higher position along the cortical hierarchy. Consistent with this, neuronal timescales under placebo were strongly negatively correlated with the T1w/T2w ratio (Figure 3.1b). Neuronal timescales thus increased along the cortical hierarchy, replicating previous findings (Gao et al., 2020). Furthermore, this hierarchical organization was preserved under elevated $GABA_A$ and NMDA receptor activity following administration of lorazepam and D-cycloserine, respectively (Figure 3.1a and c).

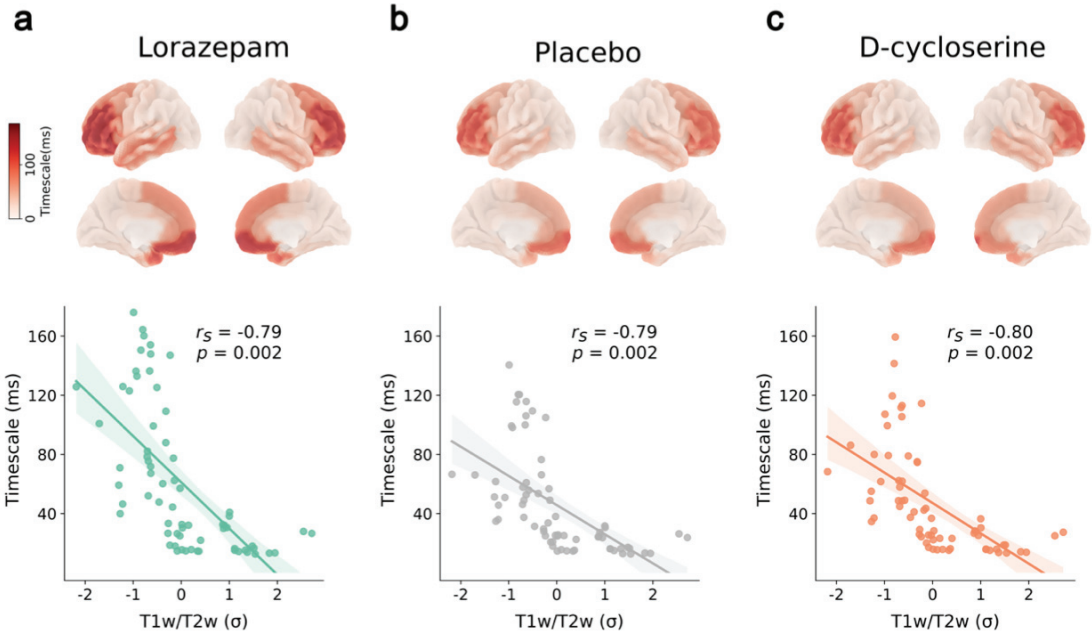

Figure 3.1: Hierarchical organization of neuronal timescales across the cortex. Neuronal timescales (ms), averaged across participants, and projected onto the cortical surface (**top row**) for (**a**) lorazepam, (**b**) placebo and (**c**) D-cycloserine. **Bottom row**: Neuronal timescales across 68 cortical regions as a function of cortical hierarchy, approximated with the T1w/T2w ratio. Solid lines represent the regression line, with shaded areas indicating 95% confidence intervals. r_S = Spearman correlation coefficient. *p*-values were computed while accounting for spatial autocorrelation. Reproduced from Dias Maile, Kohl, et al. (2026). CC BY 4.0.

We further hypothesized that lorazepam and D-cycloserine would prolong neuronal timescales, consistent with the slower decay kinetics of $GABA_A$ and NMDA receptor-mediated activity relative to AMPA (Angulo et al., 1999; Gupta et al., 2000; Sah et al.,

1990). A two-tailed paired-sample permutation t-test revealed that lorazepam significantly increased neuronal timescales in 48 of 68 cortical regions, distributed across both hemispheres (Figure 3.2a). To test whether lorazepam effects on neuronal timescales depended on a region's position within the cortical hierarchy, a linear mixed-effects model was implemented. As such, cortical hierarchy (T1w/T2w ratio), drug condition and their interaction were used as predictors for neuronal timescales. A hierarchy-dependent drug effect would be reflected in a significant interaction between the factors drug and T1w/T2w ratio, as this would imply that the drugs change the slope of the relationship between cortical hierarchy and neuronal timescales. Consistent with the region-wise analysis, lorazepam significantly increased neuronal timescales, as indicated by a significant positive main effect. In addition, T1w/T2w ratio had a significant negative main effect on neuronal timescales. A trend-level interaction between lorazepam and T1w/T2w ratio suggested that lorazepam effects were largely independent of cortical hierarchy with a tendency to steepen the hierarchical gradient (Figure 3.2c). This was likely driven by larger increases of neuronal timescales in frontal compared to occipital cortical regions (Figure 3.2a). Accordingly, previous work suggests that neuronal timescales are related to regional GABA receptor expression beyond their position in the cortical hierarchy (Gao et al., 2020). Importantly, the lorazepam effects on neuronal timescales were not explained by lorazepam-related changes in participants' vital signs, visuomotor abilities or mood (alertness, calmness and contentedness). Unlike lorazepam, D-cycloserine had no significant effect on neuronal timescales (Figure 3.2b) and showed no interaction with cortical hierarchy.

Taken together, neuronal timescales followed a hierarchical gradient across the cortex, which was preserved under elevated $GABA_A$ and NMDA receptor activity. Furthermore, neuronal timescales were increased across widespread cortical regions under elevated GABAergic activity. While this effect was largely independent of cortical hierarchy, it tended to be stronger in frontal regions, resulting in a trend towards a steeper hierarchical gradient.

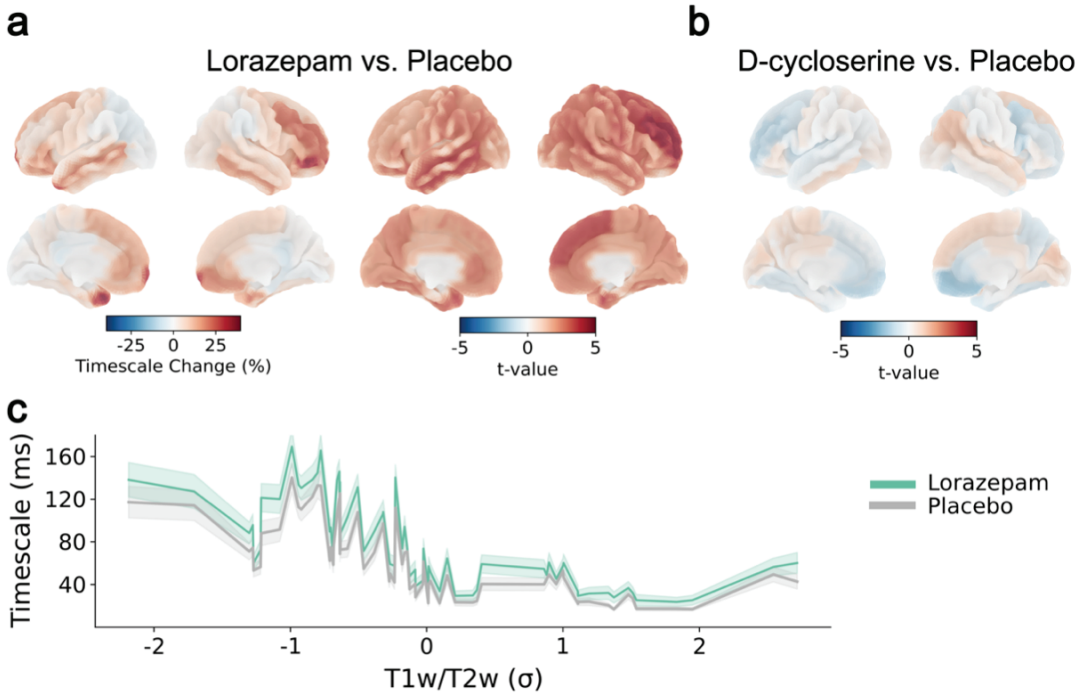

Figure 3.2: Pharmacological modulation of neuronal timescales. (**a**) lorazepam significantly increased neuronal timescales across the cortex as shown by the percent change of timescales relative to placebo (**left panel**) and the corresponding t-statistic (**right panel**), both projected onto the cortical surface. (**b**) D-cycloserine had not significant effect on cortical timescales, as indicated by the t-statistic projected onto the cortical surface. (**c**) T1w/T2w ratio plotted as a function of neuronal timescales for lorazepam and placebo. The 95%-confidence intervals are represented by shades. Lorazepam increased neuronal timescales largely independent of cortical hierarchy, with a trend towards a steeper hierarchical gradient. Reproduced from Dias Maile, Kohl, et al. (2026). CC BY 4.0.

3.1.2 Cortical networks show varying neuronal timescales and are differentially modulated by lorazepam

A TDE-HMM applied to the MEG timeseries identified eight dynamic large-scale cortical networks (Section 2.2.4). Visits to these network states were associated with distinct neuronal timescales (Figure 3.3a). Compared to global timescales, six states showed predominantly shorter (Sate 2, 4, 7 and 8) or mixed effects (State 6), whereas two states were associated with longer neuronal timescales (State 1 and 3).

Given the absence of significant effects of D-cycloserine in regions-wise analyses, drug-related changes of state-specific neuronal timescales were examined for lorazepam only. Lorazepam significantly increased neuronal timescales across distinct network states (Figure 3.3b). The strongest effects were observed during visits to State 1 and State 3 (Figure 3.4). These states have been linked to the dorsal attention network (DAN) and the frontal default mode network (DMN), respectively (Baker et al., 2014; Rossi et al., 2023; Rossi et al., 2024; van Es et al., 2025; Vidaurre et al., 2018).

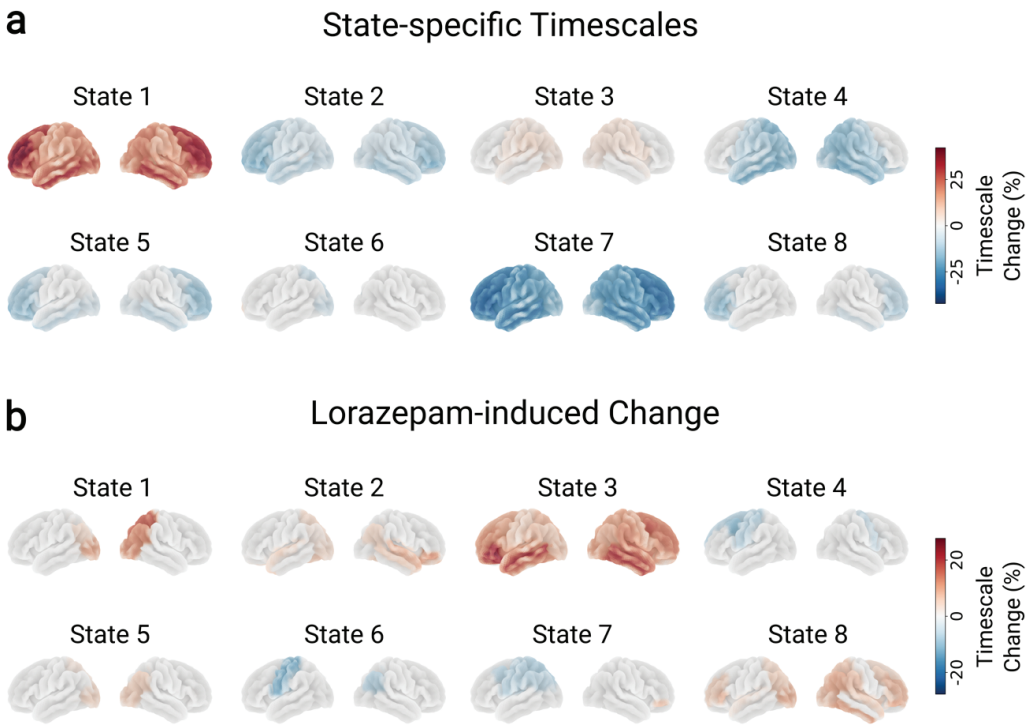

Figure 3.3: State-specific neuronal timescales. (**a**) Percent change relative to the global timescales projected onto the cortical surface. Network states exhibited distinct neuronal timescales (**b**) Percent change under lorazepam relative to placebo projected onto the cortical surface for regions showing significant effects. Lorazepam modulated timescales across states, with the strongest effects during visits to State 1 and 3. Reproduced from Dias Maile, Kohl, et al. (2026). CC BY 4.0.

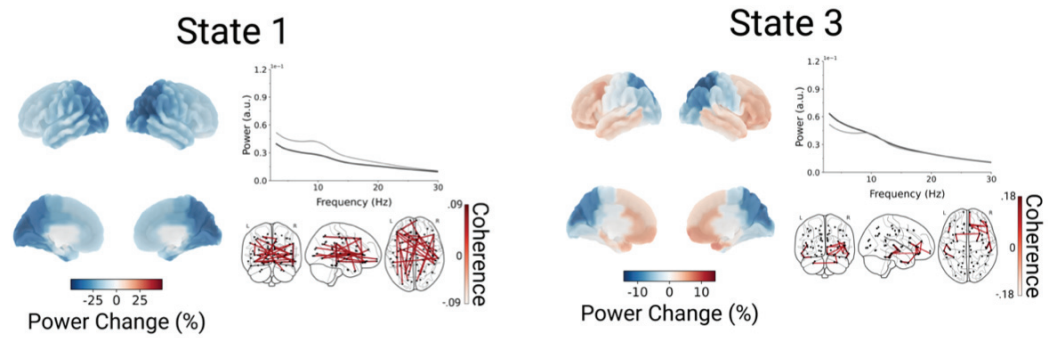

Figure 3.4: Spectral characterization of State 1 and 3 based on placebo condition. States defined by 3-30 Hz power changes relative to global power across states, projected onto the cortical surface (**left**) and averaged across the brain (**top right**, PSD). The state power spectrum in black was compared to the whole-brain average spectrum across all states (grey line). **Bottom right**: State-specific coherence networks in the 2–30 Hz range. Adapted from Dias Maile, Kohl, et al. (2026). CC BY 4.0.

Analysis of large-scale network dynamics further revealed that lorazepam increased fractional occupancy for frontal DMN (State 3) and decreased it for the DAN (State1; Figure 3.5a). In line with this, under lorazepam global neuronal timescales were strongest correlated to neuronal timescales in the frontal DMN in agreement with the increased engagement of this state.

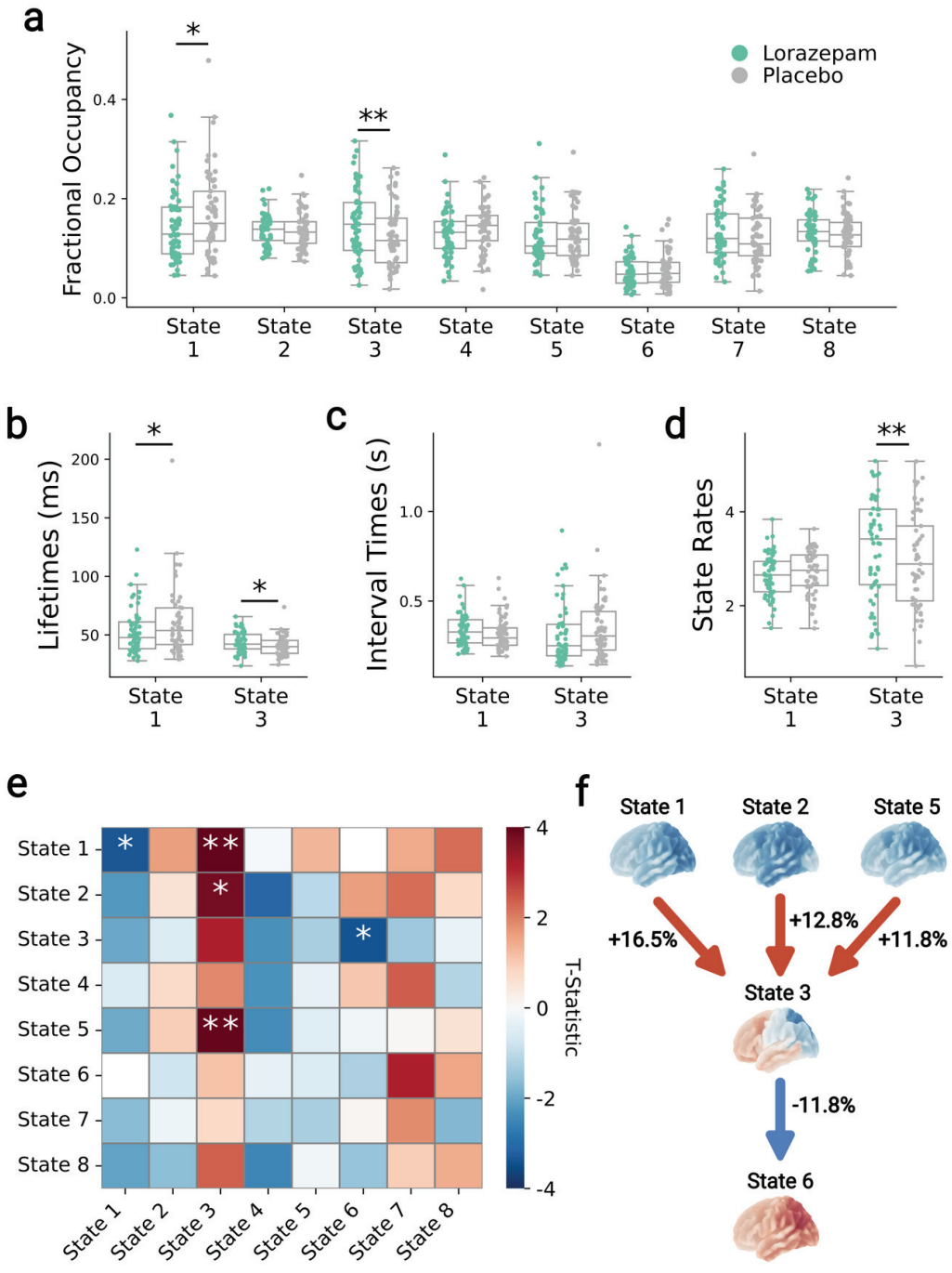

Figure 3.5: Dynamic large-scale network analysis. Lorazepam increased fractional occupancy (**a**) and state lifetimes (**b**) of State 3 compared to placebo. In contrast fractional occupancy (**a**) and state lifetimes (**b**) were reduced in State 1. (**c**) No significant drug effects on interval times. (**d**) State rates were significantly increased for State 3 under lorazepam. (**e**) State transition probabilities under lorazepam compared to placebo in a heatmap of t-statistics from within-participant GLMs. Rows indicate the current state and columns the transitions. (**f**) Lorazepam reduced self-transitions within State 1 and increased transitions from State 1, 2 and 5 into State 3. Transitions out of State 3 were reduced. Arrows indicate the transition direction paired with the percent change compared to placebo. Dots in a-d represent individual participants. Statistical significance in a-e was assessed using maximum t-statistic permutation tests including correction for multiple comparisons across states or transitions. Stars indicate significance ($p < 0.050$ = *, $p < 0.010$ = **). Reproduced from Dias Maile, Kohl, et al. (2026). CC BY 4.0.

In a next step, the fractional occupancy was decomposed into state lifetime (duration of a continuous visit), interval time (duration between successive visits) and state rate (frequency of entering a state per second; Figure 3.5b-d). The increased fractional occupancy of the frontal DMN (State 3) was driven by a longer state lifetime and an increased state rate. The reduced fractional occupancy of the DAN (State 1) was primarily driven by a shorter state lifetime. Thus, lorazepam increased both the duration of individual visits to the frontal DMN and the probability of entering this state. In contrast, the probability of entering the DAN was reduced. Network transition analysis supported these findings by showing that lorazepam significantly reduced self-transitions within the DAN (Sate1, Figure 3.5e-f). In addition, the DAN together with States 2 and 5, more frequently transitioned towards the frontal DMN (State 3), while transitions out of this state were reduced.

Together, these results indicated that dynamic large-scale cortical networks exhibited distinct neuronal timescales. Increased $GABA_A$ receptor activity largely modulated neuronal timescales of the frontal DMN and DAN and led to opposing shifts in their recruitment.

3.2 Bidirectional modulation of reward-guided decision making by dopamine (Study 2)

The following section is based on our manuscript published in Psychopharmacology (see Research articles):

Dias Maile AA, Gruendler TOJ, Fischer AG, Kurtenbach H, Kaiser LF, Froböse MI, Jocham G (2025). *Bidirectional modulation of reward-guided decision making by dopamine.* Psychopharmacology, 242(11), 2547–2559.
https://doi.org/10.1007/s00213-025-06816-9

Study 2 investigated decision strategies and their modulation by dopamine. To this end, participants performed a reward-guided decision-making task in which each choice option was associated with a reward magnitude and a probability of receiving this reward (Section 2.3.1). Participants performed the task across three pharmacological sessions, during which they were administering the D_2/D_3 receptor antagonist amisulpride and the dopamine precursor L-DOPA (Section 2.1.3) in a within-subject, placebo-controlled randomized design. Based on our hypothesis, analyses were

structured in two parts. First, we investigated which decision strategy best accounted for participants' behavior. We hypothesized that a hybrid strategy, including a combination of a multiplicative and additive value integration, would provide the best fit to the data (Farashahi et al., 2019; Figner & Voelki, 2004; Scholl et al., 2014). In a second step, we examined how the dopaminergic modulation influenced decision making. Given its critical role in decision making and risk preferences, we expected dopamine would guide the allocation of decision strategies (Burke et al., 2018; Rutledge et al., 2015; Schultz et al., 1997).

3.2.1 Hybrid integration strategy in reward-guided decision making

We compared several candidate models, including Prospect Theory models as well as models assuming multiplicative and/or additive subjective value integration (Section 2.5.1). Consistent with our hypothesis, a hybrid model provided the best fit to the behavioral data across all drug conditions, as indicated by the lowest BIC (Table 1). This suggests that participants relied on a combination of a multiplicative and additive value integration, contrary to the traditionally assumed purely multiplicative strategy in Prospect Theory.

Table 1: Model fits based on the BIC. The hybrid model explained the data best as indicated by the lowest BIC. Values represent means (SE) across all drug conditions. Adapted from Dias Maile, Gruendler, et al. (2025). CC BY 4.0.

	BIC
Hybrid model	314.67 (10.21)
Hybrid model with repetition bias	319.56 (10.13)
Additive model	336.49 (9.49)
Multiplicative model	400.95 (10.47)
Prospect Theory with magnitude distortion	319.58 (10.38)
Prospect Theory with probability distortion	364.93 (10.18)
Prospect Theory with magnitude and probability distortion	317.69 (10.15)

3.2.2 Dopamine modulates the reliance of choices on reward information

We examined how dopamine modulated the influence of task parameters on participants' choices using a general linear mixed-effects model. Amisulpride significantly reduced the effect of both reward magnitude and probability on choice, whereas L-DOPA resulted in an opposite pattern: The weighting of both choice attributes was significantly increased (Figure 3.6). Notably, neither drug affected reliance on the EV.

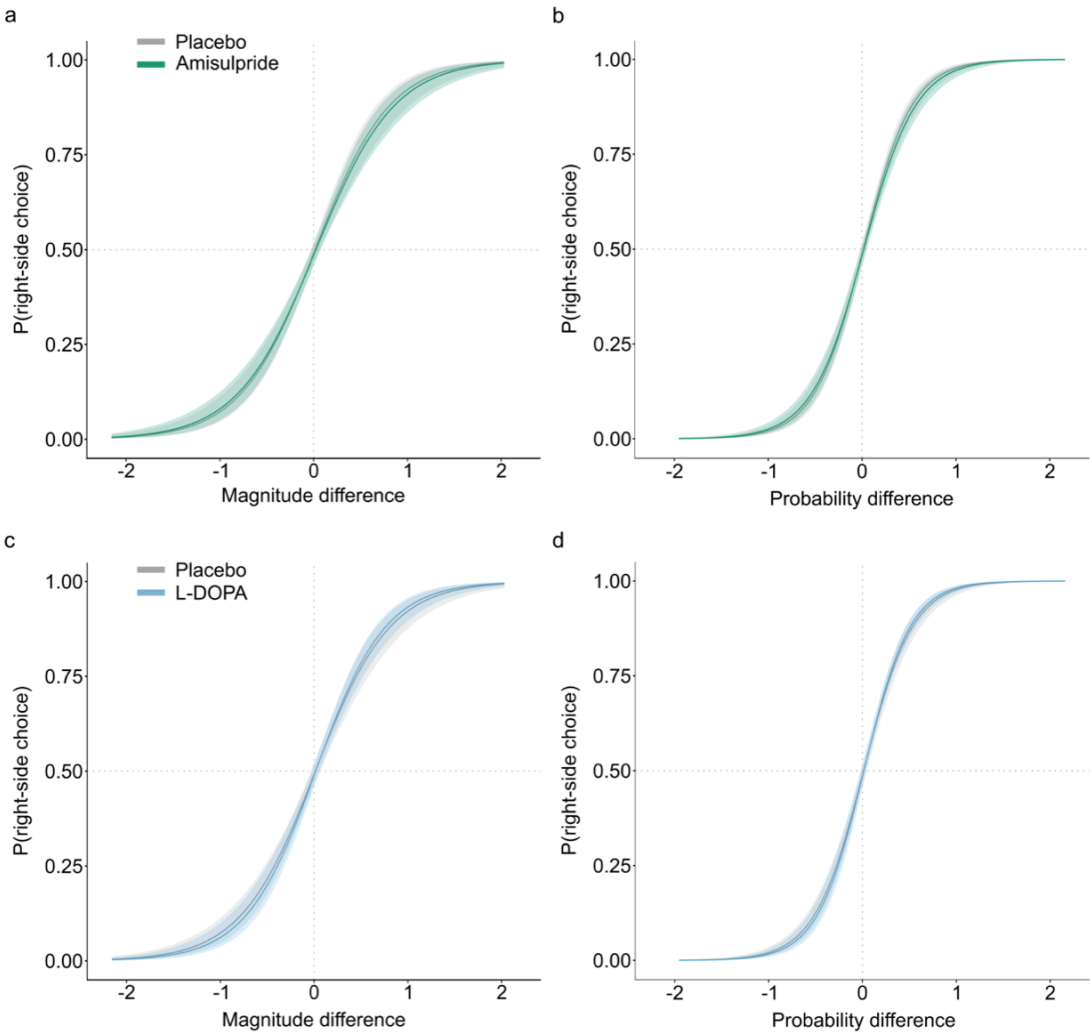

Figure 3.6: Reliance on choice attributes under amisulpride and L-DOPA. Model-predicted choice probabilities from the general linear mixed-effects model. The probability of a right-side choice as a function of the z-scored difference in reward magnitude (**a**, **c**) or reward probability (**b**, **d**) between right and left option. Amisulpride reduced the weighting of reward magnitude (**a**) and probability (**b**) on choice. L-DOPA increased the weighting of reward magnitude (**c**) and probability (**d**) on choice. Shades represent the SEM across participants. Reproduced from Dias Maile, Gruendler, et al. (2025). CC BY 4.0.

Dopaminergic effects were further analyzed within the hybrid computational model to investigate how the underlying cognitive processes were modulated. The model was implemented in a Bayesian hierarchical framework, with parameters estimated from posterior distributions and drug effects modelled as shifts on the three parameters. Credible effects were defined as those with 95% highest density intervals excluding zero. The relative contribution of additive versus multiplicative value integration was determined by the weighting parameter ω_{mult}. Parameter estimates indicated that participants relied on a nearly even combination of additive and multiplicative value computation, as reflected by the weighting parameter ω_{mult} close to 0.5 (Figure 3.7a).

However, this allocation of decision strategy was not credibly modulated by neither amisulpride or L-DOPA contrary to our hypothesis (Figure 3.7b).

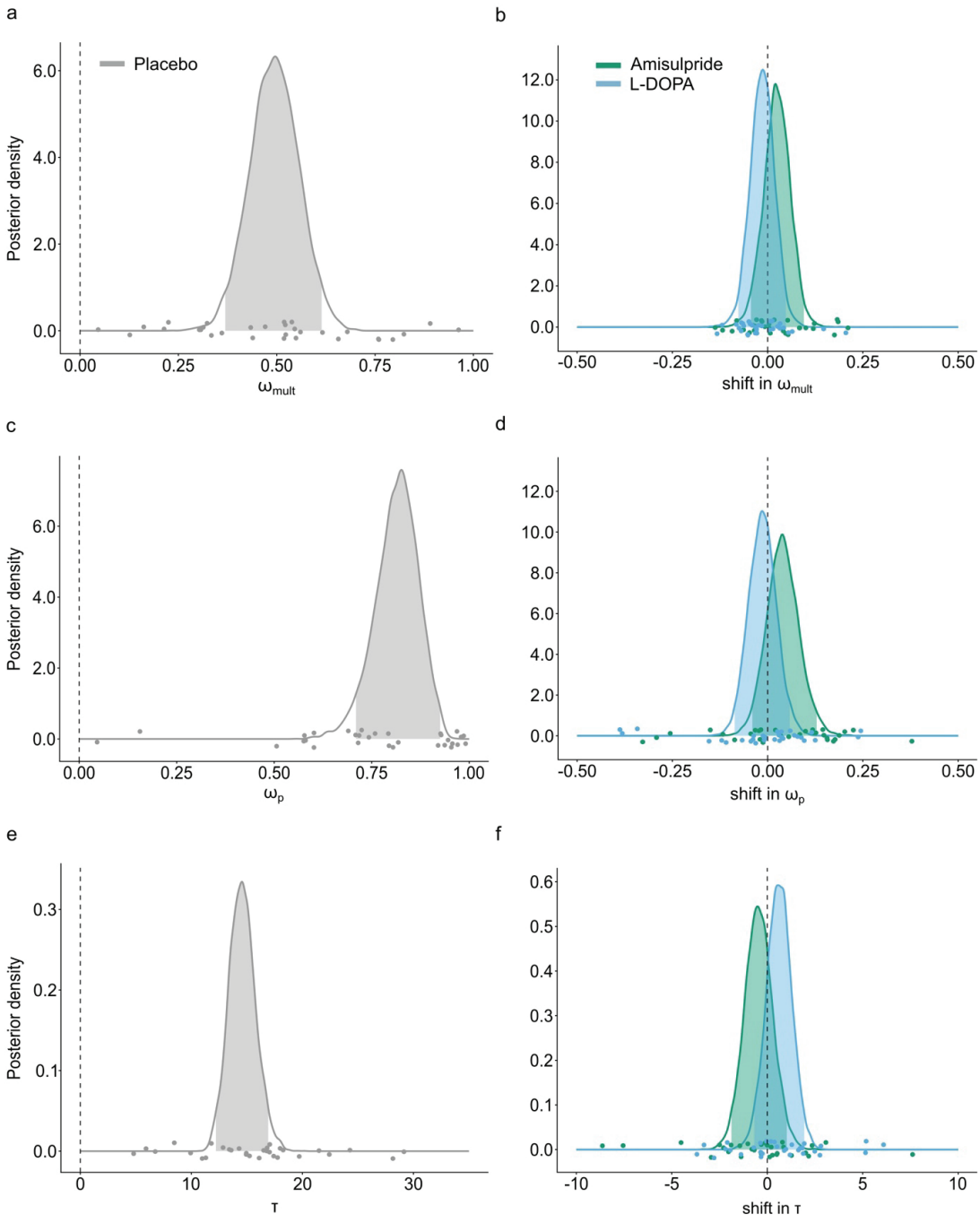

Figure 3.7: Posterior distributions of the group level estimate. Posterior distributions of the three model parameters from the Bayesian hierarchical model: (**a**) the multiplicative weight ω_{mult}, (**c**) the relative probability weight ω_P and (**e**) the softmax inverse temperature τ. (**b**, **d**, **f**) Posterior distributions of the corresponding drug shift parameters for amisulpride and L-DOPA. Shaded areas represent the 95% highest density interval. Individual subject estimates are shown as dots. Reproduced from Dias Maile, Gruendler, et al. (2025). CC BY 4.0.

Within the additive value integration, the parameter ω_p determined the relative influence of reward probabilities compared to magnitudes. Estimates of $\omega_p > 0.5$ indicated a stronger weighting of reward probabilities relative to magnitudes, consistent with risk aversive choice behavior (Figure 3.7c). But the 95% highest density interval of both drug shifts overlapped with zero, indicating no credible modulation of risk preferences by dopamine (Figure 3.7d). Likewise, the inverse softmax temperature τ, capturing choice stochasticity, was not credibly modulated by the drugs (Figure 3.7e-f). Numeric shifts were nevertheless consistent with the general linear mixed-effects results. Specifically, amisulpride was numerically associated with a reduction in τ, suggesting increased choice stochasticity. This aligns with a lower weighting of choice attributes under amisulpride in the general linear mixed-effects. In contrast, L-DOPA showed the opposite trend, whereby τ was numerically increased, suggesting reduced choice stochasticity in line with an increased weighting of choice attributes.

Together, these findings indicate that behavior in a reward-guided decision-making paradigm was best described by a hybrid response strategy combining additive and multiplicative value integration. Moreover, increased dopaminergic transmission under L-DOPA increased the influence of option attributes, whereas D_2/D_3 receptors blockade under amisulpride resulted in the opposite pattern, decreasing the influence of reward magnitude and probability.

3.3 Cholinergic and noradrenergic modulation of perceptual decision making and learning (Study 3)

The following section is based on our preprint published on bioRxiv (see Research articles):

Dias Maile AA, Andronova E, Ball F, Aravitska D, Dannenberg LK, Schnitzler A, O'Reilly JX, Jocham G (2026). *Cholinergic and noradrenergic modulation of perceptual decision making and learning.* bioRxiv. https://doi.org/10.64898/2026.06.22.732890

Study 3 investigated the role of acetylcholine and noradrenaline in shaping perception, learned expectations and the integration of these two sources of information during decision making. To this end, participants performed a modified version of the RDM, in which they reported the mean movement direction of a cloud of moving dots (Section 2.3.2). The strength of sensory evidence was manipulated by

varying the degree of motion coherence. Further, a prior probability was introduced such that one movement directions was more likely during periods of the task. Importantly, this prior probability and its changes were not explicitly signaled and therefore had to be learned from past trial outcomes. The task was performed under three drug conditions in which participants received the muscarinic acetylcholine receptor antagonist biperiden (Section 2.1.4), the β-adrenoceptor antagonist propranolol (Section 2.1.5) or a placebo. Based on previous research highlighting the role of acetylcholine and noradrenaline in perception, we expected both drugs to impair perceptual decision making (Chaudhury et al., 2009; Gelbard-Sagiv et al., 2018; Kossl & Vater, 1989; Mishra et al., 2024). In addition, we predicted opposing effects on learning. Drawing from previous work in our lab, we expected biperiden to increase the learning rate, causing a faster updating of prior beliefs (Kurtenbach et al., 2026). In contrast, propranolol has been associated with slower belief updating and we therefore hypothesized a decreased learning rate (Lawson et al., 2021). Finally, we expected both drugs to modulate the integration of bottom-up sensory information with top-down learned prior beliefs (Yu & Dayan, 2005).

3.3.1 Decision making is influenced both by motion coherence and prior expectations

Participants choices were guided by the perceptual evidence (i.e., motion coherence) and the learned prior belief, as reflected in the raw task behavior (Figure 3.8a). Overall, decisions were more strongly influenced by the perceptual evidence. However, the relative contribution of perceptual information and prior beliefs was not fixed but adapted dynamically across trials (Figure 3.8b). Participants placed greater weight on prior beliefs when sensory reliability decreased (i.e., low motion coherence), as clearly indicated by choice behavior. In contrast, when sensory evidence was strong, choices were predominantly guided by the perceptual input. This suggests that participants flexibly integrated bottom-up sensory information with top-down prior expectations, adjusting their relative weighting to the reliability of each information source.

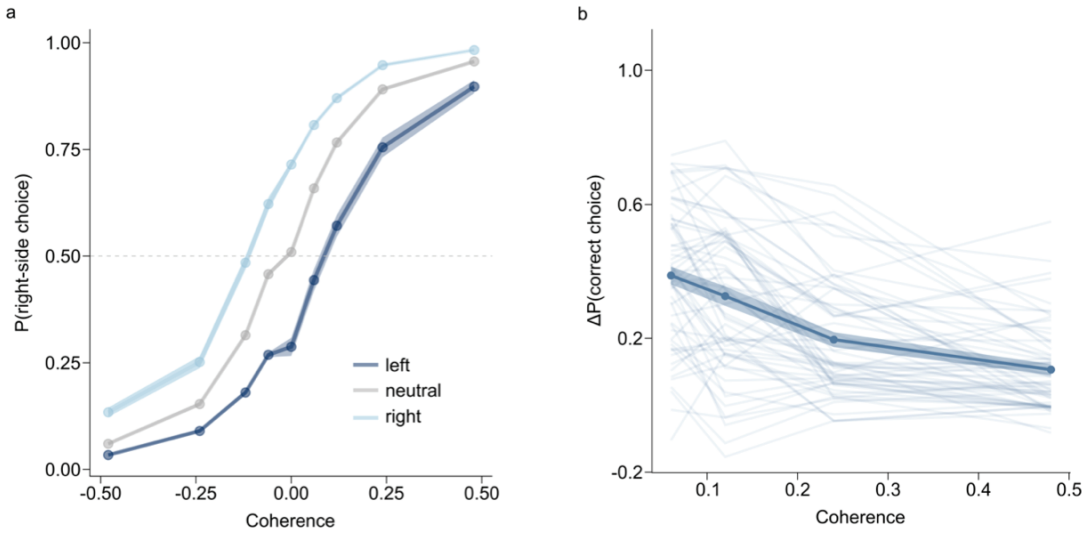

Figure 3.8: Raw task behavior averaged across drug conditions. (**a**) Probability of a right-side choice as a function of motion coherence and prior probability based on the Bayesian optimal learner (shades of blue). Leftward coherent motion is represented by negative coherence levels. (**b**) Difference between the probability of a correct choice as a function of unsigned motion coherence between congruent and incongruent trials (i.e., trials in which the Bayes-optimal prior indicated the same vs. the opposite choice as the direction of coherent motion). Light blue lines represent individual participants. The thick blue line indicates the group mean. The influence of the prior decreased with increasing perceptual evidence. Shades in **a**, **b** represent the standard error. Adapted from Dias Maile, Andronova, et al. (2026). CC BY 4.0.

3.3.2 Propranolol and biperiden modulate the updating of learned beliefs

We implemented a computational model to investigate the role of acetylcholine and noradrenaline in the underlying cognitive processes that governed participants' choices. In the model, the weighting parameter θ captured the relative contributions of perceptual evidence (i.e., motion coherence) and the learned prior. Values of $\theta > 0.5$ indicated a stronger reliance on perceptual compared to learned information. The learned prior was modelled using a Q-learning rule with a learning rate λ, which determined how strongly the prediction error updated prior estimates on each trial. Choices were generated using a softmax choice rule, including an inverse temperature τ to account for choice stochasticity. A side bias *b* was included to capture a right-side bias observed in the participants' raw choice behavior. The model was fit separately per participants and drug condition. Consistent with our hypothesis, the learning rate λ was significantly increased under biperiden. Contrary to our prediction, learning rates under propranolol were also significantly increased (Figure 3.9a-b). This indicated that participants updated prior beliefs more rapidly, placing greater weight on recent outcomes under both drugs relative to placebo. To assess whether the increased learning rate led to more optimal prior estimates, making it an adaptive adjustment of choice behavior, we computed the mean squared error (MSE) between participants'

prior estimates and statistically optimal estimates from a Bayesian learner. Under biperiden, MSE was significantly increased relative to placebo, indicating less optimal prior estimates. Thus, increased learning rates under biperiden were a maladaptive adjustment, causing nosier and less stable expectations. MSE under propranolol did not differ significantly from placebo (Figure 3.9c).

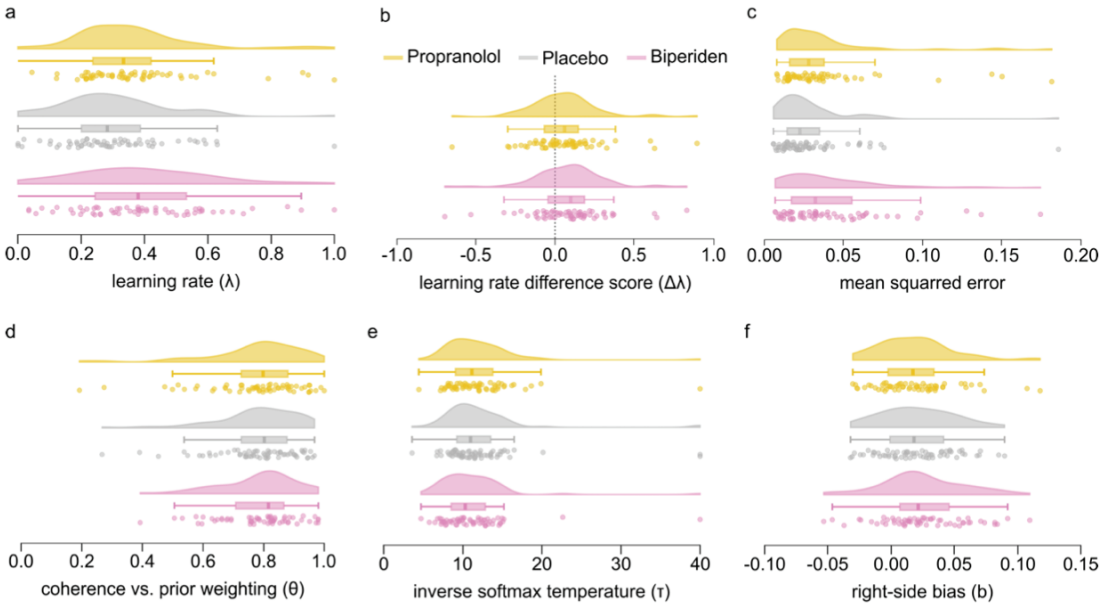

Figure 3.9: Parameter estimates per drug condition. Parameter distribution of the four model parameters across drug conditions: (**a**) learning rate (λ), (**d**) relative weighting (θ), (**e**) inverse softmax temperature (τ) and (**f**) right-side bias (*b*). (**b**) Difference scores of learning rates (Δλ; drug-placebo) where the dotted line indicates no difference. (**c**) MSE between participants prior estimates and estimates derived from a Bayesian optimal learner for each drug condition. In **a-f**, single-subject values are represented by dots. Propranolol and Biperiden significantly increased learning rates. Reproduced from Dias Maile, Andronova, et al. (2026). CC BY 4.0.

In addition, we investigated whether learning effects differed for rewarded and unrewarded trials by implementing a model with two distinct learning rates: λ_r and λ_u. Although this model did not improve the overall fit relative to the model implementing a joint learning rate, it enabled analysis of learning following reward or non-reward outcomes. The model revealed that propranolol selectively increased learning rates for rewarded choices (Figure 3.10a-b), with no significant effect on the unrewarded learning rates (Figure 3.10c-d). In contrast, biperiden increased learning rates for both rewarded and non-reward outcomes, but in line with previous reports (Kurtenbach et al., 2026), with larger effects for rewarded learning rates (Figure 3.10).

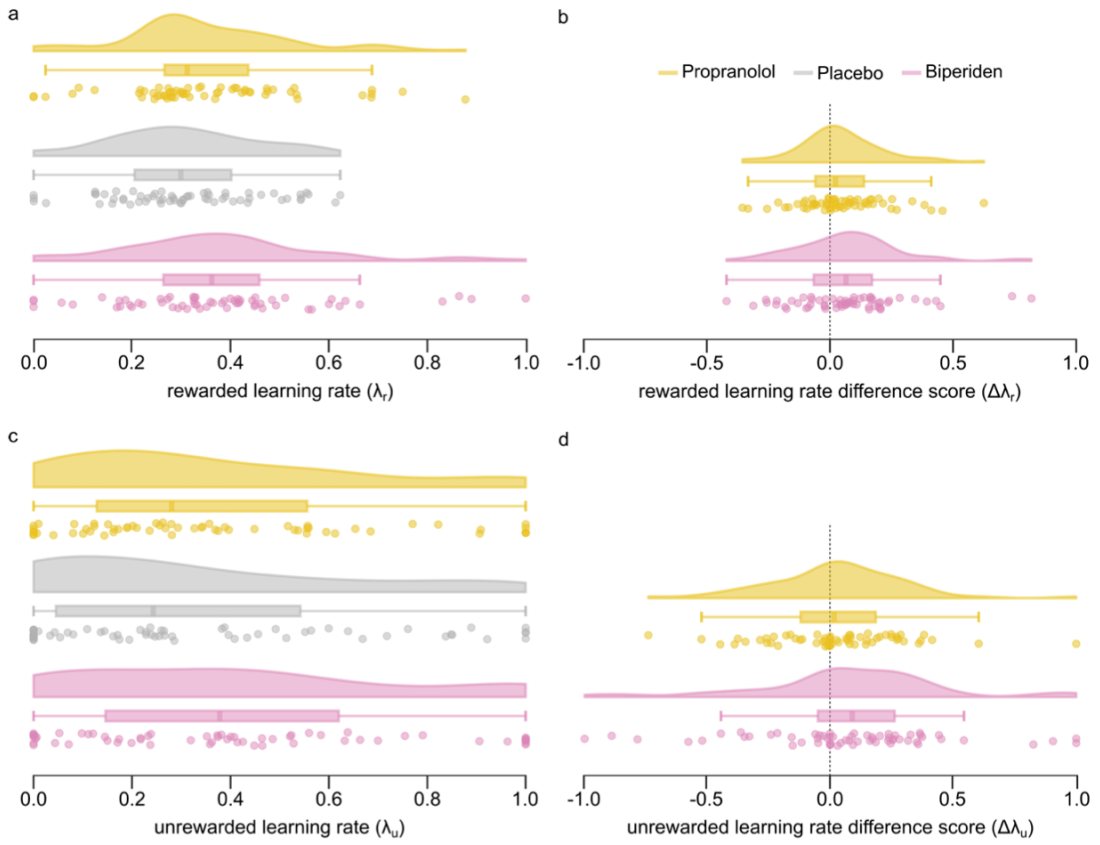

Figure 3.10: Parameter estimates for rewarded and unrewarded learning rates per drug condition. Parameter distributions for (**a**) rewarded (λ_r) and (**c**) unrewarded learning rate (λ_u) for each drug condition. Difference scores for (**b**) rewarded ($\Delta\lambda_r$) and (**d**) unrewarded learning rates ($\Delta\lambda_u$) were computes as drug minus placebo with the dotted line indicating no difference. In **a-d**, dots represent single-subject estimates. Propranolol selectively increased learning rates of rewarded outcomes, with no significant effect on the unrewarded learning rate. Biperiden increased learning rates independent of the outcome (reward/non-reward). Reproduced from Dias Maile, Andronova, et al. (2026). CC BY 4.0.

We expected a relative shift in the weighting of coherence and prior under both drugs. Contrary to our hypothesis, this weighting was not significantly modulated by either propranolol or biperiden (Figure 3.9d). However, regardless of drug condition and in line with raw behavior (Figure 3.8), the weighting parameter θ closer to 1 indicated that choices were more strongly driven by motion coherence than by the learned prior. The inverse softmax temperature τ was not significantly influenced by propranolol. Biperiden showed a trend towards a reduced τ, indicating an increased choice stochasticity (Figure 3.9d). Overall, participants showed a right-side choice bias which was not significantly modulated by the drugs (Figure 3.9e).

Taken together, these results indicated that muscarinic acetylcholine receptor antagonism and β-adrenoceptor antagonism increased the updating of learned beliefs. Once this learning effect was accounted for, neither drug influenced the relative

weighting of perceptual and learned information at the time of decision making. Blockade of muscarinic receptors additionally tended to cause more stochastic choice behavior.

4 Discussion

The present dissertation investigates how neurotransmitter systems guide decision making with a focus on the neural mechanisms underlying information integration. Across three studies, we investigated

- GABA and NMDA receptor activity in shaping neuronal timescales and large-scale network dynamics across the cortex (Study 1).
- decision strategies in reward-guided decision making and their modulation by dopamine (Study 2).
- the role of acetylcholine and noradrenaline in perception and learning, as well as in the integration of bottom-up sensory evidence with top-down expectations (Study 3).

4.1 Discussion of hypotheses

In the following section, the results are interpreted in light of our objectives, hypotheses and previous research. I provide an outlook for future research (Section 4.2) and an overall conclusion (Section 4.3).

1. Neuronal timescales follow a hierarchical gradient across the cortex.

In Study 1, we investigated the length of neuronal timescales across distinct cortical regions. We observed a strong correlation between the cortical hierarchy (approximated using the T1w/T2w ratio) and neuronal timescales under placebo. Thus, neuronal timescales increase along the cortical hierarchy, with longer timescales in higher order cortical regions. This finding is consistent with previous studies, establishing a hierarchical organization of neuronal timescales across the cortex (Cusinato et al., 2023; Murray et al., 2014; Shafiei et al., 2023; Wang, 2020). The

hierarchical gradient is essential for information processing as it enables the fast perception of new information as well as a more extended information integration (Baldassano et al., 2017; Çatal et al., 2023; Honey et al., 2012; Lerner et al., 2011). We add to existing evidence by demonstrating that this hierarchical organization was preserved under pharmacologically elevated $GABA_A$ and NMDA receptor activity. This aligns with previous findings of increased neuronal timescales during task engagement (Bernacchia et al., 2011; Manea et al., 2024), while the overall hierarchical gradient persists (Manea et al., 2024). The dynamics of task-related neuronal timescales are suggested to underlie elevated NMDA-mediated recurrent excitation paired with GABAergic feedback inhibition similar to our drug intervention (Gao et al., 2020; Wang et al., 2008; Wang et al., 2013; Wang, 1999, 2002, 2008).

2. Increased activity at NMDA and $GABA_A$ receptors prolongs neuronal timescales.

Based on the proposed neuronal mechanism underlying increased neuronal timescales during cognition, we hypothesized that elevated NMDA and $GABA_A$ receptor activity would similarly prolong neuronal timescales (Gao et al., 2020; Wang et al., 2008; Wang et al., 2013; Wang, 1999, 2002, 2008). Consistently, in Study 1, we found that strengthening GABAergic transmission through the benzodiazepine receptor agonist lorazepam prolonged neuronal timescales across widespread cortical regions. In contrast, the partial NMDA receptor agonist D-cycloserine resulted in no significant effect. In the brain, synaptic excitation is primarily driven by fast AMPA receptor activity (decay time constant ~2 ms), whereas NMDA receptors are characterized by slower decay kinetics (~50-100 ms) but have a voltage-dependent Mg^{2+} block during rest (Alberto & Hirasawa, 2010; Angulo et al., 1999; Espinosa & Kavalali, 2009; Myme et al., 2003; Sah et al., 1990; Vargas-Caballero & Robinson, 2004). Although D-cycloserine increases the channel opening probability by binding to the glycine co-agonist binding site, the emergence of NMDA currents still requires a partial postsynaptic depolarization to relief the Mg^{2+} (Thomas et al., 1988) This may explain the lack of significant D-cycloserine effects on resting-state neuronal timescales.

In turn, fast AMPA-mediated excitation is counteracted by the increased GABAergic transmission under lorazepam, which is characterized by slower decay kinetics (~5-10 ms; Chapman et al., 2022; Gupta et al., 2000; Isaacson & Scanziani, 2011), leading to the observed prolongation of neuronal timescales. This interpretation aligns with pharmacological studies observing similar effects of AMPA antagonist and

GABA agonist on resting state brain activity (Nutt et al., 2015; Routley et al., 2017). In addition, neuronal timescales have been shown to decrease with increasing AMPA/GABA receptor ratio in deeper cortical layers as indicated by a flatter slope in the aperiodic power spectrum (Halgren et al., 2021). In contrast, a steeper aperiodic slope is found under propofol anesthesia, which is thought to strengthen GABA receptor transmission, thus indicating longer timescales in line with our findings (Colombo et al., 2019; Donoghue et al., 2020; Gao et al., 2017; Waschke et al., 2021).

Finally, we observed a trend toward a steeper hierarchical gradient under lorazepam. This aligns with previous work linking $GABA_A$ receptor expression to neuronal timescales along the cortical hierarchy (Gao et al., 2020). We suggest that this effect was driven by a stronger modulation of neuronal timescales in frontal cortical areas. However, we primarily observed GABAergic modulation of neuronal timescales independent of the hierarchical gradient. This is consistent with the distributed $GABA_A$ receptor expression across the cortex and its relations with neuronal timescales beyond the cortical hierarchy (Figure 1.2; Gao et al., 2020; Norgaard et al., 2021).

3. Explorative analysis of neuronal timescales across distinct cortical networks.

In Study 1, we found that neuronal timescales varied across distinct large-scale cortical networks. This aligns with the distinct spectral signatures of transient network states (Vidaurre et al., 2018), which support cognition across diverse time windows ranging from fast sensory processing to more extended information integration (Bressler, 1995; McIntosh, 2000; Mesulam, 1998). Accordingly, the frontal DMN and DAN, which are commonly interpreted as task-relevant versus task-irrelevant thoughts, were characterized by long neuronal timescales (Fox et al., 2005; van Es et al., 2025).

4. Explorative analysis of the influence of NMDA and $GABA_A$ receptor activity on neuronal timescales across cortical networks and on network dynamics.

As our region-wise analysis found no significant modulation of neuronal timescales by D-cylcoserine, the network-specific analysis focused on lorazepam. Across large-scale networks, lorazepam increased neuronal timescales, consistent with the region-wise results. The largest increases were found in the DAN and frontal DMN, whose corresponding brain regions aligned with cortical variations in $GABA_A$ receptor density (la Fougere et al., 2011; Norgaard et al., 2021). Importantly, neuronal timescales within a given cortical region appeared to depend on the current network recruitment. This suggests that specific networks may engage distinct neuronal subpopulations

characterized by differential sensitivity to lorazepam. Consistently, $GABA_A$ receptor subtypes exhibit a distinct sensitivity to benzodiazepines, as well as distinct inhibitory profiles (Colombi et al., 2024; Patel et al., 2016; Rudolph & Knoflach, 2011). Similarly, neuronal timescales in the frontal eye field have been shown to be modulated by posterior parietal cortex activity, reflecting engagement of the frontoparietal attention network (Soyuhos et al., 2026).

Finally, these effects coincided with opposing shifts in network recruitment: Lorazepam increased the time spent in the frontal DMN while reducing it in the DAN. These bidirectional shifts align with previously reported anticorrelations between these networks (Baker et al., 2014; Fox et al., 2005; van Es et al., 2025).

5. *Reward-guided decision making is best described by a hybrid decision strategy that incorporates an additive and multiplicative value integration.*

In Study 2, we investigated which decision strategy participants relied on during reward-guided decision making. We found that a hybrid computational model combining both multiplicative and additive value integration of reward magnitude and probability provided the best fit for participants' behavior in a reward-guided decision-making paradigm. The model outperformed traditional multiplicative approaches, including Prospect Theory. This is consistent with our hypothesis and aligns with previous research showing that both humans and non-human primates rely on a flexible combination of decision strategies (Farashahi et al., 2019; Figner & Voelki, 2004; Scholl et al., 2014). Importantly, the balance between multiplicative and additive integration has been shown to shift dynamically depending on the decision context. Specifically, as risk and uncertainty increase, decision making tends to rely more on additive integration (Farashahi et al., 2019; Figner & Voelki, 2004). In the Study 2, participants' behavior reflected a similar contribution of both strategies, as indicated by the parameter ω_{mult}, which captured their relative weighting.

6. *Dopamine guides the allocation of decision strategies*.

In Study 2, we further investigated how dopamine modulates reward-guided decision making, with a focus on the allocation of decision strategies. Contrary to our hypothesis, no significant dopaminergic modulation of strategy allocation was found. Specifically, neither D_2/D_3 receptor blockade via amisulpride nor enhanced dopaminergic transmission through L-DOPA resulted in credible effect on the weighting parameter ω_{mult}, which captured the relative contribution of additive and multiplicative

value integration. Instead, the dopaminergic intervention modulated the weighting of choice attributes. Amisulpride reduced the weighting of reward magnitude and probability. In contrast, L-DOPA resulted in the opposite modulation increasing the influence of both reward magnitude and probability on choice. This bidirectional shift suggested a dopaminergic modulation of choice stochasticity, with more stochastic choices under amisulpride and less stochasticity under L-DOPA. We therefore expected these effects to be reflected in the inverse softmax temperature of the Bayesian hierarchical model. Conversely, no credible dopaminergic modulation of this parameter was found, although the numeric direction of drug effects aligned with the predicted pattern: Amisulpride tended to decrease the inverse softmax temperature (indicating more stochasticity) and L-DOPA tended to increase it (indicating less stochastic choices).

We found no credible dopaminergic modulation of risk preferences captured by the parameter ω_p, which determined the relative weighting of reward magnitude versus probability. This differs from previous research suggesting that L-DOPA increases risk-seeking behavior (Rigoli et al., 2016; Rutledge et al., 2015), while D_2 receptor antagonism reduces risk aversion (Burke et al., 2018; Ojala et al., 2018). Several factors may account for these diverging results. The reward-guided decision-making paradigm used in Study 2 included only a gain frame and did not incorporated losses, thereby disregarding loss aversion. However, previous research suggests that dopamine shapes risk preferences specifically in the gain domain (Ojala et al., 2018; Rutledge et al., 2015). Hence, this is unlikely to explain our diverging effects. Another possibility is that the short delay between the presentation of the left and right option introduced a working memory component. According to the two-state model proposed by Seamans and Yang, distinct dopaminergic receptor activity determines the processing of new input (Section 1.2.3; Seamans et al., 2001; Seamans & Yang, 2004). Thus, we cannot rule out that the dopaminergic interventions affected the processing of the first and second option differently. Finally, similar studies using a (indirect) dopamine agonist or a D_2 receptor antagonist have likewise reported no significant effects on risk preferences in healthy participants (Arrondo et al., 2015; Evers et al., 2017; Hamidovic et al., 2008; Symmonds et al., 2013; Zack & Poulos, 2007).

7. *Muscarinic acetylcholine receptor antagonism and β-adrenoceptor antagonism impair perceptual decision making.*

Based on previous research, we hypothesized that β-adrenoceptor antagonism via propranolol and muscarinic acetylcholine receptor antagonism via biperiden would reduce participants' perceptual discriminability (Eggermann & Feldmeyer, 2009; Hasselmo et al., 1997; Kasamatsu & Heggelund, 1982; Meir et al., 2018). We expected this impairment to shift the weighting parameter θ, which captured the reliance on perceptual information relative to learned beliefs. However, in Study 3, neither drug significantly modulated perceptual processing, as indicated by the absence of any modulation of θ.

Alternatively, reduced reliance on perceptual evidence, without a corresponding increase in the use of learned beliefs, would be reflected in an increased choice stochasticity. However, propranolol did not significantly alter choice stochasticity captured by the inverse softmax temperature, despite theoretical accounts proposing a role for noradrenaline in regulating this process (Doya, 2002). Biperiden showed a trend toward increased stochasticity, consistent with previous findings indicating greater decision variability under muscarinic receptor antagonism (Erfanian Abdoust et al., 2024; Kurtenbach et al., 2026). However, this effect did not reach statistical significance.

8. *Muscarinic acetylcholine receptor antagonism increases the learning rate, causing a faster updating of prior beliefs. β-adrenoceptor antagonism decreases the learning rate, causing a slower updating of learned beliefs.*

In Study 3, we observed increased learning rates under both biperiden and propranolol, indicating that prior estimates were updated more strongly based on recent outcomes. For biperiden, this finding is consistent with our hypothesis, as we expected faster updating to be reflected in an increased learning rate. This is supported by recent work from our group showing that elevated learning rates under biperiden promote faster updating of reward contingencies in volatile environments (Kurtenbach et al., 2026). Moreover, faster updating under biperiden caused learned estimates to become noisier, leading to greater deviations from the statistical optimum. This pattern was evident both in Study 3 and in prior work (Kurtenbach et al., 2026). One proposed mechanism is an insufficient adjustment of learned beliefs in response to prediction errors, which increases the tendency to infer changes in underlying contingencies,

thereby requiring a fast adjustment archived through high learning rates (Kurtenbach et al., 2026; Marshall et al., 2016; Piray & Daw, 2021; Yu & Dayan, 2005).

For propranolol, we initially expected a slower updating of learned beliefs and thus a reduced learning rate, as reported in previous studies (Lawson et al., 2021). One explanation for the discrepancy from our results is that, in the task used by Lawson et al. (2021), participants did not receive explicit veridical feedback. Instead, learning depended on the perceptual information. Consequently, changes in sensory processing and changes in prior updating could not be fully disentangled. In contrast, in our task, participants received veridical feedback following each choice, allowing learning to be based on the true outcome rather than on participants' potentially noisy interpretation of the coherent motion. Moreover, our modeling approach explicitly estimated how perceptual information and learned beliefs were integrated to guide choices. This allowed us to dissociated the contribution of perceptual evidence from the influence of prior expectations at the decision stage. Furthermore, noradrenaline is proposed to stabilize estimates of environmental volatility. Hence, noradrenergic antagonism has been shown to lead to faster updating, as unexpected outcomes are more likely to be attributed to changes in the underlying contingency (Marshall et al., 2016). This aligns with the increased learning rates under propranolol observed in Study 3. However, it is important to note that the pharmacological intervention in the previous study targeted α_1-adrenoceptors, whereas we administered a β-adrenoceptor antagonist. Nevertheless, β-adrenoceptor activity is also implicated in learning by supporting synaptic plasticity in the hippocampus essential for memory formation (Jami et al., 2023; Larsen et al., 2023; Sara et al., 1999; Straube et al., 2003; Tronel et al., 2004). We extend this finding by identifying a role of β-adrenoceptor activity in trial-by-trial learning whereby recent outcomes have a stronger influence compared to more distant experiences.

Finally, our results suggest that the effects of propranolol on learning were specific to the rewarded outcomes and that the effects of biperiden were similarly more pronounced for rewards. Coherently, previous studies indicate that biperiden modulates learning rates following rewards more strongly (Kurtenbach et al., 2026).

9. *Muscarinic acetylcholine receptor antagonism and β-adrenoceptor antagonism modulate the integration of bottom-up sensory evidence with top-down learned expectations*.

Contrary to our hypothesis, the drugs did not significantly modulate the relative weighting parameter θ, which captured the integration of top-down learned beliefs with bottom-up sensory evidence at the time of choice. Nevertheless, the observed learning effects under both propranolol and biperiden provide insights into this integration process. Specifically, the increased learning rates under both drugs suggest that learned beliefs were treated as more uncertain and therefore needed to be updated faster. As a consequence, reliance on top-down expectations was reduced in favor of learning from new bottom-up information (Yu & Dayan, 2005).

4.2 Outlook

Across the three studies presented in this dissertation, the results highlighted the mechanistic role of neurotransmitter systems in shaping decision making and learning and thereby guiding information processing in the brain. At the same time, the findings and their associated limitations promise interesting directions for future research.

Across all studies, pharmacological interventions provided important insights into the neurochemical underpinnings of cortical dynamics and cognition. However, most interventions selectively targeted a specific receptor subtype within the respective neurotransmitter system. Accordingly, in Study 3 in our investigation of the role of noradrenaline in perceptual decision making and learning, we focused on mechanisms related to β-adrenoceptor transmission. Across past research, β-adrenoceptor activity has been implicated in synaptic plasticity and memory formation, consolidation as well as retrieval (Sara et al., 1999; Schutsky et al., 2011; Straube et al., 2003; Tronel et al., 2004; Zhang et al., 2013). On the one hand, it would therefore be important to determine whether the observed modulation of learning, where more recent outcomes have a stronger influence compared to more distant experiences, also extends to impairments in memory. Especially since current evidence suggests that reduced β-adrenoceptor activity primarily affects the consolidation phase, while leaving performance immediately after learning largely unaffected (Sara et al., 1999; Tronel et al., 2004). On the other hand, future studies should investigate whether these learning effects are specific to β-adrenoceptor activity or generalize to other noradrenergic receptor subtypes. Accordingly, similar modulations of learning have been observed under α_1-adrenoceptor antagonism (Marshall et al., 2016). In the context of perception, α_1-adrenoceptors have been associated with suppression of spontaneous neuronal

activity, as well as enhancing perceptual selectivity and sensitivity of stimulus-evoked responses (Ciombor et al., 1999; Manunta & Edeline, 1997, 2004).

In Studies 2 and 3, the analysis of decision-making behavior provided a window into cognition, revealing the outcomes of otherwise hidden neuronal processes. We focused on the role of distinct neurotransmitter systems in shaping participants' choices in different decision-making paradigms. Combining such tasks with neuroimaging techniques may provide further insight into the underlying neuronal computations. In line with the observed cholinergic modulation of learning in Study 3, an auditory detection task performed by mice paired with optogenetic identification has shown that cholinergic neurons in the basal forebrain respond to reward with high temporal precision. The activity was scaled by reward unexpectedness, which suggests that it represents a reliable reinforcement-learning signal (Hangya et al., 2015). Similarly, in a Simon task performed by humans combined with fMRI recordings, post-error adjustments essential for learning were disrupted following administration of biperiden. These effects were reflected in an absence of behavioral adaptions, as well as a reduced error-related activity in the posterior medial frontal cortex, which normally modulates activity in the visual cortex (Danielmeier et al., 2015). In line with our findings, Kurtenbach et al. (2026) identify a role of acetylcholine in regulating the learning rate according to the environmental volatility. Using MEG, they found that the maladaptive increase in learning rates caused by biperiden was accompanied by a biperiden-induced reduction of activity in the lateral prefrontal cortex in the high beta-band. This signal encoded true and expected choice outcomes and hence was proposed to reflect a prediction error signal correlate. Given that these results are based on a reward-guided decision-making paradigm, it would be interesting to investigate whether similar neuronal mechanisms underlie the effects observed in the present perceptual decision-making task. Additionally, future studies should address how these cholinergic mechanisms differ from the noradrenergic role during decision making and learning, which was more specific to the rewarded outcomes.

Vice versa, it would be interesting to investigate how the cortical dynamics of neuronal timescales and network dynamics governed by GABA and NMDA receptor activity (Study 1) translate into cognition and behavior. In this context, it has been shown that the E/I balance in the ventromedial prefrontal cortex is selectively crucial for reward-guided decision making (Jocham et al., 2012; Kaiser et al., 2021). More specifically, higher GABA concentration and lower glutamate levels are associated with

more value-driven choice behavior, whereas the opposite neurochemical profile leads to more stochastic decision making (Jocham et al., 2012). Similarly, biophysically realistic models postulating attractor-state dynamics during decision making suggest that increased NMDA-mediated recurrent excitation should lead to more impulsive decisions. In contrast, increased GABA receptor mediated feedback inhibition should result in increased indecisiveness and consequently a higher rate of missed responses (Lam et al., 2022). Study 1 also included three decision-making tasks spanning the reward-guided and perceptual domains. It would be interesting to investigate how GABA and NMDA receptor mediated changes in decision making relate to changes in neuronal timescales above their inhibitory and excitatory activation profile, respectively. In this sense, previous research suggests that neuronal timescales are modulated by cognitive demands including attention (Manea et al., 2023; Zeraati et al., 2023) and notable there is some evidence that the variability of neuronal timescales predicts reaction times across diverse tasks including decision making (Boucher et al., 2022; Zeraati et al., 2023). Accordingly, longer timescales in the prefrontal cortex have been linked to improved working memory performance (Gao et al., 2020). Future research should further investigate this thereby addressing how modulation of neuronal timescales of distinct cortical regions or networks influences cognition, especially decision making.

Additionally, our results could be extended not only by combining neuroimaging techniques with choice behavior, but also by considering a more readily available source of information: reaction times. In Studies 2 and 3, we primarily focused on participants' choices. Due to the characteristics of the paradigms, reaction times were not analyzed in detail, although they contain valuable information about the underlying decision processes. In accordance with the perceptual decision-making paradigm used in Study 3, Hanks et al. (2011) propose that the brain guides the integration of top-down learned information with bottom-up sensory evidence based on the elapsed response time. Slower decisions thereby reflect a lower reliability of sensory evidence and therefore greater influence is given to learned beliefs. By implementing two different response regimes emphasizing either speed or accuracy, they derived a time-dependent accuracy function that modulated the influence of learned beliefs on evidence accumulation. Due to the limited duration of the pharmacological interventions, a similar intricate approach could not be implemented in Study 3. However, this might be possible using different drugs enabling a longer testing window

or different experimental paradigms with a shorter trial structure (Foucault et al., 2025). To this end, it would be interesting to investigate whether acetylcholine or noradrenaline modulate the time-dependent integration of learned belies with sensory evidence.

Similarly, in the reward-guided decision-making paradigm in Study 2, reaction times could not be analyzed due to the sequential task design characterized by a choice prompt. However, previous work indicates that reward contingencies modulate evidence accumulation and, by extension, reaction times. Increased reward rates have been shown to lead to faster responses by enhancing evidence accumulation and lowering decisions thresholds. In contrast, increased punishment leads to slower responses due to elevated decision thresholds (Leng et al., 2021). Dopamine is known to play a central role in reward processing including signaling expected rewards (Frank, 2005; Schultz, 1998; Schultz et al., 1993; Schultz et al., 1997). Consistent with this, increased dopaminergic transmission in a reinforcement learning paradigm has been shown to reduce decision thresholds, resulting in faster but less accurate choices (Chakroun et al., 2023). Furthermore, increased frontal dopamine transmission in a reward-guided decision-making paradigm without learning has been shown to increase value dependence of evidence accumulation (Peters et al., 2020). This is consistent with the behavioral effects observed under increased reward rates (Leng et al., 2021). In combination with neuroimaging, it has also been shown that faster reaction times under increased catecholaminergic transmission are associated with changes in the neuronal substrate of evidence accumulation, the CPP (Loughnane et al., 2019; Nuiten et al., 2023, 2024). Taken together, reaction times contain rich information about underlying decision processes. Future research should therefore clarify the role of dopamine in shaping these dynamics and examine how different decision strategies influence evidence accumulation and reaction times.

From a clinical perspective, studies investigating the neurochemical underpinnings of human cognition also provide important insights into the causes of neurological and psychiatric disorders including potential therapeutic strategies. In this context, Molina et al. (2000) were among the first to report altered risk preferences in medicated patients with Parkinson’s disease. They describe 12 cases of pathological gambling disorder during L-DOPA treatment. This observation was later corroborated by additional studies showing that unmedicated Parkinson’s disease patients tend to be more risk averse, whereas L-DOPA treatment can increase risk-seeking behavior

and in some cases even cause impulsive control disorders, such as pathological gambling (Cherkasova et al., 2019; Kobayashi et al., 2019; Moustafa et al., 2008; Weintraub et al., 2006). Moreover, unmedicated Parkinson's patients are able to slow their responses in order to maximize reward, while being less able to speed up. In contrast, medicated patients exhibit reduced ability to slow down responses to maximize reward but improved performance in response speeding (Moustafa et al., 2008). This behavior has been hypothesized to reflect a hyperactivity of the mesolimbic reward circuit under dopaminergic medication in Parkinson's disease patients with impulsive control disorders. Coherently, Parkinson's patients show increased EV signaling in the ventromedial prefrontal cortex during choices involving rewards compared to those associated with losses (Tichelaar et al., 2023). This stronger representation of the EV may also reflect a shift in decision strategy (i.e., a more multiplicative value integration). Similarly, choices of patients with Parkinson's disease have been shown to be more strongly driven by choice attributes independent of medication. In Study 2, we find a similar dopaminergic modulation of the use of choice attributes in decision making. It would be interesting to study whether Parkinson's disease does not only cause a change in risk preferences but also a broader shift in decision strategies.

Moreover, it has been shown that neuronal timescales are altered in patients with neuropsychiatric disorders such as schizophrenia or autism spectrum disorder (Watanabe et al., 2019; Wengler et al., 2020). In schizophrenia, neuronal timescales are broadly altered across the cortex compared to healthy controls, with distinct patterns associated with different symptom dimensions. More specifically, neuronal timescales are increased in primary sensory regions but decreased in higher-order association areas, resulting in a flatter hierarchical gradient across the cortex. The magnitude of this effects has been shown to correlate with the severity of hallucinations. In contrast, stronger symptoms of delusion are associated with a steeper hierarchical gradient driven by longer neuronal timescales in higher-order association regions (Wengler et al., 2020). Similarly, in autism spectrum disorder, neuronal timescales are altered in distinct cortical regions and have been shown to correlate with symptom severity. Shorter neuronal timescales in primary sensory regions, including the bilateral postcentral gyrus and right inferior occipital gyrus, are associated with overall symptom severity. Conversely, longer neuronal timescales in subcortical regions, such as the right caudate correlate with the severity of restricted

and repetitive behaviors (Watanabe et al., 2019). While the precise neurobiological causes of schizophrenia and autism remain incompletely understood, both conditions are thought to involve shifts in the E/I-balance governed by GABA and NMDA receptor activity (Gao & Penzes, 2015; Kehrer et al., 2008; Marin, 2012; Zikopoulos & Barbas, 2013). In line with this, cortical dynamics in schizophrenia show similarities to those observed in healthy participants under pharmacological manipulation of $GABA_A$ and NMDA receptor transmission. Positive symptoms more closely resemble cortical dynamics under pharmacologically increased GABAergic receptor activity. Negative symptoms correlate with dynamics under pharmacological NMDA receptor blockade (Arazi et al., 2025). These modulations in cortical activity include alterations in the aperiodic signal in patients with schizophrenia, which are normalized following pharmacological NMDA receptor blockade (Molina et al., 2020). Similar aperiodic alterations have also been found in other psychiatric disorders, including ADHD and depression (reviewed in Donoghue, 2025). Hence, a more precise understanding of neuronal dynamics including neuronal timescales shaped by the balance between glutamatergic excitation and GABAergic inhibition may improve our knowledge of the causes of distinct neuropsychiatric disorders and facilitate the development of new therapeutic strategies.

Extending this perspective to our findings in Study 3, the use of learned information in decision making has been shown to vary across psychiatric disorders. Individuals with high traits of anxiety show a greater reliance on expectations independent of the reliability of bottom-up sensory information (Kraus et al., 2021). In addition, they are impaired in updating their expectations in accordance to the environmental volatility, which has been linked to a reduced pupil dilation response to volatility (Browning et al., 2015). Since pupil diameter has been associated with locus coeruleus activity, this finding suggests a role of noradrenaline in shaping the reliance on expectations in individuals with anxiety. In our pilot data from Study 3, we found that trait anxiety was positively correlated with reliance on learned information, such that decisions of participants with higher trait anxiety were more strongly influenced by prior expectations. Moreover, higher trait anxiety was associated with increased choice switching, suggesting that these participants perceived the environment as more volatile. In the pharmacological dataset of Study 3, we were unable to replicate this finding. This may be due to the strict exclusion criteria required for pharmacological interventions. As such, participants needed to be free of neurological and psychiatric

disorders, including anxiety and depression, resulting in a restricted range of anxiety scores in our sample. For future studies, it would be interesting to clarify how anxiety modulates learning and the use of expectations and to further disentangle the involvement of the noradrenergic system.

In addition to these follow-up studies, future research should also address the limitations of the present work. Across all three studies, pharmacological interventions targeted one neurotransmitter system at a time. Consequently, our findings do not allow conclusions regarding the coordinated activity of multiple neurotransmitter systems. Although the results suggest complementary roles of different neurotransmitters, their interactions remain unclear. To this end, previous studies have shown that memory and learning deficits caused by cholinergic lesions are alleviated by reducing noradrenergic signaling (Ammassari-Teule et al., 1991; Sara et al., 1992; Yu & Dayan, 2005). These findings highlight the importance of investigating how neurotransmitter systems interact and jointly contribute to cognition. Future studies should therefore address the coordinated influence of distinct neurotransmitters on cortical dynamics which guide information integration during decision making and learning. In addition, we relied on a relatively young sample recruited from a university campus. Consequently, our findings may not generalize to older populations. In this context, it has been shown that neuronal timescales decrease with age across most cortical regions. Particularly pronounced effects are found in primary sensory and motor areas, as well as in temporal and medial frontal brain regions (Gao et al., 2020). Similarly, Study 2 and Study 3 were conducted in an exclusively male sample. Study 2 investigated reward-guided decision making and risk preferences as a function of dopamine. Previous work has demonstrated gender-specific effects of dopamine on risk preferences, suggesting that our findings may not fully generalize across sexes (Acheson & de Wit, 2008). Lastly, experimental paradigms are typically conducted in strictly controlled laboratory settings and often involve hypothetical or only very small performance-based monetary rewards. In the reward domain, this has been shown to alter decision-making behavior, leading to increased risk taking and greater choice variability (Etchart-Vincent & l'Haridon, 2011). Moreover, the ecological validity of behavior observed in artificially constructed decision-making tasks should be considered carefully (Buelow et al., 2024). This does not necessary imply a shift toward naturalistic field studies, but rather highlights the need for experimental paradigms that better approximate everyday decision making (Yartsev, 2026). As such, experimental

paradigms should move beyond discrete trial structures toward more continuous forms of decision making. This should also include more continuous response measures rather than categorical or even binary responses (Foucault et al., 2025).

4.3 Conclusion

In this dissertation, we investigated the neurochemical underpinnings of decision making with a particular focus on information integration. Across three studies, we demonstrated that distinct neurotransmitter systems play complementary roles in shaping how information is integrated and used to guide behavior. Rather than reflecting independent influences, our findings suggest that cognition emerges from the coordinated activity of different neurotransmitter systems operating across different brain regions and temporal scales.

In Study 1, we showed that $GABA_A$ receptor activity shapes cortical timescales and large-scale network dynamics at rest. This forms the basis of the temporal and spatial organization of the brain and determines how information is integration across time and distributed cortical regions. In Study 2, we investigated the role of dopamine in arbitrating between decision strategies and found a specific role in shaping the use of choice-relevant attributes during decision making. Therefore, dopamine modulated the degree by which choices were driven by the available information. In Study 3, we showed that acetylcholine and noradrenaline jointly regulated how bottom-up information is integrated with top-down beliefs during learning. Hence, acetylcholine and noradrenaline determined the dynamic reliance on existing expectations versus current information to guide learning.

Together, these findings highlight that neurotransmitter system jointly tune distinct components of neuronal processing, enabling adaptive behavior. Across all studies, pharmacological interventions enabled a causal identification of these mechanisms, providing direct evidence for the links between specific neurotransmitter systems, cognitive computations in the brain and the observed behavior. This was complemented by computational modeling which made an attribution of distinct neurochemical mechanisms to the underlying cognitive processes possible. More broadly, this work highlights the value of causal pharmacological approaches in cognitive neuroscience, enabling a mechanistic interpretation of behavior and brain activity that goes beyond correlational observations.

In conclusion, this dissertation advances our understanding of how neurotransmitter systems shape cortical dynamics, information integration and thereby decision making and learning. By linking neurochemistry, neuronal dynamics and behavior within a unified framework, this work contributes to a more integrated understanding of how the brain supports information integration at rest and during active decision making.

References

Abeysuriya, R. G., Hadida, J., Sotiropoulos, S. N., Jbabdi, S., Becker, R., Hunt, B. A. E., Brookes, M. J., & Woolrich, M. W. (2018). A biophysical model of dynamic balancing of excitation and inhibition in fast oscillatory large-scale networks. *Plos Computational Biology*, *14*(2), e1006007. https://doi.org/10.1371/journal.pcbi.1006007

Ablin, P., Cardoso, J.-F., & Gramfort, A. (2018). Faster Independent Component Analysis by preconditioning with Hessian approximations. *IEEE Transactions on Signal Processing*, *66*(15), 4040–4049. https://doi.org/10.1109/TSP.2018.2844203

Acheson, A., & de Wit, H. (2008). Bupropion improves attention but does not affect impulsive behavior in healthy young adults. *Exp Clin Psychopharmacol*, *16*(2), 113–123. https://doi.org/10.1037/1064-1297.16.2.113

Alberto, C. O., & Hirasawa, M. (2010). AMPA receptor-mediated miniature EPSCs have heterogeneous time courses in orexin neurons. *Biochem Biophys Res Commun*, *400*(4), 707–712. https://doi.org/10.1016/j.bbrc.2010.08.132

Ammassari-Teule, M., Maho, C., & Sara, S. J. (1991). Clonidine reverses spatial learning deficits and reinstates theta frequencies in rats with partial fornix section. *Behav Brain Res*, *45*(1), 1–8. https://doi.org/10.1016/s0166-4328(05)80174-3

Ananth, M. R., Rajebhosale, P., Kim, R., Talmage, D. A., & Role, L. W. (2023). Basal forebrain cholinergic signalling: development, connectivity and roles in cognition. *Nat Rev Neurosci*, *24*(4), 233–251. https://doi.org/10.1038/s41583-023-00677-x

Angulo, M. C., Rossier, J., & Audinat, E. (1999). Postsynaptic glutamate receptors and integrative properties of fast-spiking interneurons in the rat neocortex. *J Neurophysiol*, *82*(3), 1295–1302. https://doi.org/10.1152/jn.1999.82.3.1295

Arazi, A., Toso, A., Grent-'t-Jong, T., Uhlhaas, P. J., & Donner, T. H. (2025). Large-scale Dynamical Fingerprints of Distributed Synaptic Alterations in Early-Stage Psychosis. *bioRxiv*, 2024.2007.2015.603513. https://doi.org/10.1101/2024.07.15.603513

Ariwodola, O. J., & Weiner, J. L. (2004). Ethanol potentiation of GABAergic synaptic transmission may be self-limiting: role of presynaptic GABA(B) receptors. *J*

Neurosci, *24*(47), 10679–10686. https://doi.org/10.1523/JNEUROSCI.1768-04.2004

Arnsten, A. F., & Goldman-Rakic, P. S. (1985). Alpha 2-adrenergic mechanisms in prefrontal cortex associated with cognitive decline in aged nonhuman primates. *Science*, *230*(4731), 1273–1276. https://doi.org/10.1126/science.2999977

Arnsten, A. F., & Pliszka, S. R. (2011). Catecholamine influences on prefrontal cortical function: relevance to treatment of attention deficit/hyperactivity disorder and related disorders. *Pharmacol Biochem Behav*, *99*(2), 211–216. https://doi.org/10.1016/j.pbb.2011.01.020

Arrondo, G., Aznarez-Sanado, M., Fernandez-Seara, M. A., Goni, J., Loayza, F. R., Salamon-Klobut, E., Heukamp, F. H., & Pastor, M. A. (2015). Dopaminergic modulation of the trade-off between probability and time in economic decision-making. *Eur Neuropsychopharmacol*, *25*(6), 817–827. https://doi.org/10.1016/j.euroneuro.2015.02.011

Aston-Jones, G., & Bloom, F. E. (1981). Activity of norepinephrine-containing locus coeruleus neurons in behaving rats anticipates fluctuations in the sleep-waking cycle. *J Neurosci*, *1*(8), 876–886. https://doi.org/10.1523/JNEUROSCI.01-08-00876.1981

Aston-Jones, G., & Cohen, J. D. (2005). An integrative theory of locus coeruleus-norepinephrine function: adaptive gain and optimal performance. *Annu Rev Neurosci*, *28*, 403–450. https://doi.org/10.1146/annurev.neuro.28.061604.135709

Baker, A. P., Brookes, M. J., Rezek, I. A., Smith, S. M., Behrens, T., Probert Smith, P. J., & Woolrich, M. (2014). Fast transient networks in spontaneous human brain activity. *Elife*, *3*, e01867. https://doi.org/10.7554/eLife.01867

Baker, J. F., Petersen, S. E., Newsome, W. T., & Allman, J. M. (1981). Visual response properties of neurons in four extrastriate visual areas of the owl monkey (Aotus trivirgatus): a quantitative comparison of medial, dorsomedial, dorsolateral, and middle temporal areas. *J Neurophysiol*, *45*(3), 397–416. https://doi.org/10.1152/jn.1981.45.3.397

Baldassano, C., Chen, J., Zadbood, A., Pillow, J. W., Hasson, U., & Norman, K. A. (2017). Discovering Event Structure in Continuous Narrative Perception and Memory. *Neuron*, *95*(3), 709–721 e705. https://doi.org/10.1016/j.neuron.2017.06.041

Ballinger, E. C., Ananth, M., Talmage, D. A., & Role, L. W. (2016). Basal Forebrain Cholinergic Circuits and Signaling in Cognition and Cognitive Decline. *Neuron*, *91*(6), 1199–1218. https://doi.org/10.1016/j.neuron.2016.09.006

Baribault, B., & Collins, A. G. E. (2023). Troubleshooting Bayesian cognitive models. *Psychol Methods*. https://doi.org/10.1037/met0000554

Basu, S., & Suh, H. (2020). Role of Hippocampal Neurogenesis in Alcohol Withdrawal Seizures. *Brain Plast*, *6*(1), 27–39. https://doi.org/10.3233/BPL-200114

Bates, D., Kliegl, R., Vasishth, S., & Baayen, H. (2015). Parsimonious mixed models. https://arxiv.org/abs/1506.04967

Bauer, M., Kluge, C., Bach, D., Bradbury, D., Heinze, H. J., Dolan, R. J., & Driver, J. (2012). Cholinergic enhancement of visual attention and neural oscillations in

the human brain. *Curr Biol*, *22*(5), 397–402. https://doi.org/10.1016/j.cub.2012.01.022

Behrens, T. E., Woolrich, M. W., Walton, M. E., & Rushworth, M. F. (2007). Learning the value of information in an uncertain world. *Nat Neurosci*, *10*(9), 1214–1221. https://doi.org/10.1038/nn1954

Bernacchia, A., Seo, H., Lee, D., & Wang, X. J. (2011). A reservoir of time constants for memory traces in cortical neurons. *Nat Neurosci*, *14*(3), 366–372. https://doi.org/10.1038/nn.2752

Berridge, C. W. (2008). Noradrenergic modulation of arousal. *Brain Res Rev*, *58*(1), 1–17. https://doi.org/10.1016/j.brainresrev.2007.10.013

Birbaumer, N., & Schmidt, R. F. (2010). *Biologische Psychologie* (7 ed.). Springer.

Bizer, G. Y., Larsen, J. T., & Petty, R. E. (2011). Exploring the Valence-Framing Effect: Negative Framing Enhances Attitude Strength. *Political Psychology*, *32*(1), 59–80. https://doi.org/10.1111/j.1467-9221.2010.00795.x

Blatt, G. J., Andersen, R. A., & Stoner, G. R. (1990). Visual receptive field organization and cortico-cortical connections of the lateral intraparietal area (area LIP) in the macaque. *J Comp Neurol*, *299*(4), 421–445. https://doi.org/10.1002/cne.902990404

Borgstrom, L., Johansson, C. G., Larsson, H., & Lenander, R. (1981). Pharmacokinetics of propranolol. *J Pharmacokinet Biopharm*, *9*(4), 419–429. https://doi.org/10.1007/BF01060886

Boucher, P. O., Wang, T., Carceroni, L., Kane, G., Shenoy, K. V., & Chandrasekaran, C. (2022). Neural population dynamics in dorsal premotor cortex underlying a reach decision. *bioRxiv*, 2022.2006.2030.497070. https://doi.org/10.1101/2022.06.30.497070

Bouret, S., & Sara, S. J. (2005). Network reset: a simplified overarching theory of locus coeruleus noradrenaline function. *Trends Neurosci*, *28*(11), 574–582. https://doi.org/10.1016/j.tins.2005.09.002

Bowery, N. G. (2006). GABAB receptor: a site of therapeutic benefit. *Curr Opin Pharmacol*, *6*(1), 37–43. https://doi.org/10.1016/j.coph.2005.10.002

Bressler, S. L. (1995). Large-scale cortical networks and cognition. *Brain Res Brain Res Rev*, *20*(3), 288–304. https://doi.org/10.1016/0165-0173(94)00016-i

Brocks, D. R. (1999). Anticholinergic drugs used in Parkinson's disease: An overlooked class of drugs from a pharmacokinetic perspective. *J Pharm Pharm Sci*, *2*(2), 39–46.

Brown, V. A. (2021). An Introduction to Linear Mixed-Effects Modeling in R. *Advances in Methods and Practices in Psychological Science*, *4*(1). https://doi.org/10.1177/2515245920960351

Browning, M., Behrens, T. E., Jocham, G., O'Reillly, J. X., & Bishop, S. J. (2015). Anxious Individuals Have Difficulty Learning the Causal Statistics of Aversive Environments. *Biological Psychiatry*, *77*(9), 47s–48s.

Bubser, M., Byun, N., Wood, M. R., & Jones, C. K. (2012). Muscarinic receptor pharmacology and circuitry for the modulation of cognition. *Handb Exp Pharmacol*(208), 121–166. https://doi.org/10.1007/978-3-642-23274-9_7

Buelow, M. T., Okdie, B. M., & Kowalsky, J. M. (2024). Ecological validity of common behavioral decision making tasks: evidence across two samples. *J Clin Exp Neuropsychol*, *46*(3), 187–206. https://doi.org/10.1080/13803395.2024.2337759

Burke, C. J., Soutschek, A., Weber, S., Beharelle, A. R., Fehr, E., Haker, H., & Tobler, P. N. (2018). Dopamine Receptor-Specific Contributions to the Computation of Value. *Neuropsychopharmacology*, *43*(6), 1415–1424. https://doi.org/10.1038/npp.2017.302

Burt, J. B., Demirtas, M., Eckner, W. J., Navejar, N. M., Ji, J. L., Martin, W. J., Bernacchia, A., Anticevic, A., & Murray, J. D. (2018). Hierarchy of transcriptomic specialization across human cortex captured by structural neuroimaging topography. *Nat Neurosci*, *21*(9), 1251–1259. https://doi.org/10.1038/s41593-018-0195-0

Bush, A., Zou, J. F., Lipski, W. J., Kokkinos, V., & Richardson, R. M. (2024). Aperiodic components of local field potentials reflect inherent differences between cortical and subcortical activity. *Cerebral Cortex*, *34*(5). https://doi.org/10.1093/cercor/bhae186

Carlson, N. R. (2010). *Physiology of behavior / Neil R. Carlson* (10th ed.). Boston, Mass. : Pearson.

Çatal, Y., Wolman, A., Abbasi, S., & Northoff, G. (2023). Intrinsic neural timescales attenuate information transfer along the uni-transmodal hierarchy. *bioRxiv*, 2023.2007.2028.551047. https://doi.org/10.1101/2023.07.28.551047

Chakroun, K., Wiehler, A., Wagner, B., Mathar, D., Ganzer, F., van Eimeren, T., Sommer, T., & Peters, J. (2023). Dopamine regulates decision thresholds in human reinforcement learning in males. *Nat Commun*, *14*(1), 5369. https://doi.org/10.1038/s41467-023-41130-y

Chapman, C. A., Nuwer, J. L., & Jacob, T. C. (2022). The Yin and Yang of GABAergic and Glutamatergic Synaptic Plasticity: Opposites in Balance by Crosstalking Mechanisms. *Front Synaptic Neurosci*, *14*, 911020. https://doi.org/10.3389/fnsyn.2022.911020

Chaudhury, D., Escanilla, O., & Linster, C. (2009). Bulbar acetylcholine enhances neural and perceptual odor discrimination. *J Neurosci*, *29*(1), 52–60. https://doi.org/10.1523/JNEUROSCI.4036-08.2009

Cherkasova, M. V., Corrow, J. C., Taylor, A., Yeung, S. C., Stubbs, J. L., McKeown, M. J., Appel-Cresswell, S., Stoessl, A. J., & Barton, J. J. S. (2019). Dopamine replacement remediates risk aversion in Parkinson's disease in a value-independent manner. *Parkinsonism Relat Disord*, *66*, 189–194. https://doi.org/10.1016/j.parkreldis.2019.08.014

Chini, M., Pfeffer, T., Hanganu-Opatz, I., & de la Prida, L. M. (2022). An increase of inhibition drives the developmental decorrelation of neural activity. *Elife*, *11*. https://doi.org/10.7554/eLife.78811

Ciombor, K. J., Ennis, M., & Shipley, M. T. (1999). Norepinephrine increases rat mitral cell excitatory responses to weak olfactory nerve input via alpha-1 receptors in vitro. *Neuroscience*, *90*(2), 595–606. https://doi.org/10.1016/s0306-4522(98)00437-0

Clemens, S., Rye, D., & Hochman, S. (2006). Restless legs syndrome: revisiting the dopamine hypothesis from the spinal cord perspective. *Neurology*, *67*(1), 125–130. https://doi.org/10.1212/01.wnl.0000223316.53428.c9

Coghill, D. R., Seth, S., Pedroso, S., Usala, T., Currie, J., & Gagliano, A. (2014). Effects of methylphenidate on cognitive functions in children and adolescents with attention-deficit/hyperactivity disorder: evidence from a systematic review and a meta-analysis. *Biol Psychiatry*, *76*(8), 603–615. https://doi.org/10.1016/j.biopsych.2013.10.005

Cohen, M. X. (2014). *Analyzing Neural Time Series Data: Theory and Practice*. The MIT Press. https://doi.org/10.7551/mitpress/9609.001.0001

Colombi, I., Rastogi, M., Parrini, M., Alberti, M., Potenzieri, A., Chellali, M. M., Rosati, S., Chiappalone, M., Nanni, M., Contestabile, A., & Cancedda, L. (2024). Heterogeneous subpopulations of GABA(A)R-responding neurons coexist across neuronal network scales and developmental stages in health and disease. *iScience*, *27*(4), 109438. https://doi.org/10.1016/j.isci.2024.109438

Colombo, M. A., Napolitani, M., Boly, M., Gosseries, O., Casarotto, S., Rosanova, M., Brichant, J. F., Boveroux, P., Rex, S., Laureys, S., Massimini, M., Chieregato, A., & Sarasso, S. (2019). The spectral exponent of the resting EEG indexes the presence of consciousness during unresponsiveness induced by propofol, xenon, and ketamine. *Neuroimage*, *189*, 631–644. https://doi.org/10.1016/j.neuroimage.2019.01.024

Connolly, B. S., & Lang, A. E. (2014). Pharmacological Treatment of Parkinson Disease A Review. *Jama-Journal of the American Medical Association*, *311*(16), 1670–1683. https://doi.org/10.1001/jama.2014.3654

Cools, R. (2008). Role of dopamine in the motivational and cognitive control of behavior. *Neuroscientist*, *14*(4), 381–395. https://doi.org/10.1177/1073858408317009

Cools, R., Barker, R. A., Sahakian, B. J., & Robbins, T. W. (2001). Enhanced or impaired cognitive function in Parkinson's disease as a function of dopaminergic medication and task demands. *Cerebral Cortex*, *11*(12), 1136–1143. https://doi.org/10.1093/cercor/11.12.1136

Cools, R., & D'Esposito, M. (2011). Inverted-U-Shaped Dopamine Actions on Human Working Memory and Cognitive Control. *Biological Psychiatry*, *69*(12), E113–E125. https://doi.org/10.1016/j.biopsych.2011.03.028

Cubillo, A., Halari, R., Smith, A., Taylor, E., & Rubia, K. (2012). A review of fronto-striatal and fronto-cortical brain abnormalities in children and adults with Attention Deficit Hyperactivity Disorder (ADHD) and new evidence for dysfunction in adults with ADHD during motivation and attention. *Cortex*, *48*(2), 194–215. https://doi.org/10.1016/j.cortex.2011.04.007

Cusinato, R., Alnes, S. L., van Maren, E., Boccalaro, I., Ledergerber, D., Adamantidis, A., Imbach, L. L., Schindler, K., Baud, M. O., & Tzovara, A. (2023). Intrinsic Neural Timescales in the Temporal Lobe Support an Auditory Processing Hierarchy. *J Neurosci*, *43*(20), 3696–3707. https://doi.org/10.1523/JNEUROSCI.1941-22.2023

Danielmeier, C., Allen, E. A., Jocham, G., Onur, O. A., Eichele, T., & Ullsperger, M. (2015). Acetylcholine mediates behavioral and neural post-error control. *Curr Biol*, *25*(11), 1461–1468. https://doi.org/10.1016/j.cub.2015.04.022

Dayan, P., & Huys, Q. J. (2009). Serotonin in affective control. *Annu Rev Neurosci*, *32*, 95–126. https://doi.org/10.1146/annurev.neuro.051508.135607

de Lange, F. P., Heilbron, M., & Kok, P. (2018). How Do Expectations Shape Perception? *Trends in Cognitive Sciences*, *22*(9), 764–779. https://doi.org/10.1016/j.tics.2018.06.002

de Leon-Lopez, C. A. M., Carretero-Rey, M., & Khan, Z. U. (2025). AMPA Receptors in Synaptic Plasticity, Memory Function, and Brain Diseases. *Cell Mol Neurobiol*, *45*(1), 14. https://doi.org/10.1007/s10571-024-01529-7

Deco, G., & Thiele, A. (2011). Cholinergic control of cortical network interactions enables feedback-mediated attentional modulation. *Eur J Neurosci*, *34*(1), 146–157. https://doi.org/10.1111/j.1460-9568.2011.07749.x

Desikan, R. S., Segonne, F., Fischl, B., Quinn, B. T., Dickerson, B. C., Blacker, D., Buckner, R. L., Dale, A. M., Maguire, R. P., Hyman, B. T., Albert, M. S., & Killiany, R. J. (2006). An automated labeling system for subdividing the human cerebral cortex on MRI scans into gyral based regions of interest. *Neuroimage*, *31*(3), 968–980. https://doi.org/10.1016/j.neuroimage.2006.01.021

Devauges, V., & Sara, S. J. (1990). Activation of the noradrenergic system facilitates an attentional shift in the rat. *Behav Brain Res*, *39*(1), 19–28. https://doi.org/10.1016/0166-4328(90)90118-x

Devauges, V., & Sara, S. J. (1991). Memory retrieval enhancement by locus coeruleus stimulation: evidence for mediation by beta-receptors. *Behav Brain Res*, *43*(1), 93–97. https://doi.org/10.1016/s0166-4328(05)80056-7

Dias Maile, A. A., Andronova, E., Ball, F., Aravitska, D., Dannenberg, L. K., Schnitzler, A., O'Reilly, J. X., & Jocham, G. (2026). Cholinergic and noradrenergic modulation of perceptual decision making and learning. *bioRxiv*, 2026.2006.2022.732890. https://doi.org/10.64898/2026.06.22.732890

Dias Maile, A. A., Andronova, E., O'Reilly, J., & Jocham, G. (2025). *Cholinergic and noradrenergic modulation of perceptual decision making and learning*. https://osf.io/aqd2r/overview

Dias Maile, A. A., Gruendler, T. O. J., Fischer, A. G., Kurtenbach, H., Kaiser, L. F., Frobose, M. I., & Jocham, G. (2025). Bidirectional modulation of reward-guided decision making by dopamine. *Psychopharmacology (Berl)*, *242*(11), 2547–2559. https://doi.org/10.1007/s00213-025-06816-9

Dias Maile, A. A., Kohl, O., Ort, E., Froböse, M. I., Kurtenbach, H., Butz, M., Schreivogel, E., Schnitzler, A., Florin, E., & Jocham, G. (2026). Role of GABA and NMDA receptors in shaping cortical timescales and large-scale network dynamics. *bioRxiv*, 2026.2005.2011.723797. https://doi.org/10.64898/2026.05.11.723797

Ditterich, J., Mazurek, M. E., & Shadlen, M. N. (2003). Microstimulation of visual cortex affects the speed of perceptual decisions. *Nat Neurosci*, *6*(8), 891–898. https://doi.org/10.1038/nn1094

Donoghue, T. (2025). A Systematic Review of Aperiodic Neural Activity in Clinical Investigations. *Eur J Neurosci*, *62*(7), e70255. https://doi.org/10.1111/ejn.70255

Donoghue, T., Haller, M., Peterson, E. J., Varma, P., Sebastian, P., Gao, R., Noto, T., Lara, A. H., Wallis, J. D., Knight, R. T., Shestyuk, A., & Voytek, B. (2020). Parameterizing neural power spectra into periodic and aperiodic components. *Nature Neuroscience*, *23*(12), 1655–U1288. https://doi.org/10.1038/s41593-020-00744-x

Doya, K. (2002). Metalearning and neuromodulation. *Neural Netw*, *15*(4-6), 495–506. https://doi.org/10.1016/s0893-6080(02)00044-8

Dudai, A., Yayon, N., Soreq, H., & London, M. (2021). Cortical VIP(+) /ChAT(+) interneurons: From genetics to function. *J Neurochem*, *158*(6), 1320–1333. https://doi.org/10.1111/jnc.15263

Eggermann, E., & Feldmeyer, D. (2009). Cholinergic filtering in the recurrent excitatory microcircuit of cortical layer 4. *Proc Natl Acad Sci U S A*, *106*(28), 11753–11758. https://doi.org/10.1073/pnas.0810062106

Eggermann, E., Kremer, Y., Crochet, S., & Petersen, C. C. H. (2014). Cholinergic signals in mouse barrel cortex during active whisker sensing. *Cell Rep*, *9*(5), 1654–1660. https://doi.org/10.1016/j.celrep.2014.11.005

Ellis, J. M. (2005). Cholinesterase inhibitors in the treatment of dementia. *J Am Osteopath Assoc*, *105*(3), 145–158.

Erfanian Abdoust, M., Frobose, M. I., Schnitzler, A., Schreivogel, E., & Jocham, G. (2024). Dopamine and acetylcholine have distinct roles in delay- and effort-based decision-making in humans. *PLoS Biol*, *22*(7), e3002714. https://doi.org/10.1371/journal.pbio.3002714

Erskine, D., Taylor, J. P., Bakker, G., Brown, A. J. H., Tasker, T., & Nathan, P. J. (2019). Cholinergic muscarinic M(1) and M(4) receptors as therapeutic targets for cognitive, behavioural, and psychological symptoms in psychiatric and neurological disorders. *Drug Discov Today*, *24*(12), 2307–2314. https://doi.org/10.1016/j.drudis.2019.08.009

Espinosa, F., & Kavalali, E. T. (2009). NMDA receptor activation by spontaneous glutamatergic neurotransmission. *J Neurophysiol*, *101*(5), 2290–2296. https://doi.org/10.1152/jn.90754.2008

Etchart-Vincent, N., & l'Haridon, O. (2011). Monetary incentives in the loss domain and behavior toward risk: An experimental comparison of three reward schemes including real losses. *Journal of Risk and Uncertainty*, *42*(1), 61–83. https://doi.org/10.1007/s11166-010-9110-0

Evans, A. H., Strafella, A. P., Weintraub, D., & Stacy, M. (2009). Impulsive and compulsive behaviors in Parkinson's disease. *Mov Disord*, *24*(11), 1561–1570. https://doi.org/10.1002/mds.22505

Evers, E. A., Stiers, P., & Ramaekers, J. G. (2017). High reward expectancy during methylphenidate depresses the dopaminergic response to gain and loss. *Soc Cogn Affect Neurosci*, *12*(2), 311–318. https://doi.org/10.1093/scan/nsw124

Farashahi, S., Donahue, C. H., Hayden, B. Y., Lee, D., & Soltani, A. (2019). Flexible combination of reward information across primates. *Nat Hum Behav*, *3*(11), 1215–1224. https://doi.org/10.1038/s41562-019-0714-3

Figner, B., & Voelki, N. (2004). Risky Decision Making in a Computer Card Game: An Information Integration Experiment. *Pol. Psychol. Bull.*, *35*.

Findling, C., Hubert, F., International Brain, L., Acerbi, L., Benson, B., Benson, J., Birman, D., Bonacchi, N., Buchanan, E. K., Bruijns, S., Carandini, M., Catarino, J. A., Chapuis, G. A., Churchland, A. K., Dan, Y., Davatolhagh, F., DeWitt, E. E. J., Engel, T. A., Fabbri, M.,…Pouget, A. (2025). Brain-wide representations of prior information in mouse decision-making. *Nature*, *645*(8079), 192–200. https://doi.org/10.1038/s41586-025-09226-1

Fleetwood-Walker, S. M., Hope, P. J., & Mitchell, R. (1988). Antinociceptive actions of descending dopaminergic tracts on cat and rat dorsal horn somatosensory neurones. *J Physiol*, *399*, 335–348. https://doi.org/10.1113/jphysiol.1988.sp017084

Foucault, C., Weber, L. A., & Hunt, L. (2025). Environmental dynamics shape human learning: change points versus random walks. *bioRxiv*, 2025.2011.2026.690700. https://doi.org/10.1101/2025.11.26.690700

Fox, M. D., Snyder, A. Z., Vincent, J. L., Corbetta, M., Van Essen, D. C., & Raichle, M. E. (2005). The human brain is intrinsically organized into dynamic, anticorrelated functional networks. *Proc Natl Acad Sci U S A*, *102*(27), 9673–9678. https://doi.org/10.1073/pnas.0504136102

Frank, M. J. (2005). Dynamic dopamine modulation in the basal ganglia: a neurocomputational account of cognitive deficits in medicated and nonmedicated Parkinsonism. *J Cogn Neurosci*, *17*(1), 51–72. https://doi.org/10.1162/0898929052880093

Froböse, M. I., & Ort, E. (2022). *Glutamatergic And GABAergic Effects On Learning And Decision Making: A Pharmacological MEG Study With Lorazepam, D-Cycloserine And Placebo*. https://osf.io/cmyh2/overview

Gao, R., & Penzes, P. (2015). Common mechanisms of excitatory and inhibitory imbalance in schizophrenia and autism spectrum disorders. *Curr Mol Med*, *15*(2), 146–167. https://doi.org/10.2174/1566524015666150303003028

Gao, R., Peterson, E. J., & Voytek, B. (2017). Inferring synaptic excitation/inhibition balance from field potentials. *Neuroimage*, *158*, 70–78. https://doi.org/10.1016/j.neuroimage.2017.06.078

Gao, R., van den Brink, R. L., Pfeffer, T., & Voytek, B. (2020). Neuronal timescales are functionally dynamic and shaped by cortical microarchitecture. *Elife*, *9*. https://doi.org/10.7554/eLife.61277

Gelbard-Sagiv, H., Magidov, E., Sharon, H., Hendler, T., & Nir, Y. (2018). Noradrenaline Modulates Visual Perception and Late Visually Evoked Activity. *Curr Biol*, *28*(14), 2239–2249 e2236. https://doi.org/10.1016/j.cub.2018.05.051

Glimcher, P. W. (2011). Understanding dopamine and reinforcement learning: the dopamine reward prediction error hypothesis. *Proc Natl Acad Sci U S A*, *108 Suppl 3*(Suppl 3), 15647–15654. https://doi.org/10.1073/pnas.1014269108

Gohil, C., Huang, R., Roberts, E., van Es, M. W. J., Quinn, A. J., Vidaurre, D., & Woolrich, M. W. (2024). osl-dynamics, a toolbox for modeling fast dynamic brain activity. *Elife*, *12*. https://doi.org/10.7554/eLife.91949

Gohil, C., Kohl, O., Huang, R., van Es, M. W. J., Parker Jones, O., Hunt, L. T., Quinn, A. J., & Woolrich, M. W. (2024). Dynamic network analysis of electrophysiological task data. *Imaging Neurosci (Camb)*, *2*. https://doi.org/10.1162/imag_a_00226

Gold, J. I., & Shadlen, M. N. (2007). The neural basis of decision making. *Annu Rev Neurosci*, *30*, 535–574. https://doi.org/10.1146/annurev.neuro.29.051605.113038

Greenblatt, D. J., Schillings, R. T., Kyriakopoulos, A. A., Shader, R. I., Sisenwine, S. F., Knowles, J. A., & Ruelius, H. W. (1976). Clinical pharmacokinetics of lorazepam. I. Absorption and disposition of oral 14C-lorazepam. *Clin Pharmacol Ther*, *20*(3), 329–341. https://doi.org/10.1002/cpt1976203329

Grimaldi, R., Perucca, E., Ruberto, G., Gelmi, C., Trimarchi, F., Hollmann, M., & Crema, A. (1986). Pharmacokinetic and pharmacodynamic studies following the intravenous and oral administration of the antiparkinsonian drug biperiden to normal subjects. *Eur J Clin Pharmacol*, *29*(6), 735–737. https://doi.org/10.1007/BF00615970

Gupta, A., Wang, Y., & Markram, H. (2000). Organizing principles for a diversity of GABAergic interneurons and synapses in the neocortex. *Science*, *287*(5451), 273–278. https://doi.org/10.1126/science.287.5451.273

Halgren, M., Kang, R., Voytek, B., Ulbert, I., Fabo, D., Eross, L., Wittner, L., Madsen, J., Doyle, W. K., Devinsky, O., Halgren, E., Harnett, M. T., & Cash, S. S. (2021). The timescale and magnitude of 1/f aperiodic activity decrease with cortical depth in humans, macaques, and mice. *bioRxiv*, 2021.2007.2028.454235. https://doi.org/10.1101/2021.07.28.454235

Hamid, A. A., Pettibone, J. R., Mabrouk, O. S., Hetrick, V. L., Schmidt, R., Vander Weele, C. M., Kennedy, R. T., Aragona, B. J., & Berke, J. D. (2016). Mesolimbic dopamine signals the value of work. *Nat Neurosci*, *19*(1), 117–126. https://doi.org/10.1038/nn.4173

Hamidovic, A., Kang, U. J., & de Wit, H. (2008). Effects of low to moderate acute doses of pramipexole on impulsivity and cognition in healthy volunteers. *J Clin Psychopharmacol*, *28*(1), 45–51. https://doi.org/10.1097/jcp.0b013e3181602fab

Hamon-Vilcot, B., Chaufour, S., Deschamps, C., Canal, M., Zieleniuk, I., Ahtoy, P., Chretien, P., Rosenzweig, P., Nasr, A., & Piette, F. (1998). Safety and pharmacokinetics of a single oral dose of amisulpride in healthy elderly volunteers. *Eur J Clin Pharmacol*, *54*(5), 405–409. https://doi.org/10.1007/s002280050483

Hangya, B., Ranade, S. P., Lorenc, M., & Kepecs, A. (2015). Central Cholinergic Neurons Are Rapidly Recruited by Reinforcement Feedback. *Cell*, *162*(5), 1155–1168. https://doi.org/10.1016/j.cell.2015.07.057

Hanks, T. D., Mazurek, M. E., Kiani, R., Hopp, E., & Shadlen, M. N. (2011). Elapsed decision time affects the weighting of prior probability in a perceptual decision task. *J Neurosci*, *31*(17), 6339–6352. https://doi.org/10.1523/JNEUROSCI.5613-10.2011

Hanks, T. D., & Summerfield, C. (2017). Perceptual Decision Making in Rodents, Monkeys, and Humans. *Neuron*, *93*(1), 15–31. https://doi.org/10.1016/j.neuron.2016.12.003

Hansen, J. Y., Shafiei, G., Markello, R. D., Smart, K., Cox, S. M. L., Norgaard, M., Beliveau, V., Wu, Y., Gallezot, J. D., Aumont, E., Servaes, S., Scala, S. G., DuBois, J. M., Wainstein, G., Bezgin, G., Funck, T., Schmitz, T. W., Spreng, R.

N., Galovic, M.,…Misic, B. (2022). Mapping neurotransmitter systems to the structural and functional organization of the human neocortex. *Nat Neurosci*, *25*(11), 1569–1581. https://doi.org/10.1038/s41593-022-01186-3

Hari, M., PhD, Riitta, & Puce, P., Aina. (2017). *MEG-EEG Primer*. Oxford University Press. https://doi.org/10.1093/med/9780190497774.001.0001

Harrison, X. A., Donaldson, L., Correa-Cano, M. E., Evans, J., Fisher, D. N., Goodwin, C. E. D., Robinson, B. S., Hodgson, D. J., & Inger, R. (2018). A brief introduction to mixed effects modelling and multi-model inference in ecology. *PeerJ*, *6*, e4794. https://doi.org/10.7717/peerj.4794

Hasselmo, M. E., Linster, C., Patil, M., Ma, D., & Cekic, M. (1997). Noradrenergic suppression of synaptic transmission may influence cortical signal-to-noise ratio. *J Neurophysiol*, *77*(6), 3326–3339. https://doi.org/10.1152/jn.1997.77.6.3326

Hasselmo, M. E., Wyble, B. P., & Wallenstein, G. V. (1996). Encoding and retrieval of episodic memories: role of cholinergic and GABAergic modulation in the hippocampus. *Hippocampus*, *6*(6), 693–708. https://doi.org/10.1002/(SICI)1098-1063(1996)6:6<693::AID-HIPO12>3.0.CO;2-W

He, W., Donoghue, T., Sowman, P. F., Seymour, R. A., Brock, J., Crain, S., Voytek, B., & Hillebrand, A. (2019). Co-Increasing Neuronal Noise and Beta Power in the Developing Brain. *bioRxiv*, 839258. https://doi.org/10.1101/839258

Heishman, S. J., Kleykamp, B. A., & Singleton, E. G. (2010). Meta-analysis of the acute effects of nicotine and smoking on human performance. *Psychopharmacology (Berl)*, *210*(4), 453–469. https://doi.org/10.1007/s00213-010-1848-1

Helson, P., Lundqvist, D., Svenningsson, P., Vinding, M. C., & Kumar, A. (2023). Cortex-wide topography of 1/f-exponent in Parkinson's disease. *NPJ Parkinsons Dis*, *9*(1), 109. https://doi.org/10.1038/s41531-023-00553-6

Herrero, J. L., Gieselmann, M. A., & Thiele, A. (2017). Muscarinic and Nicotinic Contribution to Contrast Sensitivity of Macaque Area V1 Neurons. *Front Neural Circuits*, *11*, 106. https://doi.org/10.3389/fncir.2017.00106

Herrero, J. L., Roberts, M. J., Delicato, L. S., Gieselmann, M. A., Dayan, P., & Thiele, A. (2008). Acetylcholine contributes through muscarinic receptors to attentional modulation in V1. *Nature*, *454*(7208), 1110–1114. https://doi.org/10.1038/nature07141

Higley, M. J., Gittis, A. H., Oldenburg, I. A., Balthasar, N., Seal, R. P., Edwards, R. H., Lowell, B. B., Kreitzer, A. C., & Sabatini, B. L. (2011). Cholinergic interneurons mediate fast VGluT3-dependent glutamatergic transmission in the striatum. *Plos One*, *6*(4), e19155. https://doi.org/10.1371/journal.pone.0019155

Hillebrand, A., & Barnes, G. R. (2002). A quantitative assessment of the sensitivity of whole-head MEG to activity in the adult human cortex. *Neuroimage*, *16*(3 Pt 1), 638–650. https://doi.org/10.1006/nimg.2002.1102

Honey, C. J., Thesen, T., Donner, T. H., Silbert, L. J., Carlson, C. E., Devinsky, O., Doyle, W. K., Rubin, N., Heeger, D. J., & Hasson, U. (2012). Slow cortical dynamics and the accumulation of information over long timescales. *Neuron*, *76*(2), 423–434. https://doi.org/10.1016/j.neuron.2012.08.011

Isaacson, J. S., & Scanziani, M. (2011). How inhibition shapes cortical activity. *Neuron*, *72*(2), 231–243. https://doi.org/10.1016/j.neuron.2011.09.027

Ito, T., Hearne, L. J., & Cole, M. W. (2020). A cortical hierarchy of localized and distributed processes revealed via dissociation of task activations, connectivity changes, and intrinsic timescales. *Neuroimage*, *221*, 117141. https://doi.org/10.1016/j.neuroimage.2020.117141

Iversen, P., Leslie, Iversen, P., Susan, Bloom, M., Floyd E, & Roth, P., Robert H. (2009). *Introduction to Neuropsychopharmacology*. Oxford University Press. https://doi.org/10.1093/med/9780195380538.001.0001

Jaeger, T. F. (2008). Categorical Data Analysis: Away from ANOVAs (transformation or not) and towards Logit Mixed Models. *J Mem Lang*, *59*(4), 434–446. https://doi.org/10.1016/j.jml.2007.11.007

Jami, S. A., Wilkinson, B. J., Guglietta, R., Hartel, N., Babiec, W. E., Graham, N. A., Coba, M. P., & O'Dell, T. J. (2023). Functional and phosphoproteomic analysis of beta-adrenergic receptor signaling at excitatory synapses in the CA1 region of the ventral hippocampus. *Sci Rep*, *13*(1), 7493. https://doi.org/10.1038/s41598-023-34401-7

Jimenez-Martin, J., Potapov, D., Potapov, K., Knopfel, T., & Empson, R. M. (2021). Cholinergic modulation of sensory processing in awake mouse cortex. *Sci Rep*, *11*(1), 17525. https://doi.org/10.1038/s41598-021-96696-8

Jocham, G., Furlong, P. M., Kroger, I. L., Kahn, M. C., Hunt, L. T., & Behrens, T. E. (2014). Dissociable contributions of ventromedial prefrontal and posterior parietal cortex to value-guided choice. *Neuroimage*, *100*, 498–506. https://doi.org/10.1016/j.neuroimage.2014.06.005

Jocham, G., Hunt, L. T., Near, J., & Behrens, T. E. (2012). A mechanism for value-guided choice based on the excitation-inhibition balance in prefrontal cortex. *Nat Neurosci*, *15*(7), 960–961. https://doi.org/10.1038/nn.3140

Kaiser, L. F., Gruendler, T. O. J., Speck, O., Luettgau, L., & Jocham, G. (2021). Dissociable roles of cortical excitation-inhibition balance during patch-leaving versus value-guided decisions. *Nat Commun*, *12*(1), 904. https://doi.org/10.1038/s41467-020-20875-w

Kalam, M. N., Rasool, M. F., Rehman, A. U., & Ahmed, N. (2020). Clinical Pharmacokinetics of Propranolol Hydrochloride: A Review. *Curr Drug Metab*, *21*(2), 89–105. https://doi.org/10.2174/1389200221666200414094644

Kasamatsu, T., & Heggelund, P. (1982). Single cell responses in cat visual cortex to visual stimulation during iontophoresis of noradrenaline. *Exp Brain Res*, *45*(3), 317–327. https://doi.org/10.1007/BF01208591

Kehrer, C., Maziashvili, N., Dugladze, T., & Gloveli, T. (2008). Altered Excitatory-Inhibitory Balance in the NMDA-Hypofunction Model of Schizophrenia. *Front Mol Neurosci*, *1*, 6. https://doi.org/10.3389/neuro.02.006.2008

Kish, S. J., Shannak, K., & Hornykiewicz, O. (1988). Uneven pattern of dopamine loss in the striatum of patients with idiopathic Parkinson's disease. Pathophysiologic and clinical implications. *N Engl J Med*, *318*(14), 876–880. https://doi.org/10.1056/NEJM198804073181402

Klein, M. O., Battagello, D. S., Cardoso, A. R., Hauser, D. N., Bittencourt, J. C., & Correa, R. G. (2019). Dopamine: Functions, Signaling, and Association with

Neurological Diseases. *Cell Mol Neurobiol*, *39*(1), 31–59. https://doi.org/10.1007/s10571-018-0632-3

Kobayashi, S., Asano, K., Matsuda, N., & Ugawa, Y. (2019). Dopaminergic influences on risk preferences of Parkinson's disease patients. *Cogn Affect Behav Neurosci*, *19*(1), 88–97. https://doi.org/10.3758/s13415-018-00646-3

Kok, P., Brouwer, G. J., van Gerven, M. A., & de Lange, F. P. (2013). Prior expectations bias sensory representations in visual cortex. *J Neurosci*, *33*(41), 16275–16284. https://doi.org/10.1523/JNEUROSCI.0742-13.2013

Kossl, M., & Vater, M. (1989). Noradrenaline enhances temporal auditory contrast and neuronal timing precision in the cochlear nucleus of the mustached bat. *J Neurosci*, *9*(12), 4169–4178. https://doi.org/10.1523/JNEUROSCI.09-12-04169.1989

Kraus, N., Niedeggen, M., & Hesselmann, G. (2021). Trait anxiety is linked to increased usage of priors in a perceptual decision making task. *Cognition*, *206*. https://doi.org/10.1016/j.cognition.2020.104474

Kroeger, D., Ferrari, L. L., Petit, G., Mahoney, C. E., Fuller, P. M., Arrigoni, E., & Scammell, T. E. (2017). Cholinergic, Glutamatergic, and GABAergic Neurons of the Pedunculopontine Tegmental Nucleus Have Distinct Effects on Sleep/Wake Behavior in Mice. *J Neurosci*, *37*(5), 1352–1366. https://doi.org/10.1523/JNEUROSCI.1405-16.2016

Kuchibhotla, K. V., Gill, J. V., Lindsay, G. W., Papadoyannis, E. S., Field, R. E., Sten, T. A., Miller, K. D., & Froemke, R. C. (2017). Parallel processing by cortical inhibition enables context-dependent behavior. *Nat Neurosci*, *20*(1), 62–71. https://doi.org/10.1038/nn.4436

Kurtenbach, H., Froböse, M. I., Ort, E., Bahners, B., Butz, M., Schnitzler, A., Hirschmann, J., & Jocham, G. (2026). Cholinergic modulation of reinforcement learning and prefrontal value computations under uncertainty. *bioRxiv*, 2024.2009.2020.614105. https://doi.org/10.1101/2024.09.20.614105

la Fougere, C., Grant, S., Kostikov, A., Schirrmacher, R., Gravel, P., Schipper, H. M., Reader, A., Evans, A., & Thiel, A. (2011). Where in-vivo imaging meets cytoarchitectonics: the relationship between cortical thickness and neuronal density measured with high-resolution [18F]flumazenil-PET. *Neuroimage*, *56*(3), 951–960. https://doi.org/10.1016/j.neuroimage.2010.11.015

Lam, N. H., Borduqui, T., Hallak, J., Roque, A., Anticevic, A., Krystal, J. H., Wang, X. J., & Murray, J. D. (2022). Effects of Altered Excitation-Inhibition Balance on Decision Making in a Cortical Circuit Model. *J Neurosci*, *42*(6), 1035–1053. https://doi.org/10.1523/JNEUROSCI.1371-20.2021

Larsen, M. E., Buonarati, O. R., Qian, H., Hell, J. W., & Bayer, K. U. (2023). Stimulating beta-adrenergic receptors promotes synaptic potentiation by switching CaMKII movement from LTD to LTP mode. *J Biol Chem*, *299*(6), 104706. https://doi.org/10.1016/j.jbc.2023.104706

Latif, S., Jahangeer, M., Maknoon Razia, D., Ashiq, M., Ghaffar, A., Akram, M., El Allam, A., Bouyahya, A., Garipova, L., Ali Shariati, M., Thiruvengadam, M., & Azam Ansari, M. (2021). Dopamine in Parkinson's disease. *Clin Chim Acta*, *522*, 114–126. https://doi.org/10.1016/j.cca.2021.08.009

Lawson, R. P., Bisby, J., Nord, C. L., Burgess, N., & Rees, G. (2021). The Computational, Pharmacological, and Physiological Determinants of Sensory Learning under Uncertainty. *Curr Biol*, *31*(1), 163–172 e164. https://doi.org/10.1016/j.cub.2020.10.043

Leach, N. D., Nodal, F. R., Cordery, P. M., King, A. J., & Bajo, V. M. (2013). Cortical cholinergic input is required for normal auditory perception and experience-dependent plasticity in adult ferrets. *J Neurosci*, *33*(15), 6659–6671. https://doi.org/10.1523/JNEUROSCI.5039-12.2013

Lendner, J. D., Lin, J. J., Larsson, P. G., & Helfrich, R. F. (2024). Multiple Intrinsic Timescales Govern Distinct Brain States in Human Sleep. *J Neurosci*, *44*(42). https://doi.org/10.1523/JNEUROSCI.0171-24.2024

Lendner, J. D., Niethard, N., Mander, B. A., van Schalkwijk, F. J., Schuh-Hofer, S., Schmidt, H., Knight, R. T., Born, J., Walker, M. P., Lin, J. J., & Helfrich, R. F. (2023). Human REM sleep recalibrates neural activity in support of memory formation. *Sci Adv*, *9*(34), eadj1895. https://doi.org/10.1126/sciadv.adj1895

Leng, X., Yee, D., Ritz, H., & Shenhav, A. (2021). Dissociable influences of reward and punishment on adaptive cognitive control. *Plos Computational Biology*, *17*(12), e1009737. https://doi.org/10.1371/journal.pcbi.1009737

Lerner, Y., Honey, C. J., Silbert, L. J., & Hasson, U. (2011). Topographic mapping of a hierarchy of temporal receptive windows using a narrated story. *J Neurosci*, *31*(8), 2906–2915. https://doi.org/10.1523/JNEUROSCI.3684-10.2011

Levey, A. I., Kitt, C. A., Simonds, W. F., Price, D. L., & Brann, M. R. (1991). Identification and localization of muscarinic acetylcholine receptor proteins in brain with subtype-specific antibodies. *J Neurosci*, *11*(10), 3218–3226. https://doi.org/10.1523/JNEUROSCI.11-10-03218.1991

Li, B. M., & Mei, Z. T. (1994). Delayed-response deficit induced by local injection of the alpha 2-adrenergic antagonist yohimbine into the dorsolateral prefrontal cortex in young adult monkeys. *Behav Neural Biol*, *62*(2), 134–139. https://doi.org/10.1016/s0163-1047(05)80034-2

Littleton, J. (1998). Neurochemical mechanisms underlying alcohol withdrawal. *Alcohol Health Res World*, *22*(1), 13–24.

Liu, T. S., & Pleskac, T. J. (2011). Neural correlates of evidence accumulation in a perceptual decision task. *Journal of Neurophysiology*, *106*(5), 2383–2398. https://doi.org/10.1152/jn.00413.2011

Loughnane, G. M., Brosnan, M. B., Barnes, J. J. M., Dean, A., Nandam, S. L., O'Connell, R. G., & Bellgrove, M. A. (2019). Catecholamine Modulation of Evidence Accumulation during Perceptual Decision Formation: A Randomized Trial. *J Cogn Neurosci*, *31*(7), 1044–1053. https://doi.org/10.1162/jocn_a_01393

Lowe, A. T., Petzka, M., Tzegka, M. M., & Schuck, N. W. (2025). N2 sleep promotes the occurrence of 'aha' moments in a perceptual insight task. *PLoS Biol*, *23*(6), e3003185. https://doi.org/10.1371/journal.pbio.3003185

Lowenthal, D. T. (1984). The clinical pharmacology of beta-adrenergic blockers. *Cardiovasc Clin*, *14*(3), 61–71.

Luck, S. J. (2005). *An Introduction to the Event-Related Potential Technique*. MIT Press.

Lynch, J. C., Graybiel, A. M., & Lobeck, L. J. (1985). The differential projection of two cytoarchitectonic subregions of the inferior parietal lobule of macaque upon the deep layers of the superior colliculus. *J Comp Neurol*, *235*(2), 241–254. https://doi.org/10.1002/cne.902350207

Malmivuo, J., Suihko, V., & Eskola, H. (1997). Sensitivity distributions of EEG and MEG measurements. *IEEE Trans Biomed Eng*, *44*(3), 196–208. https://doi.org/10.1109/10.554766

Manea, A. M. G., Maisson, D. J., Voloh, B., Zilverstand, A., Hayden, B., & Zimmermann, J. (2024). Neural timescales reflect behavioral demands in freely moving rhesus macaques. *Nat Commun*, *15*(1), 2151. https://doi.org/10.1038/s41467-024-46488-1

Manea, A. M. G., Zilverstand, A., Hayden, B., & Zimmermann, J. (2023). Neural timescales reflect behavioral demands in freely moving rhesus macaques. *bioRxiv*, 2023.2003.2027.534470. https://doi.org/10.1101/2023.03.27.534470

Manunta, Y., & Edeline, J. M. (1997). Effects of noradrenaline on frequency tuning of rat auditory cortex neurons. *Eur J Neurosci*, *9*(4), 833–847. https://doi.org/10.1111/j.1460-9568.1997.tb01433.x

Manunta, Y., & Edeline, J. M. (2004). Noradrenergic induction of selective plasticity in the frequency tuning of auditory cortex neurons. *J Neurophysiol*, *92*(3), 1445–1463. https://doi.org/10.1152/jn.00079.2004

Marin, O. (2012). Interneuron dysfunction in psychiatric disorders. *Nat Rev Neurosci*, *13*(2), 107–120. https://doi.org/10.1038/nrn3155

Marshall, L., Mathys, C., Ruge, D., de Berker, A. O., Dayan, P., Stephan, K. E., & Bestmann, S. (2016). Pharmacological Fingerprints of Contextual Uncertainty. *PLoS Biol*, *14*(11), e1002575. https://doi.org/10.1371/journal.pbio.1002575

Marshall, T. R., Ruesseler, M., Hunt, L. T., & O'Reilly, J. X. (2024). The representation of priors and decisions in the human parietal cortex. *PLoS Biol*, *22*(1), e3002383. https://doi.org/10.1371/journal.pbio.3002383

Maunsell, J. H., & Van Essen, D. C. (1983). Functional properties of neurons in middle temporal visual area of the macaque monkey. I. Selectivity for stimulus direction, speed, and orientation. *J Neurophysiol*, *49*(5), 1127–1147. https://doi.org/10.1152/jn.1983.49.5.1127

McIntosh, A. R. (2000). Towards a network theory of cognition. *Neural Netw*, *13*(8-9), 861–870. https://doi.org/10.1016/s0893-6080(00)00059-9

McKeage, K., & Plosker, G. L. (2004). Amisulpride: a review of its use in the management of schizophrenia. *CNS Drugs*, *18*(13), 933–956. https://doi.org/10.2165/00023210-200418130-00007

McLean, J., & Waterhouse, B. D. (1994). Noradrenergic modulation of cat area 17 neuronal responses to moving visual stimuli. *Brain Res*, *667*(1), 83–97. https://doi.org/10.1016/0006-8993(94)91716-7

Meir, I., Katz, Y., & Lampl, I. (2018). Membrane Potential Correlates of Network Decorrelation and Improved SNR by Cholinergic Activation in the Somatosensory Cortex. *J Neurosci*, *38*(50), 10692–10708. https://doi.org/10.1523/JNEUROSCI.1159-18.2018

Mesulam, M. M. (1998). From sensation to cognition. *Brain*, *121 (Pt 6)*, 1013–1052. https://doi.org/10.1093/brain/121.6.1013

Miederer, I., Buchholz, H. G., Rademacher, L., Eckart, C., Kraft, D., Piel, M., Fiebach, C. J., & Schreckenberger, M. (2025). Dopaminergic Mechanisms of Cognitive Flexibility: An [(18)F]Fallypride PET Study. *J Nucl Med*, *66*(3), 405–409. https://doi.org/10.2967/jnumed.124.268317

Mishra, W., Kheradpezhouh, E., & Arabzadeh, E. (2024). Activation of M1 cholinergic receptors in mouse somatosensory cortex enhances information processing and detection behaviour. *Commun Biol*, *7*(1), 3. https://doi.org/10.1038/s42003-023-05699-w

Mitsushima, D., Sano, A., & Takahashi, T. (2013). A cholinergic trigger drives learning-induced plasticity at hippocampal synapses. *Nat Commun*, *4*, 2760. https://doi.org/10.1038/ncomms3760

Molina, J. A., Sainz-Artiga, M. J., Fraile, A., Jimenez-Jimenez, F. J., Villanueva, C., Orti-Pareja, M., & Bermejo, F. (2000). Pathologic gambling in Parkinson's disease: a behavioral manifestation of pharmacologic treatment? *Mov Disord*, *15*(5), 869–872. https://doi.org/10.1002/1531-8257(200009)15:5<869::aid-mds1016>3.0.co;2-i

Molina, J. L., Voytek, B., Thomas, M. L., Joshi, Y. B., Bhakta, S. G., Talledo, J. A., Swerdlow, N. R., & Light, G. A. (2020). Memantine Effects on Electroencephalographic Measures of Putative Excitatory/Inhibitory Balance in Schizophrenia. *Biol Psychiatry Cogn Neurosci Neuroimaging*, *5*(6), 562–568. https://doi.org/10.1016/j.bpsc.2020.02.004

Moore, R. Y., & Bloom, F. E. (1979). Central catecholamine neuron systems: anatomy and physiology of the norepinephrine and epinephrine systems. *Annu Rev Neurosci*, *2*, 113–168. https://doi.org/10.1146/annurev.ne.02.030179.000553

Moustafa, A. A., Cohen, M. X., Sherman, S. J., & Frank, M. J. (2008). A role for dopamine in temporal decision making and reward maximization in parkinsonism. *J Neurosci*, *28*(47), 12294–12304. https://doi.org/10.1523/JNEUROSCI.3116-08.2008

Murray, J. D., Bernacchia, A., Freedman, D. J., Romo, R., Wallis, J. D., Cai, X., Padoa-Schioppa, C., Pasternak, T., Seo, H., Lee, D., & Wang, X. J. (2014). A hierarchy of intrinsic timescales across primate cortex. *Nat Neurosci*, *17*(12), 1661–1663. https://doi.org/10.1038/nn.3862

Myme, C. I., Sugino, K., Turrigiano, G. G., & Nelson, S. B. (2003). The NMDA-to-AMPA ratio at synapses onto layer 2/3 pyramidal neurons is conserved across prefrontal and visual cortices. *J Neurophysiol*, *90*(2), 771–779. https://doi.org/10.1152/jn.00070.2003

Nagatsua, T., & Sawadab, M. (2009). L-dopa therapy for Parkinson's disease: past, present, and future. *Parkinsonism Relat Disord*, *15 Suppl 1*, S3–8. https://doi.org/10.1016/S1353-8020(09)70004-5

Neumann, J. v., & Morgenstern, O. (1944). Theory of games and economic behavior. In: Princeton university press Princeton.

Norgaard, M., Beliveau, V., Ganz, M., Svarer, C., Pinborg, L. H., Keller, S. H., Jensen, P. S., Greve, D. N., & Knudsen, G. M. (2021). A high-resolution in vivo atlas of

the human brain's benzodiazepine binding site of GABA(A) receptors. *Neuroimage*, *232*, 117878. https://doi.org/10.1016/j.neuroimage.2021.117878

Nuiten, S. A., de Gee, J. W., Zantvoord, J. B., Fahrenfort, J. J., & van Gaal, S. (2023). Catecholaminergic neuromodulation and selective attention jointly shape perceptual decision-making. *Elife*, *12*. https://doi.org/10.7554/eLife.87022

Nuiten, S. A., De Gee, J. W., Zantvoord, J. B., Fahrenfort, J. J., & van Gaal, S. (2024). Pharmacological elevation of catecholamine levels improves perceptual decisions, but not metacognitive insight. *Eneuro*. https://doi.org/10.1523/ENEURO.0019-24.2024

Nutt, D., Wilson, S., Lingford-Hughes, A., Myers, J., Papadopoulos, A., & Muthukumaraswamy, S. (2015). Differences between magnetoencephalographic (MEG) spectral profiles of drugs acting on GABA at synaptic and extrasynaptic sites: a study in healthy volunteers. *Neuropharmacology*, *88*, 155–163. https://doi.org/10.1016/j.neuropharm.2014.08.017

O'Connell, R. G., Dockree, P. M., & Kelly, S. P. (2012). A supramodal accumulation-to-bound signal that determines perceptual decisions in humans. *Nat Neurosci*, *15*(12), 1729–1735. https://doi.org/10.1038/nn.3248

Ojala, K. E., Janssen, L. K., Hashemi, M. M., Timmer, M. H. M., Geurts, D. E. M., ter Huurne, N. P., Cools, R., & Sescousse, G. (2018). Dopaminergic Drug Effects on Probability Weighting during Risky Decision Making. *Eneuro*, *5*(2). https://doi.org/10.1523/ENEURO.0330-18.2018

Paoletti, P., & Neyton, J. (2007). NMDA receptor subunits: function and pharmacology. *Curr Opin Pharmacol*, *7*(1), 39–47. https://doi.org/10.1016/j.coph.2006.08.011

Pare, M., & Wurtz, R. H. (1997). Monkey posterior parietal cortex neurons antidromically activated from superior colliculus. *J Neurophysiol*, *78*(6), 3493–3497. https://doi.org/10.1152/jn.1997.78.6.3493

Pascoa Dos Santos, F., & Verschure, P. (2025). Metastable dynamics emerge from local excitatory-inhibitory homeostasis in the cortex at rest. *Netw Neurosci*, *9*(3), 938–968. https://doi.org/10.1162/netn_a_00460

Pasquini, J., Brooks, D. J., & Pavese, N. (2025). The involvement of the cholinergic system in Parkinson disease. *Handb Clin Neurol*, *211*, 215–229. https://doi.org/10.1016/B978-0-443-19088-9.00001-9

Patel, B., Bright, D. P., Mortensen, M., Frolund, B., & Smart, T. G. (2016). Context-Dependent Modulation of GABAAR-Mediated Tonic Currents. *J Neurosci*, *36*(2), 607–621. https://doi.org/10.1523/JNEUROSCI.2047-15.2016

Patel, D. S., Sharma, N., Patel, M. C., Patel, B. N., Shrivastav, P. S., & Sanyal, M. (2011). Development and validation of a selective and sensitive LC-MS/MS method for determination of cycloserine in human plasma: application to bioequivalence study. *J Chromatogr B Analyt Technol Biomed Life Sci*, *879*(23), 2265–2273. https://doi.org/10.1016/j.jchromb.2011.06.011

Perry, E. K., Perry, R. H., Blessed, G., & Tomlinson, B. E. (1978). Changes in brain cholinesterases in senile dementia of Alzheimer type. *Neuropathol Appl Neurobiol*, *4*(4), 273–277. https://doi.org/10.1111/j.1365-2990.1978.tb00545.x

Peters, J., Vega, T., Weinstein, D., Mitchell, J., & Kayser, A. (2020). Dopamine and Risky Decision-Making in Gambling Disorder. *Eneuro*, *7*(3). https://doi.org/10.1523/ENEURO.0461-19.2020

Petzold, J., Kienast, A., Lee, Y., Pooseh, S., London, E. D., Goschkes, T., & Smolka, M. N. (2019). Baseline impulsivity may moderate L-DOPA effects on value-based decision-making. *Scientific Reports*, *9*. https://doi.org/10.1038/s41598-019-42124-x

Pfister, H., Kaynig, V., Botha, C. P., Bruckner, S., Dercksen, V. J., Hege, H.-C., & Roerdink, J. B. T. M. (2014). Visualization in Connectomics. In C. D. Hansen, M. Chen, C. R. Johnson, A. E. Kaufman, & H. Hagen (Eds.), *Scientific Visualization: Uncertainty, Multifield, Biomedical, and Scalable Visualization* (pp. 221–245). Springer London. https://doi.org/10.1007/978-1-4471-6497-5_21

Pinheiro, P., & Mulle, C. (2006). Kainate receptors. *Cell Tissue Res*, *326*(2), 457–482. https://doi.org/10.1007/s00441-006-0265-6

Pinto, L., Goard, M. J., Estandian, D., Xu, M., Kwan, A. C., Lee, S. H., Harrison, T. C., Feng, G., & Dan, Y. (2013). Fast modulation of visual perception by basal forebrain cholinergic neurons. *Nat Neurosci*, *16*(12), 1857–1863. https://doi.org/10.1038/nn.3552

Piray, P., & Daw, N. D. (2021). A model for learning based on the joint estimation of stochasticity and volatility. *Nat Commun*, *12*(1), 6587. https://doi.org/10.1038/s41467-021-26731-9

Platt, M. L., & Glimcher, P. W. (1999). Neural correlates of decision variables in parietal cortex. *Nature*, *400*(6741), 233–238. https://doi.org/10.1038/22268

Quinn, A. J., Vidaurre, D., Abeysuriya, R., Becker, R., Nobre, A. C., & Woolrich, M. W. (2018). Task-Evoked Dynamic Network Analysis Through Hidden Markov Modeling. *Frontiers in Neuroscience*, *12*. https://doi.org/10.3389/fnins.2018.00603

Rangel, A., Camerer, C., & Montague, P. R. (2008). A framework for studying the neurobiology of value-based decision making. *Nat Rev Neurosci*, *9*(7), 545–556. https://doi.org/10.1038/nrn2357

Ratcliff, R. (1978). Theory of Memory Retrieval. *Psychological Review*, *85*(2), 59–108. https://doi.org/10.1037//0033-295x.85.2.59

Reiner, A., & Levitz, J. (2018). Glutamatergic Signaling in the Central Nervous System: Ionotropic and Metabotropic Receptors in Concert. *Neuron*, *98*(6), 1080–1098. https://doi.org/10.1016/j.neuron.2018.05.018

Rescorla, R. A., & Wagner, A. R. (1972). A theory of Pavlovian conditioning: Variations in the effectiveness of reinforcement and non-reinforcement. In *Classical conditioning II: Current research and theory* (pp. 64–69). Appleton-Century-Crofts.

Rigoli, F., Rutledge, R. B., Chew, B., Ousdal, O. T., Dayan, P., & Dolan, R. J. (2016). Dopamine Increases a Value-Independent Gambling Propensity. *Neuropsychopharmacology*, *41*(11), 2658–2667. https://doi.org/10.1038/npp.2016.68

Riss, J., Cloyd, J., Gates, J., & Collins, S. (2008). Benzodiazepines in epilepsy: pharmacology and pharmacokinetics. *Acta Neurol Scand*, *118*(2), 69–86. https://doi.org/10.1111/j.1600-0404.2008.01004.x

Roitman, J. D., & Shadlen, M. N. (2002). Response of neurons in the lateral intraparietal area during a combined visual discrimination reaction time task. *J Neurosci*, *22*(21), 9475–9489. https://doi.org/10.1523/JNEUROSCI.22-21-09475.2002

Rokem, A., & Silver, M. A. (2010). Cholinergic enhancement augments magnitude and specificity of visual perceptual learning in healthy humans. *Curr Biol*, *20*(19), 1723–1728. https://doi.org/10.1016/j.cub.2010.08.027

Rokem, A., & Silver, M. A. (2013). The benefits of cholinergic enhancement during perceptual learning are long-lasting. *Front Comput Neurosci*, *7*, 66. https://doi.org/10.3389/fncom.2013.00066

Roland, J. J., Stewart, A. L., Janke, K. L., Gielow, M. R., Kostek, J. A., Savage, L. M., Servatius, R. J., & Pang, K. C. (2014). Medial septum-diagonal band of Broca (MSDB) GABAergic regulation of hippocampal acetylcholine efflux is dependent on cognitive demands. *J Neurosci*, *34*(2), 506–514. https://doi.org/10.1523/JNEUROSCI.2352-13.2014

Rolls, E. T., McCabe, C., & Redoute, J. (2008). Expected value, reward outcome, and temporal difference error representations in a probabilistic decision task. *Cerebral Cortex*, *18*(3), 652–663. https://doi.org/10.1093/cercor/bhm097

Rossi, C., Vidaurre, D., Costers, L., Akbarian, F., Woolrich, M., Nagels, G., & Van Schependom, J. (2023). A data-driven network decomposition of the temporal, spatial, and spectral dynamics underpinning visual-verbal working memory processes. *Commun Biol*, *6*(1), 1079. https://doi.org/10.1038/s42003-023-05448-z

Rossi, C., Vidaurre, D., Costers, L., D'Hooghe M, B., Akbarian, F., D'Haeseleer, M., Woolrich, M., Nagels, G., & Van Schependom, J. (2024). Disrupted working memory event-related network dynamics in multiple sclerosis. *Commun Biol*, *7*(1), 1592. https://doi.org/10.1038/s42003-024-07283-2

Routley, B. C., Singh, K. D., Hamandi, K., & Muthukumaraswamy, S. D. (2017). The effects of AMPA receptor blockade on resting magnetoencephalography recordings. *J Psychopharmacol*, *31*(12), 1527–1536. https://doi.org/10.1177/0269881117736915

Rudolph, U., & Knoflach, F. (2011). Beyond classical benzodiazepines: novel therapeutic potential of GABAA receptor subtypes. *Nat Rev Drug Discov*, *10*(9), 685–697. https://doi.org/10.1038/nrd3502

Ruggeri, K., Ali, S., Berge, M. L., Bertoldo, G., Bjorndal, L. D., Cortijos-Bernabeu, A., Davison, C., Demic, E., Esteban-Serna, C., Friedemann, M., Gibson, S. P., Jarke, H., Karakasheva, R., Khorrami, P. R., Kveder, J., Andersen, T. L., Lofthus, I. S., McGill, L., Nieto, A. E.,…Folke, T. (2020). Replicating patterns of prospect theory for decision under risk. *Nat Hum Behav*, *4*(6), 622–633. https://doi.org/10.1038/s41562-020-0886-x

Rutledge, R. B., Skandali, N., Dayan, P., & Dolan, R. J. (2015). Dopaminergic Modulation of Decision Making and Subjective Well-Being. *J Neurosci*, *35*(27), 9811–9822. https://doi.org/10.1523/JNEUROSCI.0702-15.2015

Sah, P., Hestrin, S., & Nicoll, R. A. (1990). Properties of excitatory postsynaptic currents recorded in vitro from rat hippocampal interneurones. *J Physiol*, *430*, 605–616. https://doi.org/10.1113/jphysiol.1990.sp018310

Salzman, C. D., Britten, K. H., & Newsome, W. T. (1990). Cortical microstimulation influences perceptual judgements of motion direction. *Nature*, *346*(6280), 174–177. https://doi.org/10.1038/346174a0

Sara, S. J. (2009). The locus coeruleus and noradrenergic modulation of cognition. *Nat Rev Neurosci*, *10*(3), 211–223. https://doi.org/10.1038/nrn2573

Sara, S. J., Dyon-Laurent, C., Guibert, B., & Leviel, V. (1992). Noradrenergic hyperactivity after partial fornix section: role in cholinergic dependent memory performance. *Exp Brain Res*, *89*(1), 125–132. https://doi.org/10.1007/BF00229009

Sara, S. J., Roullet, P., & Przybyslawski, J. (1999). Consolidation of memory for odor-reward association: beta-adrenergic receptor involvement in the late phase. *Learn Mem*, *6*(2), 88–96.

Schade, S., & Paulus, W. (2016). D-Cycloserine in Neuropsychiatric Diseases: A Systematic Review. *Int J Neuropsychopharmacol*, *19*(4). https://doi.org/10.1093/ijnp/pyv102

Schaworonkow, N., & Voytek, B. (2021). Longitudinal changes in aperiodic and periodic activity in electrophysiological recordings in the first seven months of life. *Developmental Cognitive Neuroscience*, *47*. https://doi.org/10.1016/j.dcn.2020.100895

Schmidt, F., Danböck, S. K., Trinka, E., Demarchi, G., & Weisz, N. (2023). Age-related changes in “cortical” 1/f dynamics are linked to cardiac activity. *bioRxiv*, 2022.2011.2007.515423. https://doi.org/10.1101/2022.11.07.515423

Schneider, F., & Blank, H. (2026). Sensory sharpening and semantic prediction errors unify competing models of predictive processing in human speech comprehension. *PLoS Biol*, *24*(1), e3003588. https://doi.org/10.1371/journal.pbio.3003588

Schneider, F., Erisson, L., Beygi, H., Bradbury, M., Cohen-Barak, O., Grachev, I. D., Guzy, S., Loupe, P. S., Levi, M., McDonald, M., Savola, J. M., Papapetropoulos, S., Tracewell, W. G., Velinova, M., & Spiegelstein, O. (2018). Pharmacokinetics, metabolism and safety of deuterated L-DOPA (SD-1077)/carbidopa compared to L-DOPA/carbidopa following single oral dose administration in healthy subjects. *Br J Clin Pharmacol*, *84*(10), 2422–2432. https://doi.org/10.1111/bcp.13702

Schoemaker, H., Claustre, Y., Fage, D., Rouquier, L., Chergui, K., Curet, O., Oblin, A., Gonon, F., Carter, C., Benavides, J., & Scatton, B. (1997). Neurochemical characteristics of amisulpride, an atypical dopamine D-2/D-3 receptor antagonist with both presynaptic and limbic selectivity. *Journal of Pharmacology and Experimental Therapeutics*, *280*(1), 83–97.

Scholl, J., Gunthner, J., Kolling, N., Favaron, E., Rushworth, M. F., Harmer, C. J., & Reinecke, A. (2014). A role beyond learning for NMDA receptors in reward-based decision-making-a pharmacological study using d-cycloserine. *Neuropsychopharmacology*, *39*(12), 2900–2909. https://doi.org/10.1038/npp.2014.144

Scholz, V., Hook, R. W., Kandroodi, M. R., Algermissen, J., Ioannidis, K., Christmas, D., Valle, S., Robbins, T. W., Grant, J. E., Chamberlain, S. R., & den Ouden, H. E. M. (2022). Cortical dopamine reduces the impact of motivational biases governing automated behaviour. *Neuropsychopharmacology*, *47*(8), 1503–1512. https://doi.org/10.1038/s41386-022-01291-8

Schultz, W. (1998). Predictive reward signal of dopamine neurons. *J Neurophysiol*, *80*(1), 1–27. https://doi.org/10.1152/jn.1998.80.1.1

Schultz, W., Apicella, P., & Ljungberg, T. (1993). Responses of monkey dopamine neurons to reward and conditioned stimuli during successive steps of learning a delayed response task. *J Neurosci*, *13*(3), 900–913. https://doi.org/10.1523/JNEUROSCI.13-03-00900.1993

Schultz, W., Dayan, P., & Montague, P. R. (1997). A neural substrate of prediction and reward. *Science*, *275*(5306), 1593–1599. https://doi.org/10.1126/science.275.5306.1593

Schutsky, K., Ouyang, M., Castelino, C. B., Zhang, L., & Thomas, S. A. (2011). Stress and glucocorticoids impair memory retrieval via beta2-adrenergic, Gi/o-coupled suppression of cAMP signaling. *J Neurosci*, *31*(40), 14172–14181. https://doi.org/10.1523/JNEUROSCI.2122-11.2011

Seamans, J. K., Gorelova, N., Durstewitz, D., & Yang, C. R. (2001). Bidirectional dopamine modulation of GABAergic inhibition in prefrontal cortical pyramidal neurons. *J Neurosci*, *21*(10), 3628–3638. https://doi.org/10.1523/JNEUROSCI.21-10-03628.2001

Seamans, J. K., & Yang, C. R. (2004). The principal features and mechanisms of dopamine modulation in the prefrontal cortex (vol 74, pg 1, 2004). *Progress in Neurobiology*, *74*(5), 321–321. https://doi.org/10.1016/j.pneurobio.2004.10.002

Sekihara, K., & Nagarajan, S. S. (2008). *Adaptive Spatial Filters for Electromagnetic Brain Imaging*. Springer. https://doi.org/10.1007/978-3-540-79370-0

Shadlen, M. N., & Kiani, R. (2013). Decision Making as a Window on Cognition. *Neuron*, *80*(3), 791–806. https://doi.org/10.1016/j.neuron.2013.10.047

Shafiei, G., Fulcher, B. D., Voytek, B., Satterthwaite, T. D., Baillet, S., & Misic, B. (2023). Neurophysiological signatures of cortical micro-architecture. *Nat Commun*, *14*(1), 6000. https://doi.org/10.1038/s41467-023-41689-6

Sigel, E., & Steinmann, M. E. (2012). Structure, function, and modulation of GABA(A) receptors. *J Biol Chem*, *287*(48), 40224–40231. https://doi.org/10.1074/jbc.R112.386664

Soyuhos, O., Zirnsak, M., Chaudhuri, R., & Chen, X. (2026). Selective control of prefrontal neural timescales by parietal cortex. *Nat Commun*. https://doi.org/10.1038/s41467-026-70326-1

Straube, T., Korz, V., Balschun, D., & Frey, J. U. (2003). Requirement of beta-adrenergic receptor activation and protein synthesis for LTP-reinforcement by novelty in rat dentate gyrus. *J Physiol*, *552*(Pt 3), 953–960. https://doi.org/10.1113/jphysiol.2003.049452

Strawn, J. R., & Geracioti, T. D., Jr. (2008). Noradrenergic dysfunction and the psychopharmacology of posttraumatic stress disorder. *Depress Anxiety*, *25*(3), 260–271. https://doi.org/10.1002/da.20292

Sutton, R. S., & Barto, A. G. (2018). *Reinforcement Learning: An Introduction* (2 ed.). MIT Press.

Symmonds, M., Wright, N. D., Fagan, E., & Dolan, R. J. (2013). Assaying the effect of levodopa on the evaluation of risk in healthy humans. *Plos One*, *8*(7), e68177. https://doi.org/10.1371/journal.pone.0068177

Syvalahti, E. K., Lauren, L., Markkanen, J., & Kunelius, R. (1987). Interaction of psychotropic drugs with brain muscarinic cholinoceptors: similarities of biperiden with pirenzepine in receptor binding properties. *Pharmacol Toxicol*, *60*(1), 66–69. https://doi.org/10.1111/j.1600-0773.1987.tb01722.x

Tallman, J. F., Thomas, J. W., & Gallager, D. W. (1978). GABAergic modulation of benzodiazepine binding site sensitivity. *Nature*, *274*(5669), 383–385. https://doi.org/10.1038/274383a0

Thaler, R. (1980). Toward a Positive Theory of Consumer Choice. *Journal of Economic Behavior & Organization*, *1*(1), 39–60. https://doi.org/10.1016/0167-2681(80)90051-7

Thiele, A. (2013). Muscarinic signaling in the brain. *Annu Rev Neurosci*, *36*, 271–294. https://doi.org/10.1146/annurev-neuro-062012-170433

Thomas, J. W., Hood, W. F., Monahan, J. B., Contreras, P. C., & O'Donohue, T. L. (1988). Glycine modulation of the phencyclidine binding site in mammalian brain. *Brain Res*, *442*(2), 396–398. https://doi.org/10.1016/0006-8993(88)91533-8

Thomson, J. J. (1976). Killing, letting die, and the trolley problem. *Monist*, *59*(2), 204–217. https://doi.org/10.5840/monist197659224

Tichelaar, J. G., Sayali, C., Helmich, R. C., & Cools, R. (2023). Impulse control disorder in Parkinson's disease is associated with abnormal frontal value signalling. *Brain*, *146*(9), 3676–3689. https://doi.org/10.1093/brain/awad162

Tobler, P. N., Fiorillo, C. D., & Schultz, W. (2005). Adaptive coding of reward value by dopamine neurons. *Science*, *307*(5715), 1642–1645. https://doi.org/10.1126/science.1105370

Tremblay, R., Lee, S., & Rudy, B. (2016). GABAergic Interneurons in the Neocortex: From Cellular Properties to Circuits. *Neuron*, *91*(2), 260–292. https://doi.org/10.1016/j.neuron.2016.06.033

Tronel, S., Feenstra, M. G., & Sara, S. J. (2004). Noradrenergic action in prefrontal cortex in the late stage of memory consolidation. *Learn Mem*, *11*(4), 453–458. https://doi.org/10.1101/lm.74504

Tunbridge, E. M., Bannerman, D. M., Sharp, T., & Harrison, P. J. (2004). Catechol-o-methyltransferase inhibition improves set-shifting performance and elevates stimulated dopamine release in the rat prefrontal cortex. *J Neurosci*, *24*(23), 5331–5335. https://doi.org/10.1523/JNEUROSCI.1124-04.2004

Turrigiano, G. G., & Nelson, S. B. (2004). Homeostatic plasticity in the developing nervous system. *Nat Rev Neurosci*, *5*(2), 97–107. https://doi.org/10.1038/nrn1327

Tversky, A., & Kahneman, D. (1979). Prospect Theory: An Analysis of Decision under Risk. *Econometrica*, *47*(2), 263–292. https://doi.org/https://www.jstor.org/stable/1914185

Tversky, A., & Kahneman, D. (1986). The Framing of Decisions and the Evaluation of Prospects. In R. Barcan Marcus, G. J. W. Dorn, & P. Weingartner (Eds.), *Studies in Logic and the Foundations of Mathematics* (Vol. 114, pp. 503–520). Elsevier. https://doi.org/https://doi.org/10.1016/S0049-237X(09)70710-4

Tversky, A., & Kahneman, D. (1992). Advances in Prospect-Theory - Cumulative Representation of Uncertainty. *Journal of Risk and Uncertainty*, *5*(4), 297–323. https://doi.org/10.1007/Bf00122574

van Berckel, B. N., Lipsch, C., Gispen-de Wied, C., Wynne, H. J., Blankenstein, M. A., van Ree, J. M., & Kahn, R. S. (1998). The partial NMDA agonist D-cycloserine stimulates LH secretion in healthy volunteers. *Psychopharmacology (Berl)*, *138*(2), 190–197. https://doi.org/10.1007/s002130050662

van Es, M. W. J., Higgins, C., Gohil, C., Quinn, A. J., Vidaurre, D., & Woolrich, M. W. (2025). Large-scale cortical functional networks are organized in structured cycles. *Nat Neurosci*, *28*(10), 2118–2128. https://doi.org/10.1038/s41593-025-02052-8

van Schouwenburg, M. R., den Ouden, H. E., & Cools, R. (2010). The human basal ganglia modulate frontal-posterior connectivity during attention shifting. *J Neurosci*, *30*(29), 9910–9918. https://doi.org/10.1523/JNEUROSCI.1111-10.2010

van van Hugte, E. J. H., Schubert, D., & Nadif Kasri, N. (2023). Excitatory/inhibitory balance in epilepsies and neurodevelopmental disorders: Depolarizing gamma-aminobutyric acid as a common mechanism. *Epilepsia*, *64*(8), 1975–1990. https://doi.org/10.1111/epi.17651

Vargas-Caballero, M., & Robinson, H. P. (2004). Fast and slow voltage-dependent dynamics of magnesium block in the NMDA receptor: the asymmetric trapping block model. *J Neurosci*, *24*(27), 6171–6180. https://doi.org/10.1523/JNEUROSCI.1380-04.2004

Vidaurre, D., Hunt, L. T., Quinn, A. J., Hunt, B. A. E., Brookes, M. J., Nobre, A. C., & Woolrich, M. W. (2018). Spontaneous cortical activity transiently organises into frequency specific phase-coupling networks. *Nature Communications*, *9*. https://doi.org/10.1038/s41467-018-05316-z

Vidaurre, D., Quinn, A. J., Baker, A. P., Dupret, D., Tejero-Cantero, A., & Woolrich, M. W. (2016). Spectrally resolved fast transient brain states in electrophysiological data. *Neuroimage*, *126*, 81–95. https://doi.org/10.1016/j.neuroimage.2015.11.047

Voytek, B., Kramer, M. A., Case, J., Lepage, K. Q., Tempesta, Z. R., Knight, R. T., & Gazzaley, A. (2015). Age-Related Changes in 1/f Neural Electrophysiological Noise. *Journal of Neuroscience*, *35*(38), 13257–13265. https://doi.org/10.1523/Jneurosci.2332-14.2015

Wang, H., Stradtman, G. G., 3rd, Wang, X. J., & Gao, W. J. (2008). A specialized NMDA receptor function in layer 5 recurrent microcircuitry of the adult rat prefrontal cortex. *Proc Natl Acad Sci U S A*, *105*(43), 16791–16796. https://doi.org/10.1073/pnas.0804318105

Wang, M., Yang, Y., Wang, C. J., Gamo, N. J., Jin, L. E., Mazer, J. A., Morrison, J. H., Wang, X. J., & Arnsten, A. F. (2013). NMDA receptors subserve persistent

neuronal firing during working memory in dorsolateral prefrontal cortex. *Neuron*, *77*(4), 736–749. https://doi.org/10.1016/j.neuron.2012.12.032

Wang, X. J. (1999). Synaptic basis of cortical persistent activity: the importance of NMDA receptors to working memory. *J Neurosci*, *19*(21), 9587–9603. https://doi.org/10.1523/JNEUROSCI.19-21-09587.1999

Wang, X. J. (2002). Probabilistic decision making by slow reverberation in cortical circuits. *Neuron*, *36*(5), 955–968. https://doi.org/10.1016/s0896-6273(02)01092-9

Wang, X. J. (2008). Decision making in recurrent neuronal circuits. *Neuron*, *60*(2), 215–234. https://doi.org/10.1016/j.neuron.2008.09.034

Wang, X. J. (2020). Macroscopic gradients of synaptic excitation and inhibition in the neocortex. *Nat Rev Neurosci*, *21*(3), 169–178. https://doi.org/10.1038/s41583-020-0262-x

Wang, X. J., Tegner, J., Constantinidis, C., & Goldman-Rakic, P. S. (2004). Division of labor among distinct subtypes of inhibitory neurons in a cortical microcircuit of working memory. *Proc Natl Acad Sci U S A*, *101*(5), 1368–1373. https://doi.org/10.1073/pnas.0305337101

Waschke, L., Donoghue, T., Fiedler, L., Smith, S., Garrett, D. D., Voytek, B., & Obleser, J. (2021). Modality-specific tracking of attention and sensory statistics in the human electrophysiological spectral exponent. *Elife*, *10*. https://doi.org/10.7554/eLife.70068

Watanabe, T., Rees, G., & Masuda, N. (2019). Atypical intrinsic neural timescale in autism. *Elife*, *8*. https://doi.org/10.7554/eLife.42256

Waterhouse, B. D., Moises, H. C., & Woodward, D. J. (1998). Phasic activation of the locus coeruleus enhances responses of primary sensory cortical neurons to peripheral receptive field stimulation. *Brain Res*, *790*(1-2), 33–44. https://doi.org/10.1016/s0006-8993(98)00117-6

Waterhouse, B. D., & Woodward, D. J. (1980). Interaction of norepinephrine with cerebrocortical activity evoked by stimulation of somatosensory afferent pathways in the rat. *Exp Neurol*, *67*(1), 11–34. https://doi.org/10.1016/0014-4886(80)90159-4

Weinshenker, D., & Schroeder, J. P. (2007). There and back again: a tale of norepinephrine and drug addiction. *Neuropsychopharmacology*, *32*(7), 1433–1451. https://doi.org/10.1038/sj.npp.1301263

Weintraub, D., Siderowf, A. D., Potenza, M. N., Goveas, J., Morales, K. H., Duda, J. E., Moberg, P. J., & Stern, M. B. (2006). Association of dopamine agonist use with impulse control disorders in Parkinson disease. *Archives of Neurology*, *63*(7), 969–973. https://doi.org/10.1001/archneur.63.7.969

Wengler, K., Goldberg, A. T., Chahine, G., & Horga, G. (2020). Distinct hierarchical alterations of intrinsic neural timescales account for different manifestations of psychosis. *Elife*, *9*. https://doi.org/10.7554/eLife.56151

Westner, B. U., Dalal, S. S., Gramfort, A., Litvak, V., Mosher, J. C., Oostenveld, R., & Schoffelen, J. M. (2022). A unified view on beamformers for M/EEG source reconstruction. *Neuroimage*, *246*, 118789. https://doi.org/10.1016/j.neuroimage.2021.118789

Wezenberg, E., Verkes, R. J., Sabbe, B. G., Ruigt, G. S., & Hulstijn, W. (2005). Modulation of memory and visuospatial processes by biperiden and rivastigmine in elderly healthy subjects. *Psychopharmacology (Berl)*, *181*(3), 582–594. https://doi.org/10.1007/s00213-005-0083-7

White, T. L., Lejuez, C. W., & de Wit, H. (2007). Personality and gender differences in effects of d-amphetamine on risk taking. *Exp Clin Psychopharmacol*, *15*(6), 599–609. https://doi.org/10.1037/1064-1297.15.6.599

Wiest, C., Torrecillos, F., Pogosyan, A., Bange, M., Muthuraman, M., Groppa, S., Hulse, N., Hasegawa, H., Ashkan, K., Baig, F., Morgante, F., Pereira, E. A., Mallet, N., Magill, P. J., Brown, P., Sharott, A., & Tan, H. L. (2023). The aperiodic exponent of subthalamic field potentials reflects excitation/inhibition balance in Parkinsonism. *Elife*, *12*. https://doi.org/10.7554/eLife.82467

Willard, S. S., & Koochekpour, S. (2013). Glutamate, glutamate receptors, and downstream signaling pathways. *Int J Biol Sci*, *9*(9), 948–959. https://doi.org/10.7150/ijbs.6426

Williams, G. V., & Goldman-Rakic, P. S. (1995). Modulation of memory fields by dopamine D1 receptors in prefrontal cortex. *Nature*, *376*(6541), 572–575. https://doi.org/10.1038/376572a0

Wilson, R. C., & Collins, A. G. (2019). Ten simple rules for the computational modeling of behavioral data. *Elife*, *8*. https://doi.org/10.7554/eLife.49547

Wong, K. F., & Wang, X. J. (2006). A recurrent network mechanism of time integration in perceptual decisions. *J Neurosci*, *26*(4), 1314–1328. https://doi.org/10.1523/JNEUROSCI.3733-05.2006

Wunderlich, K., Rangel, A., & O'Doherty, J. P. (2009). Neural computations underlying action-based decision making in the human brain. *Proc Natl Acad Sci U S A*, *106*(40), 17199–17204. https://doi.org/10.1073/pnas.0901077106

Wunderlich, K., Rangel, A., & O'Doherty, J. P. (2010). Economic choices can be made using only stimulus values. *Proc Natl Acad Sci U S A*, *107*(34), 15005–15010. https://doi.org/10.1073/pnas.1002258107

Xue, M. S., Atallah, B. V., & Scanziani, M. (2014). Equalizing excitation-inhibition ratios across visual cortical neurons. *Nature*, *511*(7511), 596–+. https://doi.org/10.1038/nature13321

Yartsev, M. M. (2026). Natural behavior is what you do, not just where you are. *Nat Neurosci*, *29*(4), 763–766. https://doi.org/10.1038/s41593-026-02225-z

Yu, A. J., & Dayan, P. (2005). Uncertainty, neuromodulation, and attention. *Neuron*, *46*(4), 681–692. https://doi.org/10.1016/j.neuron.2005.04.026

Zack, M., & Poulos, C. X. (2007). A D2 antagonist enhances the rewarding and priming effects of a gambling episode in pathological gamblers. *Neuropsychopharmacology*, *32*(8), 1678–1686. https://doi.org/10.1038/sj.npp.1301295

Zeraati, R., Shi, Y. L., Steinmetz, N. A., Gieselmann, M. A., Thiele, A., Moore, T., Levina, A., & Engel, T. A. (2023). Intrinsic timescales in the visual cortex change with selective attention and reflect spatial connectivity. *Nat Commun*, *14*(1), 1858. https://doi.org/10.1038/s41467-023-37613-7

Zhang, L., Ouyang, M., Ganellin, C. R., & Thomas, S. A. (2013). The slow afterhyperpolarization: a target of beta1-adrenergic signaling in hippocampus-dependent memory retrieval. *J Neurosci*, *33*(11), 5006–5016. https://doi.org/10.1523/JNEUROSCI.3834-12.2013

Zikopoulos, B., & Barbas, H. (2013). Altered neural connectivity in excitatory and inhibitory cortical circuits in autism. *Front Hum Neurosci*, *7*, 609. https://doi.org/10.3389/fnhum.2013.00609

Zilio, F., Gomez-Pilar, J., Cao, S., Zhang, J., Zang, D., Qi, Z., Tan, J., Hiromi, T., Wu, X., Fogel, S., Huang, Z., Hohmann, M. R., Fomina, T., Synofzik, M., Grosse-Wentrup, M., Owen, A. M., & Northoff, G. (2021). Are intrinsic neural timescales related to sensory processing? Evidence from abnormal behavioral states. *Neuroimage*, *226*, 117579. https://doi.org/10.1016/j.neuroimage.2020.117579

List of abbreviations

ADHD	attention deficit hyperactivity disorder
AMPA	α-amino-3-hydroxy-5-methyl-4-isoxazolepropionic acid
ANOVA	analysis of variance
AP-4	1,2-amino-4-phosphonobutyrate
BIC	Bayesian information criterion
CA^{2+}	calcium
cAMP	cyclic adenosine monophosphate
Cl^-	chloride
COMT	catechol-o-methyltransferase
CPP	centroparietal positivity
DAN	dorsal attention network
DMN	default mode network
EEG	electroencephalography
E/I balance	excitation-inhibition-balance
EV	expected value
fMRI	functional magnetic resonance imaging
GABA	γ-aminobutyric acid
ICA	independent component analysis
K^+	potassium
LCMV	linear-constraint minimum-variance
L-DOPA	levodopa
MAO	monoamine oxidase
MEG	magnetoencephalography
Mg^{2+}	magnesium

MRI	magnetic resonance imaging
MSE	mean squared error
NA^+	sodium
NMDA	N-Methyl-D-aspartate
PSD	power spectral density
PV	parvalbumin
RDM	random dot motion task
REM	rapid eye movement
SST	somatostatin
FFT	fast Fourier transform
SQUID	superconducting quantum interference device
TDE-HMM	Time-Delay Embedded Hidden Markov Models
VIP	vasoactive intestinal peptide

List of publications

Dias Maile AA[*], Kohl O[*], Ort E, Froböse MI, Kurtenbach H, Butz M, Schreivogel E, Schnitzler A, Florin E[†], Jocham G[†] (2026). *Role of GABA and NMDA receptors in shaping cortical timescales and large-scale network dynamics*. bioRxiv. https://doi.org/10.64898/2026.05.11.723797

Statement of contributions

* These authors contributed equally to this work

† These authors contributed equally to this work

Study conception and design (EO, MIF, HK, GJ), data acquisition (EO, MIF, HK, AADM, ES), data analysis (AADM, OK, EO), interpretation of data for the work (all authors), drafting the article (AADM, OK, EF, GJ), revising it for intellectual content (all authors), approving the final version of the manuscript (all authors)

Dias Maile AA, Gruendler TOJ, Fischer AG, Kurtenbach H, Kaiser LF, Froböse MI, Jocham G (2025). *Bidirectional modulation of reward-guided decision making by dopamine.* Psychopharmacology, 242(11), 2547–2559. https://doi.org/10.1007/s00213-025-06816-9

Statement of contributions

Study conception and design (TOJG, GJ), data acquisition (TOJG, AGF), data analysis (AADM, HK, LFK, MIF, GJ), interpretation of data for the work (all authors), drafting the article (AADM, MIF, GJ), revising it for intellectual content (all authors), approving the final version of the manuscript (all authors).

Dias Maile AA, Andronova E, Ball F, Aravitska D, Dannenberg LK, Schnitzler A, O'Reilly JX, Jocham G (2026). *Cholinergic and noradrenergic modulation of perceptual decision making and learning.* bioRxiv. https://doi.org/10.64898/2026.06.22.732890

Statement of contributions

Study conception and design (AADM, FB, JXOR, GJ), data acquisition (AADM, EA, FB, DA, LKD), data analysis (AADM, JXOR, GJ), interpretation of data for the work (AADM, JXOR, GJ), drafting the article (AADM, JXOR, GJ), revising it for intellectual content (all authors), approving the final version of the manuscript (all authors)

Conference contributions and talks

Dias Maile AA, Kohl O. *Role of GABA and NMDA receptors in shaping cortical timescales and large-scale network dynamics.* Research colloquium of the Institute of Clinical Neuroscience and Medical Psychology 2026 in Düsseldorf, Germany (invited talk)

Dias Maile AA, Ort E, Froböse MI, Kurtenbach H, Bahners BH, Butz M, Schnitzler A, Jocham G. *Glutamatergic and GABAergic modulation of cortical temporal dynamics.* 12th Symposium on the Biology of Decision Making 2025 in Lyon, France (poster)

Dias Maile AA, Ort E, Froböse MI, Kurtenbach H, Bahners BH, Butz M, Schnitzler A, Jocham G. *Glutamatergic and GABAergic modulation of cortical temporal dynamics*. 49. Jahrestagung Psychologie & Gehirn 2024 in Hamburg, Germany (poster).

Dias Maile AA, Gründler TOJ, Froböse MJ, Kaiser LF, Jocham G. *Bidirectional Modulation of Reward-Guided Decision Making by Dopamine*. 48. Jahrestagung Psychologie & Gehirn 2023 in Tübingen, Germany (poster).

Dias Maile AA, Gründler TOJ, Froböse MJ, Kaiser LF, Jocham G. *Bidirectional Modulation of Reward-Guided Decision Making by Dopamine*. 11th Symposium on the Biology of Decision Making 2023 in Paris, France (poster)

Research articles

Study 1: Role of GABA and NMDA receptors in shaping cortical timescales and large-scale network dynamics

Currently under review at eLife and reproduced from

Dias Maile AA[*], Kohl O[*], Ort E, Froböse MI, Kurtenbach H, Butz M, Schreivogel E, Schnitzler A, Florin E[†], Jocham G[†] (2026). *Role of GABA and NMDA receptors in shaping cortical timescales and large-scale network dynamics*. bioRxiv. https://doi.org/10.64898/2026.05.11.723797

* These authors contributed equally to this work

† These authors contributed equally to this work

Role of GABA and NMDA receptors in shaping cortical timescales and large-scale network dynamics

Ana Antonia Dias Maile[1*], Oliver Kohl[2*], Eduard Ort[1], Monja I Froböse[1], Hannah Kurtenbach[1], Markus Butz[2], Elisabeth Schreivogel[3], Alfons Schnitzler[2,3], Esther Florin[2†], Gerhard Jocham[1†]

* These authors contributed equally to this work.

† These authors contributed equally to this work.

[1]Biological Psychology of Decision Making, Institute of Experimental Psychology, Heinrich Heine University Düsseldorf, 40225 Düsseldorf, Germany

[2]Institute of Clinical Neuroscience and Medical Psychology, Medical Faculty, Heinrich Heine University Düsseldorf, 40225 Düsseldorf, Germany

[3]Department of Neurology, Centre for Movement Disorders and Neuromodulation, Medical Faculty, Heinrich Heine University Düsseldorf, 40225 Düsseldorf, Germany

Author contributions

- Study conception and design (EO, MIF, HK, GJ), data acquisition (EO, MIF, HK, AADM, ES), data analysis (AADM, OK, EO), interpretation of data for the work (all authors)
- Drafting the article (AADM, OK, EF, GJ), revising it for intellectual content (all authors)
- Approving the final version of the manuscript (all authors)

Correspondence: Ana Antonia Dias Maile and Oliver Kohl
ana.dias.maile@hhu.de
oliver.kohl@hhu.de

Acknowledgements

We thank Hanin Alejel, Helena El Kholy, Judith Geusen, Paul Höchter, Marlene Hüsken, Christina Kalinicenko, Joshua Saal, Kouta Sasaki, Georg Schäfer, and Helena Schmidt for their support during data acquisition. We thank the MRI Core Facility of the University Hospital Düsseldorf, particularly Erika Rädisch and Eric Bechler, for help with the MRI recordings. We further thank Bradley Voytek for his advice regarding aperiodic data analysis and cortical parcellation, and Thomas Pirenne

for valuable discussions on data analysis, interpretation, and visualization. Computational infrastructure and support were provided by the Centre for Information and Media Technology at Heinrich Heine University Düsseldorf.

Funding

This work was supported by an ERC Consolidator Grant from the European Research Council (ERC-CoG 771432) to GJ.

Competing Interests

On behalf of all authors, the corresponding authors state that there is no conflict of interest.

Abstract

Cortical brain regions integrate information across different timescales, ranging from fast sensory processing to longer integration windows, allowing cognitive functions like working memory. At the large-scale, brain regions organize into transient network states that rapidly switch over time and similarly contribute to cognition. Both cortical timescales and large-scale network dynamics are proposed to be determined by the balance between recurrent synaptic excitation and GABAergic inhibition. Here, we pharmacologically manipulated synaptic transmission at $GABA_A$ and NMDA receptors in 60 healthy male participants and acquired resting-state magnetoencephalography. Neuronal timescales followed a hierarchical gradient with shorter timescales in early sensory regions. Increasing GABAergic activity prolonged neuronal timescales across cortical regions. This effect was most prominent in the frontal default mode and in the dorsal attention network. Notably, dynamic network analyses revealed that the occurrence probability of the frontal default mode network increased, whereas the occurrence of the dorsal attention network was reduced. NMDA receptor modulation resulted in no significant changes. Together, these findings provide causal evidence that GABAergic inhibition is a key regulator of cortical temporal organization, linking microscale synaptic mechanisms to neuronal timescales and network dynamics that support diverse cognitive function.

Introduction

Neurons throughout the brain process information over multiple timescales (Murray et al., 2014). This enables complex perception and cognition, such as following the storyline of a movie: In primary sensory regions, short timescales allow the fast detection of perceptual changes from frame to frame, whereas longer timescales in association regions allow integration of this information into coherent scenes and narratives (Baldassano et al., 2017; Çatal et al., 2023; Honey et al., 2012; Lerner et al., 2011). The spatial distribution of neuronal timescales follows a hierarchical gradient across the cortex, with short timescales in early sensory areas and increasingly longer timescales in higher-order association areas (Murray et al., 2014; Shafiei et al., 2023; Wang, 2020), a pattern that has been replicated across different species and tasks (Cusinato et al., 2023; Halgren et al., 2021). This gradient and its dynamic adaptation to cognitive demands play a fundamental role in information processing and working memory (Bernacchia et al. 2011; Gao et al., 2020; Ito et al., 2020; Lendner et al. 2024; Manea et al., 2024). In addition to these local dynamics, distant brain regions also spontaneously organize into short-lived, transient network states with distinct spectral signatures (Vidaurre et al. 2018) that likewise support cognitive processes on different timescales (Quinn et al., 2018; Gohil et al., 2024; Rossi et al., 2023; Rossi et al., 2024). This ability of the brain to explore a diverse repertoire of large-scale network configurations can be seen as sequential activation of recurring, metastable states (Rabinovich et al., 2008; Tognoli & Kelso, 2014).

Neuronal timescales and metastable resting-state dynamics are proposed to emerge from the balance between glutamatergic excitation and GABAergic inhibition (Excitation-inhibition-balance, or short, E/I balance; Abeysuriya et al., 2018; Gao et al., 2017; Murray et al., 2014; Pascoa Dos Santos & Verschure, 2025; Wang, 2020). Areas

at the top of the cortical hierarchy, like the prefrontal cortex are rich in recurrent connections endowed with NMDA glutamate receptors (Burt et al., 2018). Owing to their long time constant, they enable persistent neural activity and information integration over long timescales critical for working memory and decision making (Wang et al., 2008; Wang, 1999, 2002, 2008). In contrast, NMDA receptor expression is less pronounced in early sensory areas (Burt et al., 2018). Consequently, neural activity there fluctuates on shorter timescales and closely tracks the current sensory input (Baldassano et al., 2017; Honey et al., 2012). Recurrent excitation is balanced by shorter GABAergic feedback inhibition, which displays a similar hierarchical gradient (Burt et al., 2018). Despite these findings, it is not known how NMDA- and GABA-mediated activity causally shapes neuronal timescales across cortical regions. It further remains unclear whether different large-scale cortical networks have distinct neuronal timescales and how transitions between network states are governed by changes in transmission at GABA and NMDA receptors.

In the present study, we examine how NMDA and $GABA_A$ receptors influence both neuronal timescales across cortical regions and the dynamical organization of large-scale cortical networks. To this end, we increased activity at NMDA and $GABA_A$ receptors by administering the partial NMDA receptor agonist D-cycloserine and the benzodiazepine receptor agonist lorazepam, respectively, and examined their effects on the hierarchical organization of cortical timescales and on large-scale network dynamics during rest. Given the slower kinetics of NMDA and GABA receptors relative to the predominant AMPA-mediated excitation (Angulo et al., 1999; Gupta et al., 2000; Sah et al., 1990), we hypothesized that both manipulations would prolong neuronal timescales. In brief, we find that increased GABAergic activity prolongs neuronal timescales across the cortex, differentially modulates timescales across dynamic

large-scale cortical networks, and alters network dynamics by biasing transitions toward the frontal default mode network. Modulation of NMDA receptor activity did not significantly alter neuronal timescales or large-scale network dynamics.

Results

We examined how NMDA and $GABA_A$ receptors influence neuronal timescales across cortical regions and the dynamical organization of large-scale cortical networks by analyzing five minutes of open-eyed resting-state data. To this end, we collected magnetoencephalography (MEG) recordings from 60 healthy participants under the influence of lorazepam (1 mg), D-cycloserine (250 mg), or placebo in a double-blind, within-subject, crossover design. Lorazepam is a benzodiazepine receptor agonist that binds allosterically at $GABA_A$ receptors (Riss et al., 2008; Tallman et al., 1978). D-cycloserine is a glutamatergic partial NMDA agonist acting at the glycine-binding site (Thomas et al., 1988). Three participants were excluded due to excessive noise in the MEG data, resulting in a final sample of 57 participants.

Timescales follow a hierarchical cortical gradient

Neuronal timescales reflect the decay rate of the autocorrelation function of a neural signal (i.e., the signal's decreasing self-similarity across time). Timescales were estimated per cortical region of the Desikan-Killiany atlas (34 parcels per hemisphere; Desikan et al., 2006) based on the aperiodic knee frequency fitted with the FOOOF toolbox (version 1.0.0; Donoghue et al., 2020; Gao et al., 2020, see Methods for more details). As an initial validation, we first assessed the spatial similarity between the estimated timescales under placebo and the publicly available intrinsic timescale map (Glasser et al., 2016; Shafiei et al., 2023). We observe a strong correlation of r_s = 0.91,

supporting the validity of our estimates (p < 0.001; permutation test preserving the spatial autocorrelation; see Methods).

As it has been indicated that timescales follow a hierarchical gradient (Gao et al., 2020; Murray et al., 2014; Shafiei et al., 2023; Wang, 2020), we tested how timescales relate to the T1w/T2w ratio, an MRI-based index for myelinization commonly used as a proxy for a cortical region's position on the cortical hierarchy, with lower ratios indicating higher hierarchical position (Glasser et al., 2016). In agreement with this, timescales under placebo - but also under both drug conditions - were strongly negatively correlated with the T1w/T2w ratio (all r_s < -0.79, p = 0.002; permutation test preserving the spatial autocorrelation; see Methods and Figure 1). Thus, we confirm that neuronal timescales increase with higher position in the cortical hierarchy. Importantly, this gradient was preserved under pharmacological increase of $GABA_A$ and NMDA receptor-mediated transmission.

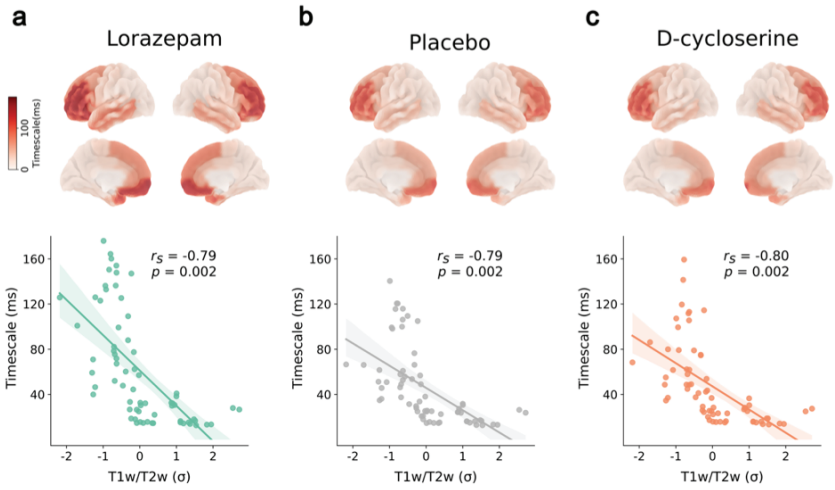

Fig. 1: Hierarchical gradient of neuronal timescales. Timescales for lorazepam **(a)**, placebo **(b)**, and D-cycloserine **(c). Top row:** Distribution of neuronal timescales in milliseconds (averaged across participants) across the cortex. **Bottom row:** Timescales of all 68 cortical areas (averaged across participants) as a function of T1w/T2w ratio (z-scored), an index of the hierarchical position of a cortical

area. Shades around the regression line represent the 95% confidence interval. r_S = Spearman correlation coefficient. Spatial autocorrelation was preserved for the computation of *p*-values.

Pharmacological modulation of neuronal timescales

Recurrent excitation at NMDA receptors and GABAergic feedback inhibition is thought to shape temporal integration of neurons (Wang, 2020). In line with this, lorazepam, compared with placebo, significantly increased neuronal timescales across 48 of 68 parcels in both hemispheres (Figure 2a and Supplement 1; see Supplement 2 for drug effects on all aperiodic parameters; two-tailed paired-sample permutation t-test, all $t > 2.14$, $p < 0.044$ with FDR correction for multiple comparisons). In contrast, D-cycloserine resulted in no significant changes in neuronal timescales (Figure 2b).

Previous work suggests a relation between a brain region's level of GABA receptor expression and its neuronal timescale, above and beyond the regions' hierarchical position (Gao et al., 2020). Therefore, we next examined whether the effects of lorazepam were independent of the position of the cortical parcels in the cortical hierarchy. A hierarchy-dependent effect of lorazepam would be evident from a change in the slope of the regression line between cortical hierarchy and neural timescales (Figure 1a). To this end, we implemented a linear mixed-effects regression on neuronal timescales, including the predictors cortical hierarchy (T1w/T2w ratio), drug condition, and their interaction. In line with the previous analyses, the T1w/T2w ratio had a significant main effect on neuronal timescales ($\beta = -3.06$, $SE = 0.17$, $t_{75880} = -17.64$, $p < 0.001$; supplement 3), indicating that increased myelination was associated with shorter timescales. Moreover, lorazepam showed a significant positive main effect ($\beta = 0.39$, $SE = 0.15$, $t_{5146000} = 2.55$, $p = 0.011$), confirming that lorazepam prolongs neuronal timescales. There was also a trend for an interaction between drug condition and T1w/T2w ratio ($\beta = -0.19$, $SE = 0.11$, $t_{11190000} = -1.75$, $p = 0.081$; Figure 2c). This trend points towards an increased hierarchical gradient under lorazepam,

likely due to a larger increase of neuronal timescales in frontal cortex compared to occipital cortex (Figure 2a). Importantly, the increase in timescales under lorazepam, but also the trend-wise interaction of lorazepam with the cortical hierarchy, are independent of the significant effects of lorazepam on various control measures we collected (i.e., alertness, calmness, contentedness, anxiety, visuomotor abilities, and vital parameters; see Supplement 4 and 5). Consistent with the results obtained from the permutation t-test across cortical regions (Fig. 2b), D-cycloserine had neither a significant main effect (β = -0.08, SE = 0.15, $t_{9952000}$ = -0.54, p = 0.586) nor an interaction with the cortical hierarchy (β = 0.08, SE = 0.11, $t_{11180000}$ = 0.71, p = 0.477), nor on control parameters (see Supplement 4).

In sum, neuronal timescales increase along the cortical hierarchy and are further prolonged by lorazepam. While this effect appears largely independent of the hierarchical gradient, there is a trend toward stronger modulation in the frontal cortex, leading to a steeper cortical gradient.

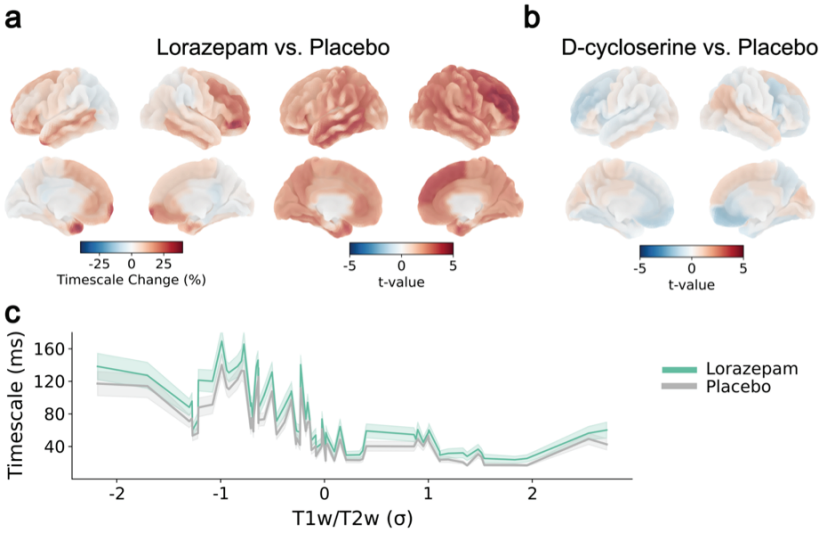

Fig. 2: Drug effects on neuronal timescales and their hierarchical gradient. a Left panel: percent change of timescales under lorazepam compared to placebo. Right panel: *t*-statistic on neuronal timescales, permutation test of the effect of lorazepam compared to placebo, projected onto the cortical surface. **b** *t*-statistic on neuronal timescales, permutation test of the effect of D-cycloserine on neuronal timescales compared to placebo, projected onto the cortical surface. D-cycloserine did not significantly modulate neuronal timescales. **c** Cortical hierarchy (operationalized via the z-scored T1w/T2w ratio) of neuronal timescales as a function of drug condition (lorazepam or placebo). Shades depict the 95%-confidence intervals.

Dynamic cortical large-scale networks exhibit varying timescales

Having established that local neuronal timescales vary systematically across the cortical hierarchy and are increased by lorazepam, we next examined timescales of dynamic large-scale cortical networks. To this end, we applied a Time-Delay Embedded Hidden Markov Model (TDE-HMM) to the parcellated MEG time series to extract spectrally and temporally resolved large-scale cortical networks. The resulting eight networks (Figure 3) closely resemble previously reported TDE-HMM-derived cortical networks (Gohil et al., 2024; Kohl et al., 2025; Rossi et al., 2023; Rossi et al., 2024; Vidaurre et al., 2018). All states were expressed in every participant, with fractional occupancies ranging from 1 % to 48 %. Fractional occupancy refers to the percent of the entire recording time the brain spent in the respective state. This demonstrates that no single state dominated individual recordings and that each network contributed to ongoing cortical dynamics.

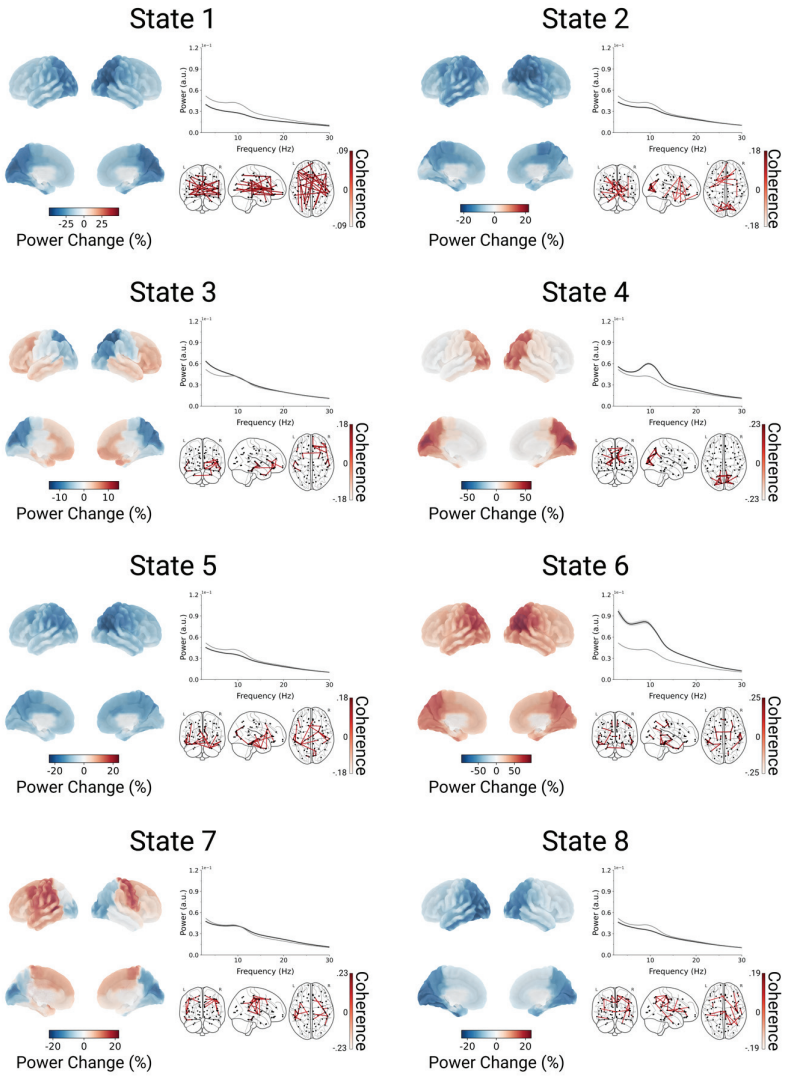

Fig. 3: Spectral characterization of dynamic large-scale cortical networks. For each state, three representations are presented, averaged across all participants in the placebo condition. **Left:** Cortical maps of state-specific 3-30 Hz power changes relative to the time-averaged power across states. **Top right:** Whole-brain average power spectrum for each state (black) compared with the whole-brain

average spectrum across all states (grey). **Bottom right:** State-specific coherence networks in the 2–30 Hz range, thresholded at the 98th percentile to highlight the strongest functional connections.

Next, we estimated state-specific timescales from each state's power spectrum, using the same procedure as reported above for time-averaged spectra. These state-specific timescales were then compared to each participant's global timescales using General Linear Models (GLMs) to determine whether neuronal timescales systematically varied with the occurrence of specific cortical networks. Visits to two states were associated with significant increases in timescales compared to the global timescales across multiple cortical regions (State 1 and State 3: all $t_{55} > 4.79$, $p < 0.001$; max change = +5.46% to +21.7%; Figure 4a). In contrast, for the remaining states, the time-scales predominantly decreased significantly (State 2, 4, 5, 7, and 8: all $t_{55} < -2.18$, $p < 0.030$; max change = -2.22% to –27.87 %) or the pattern was mixed (State 6: six parcels increased: all $t_{55} > 3.11$, $p < 0.001$; 3 parcels decreased: all $t_{55} < -2.75$, $p < 0.006$; max change = -15.10 % to +8.99 %, Figure 4a). This suggests that large-scale cortical networks operate on distinct timescales, indicating a flexible temporal organization of cortical processing.

Pharmacological modulation of network-specific time scales

The above analyses demonstrate that large-scale cortical networks operate on different timescales. Next, we investigated how our pharmacological intervention modulates these state-specific timescales. As D-cycloserine showed no significant effects on neuronal timescales, the subsequent analyses focus exclusively on lorazepam. GLMs comparing state-specific timescales between the lorazepam and placebo condition revealed significantly increased timescales during visits to State 1 (n = 12/68 significant parcels; max increase = 17.52%, $t_{55} = 4.75$, $p < 0.001$), State 2 (n = 21/68 significant parcels; max increase = 6.38%, $t_{55} = 3.9$, $p < 0.001$), State 3 (n

= 59/68 significant parcels; max increase = 24.02, t_{55} = 5.34, p < 0.001), State 5 (n = 10/68 significant parcels; max increase = 6.39, t_{55} = 4.15, p < 0.001), and State 8 (n = 34/68 significant parcels; max increase = 9.8, t_{55} = 5.28, p < 0.001; Figure 4b), whereas for the remaining states timescales significantly decreased (all t_{55}< -1.86, p < 0.020; max decrease = -5.47% to -13.82%). This pattern indicates that lorazepam exerts network-specific effects on neuronal timescales, such that its influence on a given cortical region varies depending on which large-scale network is currently active.

The lorazepam-related increase in neuronal timescales across most networks is consistent with the widespread prolongation of cortical timescales observed in our time-averaged region-wise analysis. Among the networks, the strongest lorazepam-induced increases of neuronal timescales were observed for State 3 (~24%) and State 1 (~17.5%), which have been previously linked to the frontal default mode network (DMN; Gohil et al., 2024; Rossi et al., 2023; Rossi et al., 2024; van Es et al., 2025; Vidaurre et al., 2018) and the dorsal attention network (DAN; Baker et al., 2014; van Es et al., 2025), respectively. Despite these strong increases, repeated measures correlations across all participants and parcels indicated small but significant associations (all r < 0.22) between global and state-specific timescales for all states except the DAN (State 1; see Supplement 6). In contrast, frontal DMN (State 3) timescales exhibited the strongest coupling with global timescales (r = 22, p < .0.001). Together, these findings indicate that the frontal DMN is an important driver of the global prolongation of neuronal timescales across the cortex under lorazepam.

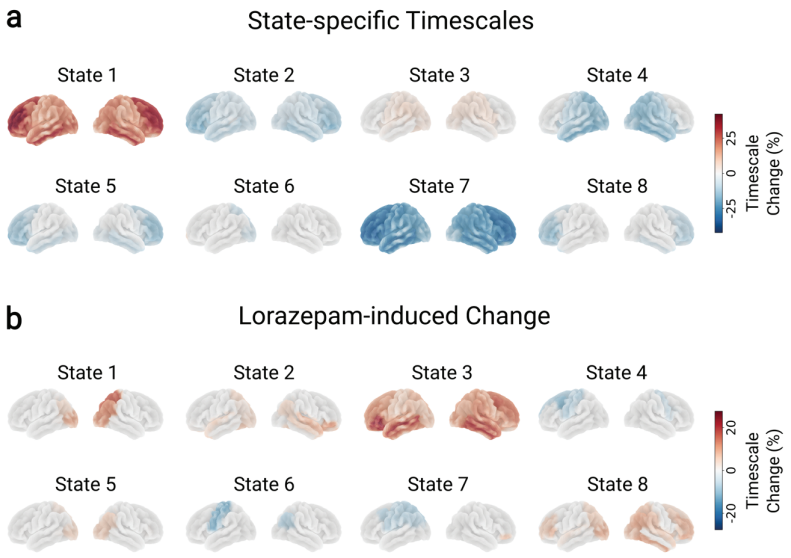

Fig. 4: Timescales vary across cortical networks and are differentially modulated by lorazepam. **a** Percent change in neuronal timescales during network occurrences relative to the time-averaged timescale across states. **b** Percent change in neuronal timescales under lorazepam relative to placebo. Only parcels with significant effects are shown ($p < 0.05$, FDR-corrected). Significance was assessed for each parcel and state using within-subject GLMs with permutation testing, comparing state-specific timescales with the time-averaged timescale (**a**) or between lorazepam and placebo (**b**). p-values were FDR-corrected across parcels and states.

Lorazepam shifts cortical dynamics toward the frontal default mode network

After identifying that neuronal timescales vary across cortical networks and are differentially modulated by lorazepam, we next examined whether lorazepam also alters large-scale network dynamics. Network dynamics were characterized using fractional occupancy (the overall proportion of time a network is active) and complementary temporal metrics: state lifetime (the average duration of continuous visits); interval time (the time between successive visits); and state rate (the frequency of network entry per second). GLMs comparing participants' fractional occupancies between the placebo and lorazepam conditions revealed a significant increase for the frontal DMN (State 3; $t_{55} = 4.33$, $p < 0.001$) and a significant decrease for the DAN

(State 1; t_{55} = -3.08, p = 0.020; Figure 5a) under lorazepam. Analyses of lifetimes, interval times, and state rates indicated that the enhanced fractional occupancy of the frontal DMN (State 3) was driven by increases in both state lifetime (t_{55} = 2.84, p = 0.040; Figure 5b) and state rate (t_{55} = 3.97, p < 0.001, Figure 5d), whereas the reduction in DAN (State1) occupancy was underpinned by shorter state lifetimes (t_{55} = -3.09, p = 0.020, Figure 5b). Interval times were not modulated by lorazepam (Figure 5c).

To further detail the mechanisms underlying the lorazepam-related increase in frontal DMN occupancy, we compared state-transition probabilities between the lorazepam and placebo conditions. This analysis tests whether the temporal progression from one network state to another differs as a function of drug condition. GLMs combined with maximum *t*-statistic permutation tests revealed that lorazepam significantly reduced DAN self-transitions (State 1; t_{55} = -3.4, p = 0.050, Figure 5e), consistent with the observed reductions in occurrence probabilities and lifetimes. Furthermore, under lorazepam, the DAN (State 1; t_{55} = 4.05, p = 0.007), State 2 (t_{55} = 3.83, p = 0.010), and State 5 (t_{55} = 4.01, p < 0.007) were significantly more likely to transition into the frontal DMN (State 3), while transitions out of the frontal DMN were significantly reduced (State 6: t_{55} = −3.45, p < 0.040; Figure 5e,f). These findings suggest that lorazepam increases transitions into and decreases transitions out of the frontal DMN, thereby increasing the time the brain spends in that state.

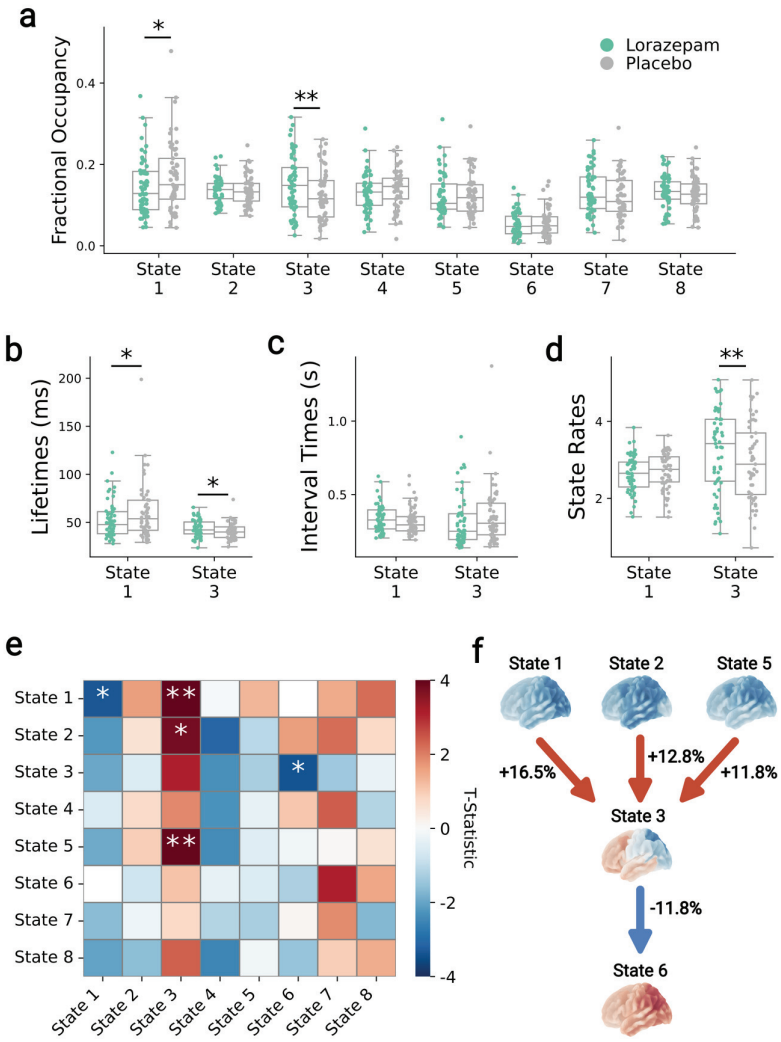

Fig. 5: Lorazepam modulates large-scale cortical network dynamics. a Lorazepam–placebo contrasts of fractional occupancy across all states. Each dot represents an individual participant. Lorazepam reduced the fractional occupancy of State 1 (dorsal attention network, DAN) and increased that of State 3 (frontal default mode network, DMN). **b-d** Lorazepam-placebo contrasts of state lifetimes (**b**), interval times (**c**), and state rates (**d**) for the DAN and frontal DMN. Dots indicate individual participants. **e** Lorazepam-placebo contrasts of state transition probabilities. Heatmap colours represent *t*-statistics from within-participant GLMs. Rows denote the current state and columns the subsequent

state. Lorazepam reduced DAN self-transitions, increased transitions from the DAN and other networks into the frontal DMN, and reduced transitions out of the frontal DMN. **f** Schematic summary of significant lorazepam-induced transition changes involving the frontal DMN. Values indicate percentage change relative to placebo, with arrows denoting transition direction. Statistical significance in **a-e** was assessed using maximum *t*-statistic permutation tests, correcting for multiple comparisons across states or transitions. Asterisks indicate significance: $p < 0.050$ = *, $p < 0.010$ = **.

Robustness Analyses

TDE-HMM analyses require a priori specification of state number, as standard model selection metrics do not identify a clear optimum (Gohil et al., 2026). We therefore repeated all key analyses using models with 10 and 12 states. Results were similar across different numbers of states for state-specific timescales, lorazepam effects on timescales (Supplement 7), and lorazepam-effects on network fractional occupancies (Supplement 8). Similarly, re-running the TDE-HMM using a different preprocessing pipeline (Supplement 9) also produced comparable states, indicating that the main findings are not dependent on state number selection or specific preprocessing choices.

Discussion

The present study examined the causal role of GABAergic and NMDA-mediated neurotransmission in shaping neuronal timescales and large-scale network dynamics. Our results demonstrate that enhancing GABAergic inhibition via lorazepam produced a widespread prolongation of neuronal timescales across the cortex, with a trend toward stronger effects in frontal regions, indicative of a steepened hierarchical gradient. These timescale changes were most pronounced during activation of the frontal DMN and DAN, and were accompanied by opposing shifts in network recruitment, with lorazepam increasing the probability of frontal DMN occurrence while reducing that of the DAN. In contrast, facilitating NMDA receptor transmission via D-cycloserine had no significant effect on cortical timescales. Together, these findings provide causal evidence that microscale synaptic inhibition directly shapes both local

neuronal timescale organization and macroscale network dynamics, thereby linking synaptic activity to the hierarchical structure of cortical processing.

In the present study, we replicate observations that neuronal timescales follow a cortical hierarchy, increasing from primary sensory to association areas (Gao et al., 2020; Murray et al., 2014). We further extended these findings by demonstrating that this hierarchy is preserved under elevated transmission at $GABA_A$ and NMDA receptors. Higher-order cognitive processes, such as working memory (Gao et al., 2020; Wang et al., 2008; Wang et al., 2013; Wang, 1999) and decision making (Wang, 2002, 2008), strongly depend on recurrent NMDA-mediated excitation. Increased NMDA-mediated recurrent excitation is thought to prolong neuronal timescales, which fits with the observation that, during behavioral tasks, neuronal timescales are similarly expanded (Bernacchia et al. 2011; Manea et al., 2024), while the general hierarchy is preserved (Manea et al., 2024). We hypothesized that pharmacologically increasing transmission at NMDA receptors with D-cycloserine would likewise increase neuronal timescales. However, we observed no significant effects of D-cycloserine. By contrast, and consistent with our hypothesis for GABAergic modulation, lorazepam prolonged neuronal timescales across almost the entire cortex. Glutamatergic and GABAergic receptors exhibit distinct timescales, with AMPA receptors operating on the shortest timescale (~2 ms) followed by GABA (~5-10 ms; Gupta et al., 2000) and NMDA (~50-100 ms; Angulo et al., 1999; Sah et al., 1990) receptors. At rest, the E/I balance is dominated by GABAergic inhibition and AMPA-mediated excitation, whereas NMDA receptor activity has a reduced contribution due to the voltage-dependent Mg^{2+} block (Alberto & Hirasawa, 2010; Espinosa & Kavalali, 2009; Myme et al., 2003; Vargas-Caballero & Robinson, 2004). Although D-cycloserine binds allosterically at the NMDA receptor and thus increases the probability of channel opening, postsynaptic

depolarization is still required for NMDA currents to emerge (Thomas et al., 1988). This may explain the absence of significant effects of D-cycloserine on neuronal timescales at rest. This reasoning also explains the direction of the GABAergic effect: lorazepam prolongs neuronal timescales by strengthening slower GABAergic inhibition and reducing faster AMPA-mediated excitation (Chapman et al., 2022; Isaacson & Scanziani, 2011). Consistent with this interpretation, AMPA antagonists modulate resting state periodic brain activity in a manner similar to what has been observed under GABA agonists (Nutt et al., 2015; Routley et al., 2017). Likewise, propofol anesthesia, which is thought to increase GABAergic inhibition, steepens the aperiodic slope indicative of longer neuronal timescales (Colombo et al., 2019; Gao et al., 2017; Waschke et al., 2021).

In the present study, we observed not only an overall prolongation of timescales but also a trend for greater effects in frontal cortical regions. In line with these findings, neuronal timescales correlate with cortical expression patterns of genes encoding $GABA_A$ receptors, both along the cortical hierarchy and beyond it (Gao et al., 2020). In sum, increased GABAergic transmission via lorazepam led to a widespread prolongation of neuronal timescales across the cortex, while modulation of NMDA-mediated receptor activity by D-cycloserine had no significant effects.

In addition to local region-wise differences between brain regions, timescales systematically differed across large-scale cortical networks. These networks are thought to play a central role in the organization of information processing in the brain and have been implicated in a wide range of functions, including sensory processing and higher-order information integration (Bressler, 1995; McIntosh, 2000; Mesulam, 1998). In line with the hierarchical gradient of neuronal timescales, states involved in higher-order processing, such as State 1 (DAN) and State 3 (DMN), were

characterized by higher intrinsic timescales, relative to global timescales. In contrast, states reflecting sensorimotor or visual networks (Gohil, Kohl, et al., 2024; Quinn et al., 2018), which are more closely tied to bottom-up processing, exhibited shorter timescales. These findings support the notion that the temporal properties of neuronal dynamics support the functional roles of large-scale cortical networks.

Comparisons of network-specific timescales between placebo and lorazepam revealed prolonged timescales for most networks, consistent with our global analysis. The largest increases in timescale occurred in the occipito-parietal areas of the DAN (State 1) and the prefrontal-temporal areas of the frontal DMN (State 3). These cortical areas overlap with regions of high $GABA_A$ receptor density (la Fougere et al., 2011; Norgaard et al., 2021), suggesting that regional receptor distribution modulates lorazepam-induced timescale prolongation. Despite this, both the magnitude and direction of lorazepam's effects varied across resting-state networks and cortical regions. Notably, state-specific spectral power in sensorimotor regions was either increased or decreased by lorazepam depending on current network activation. This pattern suggests that network-specific variability cannot be explained solely by differences in regional recruitment across networks. Instead, the effects of lorazepam on individual cortical regions were not fixed but depended on the present large-scale network activation, indicating state-dependent GABAergic modulation. A plausible explanation is that distinct networks preferentially recruit neuronal subpopulations with differing sensitivity to lorazepam. Benzodiazepines act on multiple $GABA_A$ receptor subtypes, which are heterogeneously distributed (Fritschy & Mohler, 1995; Rudolph & Knoflach, 2011) and differentially shape inhibitory gain (Colombi et al., 2024; Patel et al., 2016) and oscillatory dynamics (Heistek et al., 2013). If different networks engage circuits with distinct receptor profiles, this could account for the observed network-

specific effects. In support of this, neuronal timescales of the frontal eye field depend on activation of the frontoparietal network, likely reflecting the recruitment of distinct neuronal subpopulations (Soyuhos et al., 2026). In sum, lorazepam effects vary across large-scale cortical networks, highlighting interactions between microscale GABAergic activity and macroscale network dynamics that may be important to consider when investigating pharmacological effects on brain activity.

Analysis of large-scale network dynamics revealed that increasing GABAergic activity via lorazepam modulated not only the intrinsic timescales of the frontal DMN (State 3) and DAN (State 1), but also their temporal expression. Specifically, lorazepam increased the probability of frontal DMN activation, driven by prolonged state lifetimes and higher occurrence rates, while reducing DAN expression, primarily through shortened lifetimes. Analyses of state transition probabilities further suggested that these effects may be underpinned by attractor strength of the frontal DMN, reflected in greater transition rates from multiple networks, including the DAN, into the frontal DMN, and reduced transitions from the frontal DMN into State 6. The opposing modulation on DMN and DAN activity is consistent with their well-established anticorrelation (Baker et al., 2014; Fox et al., 2005; van Es et al., 2025), commonly interpreted as reflecting a balance between internally and externally oriented modes of processing, or task-relevant versus task-irrelevant thoughts (Fox et al., 2005). Taken together, these results suggest that increased GABAergic activity biases large-scale brain dynamics toward internally oriented processing while attenuating responsiveness to external stimuli, consistent with the known sedative effects of lorazepam.

Critically, the observation that pharmacological manipulation of GABAergic activity altered large-scale network engagement demonstrates that microscale synaptic properties shape macroscale network recruitment. This finding aligns with

models highlighting local E/I balance as critical for metastable cortical dynamics (Abeysuriya et al., 2018; Pascoa Dos Santos & Verschure, 2025) and raises the possibility that task-dependent changes in network recruitment, as observed during working memory (Rossi et al., 2023; Rossi et al., 2024) and motor processing (Gohil et al., 2024; Quinn et al., 2018), may reflect underlying adjustments in local timescales or E/I balance (Gao et al., 2020; Manea et al., 2024; Wilson et al., 2022). Future work combining large-scale network analyses with task-based timescale manipulation or targeted manipulation of the regional E/I balance via brain stimulation will be needed to determine whether the effects observed here are specific to the frontal DMN and DAN, or reflect a more general mechanism of network regulation.

Taken together, our findings demonstrate that microscale GABAergic modulation shapes timescales of regional neuronal populations and large-scale network dynamics, highlighting that microscale synaptic properties can drive macroscale cortical organization.

Methods

This study is part of a larger project that also involves task-based MEG data. The preregistration for the entire experimental protocol can be found at https://doi.org/10.17605/OSF.IO/CMYH2).

Participants

Sixty male participants took part in the study. Due to excessive noise in the MEG signal, three participants (two of whom had non-magnetic retainers) had to be excluded from analysis, leading to a final sample of 57 participants (Age: 23.58 ± 3.36 years, body weight: 74.9 ± 8.36 kg, body mass index: 22.9 ± 2.12, mean ± SD) with normal or corrected to normal vision (N = 13). Most were right-handed (N = 52). Due to the

pharmacological manipulation, we only included participants that did not have certain preexisting medical conditions, such as psychiatric or neurological disorders (full list of exclusion criteria in Supplement 10). Participants were compensated at a fixed rate plus an additional bonus based on their performance in the experimental tasks (see procedure). All participants were naïve to the purpose of the study and gave written informed consent. All procedures were approved by the local Ethics Committee of the Medical Faculty of the Heinrich Heine University Düsseldorf (reference 2018-211_1). The study was performed in compliance with the Code of Ethics of the World Medical Association (Declaration of Helsinki, 1975).

Procedure

The study consisted of a medical screening, three pharmacological MEG sessions, and a structural MRI scan. In the screening, it was ensured that participants met the inclusion criteria (full list in Supplement 12). They filled out the Beck's Depression Inventory (BDI; Beck et al., 1996) and the State-Trait Anxiety Inventory (STAI; Spielberger et al., 1983). Moreover, participants familiarized themselves with the experimental tasks: a value-based decision-making task (VBM), a random-dot motion task (RDM), and a value-based learning task (VBL; experimental tasks will not be explained here but details can be found at https://doi.org/10.17605/OSF.IO/CMYH2). They needed to meet pre-defined performance criteria to participate in the study (see performance-based exclusion criteria in Supplement 10).

The three pharmacological MEG sessions followed identical procedures, only the drug (or placebo) administered differed. In a within-subject, double-blind, cross-over design, participants were given a single oral dose of lorazepam (Tavor®, Pfizer, 1.0mg), D-cycloserine (Thai Meiji Pharmaceutical Co., Ltd., 250 mg), or placebo. MEG sessions were restricted to the morning and separated by at least six days to allow

complete washout, based on the drugs' half-lives (Greenblatt et al., 1979; Patel et al., 2011; Riss et al., 2008; van Berckel et al., 1998). Participants were given a standardized breakfast. Heart rate and blood pressure were measured at three time points per session: before the drug administration, before the MEG measurement, and after the MEG measurement. At the same three time points, participants also filled out the Bond and Lader Visual Analogue Scales to assess drug-related changes in mood (BL-VAS; Bond & Lader, 1974) along with the STAI. Additionally, to control for pharmacological effects on visuomotor processes, participants completed a modified trail-making test before the MEG measurement (Rodewald et al., 2012). The MEG measurement began 2.5 h after drug intake in accordance with the average time for peak plasma concentrations (Greenblatt et al., 1979; Patel et al., 2011; Riss et al., 2008; van Berckel et al., 1998). It started with a 5-minute eyes-open resting state measurement followed by the three experimental tasks (VBM: 30 min, RDM: 50 min, VBL: 20 min). The present analysis focuses on the resting state measurement, and hence the experimental tasks will not be explained here. On the third session, participants were asked to guess the order of drug administration. A total of 26 participants correctly guessed the day they received lorazepam with a mean certainty of m = 58.58% (sd = 20.44%). Similarly, 25 participants correctly guessed the D-cycloserine session, reporting a certainty of m = 56.04% (sd = 21.95%). Lastly, a structural MRI scan was recorded on a separate day for each participant.

Apparatus & resting state measurement

MEG recordings were conducted in a 306-channels whole head MEG system (Elekta Neuromag, Vectorview) with a sampling rate of 1 kHz. Participants' head position inside the scanner was recorded using four head position indicator (HPI) coils placed at the sides of the forehead and both mastoids. Additionally, eye movement and heart

rate were tracked with vertical and horizontal electrooculograms (EOG) and an electrocardiogram (ECG). A full-brain, high-resolution, standard T1-weighted structural magnetic resonance image was acquired from each participant to enable subsequent source reconstruction. To this end, approximately 100 point coordinates were digitized on the participants' scalp to facilitate accurate co-registration of participants' MRI scans with MEG data. We recorded 5-minutes eyes-open resting state measurements during which participants were presented with a fixation dot (radius = 0.4 degrees of visual angle; Thaler et al., 2013). It was designed using the PsychoPy software package (version 3.1.5; Peirce, 2007) and presented on a projector (Panasonic PT-D7700E). The screen dimensions were 43 cm x 35 cm with a resolution of 1,280 × 1,024 pixels and a refresh rate of 60 Hz. Participants were placed at a viewing distance of 80 cm.

Data preprocessing

MEG data was preprocessed with MNE-Python (version 1.0.2; Gramfort et al., 2013) Power line artifacts were removed using the ZapLine method (Rodewald et al., 2012). A 0.1 Hz high-pass filter (FIR filter) was applied. After discarding bad channels based on visual inspection, an independent component analysis (with 60 components) was run (Ablin et al., 2018). Components related to eye movement or heartbeat were removed from the data. Bad time segments were identified through visual inspection and excluded.

Source reconstruction

Source reconstruction and all subsequent analyses were performed on the gradiometer time series. Forward models were constructed using individual anatomical MRIs with a boundary element model (BEM). Noise covariance matrices were estimated from empty-room recordings acquired at the end of each participant's MEG

session. A linearly constrained minimum variance (LCMV; Sekihara & Nagarajan, 2008) beamformer with a regularization parameter of 5 % was computed using the forward model, noise covariance, and data covariance based on the 5 min measurements. Filters were oriented according to the direction of maximal power. Because MEG is less sensitive to radial sources, the denominator rank was reduced by one at each spatial location.

Data analyses

Estimating neuronal timescales

First, we computed the power spectral densities (PSDs) for time series of each vertex using the modified Welch's method, averaging over time segments with the median instead of the mean to reduce the effect of artefacts (10 s segments with 5 s overlap, Hanning window; Gao et al., 2020; Shafiei et al., 2023). The resulting PSDs were split into periodic and aperiodic activity using the FOOOF toolbox (version 1.0.0; Donoghue et al., 2020). Fitting parameters followed recommendations by Donoghue et al. (2020): A maximum number of 6 peaks were fitted with a peak width between 1 – 6 Hz and a height of at least 0.1 log(Hz). The aperiodic mode was set to "knee" in order to capture the bend in the aperiodic signal. As spectral power settled into a rather steady low level at values higher than 40 Hz, we restricted the frequency range to 0.5 – 40 Hz (Lendner et al., 2024). In cases where no aperiodic knee could be fitted to a power spectrum, it was refitted with the aperiodic mode set to "fixed" (this was the case for 14.21 % out of 1417113 vertices). These fits were disregarded for the analysis of timescales, but for completeness, they were included in the supplementary analyses of drug effects on the aperiodic parameters. All resulting models achieved an average goodness of fit of R^2 = 0.94 (*sd* = 0.03).

The aperiodic activity *L* was estimated using a Lorentzian function characterized by an offset *b*, exponent *x*, and knee *k* (Donoghue et al., 2020).:

$$L = b - \log(k + F^x) \quad (1)$$

with F denoting frequency (Hz). We then transformed the knee to the knee frequency (f_k) using the exponent (Donoghue et al., 2020):

$$f_k = k^{\frac{1}{x}} \quad (2)$$

The knee frequency defines the frequency at which the power is no longer constant across frequencies, but instead decreases with increasing frequencies (Donoghue et al., 2020). Finally, using the knee frequency, we could estimate the decay time constant τ of each vertex (Gao et al., 2020):

$$\tau = \frac{1}{2\pi f_k} \quad (3)$$

The decay time constant describes the rate at which the autocorrelation function, which quantifies the signal's self-similarity, decreases over time. For each drug condition, we parcellated the decay time constants into the Desikan-Killiany atlas with 34 cortical regions per hemisphere by computing the median timescale of all vertices in each parcel (Desikan et al., 2006; Shafiei et al., 2023). As a validation check, we correlated our resulting timescale maps with the publicly available intrinsic timescale map (Shafiei et al., 2023; Van Essen et al., 2013).

Analyzing pharmacological effects on timescales

To investigate whether our timescale map follows the anatomical cortical hierarchy, we correlated our map, for each drug condition, with the T1w/T2w ratio, a structural MRI marker of cortical hierarchy (see statistical analyses; Glasser et al., 2016). Drug effects on neuronal timescales were analyzed per parcel using a permutation test. We further analyzed whether the drug effects on the timescales of each parcel were modulated

by their position in the cortical hierarchy. To this end, we implemented a linear mixed-effects model since this approach allows estimating both within- and between-subject variability in accordance with our experimental design (Brown, 2021; Harrison et al., 2018; Jaeger, 2008). Furthermore, we verified that drug effects on neuronal timescales were independent of their effects on control measures (alertness, calmness, contentedness, anxiety, visuomotor processes, heart rate, and blood pressure). For visualization of lorazepam-induced changes in timescales, we computed the percentage change from the placebo to the lorazepam condition.

TDE-HMM on MEG data

Dynamic large-scale cortical networks were identified using a Time-Delay Embedded Hidden Markov Model (TDE-HMM; Vidaurre et al., 2018) as implemented in osl-dynamics (Gohil, Huang, et al., 2024). This data-driven approach identifies transient brain activity states, each representing distinct patterns of multi-regional oscillatory power and phase synchrony, thereby linking local activity to large-scale network dynamics.

Before the HMM analysis, vertex time courses were parcellated according to the Desikan–Killiany atlas (Desikan et al., 2006). For each parcel, the first principal component across all vertices, assigned to the respective parcel, was extracted to generate a representative parcel-level time series, which was then resampled to 250 Hz. Symmetric multivariate leakage correction (Colclough et al., 2015) and sign-flipping (Vidaurre et al., 2016) were subsequently applied to the 68 parcel time series to minimize spatial leakage and resolve dipole orientation ambiguity. The leakage correction reduced direct and inherited signal spread, as well as “ghost interactions” (Palva et al., 2018), while sign-flipping aligned parcel time-course polarities across participants.

Next, the obtained standardized time series were time-delay embedded (± 7 samples) and reduced to 120 principal components via PCA to capture auto- and cross-covariance structures across regions, while reducing computational costs and avoiding overfitting. On these time series, an HMM was run, inferring 8 states that represent unique covariance patterns reflecting specific spectral power and phase-locking profiles.

Since the HMM inference is randomly initialized, repeated runs with identical parameters can produce slightly different results. Accordingly, the fitting procedure was repeated 10 times, and the 8-state TDE-HMM with the lowest variational free energy is presented in the main analyses. To further ensure robustness across the hyperparameter number of states, all analyses were also replicated using models with 10 and 12 states.

State-specific spectral descriptions

Participant-specific spectral state descriptions were estimated post hoc by applying a multi-taper approach to the source-reconstructed data, weighted by the TDE-HMM a-posteriori state probabilities (Vidaurre et al., 2016). Time-resolved power and coherence were computed using seven Slepian tapers with a 2 s window, providing ~2 Hz spectral smoothing. Spectral estimates reflect all occurrences of a given network across visits rather than individual episodes. For visualization, coherence values were thresholded at the 98th percentile to highlight the strongest connections.

State-specific timescales

State-specific timescales were estimated analogously to the state-specific spectral descriptions but using vertex-level rather than parcel-level time series. To reduce the computational load, Welch's method was applied to the weighted, source-

reconstructed data with the same parameters as in the time-averaged spectral analysis (10 s segments, 5 s overlap, Hanning window). As in the time-averaged analysis, state-specific timescales were derived from vertex-level power spectra, and parcel-level estimates were obtained as the median across all vertices within each parcel. For the visualization of state-specific changes in timescales, we computed the percentage change from the placebo to the lorazepam condition.

Transition probability analysis

To assess whether transitions between large-scale cortical networks were modulated by the drug condition, transition probability matrices were estimated post hoc from each participant's hard-classified state time course under placebo and lorazepam. Hard-classified state time courses were obtained by assigning each time point to the most likely HMM state based on the posterior probabilities. For visualization, changes in transition probabilities were expressed as percentage differences between conditions.

Statistical analyses

Within-subject comparisons

To assess timescale alterations between pharmacological conditions and between state-specific and time-averaged spectra within participants, two-tailed permutation tests with 10,000 permutations were conducted (Nichols & Holmes, 2002). Resulting *p*-values were corrected for multiple comparisons across parcels, or across parcels and states, using the false discovery rate (FDR) procedure (Genovese et al., 2002). Comparisons were considered significant when FDR-corrected values fell below α = 0.05, both for these analyses and for all other statistical tests.

Drug-related alterations in transition probabilities and state metrics were also assessed using within-participant, two-tailed permutation tests with 10,000

permutations (Nichols & Holmes, 2002). To account for potential dependencies between tests (including the negative correlations arising from row-sum constraints in transition probabilities and the compositional nature of state metrics) statistical significance was determined using maximum t-statistic pooling, as implemented in GLMTOOLs (Quinn et al., 2024), across states, or across states and state transitions, to control for multiple comparisons.

We used a linear mixed-effects model to investigate if the drug effects on the timescales of each parcel were modulated by their position in the cortical hierarchy. The model was implemented in R using the lme4 package (R version 4.2.2; lme4 version 1.1.34; D. Bates et al., 2015; R Development Core Team, 2022). We applied a logarithmic transformation to the outcome variable "timescales" since the distribution was positively skewed. Fixed effects included the main effects and interactions of cortical hierarchy (defined by the T1w/T2w) and drug (lorazepam vs. placebo and D-cycloserine vs. placebo). Following a PCA, the random effect structure includes the main effects of both cortical hierarchy and drug (Douglas Bates et al., 2015). Additionally, as a control analysis, we verified that our drug effects were independent of session order by adding it to the model as a fixed effect. The same approach was implemented for other control measures (mood, anxiety, visuomotor processes, heart rate, and blood pressure) that were significantly modulated by the drug condition.

Spatial comparisons

To compare our estimated timescales with a publicly available intrinsic timescale brain map (Shafiei et al., 2023; Van Essen et al., 2013) and an MRI-based T1w/T2w ratio brain map (Glasser et al., 2016), we ran Spearman correlations and computed significance using spatial autocorrelation-preserving permutation tests (Alexander-Bloch et al., 2018; Hansen et al., 2022; Markello et al., 2022; Vása & Misic, 2022).

Before spatial comparisons, both maps were parcellated into the cortical Desikan-Killiany parcellation (Cammoun et al., 2012; Desikan et al., 2006). Additionally, the publicly available intrinsic timescale map was transformed from 4k to 32k density (Robinson et al., 2018; Robinson et al., 2014).

Data and code availability

The conditions of our ethics approval do not permit public archiving of the data supporting this study. Sharing data requires a formal data-sharing agreement following ethics procedures governing the re-use of sensitive data. Readers seeking access to the data should contact the first authors. All analysis scripts are publicly available on GitHub: https://github.com/anadiasmaile/GABA-NMDA-timescales.

References

Abeysuriya, R. G., Hadida, J., Sotiropoulos, S. N., Jbabdi, S., Becker, R., Hunt, B. A. E., Brookes, M. J., & Woolrich, M. W. (2018). A biophysical model of dynamic balancing of excitation and inhibition in fast oscillatory large-scale networks. *Plos Computational Biology*, *14*(2), e1006007. https://doi.org/10.1371/journal.pcbi.1006007

Ablin, P., Cardoso, J.-F., & Gramfort, A. (2018). Faster Independent Component Analysis by preconditioning with Hessian approximations. *IEEE Transactions on Signal Processing*, *66*(15), 4040–4049. https://doi.org/10.1109/TSP.2018.2844203

Alberto, C. O., & Hirasawa, M. (2010). AMPA receptor-mediated miniature EPSCs have heterogeneous time courses in orexin neurons. *Biochem Biophys Res Commun*, *400*(4), 707–712. https://doi.org/10.1016/j.bbrc.2010.08.132

Alexander-Bloch, A. F., Shou, H. C., Liu, S. Y., Satterthwaite, T. D., Glahn, D. C., Shinohara, R. T., Vandekar, S. N., & Raznahan, A. (2018). On testing for spatial correspondence between maps of human brain structure and function. *Neuroimage*, *178*, 540–551. https://doi.org/10.1016/j.neuroimage.2018.05.070

Angulo, M. C., Rossier, J., & Audinat, E. (1999). Postsynaptic glutamate receptors and integrative properties of fast-spiking interneurons in the rat neocortex. *J Neurophysiol*, *82*(3), 1295–1302. https://doi.org/10.1152/jn.1999.82.3.1295

Baker, A. P., Brookes, M. J., Rezek, I. A., Smith, S. M., Behrens, T., Probert Smith, P. J., & Woolrich, M. (2014). Fast transient networks in spontaneous human brain activity. *Elife*, *3*, e01867. https://doi.org/10.7554/eLife.01867

Baldassano, C., Chen, J., Zadbood, A., Pillow, J. W., Hasson, U., & Norman, K. A. (2017). Discovering Event Structure in Continuous Narrative Perception and Memory. *Neuron*, *95*(3), 709–721 e705. https://doi.org/10.1016/j.neuron.2017.06.041

Bates, D., Kliegl, R., Vasishth, S., & Baayen, H. (2015). Parsimonious mixed models. https://arxiv.org/abs/1506.04967

Bates, D., Machler, M., Bolker, B. M., & Walker, S. C. (2015). Fitting Linear Mixed-Effects Models Using lme4. *Journal of Statistical Software*, *67*(1), 1–48. https://doi.org/DOI 10.18637/jss.v067.i01

Beck, A. T., Steer, R. A., & Brown, G. K. (1996). *Manual for the Beck Depression Inventory–II*. Psychological Corporation.

Bernacchia, A., Seo, H., Lee, D., & Wang, X. J. (2011). A reservoir of time constants for memory traces in cortical neurons. *Nat Neurosci*, *14(3)*, 366–372. https://doi.org/10.1038/nn.2752

Bond, A., & Lader, M. (1974). The use of analogue scales in rating subjective feelings. *British Journal of Medical Psychology*.

Bressler, S. L. (1995). Large-scale cortical networks and cognition. *Brain Res Brain Res Rev*, *20*(3), 288–304. https://doi.org/10.1016/0165-0173(94)00016-I

Brown, V. A. (2021). An Introduction to Linear Mixed-Effects Modeling in R. *Advances in Methods and Practices in Psychological Science*, *4*(1). https://doi.org/10.1177/2515245920960351

Burt, J. B., Demirtas, M., Eckner, W. J., Navejar, N. M., Ji, J. L., Martin, W. J., Bernacchia, A., Anticevic, A., & Murray, J. D. (2018). Hierarchy of transcriptomic specialization across human cortex captured by structural neuroimaging topography. *Nat Neurosci*, *21(9)*, 1251–1259. https://doi.org/10.1038/s41593-018-0195-0

Cammoun, L., Gigandet, X., Meskaldji, D., Thiran, J. P., Sporns, O., Do, K. Q., Maeder, P., Meuli, R., & Hagmann, P. (2012). Mapping the human connectome at multiple scales with diffusion spectrum MRI. *Journal of Neuroscience Methods*, *203*(2), 386–397. https://doi.org/10.1016/j.jneumeth.2011.09.031

Çatal, Y., Wolman, A., Abbasi, S., & Northoff, G. (2023). Intrinsic neural timescales attenuate information transfer along the uni-transmodal hierarchy. *bioRxiv*, 2023.2007.2028.551047. https://doi.org/10.1101/2023.07.28.551047

Chapman, C. A., Nuwer, J. L., & Jacob, T. C. (2022). The Yin and Yang of GABAergic and Glutamatergic Synaptic Plasticity: Opposites in Balance by Crosstalking Mechanisms. *Front Synaptic Neurosci*, *14*, 911020. https://doi.org/10.3389/fnsyn.2022.911020

Colclough, G. L., Brookes, M. J., Smith, S. M., & Woolrich, M. W. (2015). A symmetric multivariate leakage correction for MEG connectomes. *Neuroimage*, *117*, 439–448. https://doi.org/10.1016/j.neuroimage.2015.03.071

Colombi, I., Rastogi, M., Parrini, M., Alberti, M., Potenzieri, A., Chellali, M. M., Rosati, S., Chiappalone, M., Nanni, M., Contestabile, A., & Cancedda, L. (2024). Heterogeneous subpopulations of GABA(A)R-responding neurons coexist across neuronal network scales and developmental stages in health and disease. *iScience*, *27*(4), 109438. https://doi.org/10.1016/j.isci.2024.109438

Colombo, M. A., Napolitani, M., Boly, M., Gosseries, O., Casarotto, S., Rosanova, M., Brichant, J. F., Boveroux, P., Rex, S., Laureys, S., Massimini, M., Chieregato, A., & Sarasso, S. (2019). The spectral exponent of the resting EEG indexes the presence of consciousness during unresponsiveness induced by propofol, xenon, and ketamine. *Neuroimage*, *189*, 631–644. https://doi.org/10.1016/j.neuroimage.2019.01.024

Cusinato, R., Alnes, S. L., van Maren, E., Boccalaro, I., Ledergerber, D., Adamantidis, A., Imbach, L. L., Schindler, K., Baud, M. O., & Tzovara, A. (2023). Intrinsic Neural Timescales in the Temporal Lobe Support an Auditory Processing Hierarchy. *J Neurosci*, *43*(20), 3696–3707. https://doi.org/10.1523/JNEUROSCI.1941-22.2023

Desikan, R. S., Segonne, F., Fischl, B., Quinn, B. T., Dickerson, B. C., Blacker, D., Buckner, R. L., Dale, A. M., Maguire, R. P., Hyman, B. T., Albert, M. S., & Killiany, R. J. (2006). An automated labeling system for subdividing the human cerebral cortex on MRI scans into gyral based regions of interest. *Neuroimage*, *31*(3), 968–980. https://doi.org/10.1016/j.neuroimage.2006.01.021

Di Lazzaro, V., Oliviero, A., Saturno, E., Dileone, M., Pilato, F., Nardone, R., Ranieri, F., Musumeci, G., Fiorilla, T., & Tonali, P. (2005). Effects of lorazepam on short latency afferent inhibition and short latency intracortical inhibition in humans. *J Physiol*, *564*(Pt 2), 661–668. https://doi.org/10.1113/jphysiol.2004.061747

Di Lazzaro, V., Pilato, F., Dileone, M., Tonali, P. A., & Ziemann, U. (2005). Dissociated effects of diazepam and lorazepam on short-latency afferent inhibition. *J Physiol*, *569*(Pt 1), 315–323. https://doi.org/10.1113/jphysiol.2005.092155

Donoghue, T., Haller, M., Peterson, E. J., Varma, P., Sebastian, P., Gao, R., Noto, T., Lara, A. H., Wallis, J. D., Knight, R. T., Shestyuk, A., & Voytek, B. (2020). Parameterizing neural power spectra into periodic and aperiodic components. *Nature Neuroscience*, *23*(12), 1655–U1288. https://doi.org/10.1038/s41593-020-00744-x

Engin, E., Benham, R. S., & Rudolph, U. (2018). An Emerging Circuit Pharmacology of GABA(A) Receptors. *Trends Pharmacol Sci*, *39*(8), 710–732. https://doi.org/10.1016/j.tips.2018.04.003

Espinosa, F., & Kavalali, E. T. (2009). NMDA receptor activation by spontaneous glutamatergic neurotransmission. *J Neurophysiol*, *101*(5), 2290–2296. https://doi.org/10.1152/jn.90754.2008

Fox, M. D., Snyder, A. Z., Vincent, J. L., Corbetta, M., Van Essen, D. C., & Raichle, M. E. (2005). The human brain is intrinsically organized into dynamic, anticorrelated functional networks. *Proc Natl Acad Sci U S A*, *102*(27), 9673–9678. https://doi.org/10.1073/pnas.0504136102

Fritschy, J. M., & Mohler, H. (1995). GABAA-receptor heterogeneity in the adult rat brain: differential regional and cellular distribution of seven major subunits. *J Comp Neurol*, *359*(1), 154–194. https://doi.org/10.1002/cne.903590111

Froböse, M. I., & Ort, E. (2022). *Glutamatergic And GABAergic Effects On Learning And Decision Making: A Pharmacological MEG Study With Lorazepam, D-Cycloserine And Placebo*. https://doi.org/10.17605/OSF.IO/CMYH2

Gao, R., Peterson, E. J., & Voytek, B. (2017). Inferring synaptic excitation/inhibition balance from field potentials. *Neuroimage*, *158*, 70–78. https://doi.org/10.1016/j.neuroimage.2017.06.078

Gao, R., van den Brink, R. L., Pfeffer, T., & Voytek, B. (2020). Neuronal timescales are functionally dynamic and shaped by cortical microarchitecture. *Elife*, *9*. https://doi.org/10.7554/eLife.61277

Genovese, C. R., Lazar, N. A., & Nichols, T. (2002). Thresholding of statistical maps in functional neuroimaging using the false discovery rate. *Neuroimage*, *15*(4), 870–878. https://doi.org/10.1006/nimg.2001.1037

Glasser, M. F., Coalson, T. S., Robinson, E. C., Hacker, C. D., Harwell, J., Yacoub, E., Ugurbil, K., Andersson, J., Beckmann, C. F., Jenkinson, M., Smith, S. M., & Van Essen, D. C. (2016). A multi-modal parcellation of human cerebral cortex. *Nature*, *536*(7615), 171–+. https://doi.org/10.1038/nature18933

Gohil, C., Huang, R., Higgins, C., van Es, M. W. J., Quinn, A. J., Vidaurre, D., & Woolrich, M. W. (2026). Canonical Hidden Markov Model Networks for Studying

M/EEG. *bioRxiv*, 2025.2010.2021.683692. https://doi.org/10.1101/2025.10.21.683692

Gohil, C., Huang, R., Roberts, E., van Es, M. W. J., Quinn, A. J., Vidaurre, D., & Woolrich, M. W. (2024). osl-dynamics, a toolbox for modeling fast dynamic brain activity. *Elife*, *12*. https://doi.org/10.7554/eLife.91949

Gohil, C., Kohl, O., Huang, R., van Es, M. W. J., Parker Jones, O., Hunt, L. T., Quinn, A. J., & Woolrich, M. W. (2024). Dynamic network analysis of electrophysiological task data. *Imaging Neurosci (Camb)*, *2*. https://doi.org/10.1162/imag_a_00226

Gohil, C., Kohl, O., Pitt, J., van Es, M. W. J., Quinn, A. J., Vidaurre, D., Turner, M. R., Nobre, A. C., & Woolrich, M. W. (2024). Effects of age on resting-state cortical networks. *bioRxiv*, 2024.2009.2023.614004. https://doi.org/10.1101/2024.09.23.614004

Gramfort, A., Luessi, M., Larson, E., Engemann, D. A., Strohmeier, D., Brodbeck, C., Goj, R., Jas, M., Brooks, T., Parkkonen, L., & Hamalainen, M. (2013). MEG and EEG data analysis with MNE-Python. *Front Neurosci*, *7*, 267. https://doi.org/10.3389/fnins.2013.00267

Greenblatt, D. J., Schillings, R. T., Kyriakopoulos, A. A., Shader, R. I., Sisenwine, S. F., Knowles, J. A., & Ruelius, H. W. (1976). Clinical pharmacokinetics of lorazepam. I. Absorption and disposition of oral 14C-lorazepam. *Clin Pharmacol Ther*, *20*(3), 329–341. https://doi.org/10.1002/cpt1976203329

Gupta, A., Wang, Y., & Markram, H. (2000). Organizing principles for a diversity of GABAergic interneurons and synapses in the neocortex. *Science*, *287*(5451), 273–278. https://doi.org/10.1126/science.287.5451.273

Halgren, M., Kang, R., Voytek, B., Ulbert, I., Fabo, D., Eross, L., Wittner, L., Madsen, J., Doyle, W. K., Devinsky, O., Halgren, E., Harnett, M. T., & Cash, S. S. (2021). The timescale and magnitude of 1/f aperiodic activity decrease with cortical depth in humans, macaques, and mice. *bioRxiv*, 2021.2007.2028.454235. https://doi.org/10.1101/2021.07.28.454235

Hansen, J. Y., Shafiei, G., Markello, R. D., Smart, K., Cox, S. M. L., Norgaard, M., Beliveau, V., Wu, Y., Gallezot, J. D., Aumont, E., Servaes, S., Scala, S. G., DuBois, J. M., Wainstein, G., Bezgin, G., Funck, T., Schmitz, T. W., Spreng, R. N., Galovic, M., Misic, B. (2022). Mapping neurotransmitter systems to the structural and functional organization of the human neocortex. *Nat Neurosci*, *25*(11), 1569–1581. https://doi.org/10.1038/s41593-022-01186-3

Harrison, X. A., Donaldson, L., Correa-Cano, M. E., Evans, J., Fisher, D. N., Goodwin, C. E. D., Robinson, B. S., Hodgson, D. J., & Inger, R. (2018). A brief introduction to mixed effects modelling and multi-model inference in ecology. *PeerJ*, *6*, e4794. https://doi.org/10.7717/peerj.4794

Heistek, T. S., Ruiperez-Alonso, M., Timmerman, A. J., Brussaard, A. B., & Mansvelder, H. D. (2013). alpha2-containing GABAA receptors expressed in hippocampal region CA3 control fast network oscillations. *J Physiol*, *591*(4), 845–858. https://doi.org/10.1113/jphysiol.2012.243725

Honey, C. J., Thesen, T., Donner, T. H., Silbert, L. J., Carlson, C. E., Devinsky, O., Doyle, W. K., Rubin, N., Heeger, D. J., & Hasson, U. (2012). Slow cortical dynamics and the accumulation of information over long timescales. *Neuron*, *76*(2), 423–434. https://doi.org/10.1016/j.neuron.2012.08.011

Isaacson, J. S., & Scanziani, M. (2011). How inhibition shapes cortical activity. *Neuron*, *72*(2), 231–243. https://doi.org/10.1016/j.neuron.2011.09.027

Ito, T., Hearne, L. J., & Cole, M. W. (2020). A cortical hierarchy of localized and distributed processes revealed via dissociation of task activations, connectivity changes, and intrinsic timescales. *Neuroimage*, *221*, 117141. https://doi.org/10.1016/j.neuroimage.2020.117141

Jaeger, T. F. (2008). Categorical Data Analysis: Away from ANOVAs (transformation or not) and towards Logit Mixed Models. *J Mem Lang*, *59*(4), 434–446. https://doi.org/10.1016/j.jml.2007.11.007

Kohl, O., Gohil, C., Zokaei, N., Hu, M. T. M., Nobre, A. C., Woolrich, M., & Quinn, A. (2025). Changes in sensorimotor network dynamics in resting-state recordings in Parkinson's disease. *Brain Commun*, *7*(4), fcaf282. https://doi.org/10.1093/braincomms/fcaf282

la Fougere, C., Grant, S., Kostikov, A., Schirrmacher, R., Gravel, P., Schipper, H. M., Reader, A., Evans, A., & Thiel, A. (2011). Where in-vivo imaging meets cytoarchitectonics: the relationship between cortical thickness and neuronal density measured with high-resolution [18F]flumazenil-PET. *Neuroimage*, *56*(3), 951–960. https://doi.org/10.1016/j.neuroimage.2010.11.015

Lendner, J. D., Lin, J. J., Larsson, P. G., & Helfrich, R. F. (2024). Multiple Intrinsic Timescales Govern Distinct Brain States in Human Sleep. *J Neurosci*, *44*(42). https://doi.org/10.1523/JNEUROSCI.0171-24.2024

Lerner, Y., Honey, C. J., Silbert, L. J., & Hasson, U. (2011). Topographic mapping of a hierarchy of temporal receptive windows using a narrated story. *J Neurosci*, *31*(8), 2906–2915. https://doi.org/10.1523/JNEUROSCI.3684-10.2011

Manea, A. M. G., Maisson, D. J., Voloh, B., Zilverstand, A., Hayden, B., & Zimmermann, J. (2024). Neural timescales reflect behavioral demands in freely moving rhesus macaques. *Nat Commun*, *15*(1), 2151. https://doi.org/10.1038/s41467-024-46488-1

Markello, R. D., Hansen, J. Y., Liu, Z. Q., Bazinet, V., Shafiei, G., Suarez, L. E., Blostein, N., Seidlitz, J., Baillet, S., Satterthwaite, T. D., Chakravarty, M. M., Raznahan, A., & Misic, B. (2022). neuromaps: structural and functional interpretation of brain maps. *Nat Methods*, *19*(11), 1472–1479. https://doi.org/10.1038/s41592-022-01625-w

McIntosh, A. R. (2000). Towards a network theory of cognition. *Neural Netw*, *13*(8-9), 861–870. https://doi.org/10.1016/s0893-6080(00)00059-9

Mesulam, M. M. (1998). From sensation to cognition. *Brain*, *121 (Pt 6)*, 1013–1052. https://doi.org/10.1093/brain/121.6.1013

Murray, J. D., Bernacchia, A., Freedman, D. J., Romo, R., Wallis, J. D., Cai, X., Padoa-Schioppa, C., Pasternak, T., Seo, H., Lee, D., & Wang, X. J. (2014). A hierarchy

of intrinsic timescales across primate cortex. *Nat Neurosci*, *17*(12), 1661–1663. https://doi.org/10.1038/nn.3862

Myme, C. I., Sugino, K., Turrigiano, G. G., & Nelson, S. B. (2003). The NMDA-to-AMPA ratio at synapses onto layer 2/3 pyramidal neurons is conserved across prefrontal and visual cortices. *J Neurophysiol*, *90*(2), 771–779. https://doi.org/10.1152/jn.00070.2003

Nichols, T. E., & Holmes, A. P. (2002). Nonparametric permutation tests for functional neuroimaging: A primer with examples. *Human Brain Mapping*, *15*(1), 1–25. https://doi.org/DOI 10.1002/hbm.1058

Norgaard, M., Beliveau, V., Ganz, M., Svarer, C., Pinborg, L. H., Keller, S. H., Jensen, P. S., Greve, D. N., & Knudsen, G. M. (2021). A high-resolution in vivo atlas of the human brain's benzodiazepine binding site of GABA(A) receptors. *Neuroimage*, *232*, 117878. https://doi.org/10.1016/j.neuroimage.2021.117878

Nutt, D., Wilson, S., Lingford-Hughes, A., Myers, J., Papadopoulos, A., & Muthukumaraswamy, S. (2015). Differences between magnetoencephalographic (MEG) spectral profiles of drugs acting on GABA at synaptic and extrasynaptic sites: a study in healthy volunteers. *Neuropharmacology*, *88*, 155–163. https://doi.org/10.1016/j.neuropharm.2014.08.017

Palva, J. M., Wang, S. H., Palva, S., Zhigalov, A., Monto, S., Brookes, M. J., Schoffelen, J. M., & Jerbi, K. (2018). Ghost interactions in MEG/EEG source space: A note of caution on inter-areal coupling measures. *Neuroimage*, *173*, 632–643. https://doi.org/10.1016/j.neuroimage.2018.02.032

Pascoa Dos Santos, F., & Verschure, P. (2025). Metastable dynamics emerge from local excitatory-inhibitory homeostasis in the cortex at rest. *Netw Neurosci*, *9*(3), 938–968. https://doi.org/10.1162/netn_a_00460

Patel, B., Bright, D. P., Mortensen, M., Frolund, B., & Smart, T. G. (2016). Context-Dependent Modulation of GABAAR-Mediated Tonic Currents. *J Neurosci*, *36*(2), 607–621. https://doi.org/10.1523/JNEUROSCI.2047-15.2016

Patel, D. S., Sharma, N., Patel, M. C., Patel, B. N., Shrivastav, P. S., & Sanyal, M. (2011). Development and validation of a selective and sensitive LC-MS/MS method for determination of cycloserine in human plasma: application to bioequivalence study. *J Chromatogr B Analyt Technol Biomed Life Sci*, *879*(23), 2265–2273. https://doi.org/10.1016/j.jchromb.2011.06.011

Peirce, J. W. (2007). PsychoPy--Psychophysics software in Python. *J Neurosci Methods*, *162*(1-2), 8–13. https://doi.org/10.1016/j.jneumeth.2006.11.017

Quinn, A. J., Atkinson, L. Z., Gohil, C., Kohl, O., Pitt, J., Zich, C., Nobre, A. C., & Woolrich, M. W. (2024). The GLM-spectrum: A multilevel framework for spectrum analysis with covariate and confound modelling. *Imaging Neurosci (Camb)*, *2*. https://doi.org/10.1162/imag_a_00082

Quinn, A. J., Vidaurre, D., Abeysuriya, R., Becker, R., Nobre, A. C., & Woolrich, M. W. (2018). Task-Evoked Dynamic Network Analysis Through Hidden Markov

Modeling. *Frontiers in Neuroscience*, *12*. https://doi.org/10.3389/fnins.2018.00603

R Development Core Team. (2022). *R: A Language and Environment for Statistical Computing*. In (Version 4.2.2) R Foundation for Statistical Computing.

Rabinovich, M. I., Huerta, R., Varona, P., & Afraimovich, V. S. (2008). Transient cognitive dynamics, metastability, and decision making. *Plos Computational Biology*, *4(5)*, e1000072. https://doi.org/10.1371/journal.pcbi.1000072

Riss, J., Cloyd, J., Gates, J., & Collins, S. (2008). Benzodiazepines in epilepsy: pharmacology and pharmacokinetics. *Acta Neurol Scand*, *118*(2), 69–86. https://doi.org/10.1111/j.1600-0404.2008.01004.x

Robinson, E. C., Garcia, K., Glasser, M. F., Chen, Z. D., Coalson, T. S., Makropoulos, A., Bozek, J., Wright, R., Schuh, A., Webster, M., Hutter, J., Price, A., Grande, L. C., Hughes, E., Tusor, N., Bayly, P. V., Van Essen, D. C., Smith, S. M., Edwards, A. D., Rueckert, D. (2018). Multimodal surface matching with higher-order smoothness constraints. *Neuroimage*, *167*, 453–465. https://doi.org/10.1016/j.neuroimage.2017.10.037

Robinson, E. C., Jbabdi, S., Glasser, M. F., Andersson, J., Burgess, G. C., Harms, M. P., Smith, S. M., Van Essen, D. C., & Jenkinson, M. (2014). MSM: a new flexible framework for Multimodal Surface Matching. *Neuroimage*, *100*, 414–426. https://doi.org/10.1016/j.neuroimage.2014.05.069

Rodewald, K., Bartolovic, M., Debelak, R., Aschenbrenner, S., Weisbrod, M., & Roesch-Ely, D. (2012). Eine Normierungsstudie eines modifizierten Trail Making Tests im deutschsprachigen Raum. *Zeitschrift für Neuropsychologie*, *23*(1), 37–48. https://doi.org/10.1024/1016-264X/a000060

Rossi, C., Vidaurre, D., Costers, L., Akbarian, F., Woolrich, M., Nagels, G., & Van Schependom, J. (2023). A data-driven network decomposition of the temporal, spatial, and spectral dynamics underpinning visual-verbal working memory processes. *Commun Biol*, *6*(1), 1079. https://doi.org/10.1038/s42003-023-05448-z

Rossi, C., Vidaurre, D., Costers, L., D'Hooghe M, B., Akbarian, F., D'Haeseleer, M., Woolrich, M., Nagels, G., & Van Schependom, J. (2024). Disrupted working memory event-related network dynamics in multiple sclerosis. *Commun Biol*, *7*(1), 1592. https://doi.org/10.1038/s42003-024-07283-2

Routley, B. C., Singh, K. D., Hamandi, K., & Muthukumaraswamy, S. D. (2017). The effects of AMPA receptor blockade on resting magnetoencephalography recordings. *J Psychopharmacol*, *31*(12), 1527–1536. https://doi.org/10.1177/0269881117736915

Rudolph, U., & Knoflach, F. (2011). Beyond classical benzodiazepines: novel therapeutic potential of GABAA receptor subtypes. *Nat Rev Drug Discov*, *10*(9), 685–697. https://doi.org/10.1038/nrd3502

Sah, P., Hestrin, S., & Nicoll, R. A. (1990). Properties of excitatory postsynaptic currents recorded in vitro from rat hippocampal interneurones. *J Physiol*, *430*, 605–616. https://doi.org/10.1113/jphysiol.1990.sp018310

Sekihara, K., & Nagarajan, S. S. (2008). *Adaptive Spatial Filters for Electromagnetic Brain Imaging*. Springer. https://doi.org/10.1007/978-3-540-79370-0

Shafiei, G., Fulcher, B. D., Voytek, B., Satterthwaite, T. D., Baillet, S., & Misic, B. (2023). Neurophysiological signatures of cortical micro-architecture. *Nat Commun*, *14*(1), 6000. https://doi.org/10.1038/s41467-023-41689-6

Soyuhos, O., Zirnsak, M., Chaudhuri, R., & Chen, X. (2026). Selective control of prefrontal neural timescales by parietal cortex. *Nat Commun*. https://doi.org/10.1038/s41467-026-70326-1

Spielberger, C. D., Gorsuch, R. L., Lushene, R., Vagg, P. R., & Jacobs, G. A. (1983). *Manual for the State-Trait Anxiety Inventory (Form Y)*. Consulting Psychologists Press.

Tallman, J. F., Thomas, J. W., & Gallager, D. W. (1978). GABAergic modulation of benzodiazepine binding site sensitivity. *Nature*, *274*(5669), 383–385. https://doi.org/10.1038/274383a0

Thaler, L., Schütz, A. C., Goodale, M. A., & Gegenfurtner, K. R. (2013). What is the best fixation target? The effect of target shape on stability of fixational eye movements. *Vision Research*, *76*, 31–42. https://doi.org/10.1016/j.visres.2012.10.012

Thomas, J. W., Hood, W. F., Monahan, J. B., Contreras, P. C., & O'Donohue, T. L. (1988). Glycine modulation of the phencyclidine binding site in mammalian brain. *Brain Res*, *442*(2), 396–398. https://doi.org/10.1016/0006-8993(88)91533-8

Tognoli, E., & Kelso, J. A. (2014). The metastable brain. *Neuron*, *81(1)*, 35–48. https://doi.org/10.1016/j.neuron.2013.12.022

van Berckel, B. N., Lipsch, C., Gispen-de Wied, C., Wynne, H. J., Blankenstein, M. A., van Ree, J. M., & Kahn, R. S. (1998). The partial NMDA agonist D-cycloserine stimulates LH secretion in healthy volunteers. *Psychopharmacology (Berl)*, *138*(2), 190–197. https://doi.org/10.1007/s002130050662

van Es, M. W. J., Higgins, C., Gohil, C., Quinn, A. J., Vidaurre, D., & Woolrich, M. W. (2025). Large-scale cortical functional networks are organized in structured cycles. *Nat Neurosci*, *28*(10), 2118–2128. https://doi.org/10.1038/s41593-025-02052-8

Van Essen, D. C., Smith, S. M., Barch, D. M., Behrens, T. E., Yacoub, E., Ugurbil, K., & Consortium, W. U.-M. H. (2013). The WU-Minn Human Connectome Project: an overview. *Neuroimage*, *80*, 62–79. https://doi.org/10.1016/j.neuroimage.2013.05.041

Vargas-Caballero, M., & Robinson, H. P. (2004). Fast and slow voltage-dependent dynamics of magnesium block in the NMDA receptor: the asymmetric trapping block model. *J Neurosci*, *24*(27), 6171–6180. https://doi.org/10.1523/JNEUROSCI.1380-04.2004

Vása, F., & Misic, B. (2022). Null models in network neuroscience. *Nature Reviews Neuroscience*, *23*(8), 493–504. https://doi.org/10.1038/s41583-022-00601-9

Vidaurre, D., Hunt, L. T., Quinn, A. J., Hunt, B. A. E., Brookes, M. J., Nobre, A. C., & Woolrich, M. W. (2018). Spontaneous cortical activity transiently organises into frequency specific phase-coupling networks. *Nature Communications*, *9*. https://doi.org/10.1038/s41467-018-05316-z

Vidaurre, D., Quinn, A. J., Baker, A. P., Dupret, D., Tejero-Cantero, A., & Woolrich, M. W. (2016). Spectrally resolved fast transient brain states in electrophysiological data. *Neuroimage*, *126*, 81–95. https://doi.org/10.1016/j.neuroimage.2015.11.047

Wang, H., Stradtman, G. G., 3rd, Wang, X. J., & Gao, W. J. (2008). A specialized NMDA receptor function in layer 5 recurrent microcircuitry of the adult rat prefrontal cortex. *Proc Natl Acad Sci U S A*, *105*(43), 16791–16796. https://doi.org/10.1073/pnas.0804318105

Wang, M., Yang, Y., Wang, C. J., Gamo, N. J., Jin, L. E., Mazer, J. A., Morrison, J. H., Wang, X. J., & Arnsten, A. F. (2013). NMDA receptors subserve persistent neuronal firing during working memory in dorsolateral prefrontal cortex. *Neuron*, *77*(4), 736–749. https://doi.org/10.1016/j.neuron.2012.12.032

Wang, X. J. (1999). Synaptic basis of cortical persistent activity: the importance of NMDA receptors to working memory. *J Neurosci*, *19*(21), 9587–9603. https://doi.org/10.1523/JNEUROSCI.19-21-09587.1999

Wang, X. J. (2002). Probabilistic decision making by slow reverberation in cortical circuits. *Neuron*, *36*(5), 955–968. https://doi.org/10.1016/s0896-6273(02)01092-9

Wang, X. J. (2008). Decision making in recurrent neuronal circuits. *Neuron*, *60*(2), 215–234. https://doi.org/10.1016/j.neuron.2008.09.034

Wang, X. J. (2020). Macroscopic gradients of synaptic excitation and inhibition in the neocortex. *Nat Rev Neurosci*, *21*(3), 169–178. https://doi.org/10.1038/s41583-020-0262-x

Waschke, L., Donoghue, T., Fiedler, L., Smith, S., Garrett, D. D., Voytek, B., & Obleser, J. (2021). Modality-specific tracking of attention and sensory statistics in the human electrophysiological spectral exponent. *Elife*, *10*. https://doi.org/10.7554/eLife.70068

Wilson, L. E., da Silva Castanheira, J., & Baillet, S. (2022). Time-resolved parameterization of aperiodic and periodic brain activity. *Elife*, *11*. https://doi.org/10.7554/eLife.77348

Supplement 1: Lorazepam effect on neuronal timescales – significant parcels

Figure S1: Lorazepam effect on neuronal timescales – significant parcels. t-statistic derived from a permutation test of the effect of lorazepam on neuronal timescales compared to placebo projected onto the cortical surface. Non-significant parcels are depicted in white. Multiple comparisons across parcels were FDR-corrected. Lorazepam significantly increased neuronal timescales across almost the entire cortex.

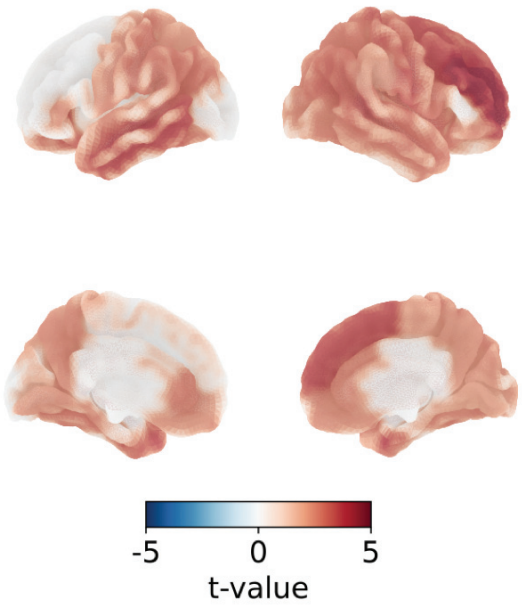

Supplement 2: Drug effects on aperiodic parameters

In order to assess the effects of lorazepam and D-cycloserine on the aperiodic signal of each cortical region, we performed a two-tailed paired-sample permutation t-test comparing the aperiodic parameters under placebo to both drugs. For each permutation test, we ran 10,000 permutations and applied FDR correction for multiple comparisons.

Figure S2: Drug effects on aperiodic exponent. (**a**) Lorazepam significantly decreased the aperiodic exponent in the left entorhinal cortex (t = -3.33, p = 0.034), left pericalcarine cortex (t = -3.37, p = 0.034) and the right lateral occipital cortex (t = -3.66, p = 0.014). Therefore, the slope of the aperiodic signal was significantly flatter in these cortical regions under Lorazepam. (**b**) In contrast, D-cycloserine had no significant effect on the aperiodic exponent.

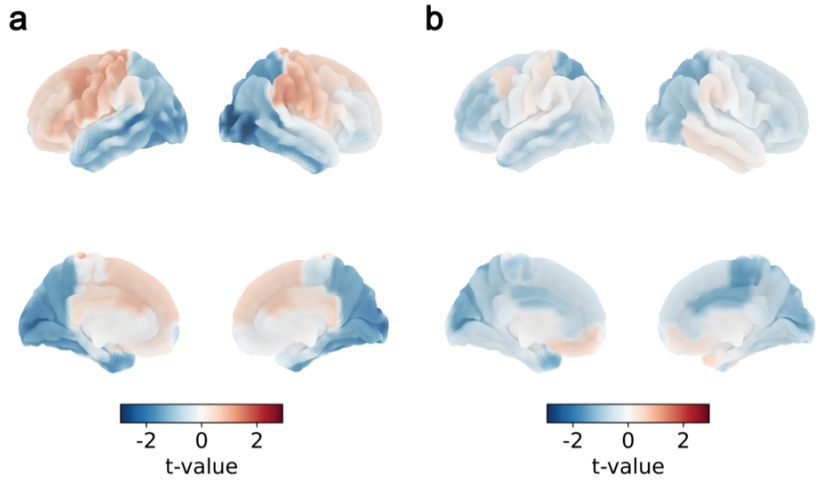

Figure S3: Drug effects on aperiodic knee frequency. (**a**) Lorazepam and (**b**) D-cycloserine had no significant effect on the cortical aperiodic knee frequency.

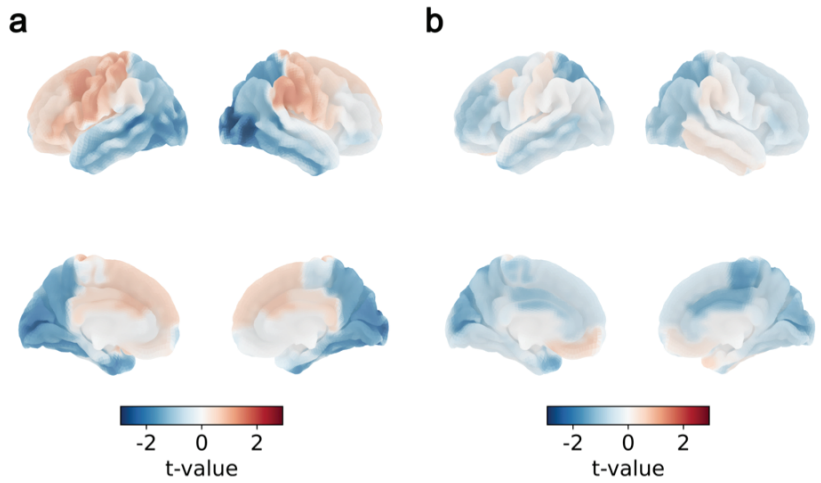

Figure S4: Drug effects on aperiodic offset. (**a**) Lorazepam significantly decreased the aperiodic offset in the right lateral occipital cortex (t = -3.33; p = 0.034). (**b**) D-cycloserine had no significant effect on the aperiodic offset.

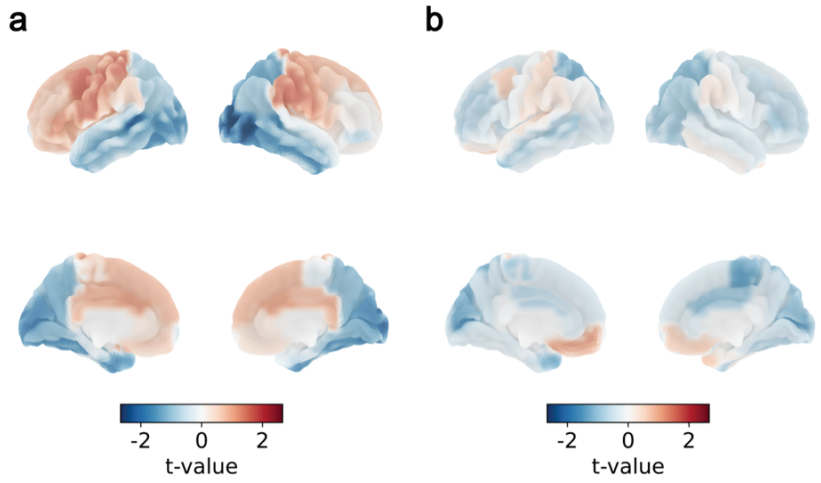

Supplement 3: Linear mixed effect results of lorazepam effect on timescales

Full results of the linear mixed model analyzing the joint effect of cortical hierarchy and the drugs on cortical timescales. Timescales significantly increase with decreasing myelination operationalized through the T1w/T2w ratio as a proxy for cortical hierarchy. While D-cycloserine has no significant effect, lorazepam significantly expands the cortical timescales. Additionally, there is a trend effect of the interaction of Lorazepam with the T1wT2w ratio. Thus, the increased timescales through Lorazepam are especially pronounced in frontal regions with typically lower degrees of myelinization.

Table S1: Linear mixed effect results. Table includes the β-weight, standard error (SE), *t*-value, degrees of freedom (df) and *p*-value for each fixed effect. Stars represent significant effects based on $p < 0.05$.

	β-weight	***SE***	**df**	***t*-value**	***p*-value**
Intercept	0.70	0.27	69.25	2.55	0.013 *
T1w/T2w	-3.06	0.17	75.88	-17.64	< 0.001 *
D-cycloserine	-0.08	0.15	9952.00	-0.54	0.586
Lorazepam	0.39	0.15	5146.00	2.55	0.011 *
T1w/T2w x D-cycloserine	0.08	0.11	11180.00	0.71	0.477
T1w/T2w x Lorazepam	-0.19	0.11	11190.00	-1.75	0.081

Supplement 4: Control measures

Bond and Lader Visual Analogue Scales and State-Trait Anxiety Inventory

Participants' mood and state anxiety was protocolled three times per session: before drug intake (T1), before (T2), and after (T3) the MEG measurement. The resting state measurement was temporally closest to T2. The effects of Lorazepam and D-cycloserine on participants' mood was assessed using linear mixed effects models. Tables include the β-weight, standard error (SE), *t*-value, degrees of freedom (df) and *p*-value for each fixed effect. Stars represent significant effects based on $p < 0.05$.

Table S2: Alertness score. Lorazepam significantly reduced alertness at T3. D-cycloserine had no significant effect.

	β-weight	***SE***	**df**	***t*-value**	***p*-value**
Intercept	7.65	0.23	99.88	33.00	< 0.001 *
D-cycloserine	0.15	0.18	447.05	0.87	0.384
Lorazepam	0.01	0.18	447.00	0.08	0.939
T2	-0.30	0.18	447.00	-1.68	0.093
T3	-1.05	0.18	447.00	-5.96	< 0.001 *
D-cycloserine x T2	-0.01	0.25	447.03	-0.06	0.953
Lorazepam x T2	-0.10	0.25	447.00	-0.41	0.685
D-cycloserine x T3	0.15	0.25	447.03	0.60	0.550
Lorazepam x T3	-0.71	0.25	447.00	-2.85	0.005 *

Table S3: Calmness score. Lorazepam and D-cycloserine had no significant effect on participants' calmness.

	β-weight	***SE***	**df**	***t*-value**	***p*-value**
Intercept	7.96	0.19	121.46	41.12	< 0.001 *
D-cycloserine	-0.06	0.17	448.00	-0.36	0.723
Lorazepam	0.18	0.17	448.00	1.05	0.293
T2	0.39	0.17	448.00	2.31	0.021 *
T3	0.24	0.17	448.00	1.44	0.151
D-cycloserine x T2	-0.04	0.24	448.00	-0.15	0.879
Lorazepam x T2	-0.25	0.24	448.00	-1.04	0.299
D-cycloserine x T3	0.01	0.24	448.00	0.04	0.972
Lorazepam x T3	-0.09	0.24	448.00	-0.37	0.709

Table S4: Contentedness score. Lorazepam and D-cycloserine had no significant effect on participants' contentedness.

	β-weight	*SE*	df	*t*-value	*p*-value
Intercept	8.25	0.17	92.76	48.86	< 0.001 *
D-cycloserine	0.01	0.12	446.04	0.10	0.920
Lorazepam	-0.01	0.12	446.04	-0.05	0.962
T2	0.01	0.12	446.00	0.06	0.949
T3	-0.09	0.12	446.00	-0.77	0.443
D-cycloserine x T2	0.03	0.17	446.02	0.16	0.876
Lorazepam x T2	0.14	0.17	446.02	0.83	0.407
D-cycloserine x T3	-0.07	0.17	446.02	-0.39	0.701
Lorazepam x T3	-0.05	0.17	446.02	-0.27	0.789

Table S5: State anxiety. Lorazepam and D-cycloserine had no significant effect on participants' state anxiety.

	β-weight	*SE*	df	*t*-value	*p*-value
Intercept	29.47	0.74	86.20	39.95	< 0.001 *
D-cycloserine	0.57	0.49	445.05	1.16	0.245
Lorazepam	0.39	0.49	445.05	0.80	0.422
T2	0.06	0.49	445.09	0.12	0.905
T3	0.76	0.49	445.09	1.54	0.124
D-cycloserine x T2	-0.08	0.69	445.05	-0.11	0.912
Lorazepam x T2	-0.04	0.69	445.05	-0.06	0.953
D-cycloserine x T3	-0.16	0.69	445.05	-0.23	0.816
Lorazepam x T3	0.17	0.69	445.05	0.25	0.802

Blood pressure and heart rate

Participants' blood pressure and heart rate was measured three times per session: before drug intake (T1), before (T2), and after (T3) the MEG measurement. The resting state measurement was temporally closest to T2. The effects of Lorazepam and D-cycloserine on participants' blood pressure and heart rate was assessed using linear mixed effects models. Tables include the β-weight, standard error (SE), *t*-value, degrees of freedom (df) and *p*-value for each fixed effect. Stars represent significant effects based on $p < 0.05$.

Table S6: Systolic blood pressure. Lorazepam significantly reduced the systolic blood pressure at T2. On sessions where D-cycloserine was administered systolic blood pressure was increased across all measuring timepoints. Thus, on these sessions systolic blood pressure was increased independently of the drug administration.

	β-weight	***SE***	**df**	***t*-value**	***p*-value**
Intercept	118.79	1.49	144.02	79.83	< 0.001 *
D-cycloserine	3.89	1.40	446.01	2.79	0.006 *
Lorazepam	1.79	1.40	446.01	1.28	0.201
T2	0.02	1.40	446.01	0.01	0.990
T3	0.56	1.41	446.18	0.39	0.694
D-cycloserine x T2	-1.88	1.98	446.01	-0.95	0.343
Lorazepam x T2	-3.91	1.98	446.01	-1.98	0.048 *
D-cycloserine x T3	1.44	1.99	446.10	0.73	0.468
Lorazepam x T3	-0.61	1.99	446.10	-0.31	0.760

Table S7: Diastolic blood pressure. Lorazepam had no significant effect on the diastolic blood pressure. On sessions where D-cycloserine was administered diastolic blood pressure was increased across all measuring timepoints. Thus, on these sessions diastolic blood pressure was increased independently of the drug administration.

	β-weight	***SE***	**df**	***t*-value**	***p*-value**
Intercept	74.18	1.07	131.80	69.28	< 0.001 *
D-cycloserine	3.35	0.97	445.95	3.47	< 0.001 *
Lorazepam	0.02	0.97	445.95	0.02	0.986
T2	-2.84	0.97	445.95	-2.94	0.003 *
T3	0.69	0.98	446.10	0.71	0.481
D-cycloserine x T2	-1.81	1.37	445.95	-1.32	0.186
Lorazepam x T2	0.53	1.37	445.95	0.39	0.700
D-cycloserine x T3	-0.35	1.37	446.03	-0.26	0.797
Lorazepam x T3	1.12	1.37	446.03	0.82	0.415

Table S8: Heart rate. Lorazepam significantly increased participants' heart rate at T2 and T3. D-cycloserine had no significant effect.

	***β*-weight**	***SE***	**df**	***t*-value**	***p*-value**
Intercept	70.81	1.40	105.62	50.62	< 0.001 *
D-cycloserine	0.77	1.11	445.99	0.70	0.486
Lorazepam	-1.18	1.11	445.99	-1.06	0.289
T2	-6.00	1.11	445.99	-5.42	< 0.001 *
T3	-11.22	1.12	446.09	-10.03	< 0.001 *
D-cycloserine x T2	-2.42	1.57	445.99	-1.55	0.123
Lorazepam x T2	3.81	1.57	445.99	2.43	0.015 *
D-cycloserine x T3	-1.75	1.57	446.04	-1.11	0.268
Lorazepam x T3	4.24	1.57	446.04	2.69	0.007 *

Trail-making test

To capture pharmacological effects on visuomotor processes, participants completed the trail-making test before the MEG measurement The effects of Lorazepam and D-cycloserine on participants' visuomotor processes were assessed using linear mixed effects models. The Table includes the β-weight, standard error (SE), *t*-value, degrees of freedom (df) and *p*-value for each fixed effect. Stars represent significant effects based on $p < 0.05$.

Table S9: Trail-making test. Lorazepam and D-cycloserine had no significant effects on participants' visuomotor processes

	β-weight	***SE***	**df**	***t*-value**	***p*-value**
Intercept	22.79	0.88	94.43	26.04	< 0.001 *
D-cycloserine	0.86	0.76	112.00	1.13	0.260
Lorazepam	0.96	0.76	112.00	1.27	0.206

Supplement 5: Control analyses regarding lorazepam effects on timescales

Lorazepam significantly reduced participants' systolic blood pressure (Table S6) and alertness (Table S2) and significantly increased their heart rate (Table S8). To control whether the lorazepam induced increase in cortical timescales was independent of the additional effect of the drug, we implemented linear mixed models including these control measures. Control measures were assessed at three times during the testing session. Since the resting state measurement was temporally closest to the timepoint 2 (right before the MEG measurement), linear mixed effect models include the difference of timepoint 2 and 1 (before the drug administration). Additionally, we also verified that the effect of lorazepam was independent of the administration order. Tables include the β-weight, standard error (SE), *t*-value, degrees of freedom (df) and *p*-value for each fixed effect. Stars represent significant effects based on $p < 0.05$.

Table S11: Linear mixed effect results including systolic blood pressure. Lorazepam increased cortical timescales independent of its effect on systolic blood pressure.

	***β*-weight**	***SE***	**df**	***t*-value**	***p*-value**
Intercept	-3.31	0.10	57.21	-33.96	< 0.001 *
T1w/T2w	-0.41	0.02	75.89	-17.64	< 0.001 *
D-cycloserine	0.02	0.03	55.82	0.61	0.542
Lorazepam	0.15	0.04	56.55	3.40	0.001 *
Systolic BP	0.03	0.02	55.82	1.25	0.216
T1w/T2w x D-cycloserine	0.01	0.01	1118.00	0.71	0.478
T1w/T2w x Lorazepam	-0.03	0.01	1119.00	-1.75	0.081
Systolic BP x D-cycloserine	-0.02	0.03	67.63	-0.78	0.440
Systolic BP x Lorazepam	-0.11	0.05	70.13	-2.35	0.021 *

Table S12: Linear mixed effect results including alertness score. Lorazepam increased cortical timescales independent of its effect on the alertness score of the Bond and Lader mood scales.

	***β*-weight**	***SE***	**df**	***t*-value**	***p*-value**
Intercept	-3.31	0.10	56.99	-33.92	< 0.001 *
T1w/T2w	-0.41	0.02	75.80	-17.62	< 0.001 *
D-cycloserine	0.02	0.03	54.59	0.86	0.392
Lorazepam	0.14	0.04	55.55	3.06	0.003 *
Alertness	0.00	0.02	56.71	-0.08	0.935
T1w/T2w x D-cycloserine	0.01	0.01	11120.00	0.75	0.453
T1w/T2w x Lorazepam	-0.03	0.01	11120.00	-1.75	0.080
Alertness x D-cycloserine	0.00	0.03	62.69	-0.07	0.942

Alertness x Lorazepam	0.01	0.04	71.39	-0.28	0.781

Table S13: Linear mixed effect results including heart rate. Lorazepam increased cortical timescales independent of its effect on the heart rate.

	***β*-weight**	***SE***	**df**	***t*-value**	***p*-value**
Intercept	-3.31	0.10	56.90	-33.92	< 0.001 *
T1w/T2w	-0.41	0.02	75.87	-17.62	< 0.001 *
D-cycloserine	0.02	0.03	56.43	0.86	0.392
Lorazepam	0.14	0.05	56.28	3.06	0.003 *
Alertness	-0.04	0.03	56.63	-0.08	0.935
T1w/T2w x D-cycloserine	0.01	0.01	11180.00	0.75	0.453
T1w/T2w x Lorazepam	-0.03	0.01	11190.00	-1.75	0.080
Alertness x D-cycloserine	0.04	0.03	61.89	-0.07	0.942
Alertness x Lorazepam	0.05	0.05	82.12	-0.28	0.781

Supplement 6: Repeated measures correlation between lorazepam effects in state-specific timescales and lorazepam effects on time-averaged timescales

Figure S5: Repeated-measures correlations between lorazepam-related changes in state-specific and time-averaged timescales. State-specific timescales for all cortical parcels were correlated with their corresponding time-averaged timescales across parcels, accounting for repeated measures within participants. Each bar represents the Spearman correlation coefficient for a given state. Statistical significance was assessed using permutation tests that shuffled timescale values within participants, with Bonferroni correction applied for multiple comparisons across states. All states except State 1 showed significant correlations, with the frontal default mode network (DMN) exhibiting the strongest association.

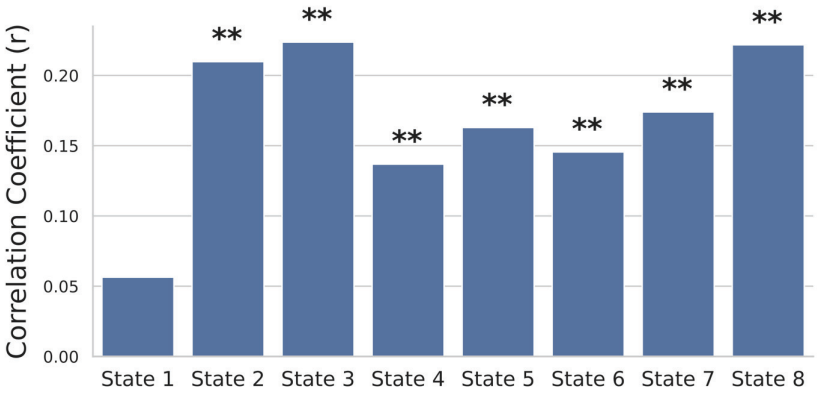

Supplement 7: Robustness of network-specific timescale findings across different numbers of states

In the main part of the manuscript, we present findings for a TDE-HMM extracting 8 states. Given that the number of states is a hyperparameter that is a priori specified, we repeated the reported analyses for TDE-HMM fits, inferring 10 and 12 States, to reassure that the main findings of this manuscript are consistent across variations of this hyperparameter. To this end we ran, analogous to the procedure for 8 States, 10 HMMs extracting 10 States and 12 States respectively. For both numbers of states, the fit with the lowest free energy, indicating the best fit to the data, was carried forward for the following analyses. States corresponding to states of interest in the main part of the manuscript (frontal DMN and State 1) were qualitatively identified in the 10- and 12-State fits based on the spectral state description. The matched states are be presented in Supplementary Figure S5.

Figure S6: Spectral description of networks of interest across TDE-HMM models with different numbers of states. Spectral descriptions of the frontal default mode network and State 1 obtained from the 8-state TDE-HMM fit reported in the main manuscript (top row) are presented alongside corresponding states from 10-state (middle row) and 12-state (bottom row) fits. For each state, three spectral representations are displayed, averaged across scans from all participants in the placebo condition. Left: Changes in 3-30 Hz power relative to the time-averaged 3-30 Hz power (averaged across all states) projected onto the cortical surface. Top right: State-specific motor cortical power spectrum (black) overlaid with the time-averaged spectrum across all states (grey). Bottom right: Coherence networks in the 2-30 Hz range, thresholded at the 98th percentile to highlight the strongest functional connections. States corresponding to the frontal DMN are outlined in orange.

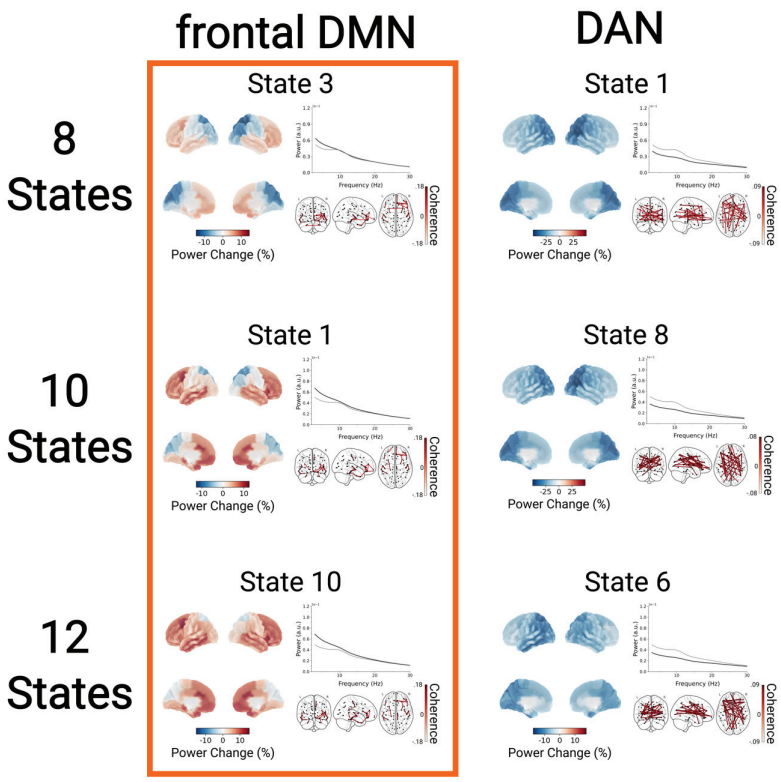

Variations in timescales across various networks are robust across different numbers of states

Repeating the analyses contrasting network-specific with time-averaged timescales (averaged across all states) produced consistent results for TDE-HMM models with 10 and 12 states (Supplementary Figure S6). In both models, the frontal DMN (10-state HMM: State 1, 52/68 significant parcels, max increase = +6.96% in lingual_lh, t_{55} = 5.83, p < 0.001; 12-state HMM: State 10, 64/68 parcels, max increase = +14.9% in rostralanteriorcingulate_rh, t_{55} = 5.21, p < 0.001) and the states corresponding to State 1 from the main analysis (10-state HMM: State 8, 68/68 parcels, max increase = +24.71% in lateraloccipital_lh, t_{55} = 7.82, p < 0.001; 12-state HMM: State 6, 68/68 parcels, max increase = +22.29% in precuneus_rh, t_{55} = 7.60, p < 0.001) showed significant increases in timescales during state visits. In contrast, most other states exhibited timescale decreases. As in the main analysis, states corresponding to State 1 displayed strong increases, exceeding those observed in the frontal DMN.

Figure S7: Network-specific variations in timescales are consistent across models with different numbers of states. Percentual changes in network-specific

timescales relative to the time-averaged scale (averaged across all states) are illustrated for TDE-HMM fits with 10 states (top) and 12 states (bottom). Only cortical parcels showing significant differences between network-specific and time-averaged timescales are displayed ($p < 0.05$, FDR-corrected across parcels and states). The state corresponding to the frontal default mode network in each TDE-HMM fit is outlined in orange.

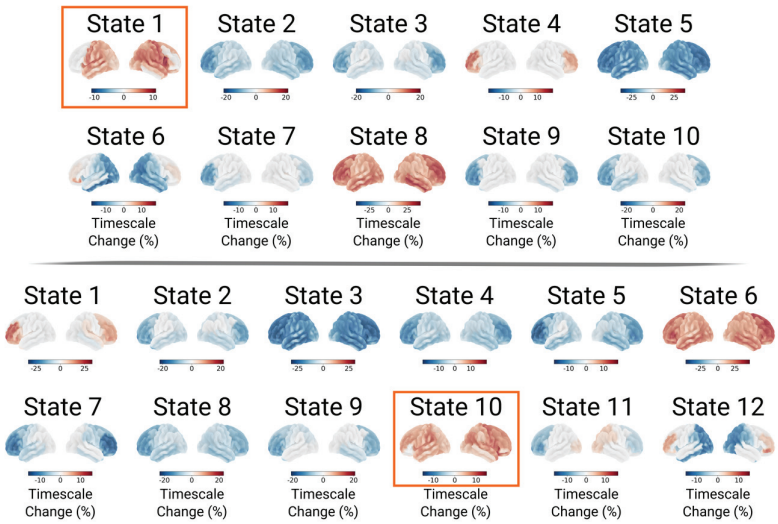

Lorazepam-related changes in state-specific timescales are robust across different numbers of states

Repeating the analyses contrasting network-specific timescales between the lorazepam and placebo conditions yielded consistent results across TDE-HMM models with 10 and 12 states (Supplementary Figure S7). Both models revealed distinct patterns of lorazepam-related increases and decreases in timescales across networks. In line with the main findings, lorazepam significantly increased timescales during visits to the frontal DMN (10-state: State 1, 44/68 significant parcels, max increase = +8.96% in lateraloccipital_rh, $t_{55} = 4.01$, $p < 0.001$; 12-state: State 10, 36/68 parcels, max increase = +14.46% in fusiform_rh, $t_{55} = 4.69$, $p < 0.001$) and in the networks corresponding to State 1 from the main analysis (10-state: State 8, 7/68 parcels, max increase = +9.84% in inferiorparietal_rh, $t_{55} = 3.40$, $p = 0.001$; 12-state: State 6, 6/68 parcels, max increase = +13.61% in inferiorparietal_rh, $t_{55} = 3.34$, $p = 0.001$). Although less pronounced, the frontal DMN still exhibited greater timescale increases than most other states in both models.

Figure S8: Lorazepam-related modulations of cortical network-specific timescales are consistent across models with different numbers of states. Percentual change in network-specific timescales after lorazepam intake relative to the placebo condition for TDE-HMM fits with 10 states (top) and 12 states (bottom). Only parcels showing significant lorazepam-related differences are displayed on the

cortical surface. Significance was assessed for each state and parcel using within-subject GLMs comparing lorazepam and placebo conditions, with FDR correction applied across all parcels and states ($p < 0.05$). The state corresponding to the frontal default mode network in each TDE-HMM fit is outlined in orange.

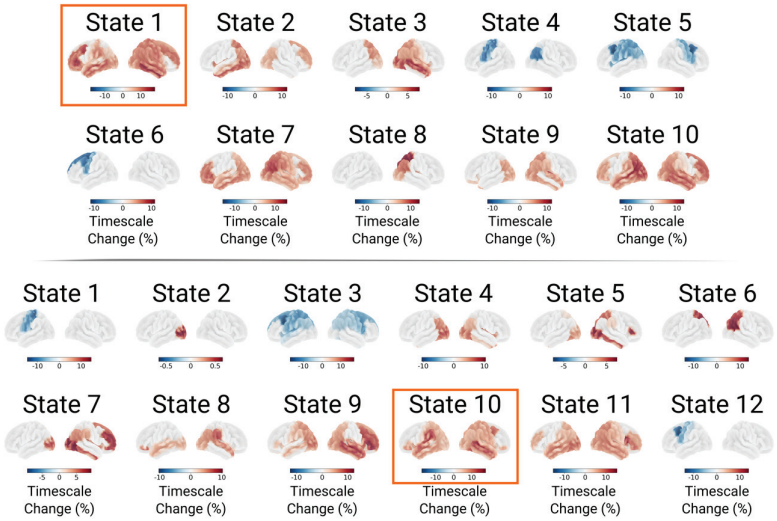

Supplement 8: Robustness of lorazepam effects on cortical network dynamics findings across different numbers of states

Lorazepam-related increases in frontal DMN occurrence probability are robust across different numbers of states

Repeating the analyses of state metrics describing network dynamics produced consistent results across TDE-HMM models with 10 and 12 states (Supplementary Figure S9). Fractional occupancy of the frontal default mode network (DMN) was significantly increased following lorazepam administration in both models (10-state HMM: State 1, t_{55} = 3.23, p = 0.02; 12-state HMM: State 10, t_{55} = 3.05, p = 0.04). Conversely, the state corresponding to State 1 from the main analysis revealed a significant reduction in occurrence probability (10-state HMM: State 8, t_{55} = -3.35, p = 0.01; 12-state HMM: State 6, t_{55} = -3.28, p = 0.02). Increases in state rates of the frontal DMN (State 1, t_{55} =3.11, p = .03) and decreases in lifetimes of the state corresponding to State 1 from the main analysis (State 8, t_{55} = -2.96, p = .03) were observed only in the 10-state TDE-HMM, but not in the 12-state model. Together, these findings suggest that lorazepam-related increases in frontal DMN occupancy and decreases in State 1 occurrence probability are robust across models with different numbers of inferred states, while the precise mechanisms underlying these changes (e.g., alterations in lifetimes or state rates) appear less consistent.

Figure S9: Lorazepam-related increases in frontal DMN occupancy are consistent across TDE-HMM models with different numbers of states. Lorazepam-related changes in state metrics of the frontal default mode network and the state corresponding to State 1 in the main manuscript are shown for TDE-HMM fits with 10 states (**a**) and 12 states (**b**). **(a**) In the 10-state model, State 1 corresponds to the frontal DMN and State 8 to State 1 in the main manuscript. Each dot represents an individual participant's metric in the respective drug condition. Condition contrasts were assessed using maximum t-statistic permutation tests, corrected for multiple comparisons across states. Lorazepam significantly increased fractional occupancy (t_{55} = 3.23, p = 0.02) and state rates (t_{55} =3.11, p = .03) for the frontal DMN, while fractional occupancy (t_{55} = –3.35, p = 0.01) and lifetimes (t_{55} = -2.96, p = .03) for State 8 were reduced. (**b**) In the 12-state model, State 10 corresponds to the frontal DMN and State 6 to State 1 in the main manuscript. Lorazepam increased fractional occupancy for the frontal DMN (t_{55} = 3.05, p = 0.04) and reduced fractional occupancy for State 6 (t_{55} = –3.28, p = 0.02). Asterisks denote significance levels: p < 0.01 (**), p < 0.05 (*).

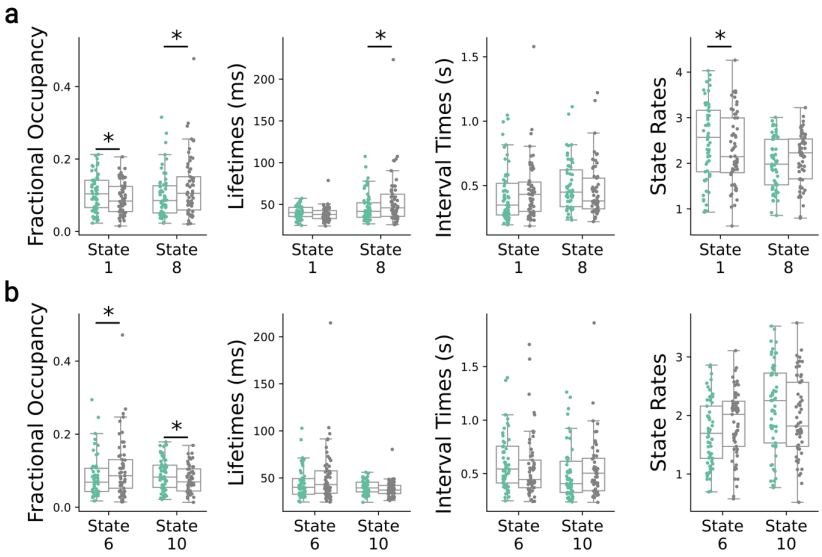

Supplement 9: Large-scale cortical network descriptions are robust across different preprocessing choices

Given that the preprocessing procedures used in the main analyses deviated in several aspects (e.g., no use vs. application of MaxFilter, use of the OSL LCMV beamformer vs. the MNE beamformer implementation, and parcellation using the Desikan–Killiany atlas vs. the Glasser52 parcellation) from pipelines commonly used in TDE-HMM analyses, we tested whether the network descriptions reported in the manuscript could be replicated using a standard preprocessing pipeline. To this end, the preprocessing was repeated following the pipeline adopted in previous studies running TDE-HMM analyses.[1–4] For a detailed description of the preprocessing pipeline, see Kohl et al. 2025.[1]

Overview of the alternative preprocessing pipeline

In short, the raw MEG data were processed using MNE-Python's Maxwell filtering pipeline, including automatic bad-channel detection and temporal signal-space separation (tSSS) for external noise suppression.[5,6] Data were bandpass filtered (0.5–125 Hz), notch-filtered at 50 Hz and 100 Hz, and resampled to 250 Hz. Artefactual segments were excluded using a window-based Generalised ESD test.[7] Cardiac and ocular artefacts were removed via signal-space projection (SSP).[8] Data quality was verified through spectral inspection, and two participants were excluded due to poor data quality.

MEG-MRI co-registration was performed using RHINO, excluding nasal points due to the limited MRI field of view. Source reconstruction employed broadband (1–45 Hz) filtered, sensor-normalised data using an LCMV beamformer (rank = 60),[9,10] and results were projected onto an 8 mm MNI152 template. Source-level signals were parcellated using a reduced Glasser atlas,[11,12] extracting the first principal component per parcel.

Before HMM analysis, symmetrical multivariate leakage correction and sign-flipping were applied to minimise spatial leakage and align dipole polarities across participants.

Comparison of large-scale cortical network descriptions

The TDE-HMM fitting procedure was performed 10 times on the alternatively pre-processed data, and the fit with the lowest free energy, indicating the best fit to the data, was carried forward for the comparison of the TDE-HMM fits on the differently pre-processed datasets.

To compare large-scale cortical network descriptions obtained from TDE-HMMs, extracting 8 states from the differently pre-processed datasets, were matched by firstly calculating the correlation distance (1 – Person Correlation) between all states' fractional occupancies in the two data sets. Afterwards, the best assignment of states between the two different HMM fits was inferred with the linear_sum_assignment function in scipy, finding the solution with the lowest overall distance between all assigned pairs.

Large-scale cortical network descriptions of the matched states are presented in Supplementary Figure S4. Qualitative comparisons of the matched states indicate that large-scale cortical network descriptions derived from differently preprocessed datasets exhibit only minor discrepancies. Overall, the patterns are very similar, enabling clear state-to-state matching.

To compare large-scale cortical network descriptions obtained from TDE-HMMs that extracted 8 states from the differently pre-processed datasets, states were matched across HMM fits by first computing the correlation distance (1 - Pearson correlation)

between the fractional occupancies of all states in the two datasets. Subsequently, the optimal one-to-one assignment of states between the two HMM fits was determined using the linear_sum_assignment function from scipy, which identifies the pairing with the lowest overall distance between all matched states.
Large-scale cortical network descriptions of the matched states are presented in Supplementary Figure S4. Qualitative comparison of the matched states revealed that, while minor discrepancies were observed, the large-scale network patterns inferred from the differently preprocessed datasets were overall highly consistent. Importantly, both TDE-HMM solutions identified a network characterized by increased wideband power in frontal and temporal regions, accompanied by power reductions in posterior areas and pronounced low-frequency power increases in the average power spectrum. These observations indicate that this network is reliably represented across both preprocessing variants, suggesting that its identification is robust to differences in the data preparation.

Figure S10: Comparison of large-scale cortical network descriptions obtained from different preprocessing pipelines. Spectral representations of cortical networks derived from the preprocessing pipeline described in the main manuscript are depicted on the left, alongside corresponding network representations obtained using preprocessing approaches commonly applied in TDE-HMM studies. States across TDE-HMM fits were matched by minimising the correlation distance between all state pairs (see above). The spectral profiles of matched states showed minor differences but were overall very similar, indicating that network estimates were robust to preprocessing choices. For a detailed description of the spectral state descriptions, refer to Figure 3 in the main text.

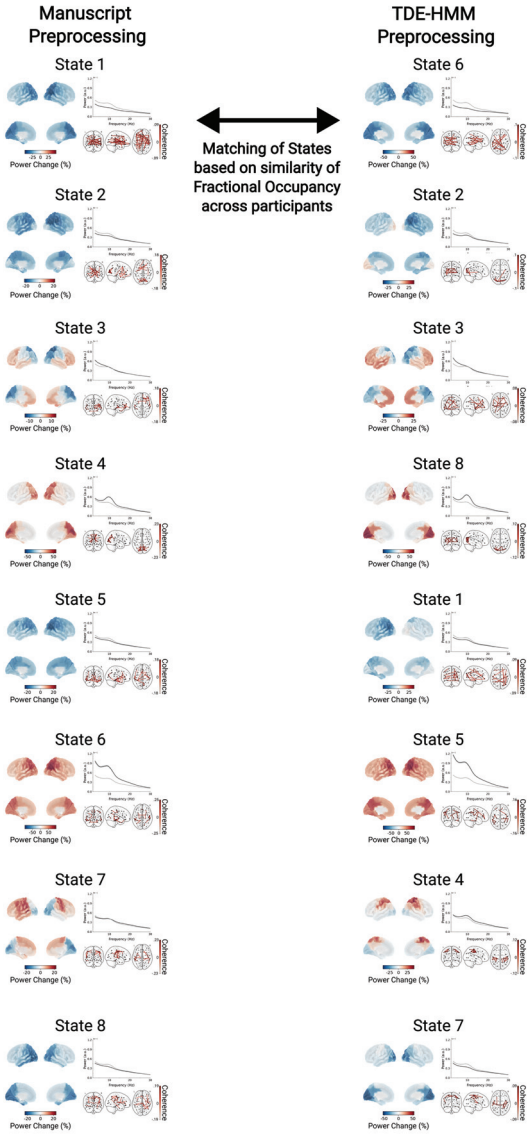
Manuscript Preprocessing
TDE-HMM Preprocessing
State 1
State 2
State 3
State 4
State 5
State 6
State 7
State 8
Matching of States based on similarity of Fractional Occupancy across participants
State 6
State 2
State 3
State 8
State 1
State 5
State 4
State 7
Power Change (%)
Coherence
Frequency (Hz)

Supplement 10: Exclusion criteria

- Female
- Age < 18 or > 35
- Body weight < 60 or > 90
- BMI < 18 or > 28
- Metal implants (e.g. Retainer) that interfered with the MEG signal or pacemaker
- Claustrophobia
- Smoking > 5 cigarettes per day
- Consumption of > 12 units alcohol per week
- (History of) significant drug abuse (cannabis, amphetamine, cocaine, ecstasy, barbiturate, tranquilizer, opiate, psychodelia, etc.). Significant is defined as:
    1. Use during the last month
    2. exceeding recreational use (> 5 times in lifetime) except or cannabis
    3. frequent use (on average more than once a month) of cannabis
- High blood pressure (systolic > 150 or diastolic > 100)
- Head injury in the past that led to loss of consciousness, or loss of consciousness with an unexplained cause in the past
- (History of) psychiatric or neurological treatment
- Beck's Depression Inventory score > 12
- Medication use interfering with lorazepam or D-cycloserine use
- Epilepsy
- Glaucoma
- Thyroid dysfunction
- Stomach or duodenal ulcer
- Stenosis in gastrointestinal tract
- (History of) gastrointestinal bleedings
- Megacolon
- Ileus
- Prostate adenoma with residual urine formation
- Diabetes
- Asthma
- Impaired liver or kidney function
- Disorders that can lead to tachycardia
- Disorders of cardiovascular system (e.g. arrythmia, high blood pressure, hemophilia)
- Performance-based exclusion:
    - VBM: choice of high expected value option < 55%
    - RDM: accuracy below chance-level, no parametric modulation as a function of coherence level
    - VBL: choice of high-expected value option and high-likelihood option < 55%

Supplement References

1. Kohl, O., Gohil, C., Zokaei, N., Hu, M. T. M., Nobre, A. C., Woolrich, M., & Quinn, A. (2025). Changes in sensorimotor network dynamics in resting-state recordings in Parkinson's disease. *Brain Commun*, *7*(4), fcaf282. https://doi.org/10.1093/braincomms/fcaf282
2. Quinn, A. J., Vidaurre, D., Abeysuriya, R., Becker, R., Nobre, A. C., & Woolrich, M. W. (2018). Task-Evoked Dynamic Network Analysis Through Hidden Markov Modeling. *Frontiers in Neuroscience*, *12*. https://doi.org/10.3389/fnins.2018.00603
3. Gohil, C., Kohl, O., Huang, R., van Es, M. W. J., Parker Jones, O., Hunt, L. T., Quinn, A. J., & Woolrich, M. W. (2024). Dynamic network analysis of electrophysiological task data. *Imaging Neurosci (Camb)*, *2*. https://doi.org/10.1162/imag_a_00226
4. Vidaurre, D., Hunt, L. T., Quinn, A. J., Hunt, B. A. E., Brookes, M. J., Nobre, A. C., & Woolrich, M. W. (2018). Spontaneous cortical activity transiently organises into frequency specific phase-coupling networks. *Nature Communications*, *9*. https://doi.org/10.1038/s41467-018-05316-z
5. Taulu, S. & Simola, J. (2006). Spatiotemporal signal space separation method for rejecting nearby interference in MEG measurements. *Phys. Med. Biol. 51*, *1759–1768.* https://doi.org/ 10.1088/0031-9155/51/7/008
6. Taulu, S. & Kajola, M. (2005). Presentation of electromagnetic multichannel data: The signal space separation method. *Journal of Applied Physics 97*, *124905.* https://doi.org/10.1063/1.1935742
7. Rosner, B. (1983). Percentage Points for a Generalized ESD Many-Outlier Procedure. *Technometrics 25*, 165–172. https://doi.org/10.1080/00401706.1983.10487848
8. Uusitalo, M. A. & Ilmoniemi, R. J. (1997). Signal-space projection method for separating MEG or EEG into components. *Med. Biol. Eng. Comput. 35*, 135–140. https://doi.org/10.1007/BF02534144
9. Van Veen, B. D. & Buckley, K. M. (1988). Beamforming: a versatile approach to spatial filtering. *IEEE ASSP Mag.* 5, 4–24. https://doi.org/10.1109/53.665
10. Woolrich, M., Hunt, L., Groves, A. & Barnes, G. (2011). MEG beamforming using Bayesian PCA for adaptive data covariance matrix regularization. *NeuroImage 57, 1466–1479.* https://doi.org/10.1016/j.neuroimage.2011.04.041
11. Glasser, M. F., Coalson, T. S., Robinson, E. C., Hacker, C. D., Harwell, J., Yacoub, E., Ugurbil, K., Andersson, J., Beckmann, C. F., Jenkinson, M., Smith, S. M., & Van Essen, D. C. (2016). A multi-modal parcellation of human cerebral cortex. *Nature*, *536*(7615), 171–+. https://doi.org/10.1038/nature18933
12. Kohl, O., Woolrich, M., Nobre, A. C. & Quinn, A. (2023). Glasser52: A parcellation for MEG-Analysis. *Zenodo* https://doi.org/10.5281/ZENODO.10401793

Study 2: Bidirectional modulation of reward-guided decision making by dopamine

Reproduced from

Dias Maile AA, Gruendler TOJ, Fischer AG, Kurtenbach H, Kaiser LF, Froböse MI, Jocham G (2025). *Bidirectional modulation of reward-guided decision making by dopamine.* Psychopharmacology, 242(11), 2547–2559.
https://doi.org/10.1007/s00213-025-06816-9

Psychopharmacology (2025) 242:2547–2559
https://doi.org/10.1007/s00213-025-06816-9

ORIGINAL INVESTIGATION

Bidirectional modulation of reward-guided decision making by dopamine

Ana Antonia Dias Maile[1] · Theo O. J. Gruendler[2] · Adrian G. Fischer[2] · Hannah Kurtenbach[1] · Luca F. Kaiser[1] · Monja I. Froböse[1] · Gerhard Jocham[1,2]

Received: 7 June 2024 / Accepted: 11 May 2025 / Published online: 29 May 2025

Abstract

Rationale The neuromodulator dopamine is known to play a key role in reward-guided decision making, where choice options are often characterized by multiple attributes. Different decision strategies can be used to merge these choice attributes with personal preferences (e.g., risk preferences) and integrate them into a single subjective value. While the influence of dopamine on risk preferences has been investigated, it is unknown whether dopamine is also involved in arbitrating between decision strategies.

Objective In the present study, we investigate the effects of pharmacological dopamine manipulations on arbitrating between different decision strategies in a healthy sample.

Methods 31 healthy male participants performed a reward-guided decision-making task under the influence of the dopamine D_2/D_3-receptor antagonist amisulpride (400 mg), the dopamine precursor L-DOPA (100 mg L-DOPA + 25 mg cardidopa), or placebo in a double-blind within-subject design. The effect of dopamine on reward-guided decisions and decision strategies was analyzed using hierarchical implementations of regressions and Bayesian models.

Results Notably, we observed that the dopaminergic interventions shifted the (overall) weighting of option attributes without changing how option attributes are integrated into a subjective value (decision strategy). These effects were bidirectional: Amisulpride *reduced* whereas L-DOPA *increased* the degree to which choices were influenced by both reward magnitude and reward probability. These effects occurred in the absence of changes in statistically optimal behavior.

Conclusion Together, our data provide evidence for a role of dopamine in controlling the influence of value parameters on choice irrespective of decision strategies.

Keywords Decision making · Risky decision making · Reward-guided decision making · Decision strategy · Dopamine · Amisulpride · L-DOPA · Pharmacology · Computational modeling

Introduction

Consider the daily commute to work and the choice of transportation: While biking boosts environmental and financial benefits, it is less comfortable and restricted by weather conditions. In contrast, driving provides flexibility and comfort, yet it has environmental and financial drawbacks. The choice of transportation thus follows from the direct comparison of various choice attributes, demanding the use of decision strategies and attribute weighting (e.g., risk preferences). Two lines of evidence suggest that decision strategies and preferences are controlled by dopamine. First, patients with the neurodegenerative disorder Parkinson's Disease (PD), which is characterized by a profound dorsal striatal dopamine depletion, exhibit motoric deficits (e.g., tremor and bradykinesia) often accompanied by an increase in risk aversive behavior (Cherkasova et al. 2019; Kobayashi et al. 2019). Conversely, treating the dopamine deficit with the dopamine-precursor levodopa (L-DOPA; Connolly and Lang 2014) improves the motor symptoms

✉ Ana Antonia Dias Maile
ana.dias.maile@uni-duesseldorf.de

[1] Biological Psychology of Decision Making, Institute of Experimental Psychology, Heinrich Heine University Düsseldorf, Universitätsstraße 1, 40225 Düsseldorf, Germany

[2] Center of Behavioral Brain Sciences, Otto Von Guericke University Magdeburg, Universitätsplatz 2, 39106 Magdeburg, Germany

but it can also increase risk seeking behavior and even cause pathological gambling (Evans et al. 2009; Molina et al. 2000; Weintraub et al. 2006).

Second, pharmacological studies in healthy volunteers have shown increased risk seeking after increasing dopamine concentrations by administering L-DOPA (Rutledge et al. 2015). Conversely, similar effects were found when administering the D_2/D_3-receptor antagonist amisulpride (Burke et al. 2018). Importantly, dopaminergic effects on risk preferences are valence-specific and were exclusively observed in the context of rewards, not losses (Burke et al. 2018; Rutledge et al. 2015). In previous work, choices were usually modelled using Prospect Theory, which posits that, following a non-linear distortion, reward probabilities and magnitudes are multiplicatively combined into an expected value (EV) which is then used to guide decisions (Kahneman and Tversky 2013; Tversky and Kahneman 1986). However, an alternative possibility would be that participants do not use such integrated EV at all, but instead rely on simpler heuristics, such as directly comparing attributes and using a weighted combination of attribute differences. Recent evidence suggests that choices of both humans and non-human primates are best characterized by a mixture of such an additive and a multiplicative strategy (Farashahi et al. 2019; Figner and Voelki 2004; Scholl et al. 2014). These results further suggested that the degree to which either of the two strategies prevails varies as a function of uncertainty about option attributes (Farashahi et al. 2019). Despite the known role of dopamine in both decision making and risk preferences, the effects of dopamine on arbitrating between decision strategies remain untested.

Therefore, in the present study we investigated the role of dopaminergic activity on decision strategies in reward-guided decision making, combining it with computational modeling approaches that take into account both multiplicative and additive strategies for value computation. Additionally, we sought to clarify the dopaminergic effect on risk preferences by including a parameter reflecting the relative balance between reliance on reward probability versus reward magnitude. Healthy participants performed a reward-guided decision-making task under the influence of either the D_2/D_3-receptor antagonist amisulpride (400 mg), the dopamine precursor L-DOPA (100 mg L-DOPA + 25 mg Carbidopa), or placebo in a double-blind within-subjects design. Notably, there was no significant dopaminergic effect on participants' decision strategies or risk preferences. Instead, the weighting of choice attributes was shifted. The degree to which participants' choices were governed by both reward magnitude and reward probability was diminished under amisulpride, but increased under L-DOPA.

Methods

Participants

A total of 33 participants took part in the study. Due to the pharmacological manipulation, participants were pre-screened on a separate day to exclude certain pre-existing medical conditions, including neurological or psychiatric disorders. Additionally, an electrocardiogram (ECG) was obtained from each potential participant and assessed by a cardiologist. Only healthy participants without ECG abnormalities were allowed to participate in the study. Due to the menstrual cycle-dependent interaction between gonadal steroids and the dopaminergic system (Becker et al. 1982; Creutz and Kritzer 2004; Dreher et al. 2007), we only included male participants, as in previous work (Jocham et al. 2011; Jocham et al. 2014a, b). Further exclusion criteria were drug abuse, and use of psychoactive drugs or medication in the two weeks before the experiment. Participants were instructed to abstain from alcohol and any other drugs of abuse during the entire course of the study.

Out of the initial 33 participants, two did not fully complete the study due to technical issues leading to the final sample of 31 participants. They were right-handed with normal or corrected-to-normal (N = 12) vision. On average, they were M = 25.71 years old (age range 21–32, SD = 3.20), body weight was M = 77.16 kg (weight range 62–90 kg, SD = 7.46). Six participants reported occasional smoking. All were naive to the purpose of the study and gave written informed consent. The present study was approved by the local ethics committee of the Medical Faculty of the Otto-von-Guericke-University Magdeburg (internal reference: 129/13) and is in line with the Helsinki Declaration of 1975. Participants were compensated for their efforts at a fixed rate, plus an additional bonus that depended on their performance during the decision-making task.

Procedure

The study comprised three pharmacological MEG-sessions in a pseudorandomized order across participants. MEG recordings will be disregarded for the purpose of the present study. Identical procedures were followed on the three sessions, only the drug (or placebo) administered differed (Fig. 1a). A physician screened participants before each session. In a double-blind cross-over design, participants received a single oral dose of either the dopamine D_2/D_3-receptor antagonist amisulpride (400 mg), the dopamine precursor levodopa (L-DOPA; 100 mg L-DOPA +25 mg cardidopa), or placebo. Because of the different pharmacokinetics of L-DOPA and amisulpride, a dummy administration procedure was used. Participants ingested two pills separated

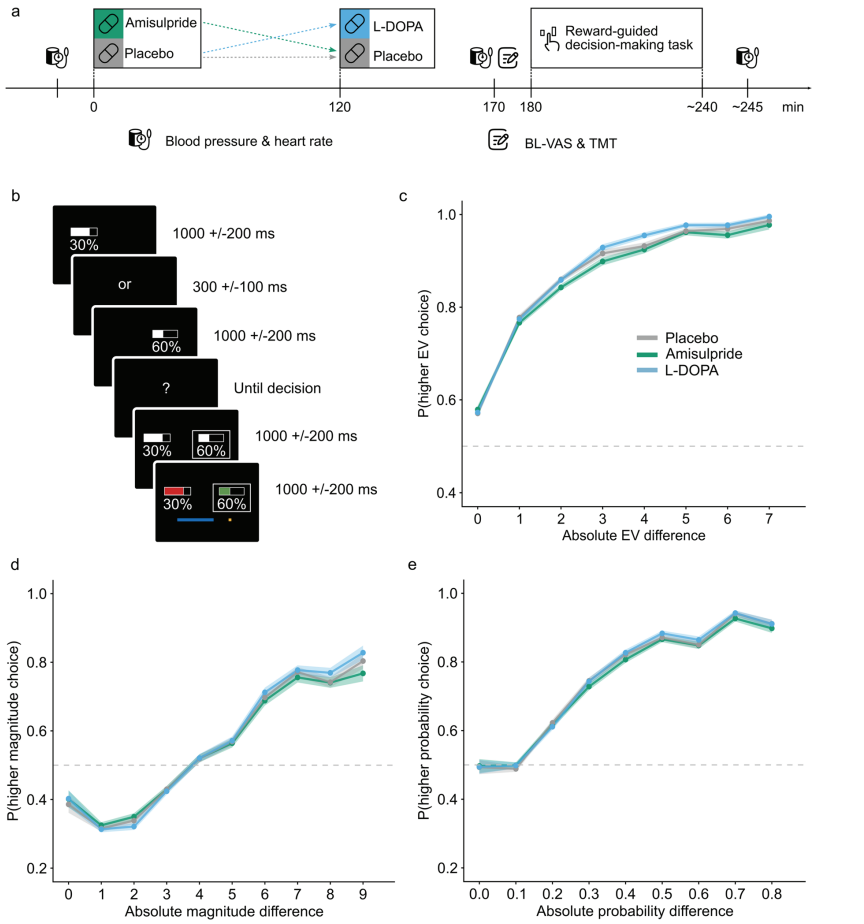

Fig. 1 Overview of study procedure, the experimental task and participants' behavior. **a** Study procedures was standardized across all sessions, only the drug (or placebo) administered differed. Due to the different pharmacokinetics of L-DOPA and amisulpride, a dummy administration procedure was used: Participants ingested two pills separated by two hours, of which at least one always contained placebo. Approximately 3 h after the first pill and 1 h after the second pill, participants performed the reward-guided decision-making task. Heart rate and blood pressure were monitored at three different time points. Immediately prior to the task, participants completed Bond & Lader visual analogue scales (BL-VAS) and the trail-making task (TMT). **b** Task schematic and trial timeline. Each choice option was associated with a reward magnitude (width of the horizontal bar) and a reward probability (percentage). The left option was always presented first, followed by a short delay before the presentation of the right option. Participants were instructed to only respond once the question mark appeared. Lastly, they were given feedback on the outcome (reward/no reward) of both the chosen and the unchosen option and reward, if obtained, was added to the progress bar (blue bar at the bottom of the screen). **c** Probability of choosing the choice option with a higher expected value (EV) depending on the absolute EV difference between the two options. Note this is not the mean-centered EV and thus not independent of reward magnitude or probability. **d** Probability of choosing the option with higher reward magnitude depending on the absolute magnitude difference between the two options. **e** Probability of choosing the option with a higher reward probability depending on the absolute probability difference between the two options. In **c**-**e**, solid lines represent the average, shaded areas represent *SEM* across participants

by two hours, of which at least one always contained placebo. In the amisulpride condition, the active substance was contained in the first pill, whereas it was contained in the second pill in the L-DOPA condition. The decision-making task began approximately 1 h after ingestion of the second pill, corresponding to 1 h after L-DOPA administration and 3 h after amisulpride administration in line with the average time for the two drugs to reach peak plasma concentration (Le Bricon et al. 1996; Nutt 2008). Immediately prior to the reward-guided decision-making task, participants completed Bond & Lader visual analogue scales (BL-VAS; Bond and Lader 1974) and the trail-making task (TMT, Reitan 1958) to assess drug effects on mood and visual attention. Heart rate and blood pressure were monitored prior to the first drug (or placebo) administration, prior to the task and after the study, before participants were released by the study physician. Sessions were separated by at least 8 days to ensure complete washout of the drug before the next session (elimination half-life of amisulpride 12 h, L-DOPA with cardidopa 1.5 h).

Reward-guided decision-making task

Participants completed 500 trials of a reward-guided decision-making task plus 12 additional trials to familiarize themselves with the task beforehand (Fig. 1b). On each trial, choices were made between two options defined by two attributes each: a reward magnitude and a probability to obtain this reward. Reward magnitudes were presented as the width of a rectangular horizontal bar and reward probabilities as a percentage written underneath these bars. Therefore, both attributes were explicit and did not have to be learned. Reward outcomes were independent of each other, meaning either of the two options, both, or none of them could be rewarded. Option values were drawn from a reward schedule that was generated before the experiment, as in previous studies (Hunt et al. 2014, 2013; Jocham et al. 2014a, b; Jocham et al. 2012). This reward schedule was designed such that correlations between factors of interest (in particular between chosen and unchosen and between left and right option value) was minimized. Furthermore, we ensured that reward magnitude and probability were never identical for the two options. To make advantageous choices, participants needed to multiply magnitude and probabilities into an integrative value estimate referred to as EV. On some trials, however, both magnitude and probability of one option were higher than on the alternative option. We refer to these trials as 'no brainer' trials. These were limited to occur no more than in 17.8% of the 500 trials (89 trials).

The two options were presented sequentially such that on every trial, the left option was always presented first, followed by a short delay (200 ms-400 ms), which was followed by a presentation of the second option on the right side. Immediately after offset of the second option, a question mark appeared prompting participants to indicate their choice. Participants were instructed to refrain from responding while the second option was onscreen and only respond after the question mark had appeared. This design choice was made in order to separate sensorimotor cortical value representations from the execution of movement in the MEG signal. Note that this design precludes a meaningful analysis of reaction times.

Options were selected by button presses with the index finger of the left and right hand, respectively. If an option was rewarded on the current trial, the bar representing the reward magnitude turned green, if it was not rewarded, it turned red. When the chosen option was rewarded, an amount proportional to the reward magnitude of that option was added to the bonus and a blue progress bar displayed at the bottom of the screen indicated this to the participant. To motivate participants, the progress bar displayed earnings towards 2 € and reset itself after reaching this goal. All earned points counted towards the reward. Rewards were rounded to the next higher value in Euro. Even though the outcome of the unchosen option was irrelevant to the bonus, the outcome of both the chosen and the unchosen option was always presented to illustrate independence of outcomes and stimulate risk seeking (i.e., occasional win of low reward probabilities). Outcome presentation was followed by an inter-trial interval (blank screen). The stimuli were presented on a grey (RGB: 60, 60, 60) background with a contrast optimized for the MEG recording chamber (white: 130, 130, 130; green: 46, 139, 60; red: 178, 70, 70; blue: 5, 105, 204).

Statistical analyses

Mixed-effects modeling

Data analyses were conducted using R (R version 4.2.2; R Development Core Team 2022). All data and codes are made available on OSF (https://osf.io/rnc94/). To evaluate drug effects on decision making, behavioral data was first analyzed using linear mixed modeling, implemented in the lme4 package (version 3.1–3; Bates et al. 2015a). In contrast to analyses of variance (ANOVAs) and linear regressions, this approach allows taking into account both within- and between-subject variability (Brown 2021; Harrison et al. 2018; Jaeger 2008). Since the dependent variable was choice (left vs. right), we used general linear mixed effects models with a binomial distribution. Fixed effects included drug (amisulpride vs. placebo and L-DOPA vs. placebo),

the option values (magnitude, probability, mean-centered EV) and a repetition bias (i.e., a tendency to choose the same choice side as in the trial before irrespective of choice attributes). Additionally, the model encompassed the interaction of drug with the option values and repetition bias. To analyze the effects of drug on option values, these were converted into the z-scaled difference scores between the two options. Hence, a drug-induced shift in risk preferences would be evident from a differential (or asymmetric) change of the interaction regression weights for reward magnitude and probability, respectively. To reduce the risk for Type I error and increase power, it is recommended to use the full random effect structure (Barr et al. 2013). However, due to convergence issues, commonly following from an overly complex random effect structure for the data (Bates et al. 2015b), we followed the recommendation by Bates et al. (2015b) and ran a PCA to inspect the amount of explained variance. Random components that explain 0.00% of variance were not kept in the model. This approach allows systematically maximizing the random effect structure. Hence, linear mixed models included both a random intercept and a random slope for the within-subject factor drug and the option values (magnitude, probability, mean-centered EV). To investigate the task effects irrespective of drug, a separate linear mixed model was set up that included the option values and a repetition bias but disregarded the factor drug. Furthermore, where we observed significant drug effects on control measures (BL-VAS, TMT, heart rate and blood pressure), these effects were added to the task models as fixed effects and we verified that the effects of interest remained unchanged. A further control analysis encompassed adding the session number as fixed effects to control for putative order effects. All *p*-values are based on asymptotic Wald tests. R^2 is reported for all models using the r.squaredGLMM procedure of the MuMIn package (version 1.48.4; Bartoń 2024).

Computational modeling

To analyze the drug effects on the underlying cognitive processes determining participants' choice behavior, we used a Bayesian hierarchical model (similar to Swart et al. 2017). This method effectively incorporates the within-subject design enabling estimation of the group-level and subject-level parameters. However, due to practicability, we first identified the best fitting model using non-hierarchical models. The first model, the multiplicative model, assumes that reward magnitudes and probabilities are multiplicatively combined (Farashahi et al. 2019):

$$sv_{i,t} = P_{i,t} \cdot M_{i,t} \tag{1}$$

where $sv_{i,t}$ is the subjective value, and $M_{i,t}$ and $P_{i,t}$ are the reward magnitude and probability, respectively, of option i presented on trial t (Farashahi et al. 2019).

In contrast, in the additive model, subjective values are computed from a weighted additive combination of reward magnitudes and probabilities:

$$sv_{i,t} = \omega_p \cdot P_{i,t} + (1 - \omega_p) \cdot M_{i,t} \tag{2}$$

where ω_p is the relative weight given to probabilities relative to magnitudes. Values of $\omega_p = 0.5$ thus indicate equal influence of probability and magnitude. Values of $\omega_p > 0.5$ indicate that choices are more strongly influenced by probabilities than magnitudes, indicating risk aversion. In contrast, values of $\omega_p < 0.5$ indicate risk seeking (Scholl et al. 2014). For this purpose, magnitudes were scaled to values between 0.10–1.00 aligning them to the value range of reward probabilities.

The third model, the hybrid model assumes that participants use a weighted combination of both the multiplicative and additive strategy:

$$sv_{i,t} = \omega_{mult} \cdot P_{i,t} \cdot M_{i,t} + (1 - \omega_{mult}) \cdot (\omega_p \cdot P_{i,t} + (1 - \omega_p) \cdot M_{i,t}) \tag{3}$$

where the relative allocation between the multiplicative and additive response strategy is governed by the parameter ω_{mult} (Farashahi et al. 2019; Scholl et al. 2014), which is bound between 0.00—1.00, with higher values of ω_{mult} indicating a dominance of the multiplicative response strategy. In all models, choices were modelled using a softmax choice rule including an inverse temperature τ to capture choice stochasticity, which then generates a probability to choose action A (in this case, left or right):

$$p_{A,t} = \frac{1}{1 + e^{-(\Delta sv_t \tau)}} \tag{4}$$

where Δsv is the subjective value difference (left minus right for A = left choice).

The linear mixed effect models revealed a (negative) choice repetition bias (see results). Therefore, we extended the best-fitting model by adding a choice bias. Furthermore, to relate to previous work and compare model fits, we used Prospect Theory. This included models where either only reward magnitude (Eq. 5), only reward probability (Eq. 6), or both (Eq. 7) were non-linearly distorted.

$$sv_{i,t} = P_{i,t} \cdot {M_{i,t}}^{\alpha} \tag{5}$$

$$sv_{i,t} = \frac{{P_{i,t}}^{\gamma}}{({P_{i,t}}^{\gamma} + (1 - P_{i,t})^{\gamma})^{\frac{1}{\gamma}}} \cdot M_{i,t} \tag{6}$$

$$sv_{i,t} = \frac{{P_{i,t}}^{\gamma}}{({P_{i,t}}^{\gamma} + (1 - P_{i,t})^{\gamma})^{\frac{1}{\gamma}}} \cdot {M_{i,t}}^{\alpha} \quad (7)$$

where α and γ are the parameters that describe the non-linear warping of objective into subjective attributes. For this purpose, reward magnitudes were not rescaled and thus ranged between 1–10. Models were implemented using the NLoptr package (version 2.0.3; Johnson 2008) with bound optimization by quadratic approximation (bobyca; Powell 2009). The maximum number of function evaluations (*maxeval*) was 10000 and the stopping criterion for relative change (*xtol_rel*) was set to 1.0e-08. Models were run with 100 iterations. The selection of the best-fitting model was based on the Bayes Information Criterion (BIC) for all testing sessions.

Next, the best-fitting model was implemented as a Bayesian hierarchical model to analyze the effects of the dopaminergic drugs. In this approach, group-level parameters (X) provide priors for the individual-level parameters (x), with $x \sim N(X, \sigma)$. A half-Cauchy with a scale of 2 defined the hyperpriors for σ. With the exception for X_{β}, the hyperpriors for X were centered around 0: $X_{mult,p} \sim N(0, 2)$, $X_{\beta} \sim N(2, 3)$. An inverse logit transform constrained ω_{mult} and ω_{p} between 0.00–1.00. The inverse temperature τ was positively bounded through an exponential transform. Parameter initials were chosen by training the model on an independent dataset using a similar task (Kurtenbach et al. 2024). We further extended the model by incorporating six parameter shifts (three per drug), enabling analysis of drug-dependent effects on the model parameters (ω_{mult}, ω_{p} and τ). These were unconstrained and their hyperpriors were specified by N(0, 3). Initial values of the parameter shifts were set to 0.00. Additionally, we used a similar approach for the best-fitting of the three variants of the Prospect Theory model, enabling a comparison of the effects of the dopaminergic drugs within a flexible attribute weighting model with the traditionally used model (Figure S2). Bayesian hierarchical models were implemented using the RStan package (version 2.21.8; Stan Development Team 2023), which enables full Bayesian inference with Markov chain Monte Carlo (MCMC) sampling methods. There were four Markov chains, comprising 500 warm-up iterations and 2500 post burn-in iterations per chain (10000 total). The target average acceptance probability (adapt_delta) was set to 0.97. Model convergence was verified using the convergence and diagnostics criteria provided by RStan which include $\widehat{R} < 1.05$.

To evaluate the best-fitting model's ability to capture our data accurately, we conducted posterior predictive checks (Baribault and Collins 2023). We generated 500 simulated datasets based on the posterior distributions of subject-level parameters obtained from the Bayesian hierarchical model. These simulated datasets were compared and correlated with key behavioral features of the real data, e.g., likelihood of choosing the option with a higher EV, reward magnitude or reward probability.

Results

Bidirectional modulation of the reliance of choices on reward information by amisulpride and L-DOPA

In the reward-guided decision-making task, participants were more likely to choose the option with a higher EV, reward magnitude or probability, as evidenced by the descriptive statistics (Fig. 1c-e). This is also confirmed by the main effects of task manipulation in the linear mixed models: EV, magnitude and probability, operationalized as a difference score between the two options, have a significant main effect on choice behavior (EV: $\beta = 0.90$, $SE = 0.12$, $z(39671) = 7.42$, $p < 0.001$; magnitude: $\beta = 2.51$, $SE = 0.24$, $z(39,671) = 10.31$, $p < 0.001$; probability: $\beta = 3.79$, $SE = 0.26$, $z(39671) = 14.37$, $p < 0.001$; marginal $R^2_{GLMM} = 0.672$; table S1). Accordingly, participants seem to weight magnitudes and probabilities more strongly than the EV as indicated by the numerically higher regression weights. As for the dopaminergic interventions, amisulpride decreased the effect of both reward magnitude and probability on choice ($\beta = -0.12$, $SE = 0.05$, $z(39655) = -2.26$, $p = 0.024$; and $\beta = -0.23$, $SE = 0.07$, $z(39655) = -3.38$, $p = 0.001$; for the interaction of amisulpride with magnitude and probability, respectively, marginal $R^2_{GLMM} = 0.674$, Fig. 2a-b). In contrast, L-DOPA increased the weighting of reward magnitude and probability on choice ($\beta = 0.17$, $SE = 0.06$, $z(39655) = 2.94$, $p = 0.003$; and $\beta = 0.21$, $SE = 0.07$, $z(39655) = 2.86$, $p = 0.004$; for the interaction of L-DOPA with magnitude and probability, respectively, marginal $R^2_{GLMM} = 0.674$, Fig. 2c-d). Notably, neither of the dopaminergic drugs had an effect on the influence of EV on choice ($\beta = -0.03$, $SE = 0.04$, $z(39655) = -0.60$, $p = 0.550$; and $\beta = 0.02$, $SE = 0.05$, $z(39655) = 0.35$, $p = 0.728$; for the interaction of amisulpride and L-DOPA with EV; marginal $R^2_{GLMM} = 0.674$; table S2). Participants displayed a tendency to alternate between right and left choices from trial to trial, evident from a negative regression weight of the repetition bias ($\beta = -0.10$, $SE = 0.04$, $z(39671) = -2.53$, $p = 0.011$, marginal $R^2_{GLMM} = 0.672$; table S1). However, this bias was not affected by the dopaminergic interventions ($\beta = -0.12$, $SE = 0.07$, $z(39655) = -1.65$, $p = 0.099$; and $\beta = 0.08$, $SE = 0.08$, $z(39655) = 1.00$, $p = 0.316$; for the interaction of amisulpride and L-DOPA with the repetition bias; marginal $R^2_{GLMM} = 0.674$; table S2). Irrespectively, due to the significant impact of the repetition bias on choice behavior, it was taken into account in the following computational modeling. For a complete overview of the linear mixed model results see table S1 and S2.

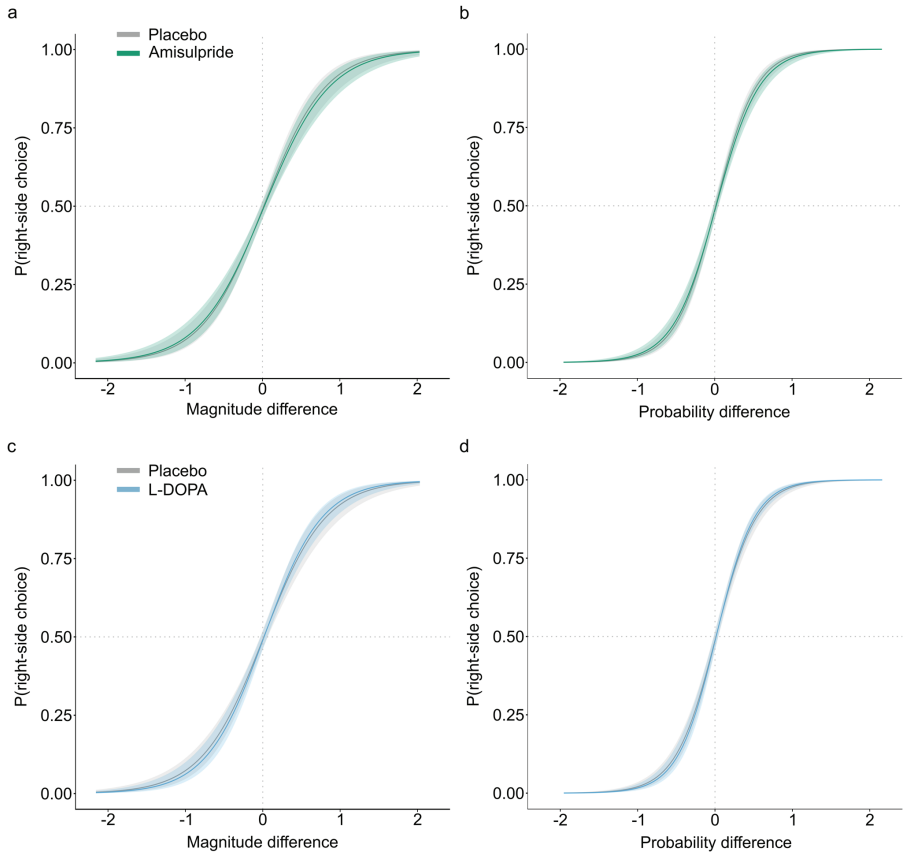

Fig. 2 General linear mixed model results. The plots indicate the modelled probability to select the right option as a function of reward magnitude (**a**, **c**) or reward probability (**b**, **d**) difference between right minus left option (z-scored difference values). Amisulpride significantly decreased the influence of both reward magnitude **a** and reward probability **b** on choice. In contrast, L-DOPA significantly increased the influence of both reward magnitude **c** and reward probability **d** on choice. Solid lines represent the average, shaded areas represent SEM across participants

We further confirmed that the drug effects were independent of the following potential confounds: All dopaminergic effects were independent of mood, visual attention, heart rate or blood pressure (note that L-DOPA increased participants' calmness independently of the effects on choice behavior; tables S3-7). When controlling for session order, the reported effects of interest were still significant, however the interaction between amisulpride and reward magnitude was no longer significant ($\beta = -0.08$, $SE = 0.06$, $z(39651) = -1.53$, $p = 0.127$, marginal $R^2_{GLMM} = 0.676$; tables S8-S9).

Computational modeling shows no dopaminergic effect on decision strategies

The above results show that amisulpride and L-DOPA changed the degree to which choices were controlled by the

individual choice attributes, magnitude and probability. Specifically, amisulpride decreased, and L-DOPA increased the effect of both reward magnitude and probability on choice behavior. Our computational models additionally allow us to further delineate whether these effects arise from an increase in choice stochasticity, as captured by the inverse softmax temperature (τ) and/or from a shift in risk preference (ω_p), the relative importance of probability vs magnitude information. Additionally, the computational models allow insights into dopaminergic effects on the selection of decision strategies (ω_{mult}). The best-fitting model for all testing sessions was the hybrid model without choice bias (BIC m = 314.67; Table 1 for model fits across sessions and Table S10 for model fits per session). In this model the parameter ω_{mult} was estimated as Mdn = 0.49 (95%-HDI: 0.37–0.61, Fig. 3a). This suggests participants used a hybrid response strategy comprising of both a multiplicative and an additive approach instead of a purely multiplicative strategy as traditionally assumed by Prospect Theory. However, this response strategy was not significantly shifted by amisulpride (Mdn = 0.02, 95%-HDI: −0.04–0.10, Fig. 3b) or L-DOPA (Mdn = −0.01, 95%-HDI: −0.08–0.05, Fig. 3b) as the posterior distributions overlap with zero. This indicates no dopaminergic effect on the selection of decision strategies. The weight parameter ω_p reflects the balance between reward probability and magnitude and thus gives insights into participants' risk preferences. It was estimated to be Mdn = 0.82 (95%-HDI: 0.71–0.93, Fig. 3c). Hence, participants weighted probabilities more strongly than magnitudes causing risk averse behavior. This parameter was not significantly shifted by amisulpride (Mdn = 0.04, 95%-HDI: −0.04–0.13, Fig. 3d) or L-DOPA (Mdn = −0.01, 95%-HDI: −0.09–0.06, Fig. 3d). Therefore, the shifted weighting of choice attributes as observed in the linear mixed models, cannot be attributed to a dopaminergic shift in risk preferences. The inverse softmax temperature τ is estimated Mdn = 14.56 (95%-HDI: 12.20–16.92, Fig. 3e). It was not significantly shifted by amisulpride (Mdn = −0.46, 95%-HDI: −1.18–1.02, Fig. 3f) or L-DOPA (Mdn = 0.62, 95%-HDI: −0.68–1.94, Fig. 3f). Hence, there is no dopaminergic effect on participants' choice stochasticity and thus this cannot clarify the dopaminergic shift of choice attributes found in the linear mixed models. Nevertheless, the direction of the drug shifts aligns with the direction of effects found in the linear mixed models: amisulpride decreases the reliance on choice attributes as demonstrated here by the numerically decreasing inverse softmax temperature leading to an increased choice stochasticity. In contrast, L-DOPA increased the weighting of choice attributes aligned with the numerically increased inverse softmax temperature and hence a decreased choice stochasticity. Table S11 depicts the parameter collinearities with all $r_s \leq 0.50$. Figure S1 shows the successful posterior predictive checks: the simulated data from the hybrid model reproduce the key features of our data indicated by the highly significant correlation between the real and simulated choice behavior (all $r_s \geq 0.83$ and $p < 0.001$). Further, the best-fitting Prospect Theory model included both a probability and magnitude distortion. Model results can be found in the Figure S2. Similar to the hybrid model, there were no significant drug shifts. Nevertheless, although it was not the best fitting model for our data, there was a trend effect for reduced probability distortion under amisulpride (Mdn = 0.11, 95%-HDI: −0.01–0.24), where 91.1% of the posterior distribution does not overlap with zero.

Table 1 Model fits for the different computational models. Bayes Information Criterion (BIC) was used to compare model fits. Lower BIC indicates better fit. The hybrid model without a bias is the best fitting model. Values are mean (SE) across all sessions

	BIC
Hybrid model	314.67 (10.21)
Hybrid model with repetition bias	319.56 (10.13)
Additive model	336.49 (9.49)
Multiplicative model	400.95 (10.47)
Prospect Theory with magnitude distortion	319.58 (10.38)
Prospect Theory with probability distortion	364.93 (10.18)
Prospect Theory with magnitude and probability distortion	317.69 (10.15)

Discussion

We investigated the effects of dopaminergic manipulation on reward-guided decision making in a double-blind within-subject design in healthy participants. We found that increasing dopaminergic transmission with L-DOPA increased the degree to which participants' choices were governed by both option attributes, reward magnitude and probability. Blockade of D_2-like receptors with amisulpride had the opposite effect, decreasing the effect of both magnitude and probability on choice.

We investigated drug effects using two main approaches. Importantly, we do not intend to suggest that the approaches make independent claims, instead results are complementary, contributing to a more comprehensive understanding. First, linear mixed modeling allowed testing the task parameters that influenced participants' choices, and how these were affected by drug. We found that the effects of reward magnitude and probability on choice were decreased under amisulpride, and increased under L-DOPA. However, the decreased effect of reward magnitude under amisulpride needs to be interpreted with caution as it was not robust to the control measure session order. In contrast, the weight of the integrated EV was affected by neither of the drugs. Because choosing on the basis of EV represents statistically

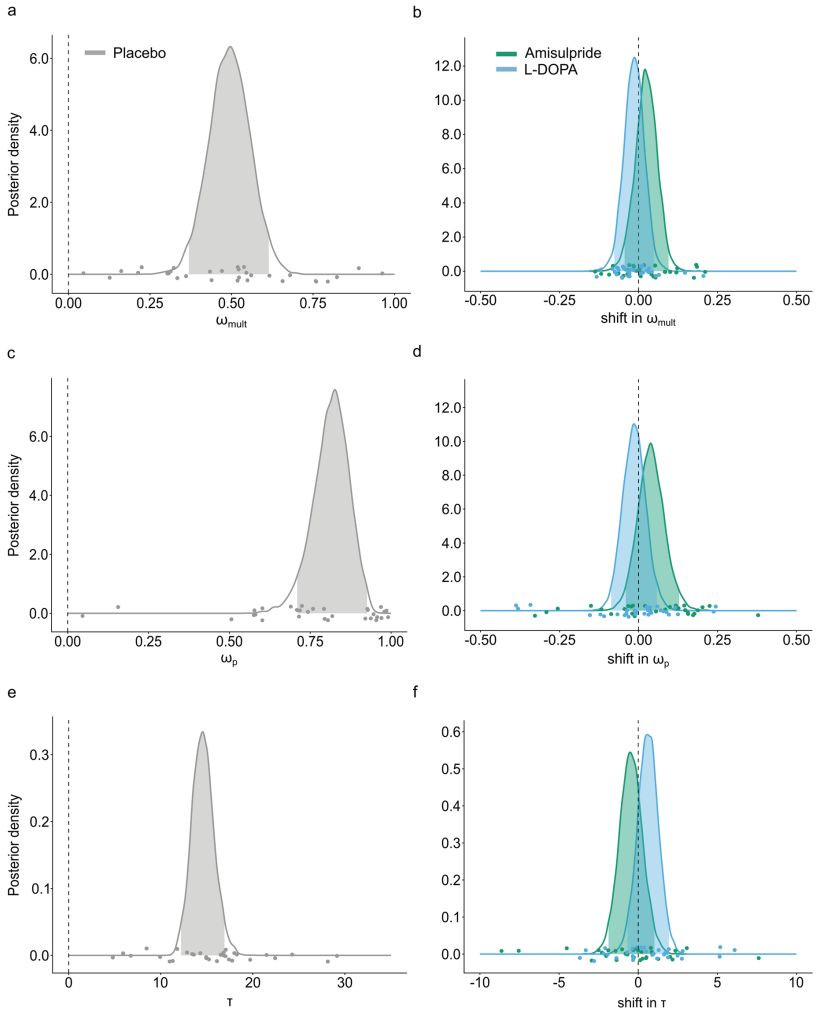

Fig. 3 Posterior distributions of the group level estimate of the parameters from the Bayesian hierarchical model. Panels on the left (**a**, **c**, **e**) are the posterior distributions of the three model parameters, the multiplicative weight ω_{mult}, the relative probability weight ω_P and the softmax inverse temperature τ. Panels on the right (**b**, **d**, **f**) are the posterior distributions of the shift parameters, color-coded for each drug. Shaded areas in the distributions are the 95%-CI. Dots represent single-subject estimates. **a** Participants use a hybrid response strategy comprising of both a multiplicative and an additive decision strategy, as evident from median ω_{mult} = 0.49. **b** This response strategy is not significantly affected by amisulpride or L-DOPA (95%-CI overlaps with zero). **c** Participants choices are guided more by reward probabilities than reward magnitudes, as evident from ω_P higher than 0.5 (median ω_P = 0.82). **d** This relative weighting is not significantly shifted by amisulpride or L-DOPA (95%-CI overlaps with zero). **e** The softmax inverse temperature τ is not significantly shif fted by amisulpride or L-DOPA (**f**), since the 95%-CI overlaps with zero

optimal behavior, this implies that drugs did not affect optimal behavior. We also observed that regression weights for the individual attributes, reward probability and reward magnitude, were higher than those for EV, an issue that we will return to in the next paragraph. Further, in agreement with previous work (Pape and Siegel 2016; Rogge et al. 2022), we found an alternation bias. That is, above and beyond the effects of value-related parameters, participants displayed a tendency to alternate between right and left choices from trial to trial. However, in contrast to previous studies, this was not modulated by drug (e.g., Rutledge et al. 2009).

Our second approach is based on computational modeling. Traditionally, multi-attribute decision making is captured with models like Prospect Theory (Kahneman and Tversky 2013; Tversky and Kahneman 1986). These approaches typically involve applying non-linear weighting functions to reward magnitude and probability prior to multiplying them into an EV. This has recently been challenged by studies showing that behavior of both humans and non-human primates is best characterized by a more flexible mixture of decision strategies (Farashahi et al. 2019; Figner and Voelki 2004; Scholl et al. 2014), comprised of both EV (multiplicative strategy) and a direct comparison of option attributes (additive strategy). The dominance of either the multiplicative or additive strategy appears to depend on uncertainty where participants have been shown to shift to preferred use of the additive strategy during risky decision making or under heightened uncertainty (Farashahi et al. 2019; Figner and Voelki 2004). Our modeling results agree with these previous studies. We found that participants' behavior was best described by a hybrid model incorporating a multiplicative and an additive strategy, which outperformed classic multiplicative models like Prospect Theory. Investigation of the parameter ω_{mult}, which captures the relative contribution of the two strategies, showed that participants' subjective values were guided to a similar degree by the multiplicative and additive component. This is in line with the linear mixed modeling regression results, where we also observed that magnitudes and probabilities influenced choice behavior numerically stronger than EV. Further, we reasoned that the dopaminergic change in weighting of the individual attributes, without a concomitant change in the role of EV, should be reflected in choice stochasticity. Therefore, we expected softmax inverse temperature to be decreased under amisulpride, and increased under L-DOPA, corresponding to more and less stochastic choices, respectively. We found no significant effects of amisulpride or L-DOPA on any of the three parameters of the Bayesian hierarchical model. Nevertheless, numerically, the direction of the drug shifts on the softmax temperature does align with our prediction: Participants' choice behavior tended to get more stochastic under amisulpride, and less stochastic under L-DOPA. The lack of change in the relative probability weighting parameter ω_P and the multiplicative term ω_{mult} is again consistent with our regression-based results. A change of ω_P would only be coherent if a drug affected the impact of probability and magnitude in opposite direction or at the very least if a change in the weight of probability was more/less pronounced than the change in the weight of magnitude. Likewise, a change in ω_{mult} should have readily been observed in the regression weight for EV.

Dopamine plays a key role in decision making, yet its involvement in arbitrating between multiplicative and additive decision strategies is not known. There is however evidence that dopamine influences risk preferences (Burke et al. 2018; Gross et al. 2021; Ojala et al. 2018; Petzold et al. 2019; Riba et al. 2008; Rigoli et al. 2016; Rutledge et al. 2015; White et al. 2007). For instance, increasing dopamine transmission with L-DOPA has been reported to increase risk seeking behavior (Rigoli et al. 2016; Rutledge et al. 2015). This effect appears to be mediated by participants' impulsivity and by their sensitivity to reward (Petzold et al. 2019; White et al. 2007). In contrast, D_2-receptor antagonism has been associated with a decreased risk aversion, as evident from a reduced probability distortion (Burke et al. 2018; Ojala et al. 2018). This is in line with our exploratory analyses on the Prospect Theory model (which was not the best fitting model for our data), where we also found a trend for amisulpride to reduce probability distortion (Fig. S2). Our linear mixed modeling effects and the non-significant shift of ω_P in our Bayesian hierarchical model diverge from these previous results. This might be caused by our task design: First, our reward-guided decision-making task consisted exclusively of a gain frame, without a loss frame. Risk preferences, and especially loss aversion, might depend on losing instead of just not receiving a reward. However, previous studies that have also exclusively included a gain frame found dopaminergic effects that were equivalent to studies including both a gain and loss frame (Ojala et al. 2018; Rutledge et al. 2015). Thus, this factor is unlikely to be the reason for our diverging effects. Second, the short offset in our task design between the presentation of the first and second choice option might have modulated the results by imposing a working memory component. The two-state model by Seamans and Yang suggests that dopamine switches prefrontal cortex networks between two states: state 1, dominated by D_2-receptor activation, allows exploration of the input space, while state 2, dominated by D_1-receptor activation, allows focusing on a limited set of representations leading to enhanced robustness of working memory representations (Seamans et al. 2001; Seamans and Yang 2004). We cannot rule out that the dopaminergic intervention might have had effects on working memory influencing

the differential processing of the first relative to the second option. Third, our sample only included young male participants. This decreases external validity. Yet, studies with a similar pharmacological manipulation and task have found effects in a male-only sample that corresponded well with a mixed sample, suggesting that gender is not a cause for our diverging effects (e.g., Burke et al. 2018; Ojala et al. 2018). Nevertheless, it would be valuable to replicate our findings recruiting a more diverse group of participants. Fourth, similar pharmacological studies have found no effects of (indirect) dopamine agonists or D_2-receptor antagonists on risk preferences (Acheson and de Wit 2008; Arrondo et al. 2015; Evers et al. 2017; Hamidovic et al. 2008; Symmonds et al. 2013; Zack and Poulos 2007).

In conclusion, participants' behavior was best described by a hybrid model where additive and multiplicative decision strategies jointly contributed to subjective value. Further, our data suggest that dopamine does not affect the relative dominance of either of the two decision strategies. However, the degree to which choices were controlled by individual attributes, was increased by L-DOPA and decreased by amisulpride. Since we did not find evidence for a stronger shift of one option attribute compared to the other, we would argue that this cannot be interpreted as change in risk preferences. Our data thus provide evidence for a role of dopamine in controlling the influence of value parameters on choice, irrespective of decision strategies and risk preferences.

Supplementary Information The online version contains supplementary material available at https://doi.org/10.1007/s00213-025-06816-9.

Acknowledgements We thank the Department of Neurology at the University Hospital of the Otto-von-Guericke University and the chair of the Department of Neurology, Prof. Dr. Hans-Jochen Heinze for invaluable support. Computational infrastructure and support were provided by the Centre for Information and Media Technology at Heinrich Heine University Düsseldorf.

Author contributions • Study conception and design (TOJG, GJ), data acquisition (TOJG, AGF), data analysis (AADM, HK, LFK, MIF, GJ), interpretation of data for the work (AADM, TOJG, AGF, HK, LFK, MIF, GJ).
• Drafting the article (AADM, MIF, GJ), revising it for intellectual content (AADM, TOJG, AGF, HK, LFK, MIF, GJ).
• Approving the final version of the manuscript (AADM, TOJG, AGF, HK, LFK, MIF, GJ).

Funding Open Access funding enabled and organized by Projekt DEAL.
This work was supported by the Deutsche Forschungsgemeinschaft (DFG JO 787/5–1), a grant from the Federal State of Saxony Anhalt and the European Regional Development Fund (ERDF 2014–2020) to GJ, project: Center for Behavioral Brain Sciences (FKZ: ZS/2016/04/78113), and a travel grant from the G.-A.-Lienert Foundation to TOJG.

Data availability All data and codes are available on OSF (https://osf.io/rnc94/).

Declarations

Ethical approval The present study was approved by the local ethics committee of the Medical Faculty of the Otto-von-Guericke-University Magdeburg (internal reference: 129/13) and is in line with the Declaration of Helsinki 1975.

Consent to participate Participants gave written informed consent before participation in the study.

Consent to publish Not applicable.

Competing interest All authors certify that they have no affiliations with or involvement in any organization or entity with any financial interest or non-financial interest in the subject matter or materials discussed in this manuscript.

References

Acheson A, de Wit H (2008) Bupropion improves attention but does not affect impulsive behavior in healthy young adults. Exp Clin Psychopharmacol 16(2):113–123. https://doi.org/10.1037/1064-1297.16.2.113

Arrondo G, Aznarez-Sanado M, Fernandez-Seara MA, Goni J, Loayza FR, Salamon-Klobut E, Heukamp FH, Pastor MA (2015) Dopaminergic modulation of the trade-off between probability and time in economic decision-making. Eur Neuropsychopharmacol 25(6):817–827. https://doi.org/10.1016/j.euroneuro.2015.02.011

Baribault B, Collins AGE (2023) Troubleshooting Bayesian cognitive models. Psychol Metho/. https://doi.org/10.1037/met0000554

Barr DJ, Levy R, Scheepers C, Tily HJ (2013) Random effects structure for confirmatory hypothesis testing: Keep it maximal. J Mem Lang 68(3). https://doi.org/10.1016/j.jml.2012.11.001

Bartoń K (2024) MuMIn: Multi-Model Inference. R package version 1.48.4, https://CRAN.R-project.org/package=MuMIn

Bates D, Mächler M, Bolker BM, Walker SC (2015a) Fitting linear mixed-effects models using lme4. J Stat Softw 67(1):1–48. https://doi.org/10.18637/jss.v067.i01

Bates D, Kliegl R, Vasishth S, Baayen H (2015b) Parsimonious mixed models. arXiv preprint arXiv:1506.04967. https://doi.org/10.48550/arXiv.1506.04967

Becker JB, Robinson TE, Lorenz KA (1982) Sex differences and estrous cycle variations in amphetamine-elicited rotational behavior. Eur J Pharmacol 80(1):65–72. https://doi.org/10.1016/0014-2999(82)90178-9

Bond A, Lader M (1974) The use of analogue scales in rating subjective feelings. Br J Med Psychol 47(3):211–218

Brown VA (2021) An introduction to linear mixed-effects modeling in R. Adv Methods Pract Psychol Sci 4(1). https://doi.org/10.1177/2515245920960351

Burke CJ, Soutschek A, Weber S, Beharelle AR, Fehr E, Haker H, Tobler PN (2018) Dopamine receptor-specific contributions to the computation of value. Neuropsychopharmacology 43(6):1415–1424. https://doi.org/10.1038/npp.2017.302

Cherkasova MV, Corrow JC, Taylor A, Yeung SC, Stubbs JL, McKeown MJ, Appel-Cresswell S, Stoessl AJ, Barton JJS (2019) Dopamine replacement remediates risk aversion in Parkinson's disease in a value-independent manner. Parkinsonism Relat Disord 66:189–194. https://doi.org/10.1016/j.parkreldis.2019.08.014

Connolly BS, Lang AE (2014) Pharmacological treatment of parkinson disease a review. Jama - J Am Med Assoc 311(16):1670–1683. https://doi.org/10.1001/jama.2014.3654

Creutz LM, Kritzer MF (2004) Mesostriatal and mesolimbic projections of midbrain neurons immunoreactive for estrogen receptor beta or androgen receptors in rats. J Comp Neurol 476(4):348–362. https://doi.org/10.1002/cne.20229

Dreher JC, Schmidt PJ, Kohn P, Furman D, Rubinow D, Berman KF (2007) Menstrual cycle phase modulates reward-related neural function in women. Proc Natl Acad Sci U S A 104(7):2465–2470. https://doi.org/10.1073/pnas.0605569104

Evans AH, Strafella AP, Weintraub D, Stacy M (2009) Impulsive and compulsive behaviors in Parkinson's disease. Mov Disord 24(11):1561–1570. https://doi.org/10.1002/mds.22505

Evers EA, Stiers P, Ramaekers JG (2017) High reward expectancy during methylphenidate depresses the dopaminergic response to gain and loss. Soc Cogn Affect Neurosci 12(2):311–318. https://doi.org/10.1093/scan/nsw124

Farashahi S, Donahue CH, Hayden BY, Lee D, Soltani A (2019) Flexible combination of reward information across primates. Nat Hum Behav 3(11):1215–1224. https://doi.org/10.1038/s41562-019-0714-3

Figner B, Voelki N (2004) Risky decision making in a computer card game: an information integration experiment. Pol Psychol Bull 35:135–139

Gross J, Faber NS, Kappes A, Nussberger AM, Cowen PJ, Browning M, Kahane G, Savulescu J, Crockett MJ, De Dreu CKW (2021) When helping is risky: the behavioral and neurobiological trade-off of social and risk preferences. Psychol Sci 32(11):1842–1855. https://doi.org/10.1177/09567976211015942

Hamidovic A, Kang UJ, de Wit H (2008) Effects of low to moderate acute doses of pramipexole on impulsivity and cognition in healthy volunteers. J Clin Psychopharmacol 28(1):45–51. https://doi.org/10.1097/jcp.0b013e3181602fab

Harrison XA, Donaldson L, Correa-Cano ME, Evans J, Fisher DN, Goodwin CED, Robinson BS, Hodgson DJ, Inger R (2018) A brief introduction to mixed effects modelling and multi-model inference in ecology. PeerJ 6:e4794. https://doi.org/10.7717/peerj.4794

Hunt LT, Woolrich MW, Rushworth MF, Behrens TE (2013) Trial-type dependent frames of reference for value comparison. PLoS Comput Biol 9(9):e1003225. https://doi.org/10.1371/journal.pcbi.1003225

Hunt LT, Dolan RJ, Behrens TE (2014) Hierarchical competitions subserving multi-attribute choice. Nat Neurosci 17(11):1613–1622. https://doi.org/10.1038/nn.3836

Jaeger TF (2008) Categorical Data Analysis: Away from ANOVAs (transformation or not) and towards Logit Mixed Models. J Mem Lang 59(4):434–446. https://doi.org/10.1016/j.jml.2007.11.007

Jocham G, Klein TA, Ullsperger M (2011) Dopamine-mediated reinforcement learning signals in the striatum and ventromedial prefrontal cortex underlie value-based choices. J Neurosci 31(5):1606–1613. https://doi.org/10.1523/JNEUROSCI.3904-10.2011

Jocham G, Hunt LT, Near J, Behrens TE (2012) A mechanism for value-guided choice based on the excitation-inhibition balance in prefrontal cortex. Nat Neurosci 15(7):960–961. https://doi.org/10.1038/nn.3140

Jocham G, Furlong PM, Kroger IL, Kahn MC, Hunt LT, Behrens TE (2014a) Dissociable contributions of ventromedial prefrontal and posterior parietal cortex to value-guided choice. Neuroimage 100:498–506. https://doi.org/10.1016/j.neuroimage.2014.06.005

Jocham G, Klein TA, Ullsperger M (2014b) Differential modulation of reinforcement learning by D2 dopamine and NMDA glutamate receptor antagonism. J Neurosci 34(39):13151–13162. https://doi.org/10.1523/JNEUROSCI.0757-14.2014

Johnson SG (2008) The NLopt nonlinear-optimization package. In (Version 2.0.3) https://nlopt.readthedocs.io/en/latest/

Kahneman D, Tversky A (2013) Prospect theory: an analysis of decision under risk. In: Handbook of the fundamentals of financial decision making: Part I. World Scientific. pp 99–127

Kobayashi S, Asano K, Matsuda N, Ugawa Y (2019) Dopaminergic influences on risk preferences of Parkinson's disease patients. Cogn Affect Behav Neurosci 19(1):88–97. https://doi.org/10.3758/s13415-018-00646-3

Kurtenbach H, Froböse MI, Ort E, Bahners BH, Hirschmann J, Butz M, Schnitzler A, Jocham G (2024) A role for acetylcholine in reinforcement learning and decision making under uncertainty. bioRxiv 2024–09. https://doi.org/10.1101/2024.09.20.614105

Le Bricon C, Hulot T, Canal M, Hortan N, Lins R (1996) Pharmacokinetics of amisulpride and its enantiomers after single and repeated doses in healthy volunteers. Eur J Drug Metab Pharmacokinet (special issue) 135–136

Molina JA, Sainz-Artiga MJ, Fraile A, Jimenez-Jimenez FJ, Villanueva C, Orti-Pareja M, Bermejo F (2000) Pathologic gambling in Parkinson's disease: a behavioral manifestation of pharmacologic treatment? Mov Disord 15(5):869–872. https://doi.org/10.1002/1531-8257(200009)15:5%3c869::aid-mds1016%3e3.0.co;2-i

Nutt JG (2008) Pharmacokinetics and pharmacodynamics of levodopa. Mov Disord 23(Suppl 3):S580-584. https://doi.org/10.1002/mds.22037

Ojala KE, Janssen LK, Hashemi MM, Timmer MHM, Geurts DEM, ter Huurne NP, Cools R, Sescousse G (2018) Dopaminergic drug effects on probability weighting during risky decision making. Eneuro 5(2). https://doi.org/10.1523/ENEURO.0330-18.2018

Pape AA, Siegel M (2016) Motor cortex activity predicts response alternation during sensorimotor decisions. Nat Commun 7:13098. https://doi.org/10.1038/ncomms13098

Petzold J, Kienast A, Lee Y, Pooseh S, London ED, Goschkes T, Smolka MN (2019) Baseline impulsivity may moderate L-DOPA effects on value-based decision-making. Sci Rep 9. https://doi.org/10.1038/s41598-019-42124-x

Powell MJ (2009) The BOBYQA algorithm for bound constrained optimization without derivatives. Cambridge NA Report NA2009/06, University of Cambridge, Cambridge, p 26

R Development Core Team (2022) R: A Language and Environment for Statistical Computing. In: (Version 4.2.2) R Foundation for Statistical Computing

Reitan RM (1958) Validity of the trail making test as an indicator of organic brain damage. Percept Mot Skills 8(3):271–276

Riba J, Kramer UM, Heldmann M, Richter S, Munte TF (2008) Dopamine agonist increases risk taking but blunts reward-related brain activity. PLoS ONE 3(6):e2479. https://doi.org/10.1371/journal.pone.0002479

Rigoli F, Rutledge RB, Chew B, Ousdal OT, Dayan P, Dolan RJ (2016) Dopamine increases a value-independent gambling propensity. Neuropsychopharmacology 41(11):2658–2667. https://doi.org/10.1038/npp.2016.68

Rogge J, Jocham G, Ullsperger M (2022) Motor cortical signals reflecting decision making and action preparation. Neuroimage 263:119667. https://doi.org/10.1016/j.neuroimage.2022.119667

Rutledge RB, Lazzaro SC, Lau B, Myers CE, Gluck MA, Glimcher PW (2009) Dopaminergic drugs modulate learning rates and perseveration in Parkinson's patients in a dynamic foraging task. J Neurosci 29(48):15104–15114. https://doi.org/10.1523/JNEUROSCI.3524-09.2009

Rutledge RB, Skandali N, Dayan P, Dolan RJ (2015) Dopaminergic modulation of decision making and subjective well-being. J Neurosci 35(27):9811–9822. https://doi.org/10.1523/JNEUROSCI.0702-15.2015

Scholl J, Gunthner J, Kolling N, Favaron E, Rushworth MF, Harmer CJ, Reinecke A (2014) A role beyond learning for NMDA receptors in reward-based decision-making-a pharmacological study using d-cycloserine. Neuropsychopharmacology 39(12):2900–2909. https://doi.org/10.1038/npp.2014.144

Seamans JK, Yang CR (2004) The principal features and mechanisms of dopamine modulation in the prefrontal cortex. Prog Neurobiol 74(5):321–321. https://doi.org/10.1016/j.pneurobio.2004.10.002

Seamans JK, Gorelova N, Durstewitz D, Yang CR (2001) Bidirectional dopamine modulation of GABAergic inhibition in prefrontal cortical pyramidal neurons. J Neurosci 21(10):3628–3638. https://doi.org/10.1523/JNEUROSCI.21-10-03628.2001

Stan Development Team (2023) RStan: the R interface to Stan. In: (Version 2.21.8) https://mc-stan.org/

Swart JC, Frobose MI, Cook JL, Geurts DE, Frank MJ, Cools R, den Ouden HE (2017) Catecholaminergic challenge uncovers distinct Pavlovian and instrumental mechanisms of motivated (in)action. Elife 6. https://doi.org/10.7554/eLife.22169

Symmonds M, Wright ND, Fagan E, Dolan RJ (2013) Assaying the effect of levodopa on the evaluation of risk in healthy humans. PLoS ONE 8(7):e68177. https://doi.org/10.1371/journal.pone.0068177

Tversky A, Kahneman D (1986) The framing of decisions and the evaluation of prospects. In: Barcan Marcus R, Dorn GJW, Weingartner P (eds) Studies in logic and the foundations of mathematics, vol 114. Elsevier, pp 503–520. https://doi.org/10.1016/S0049-237X(09)70710-4

Weintraub D, Siderowf AD, Potenza MN, Goveas J, Morales KH, Duda JE, Moberg PJ, Stern MB (2006) Association of dopamine agonist use with impulse control disorders in Parkinson disease. Arch Neurol 63(7):969–973. https://doi.org/10.1001/archneur.63.7.969

White TL, Lejuez CW, de Wit H (2007) Personality and gender differences in effects of d-amphetamine on risk taking. Exp Clin Psychopharmacol 15(6):599–609. https://doi.org/10.1037/1064-1297.15.6.599

Zack M, Poulos CX (2007) A D2 antagonist enhances the rewarding and priming effects of a gambling episode in pathological gamblers. Neuropsychopharmacology 32(8):1678–1686. https://doi.org/10.1038/sj.npp.1301295

Supplementary tables

Table S1 General linear mixed effects model: task effects. Table depicts the β-weights, *SEM*, *z*-value and *p*-value for the fixed effects. These included main effects for the intercept (side bias), z-scaled differences scores (Δ) between the two options for expected value (EV; constituting of mean-centered values for reward magnitude and reward probability), reward magnitude (M) and probability (P) and a repetition bias. The dependent variable was choice (right-side choice). The marginal R^2_{GLMM} = 0.672. Stars represent significant effects based on $p < 0.05$.

	β-weight	***SEM***	***z*-value**	***p*-value**
Intercept	-0.01	0.05	-0.15	0.885
ΔEV	0.90	0.12	7.42	< 0.001 *
ΔM	2.51	0.24	10.31	< 2e-16 *
ΔP	3.79	0.26	14.37	< 2e-16 *
Repetition	-0.10	0.04	-2.53	0.011 *

Table S2 General linear mixed effects model: drug effects. Table depicts the β-weights, *SEM*, *z*-value and *p*-value for the fixed effects. These included main effects for the intercept (side bias), drugs, z-scaled differences scores (Δ) between the two options for expected value (EV; constituting of mean-centered values for reward magnitude and reward probability), reward magnitude (M) and probability (P) and a repetition bias. Additionally, fixed effects included interactions of the drugs with the EV difference, reward magnitude difference, reward probability difference and the repetition bias. The dependent variable was choice (right-side choice). The marginal R^2_{GLMM} = 0.674. Asterisks represent significant effects based on $p < 0.05$.

	β-weight	***SEM***	***z*-value**	***p*-value**
Intercept	0.00	0.07	0.03	0.974
Amisulpride	0.04	0.06	0.75	0.454
L-DOPA	-0.05	0.06	-0.80	0.424
ΔEV	0.91	0.13	7.26	< 0.001 *
ΔM	2.51	0.25	10.14	< 2e-16 *
ΔP	3.81	0.27	14.19	< 2e-16 *
Repetition	-0.10	0.05	-1.83	0.068
Amisulpride:ΔEV	-0.03	0.04	-0.60	0.550
L-DOPA:ΔEV	0.02	0.05	0.35	0.728
Amisulpride:ΔM	-0.12	0.05	-2.26	0.024 *
L-DOPA:ΔM	0.17	0.06	2.94	0.003 *
Amisulpride:ΔP	-0.23	0.07	-3.38	< 0.001 *
L-DOPA:ΔP	0.21	0.07	2.86	0.004 *
Amisulpride:repetition	-0.12	0.07	-1.65	0.099
L-DOPA: repetition	0.08	0.08	1.00	0.316

Table S3 Linear mixed effect model for the pharmacological effects on heart rate. Table depicts the *β-weights*, *SEM*, degrees of freedom, *t*-value and *p*-value for the fixed effects. These included main effects for the intercept, the two drugs (amisulpride and L-DOPA) compared to placebo and the two measuring timepoints (prior to the first drug administration and after the study). Additionally, fixed effects included interactions of the drugs with the measuring timepoint. Asterisks represent significant effects based on $p < 0.05$. The heart rate significantly differs from zero (significant intercept) and decreases from measuring timepoint 1 to 2. There is no significant effect of the drugs on participants' heart rate. The marginal $R^2_{GLMM} = 0.257$.

	β-weight	***SEM***	**df**	***t*-value**	***p*-value**
Intercept	78.81	2.46	77.01	31.99	< 2e-16 *
Amisulpride	1.90	2.48	155.54	0.77	0.445
L-DOPA	-0.65	2.48	155.54	-0.26	0.795
Timepoint	-15.39	2.51	156.11	-6.14	< 0.001 *
Amisulpride:timepoint	-2.19	3.69	159.89	-0.59	0.554
L-DOPA:timepoint	1.13	3.69	159.89	0.31	0.759

Table S4 Linear mixed effect model for the pharmacological effects on systolic blood pressure. Table depicts the β-weights, *SEM*, degrees of freedom, *t*-value and *p*-value for the fixed effects. These included main effects for the intercept, the two drugs (amisulpride and L-DOPA) compared to placebo and the two measuring timepoints (prior to the first drug administration and after the study). Additionally, fixed effects included interactions of the drugs with the measuring timepoint. Asterisks represent significant effects based on $p < 0.05$. The systolic blood pressure significantly differs from zero (significant intercept) and there is no significant drug effect. The marginal $R^2_{GLMM} = 0.051$.

	***β*-weight**	***SEM***	**df**	***t*-value**	***p*-value**
Intercept	133.85	1.96	124.42	68.30	< 2e-16 *
Amisulpride	-3.26	2.39	161.43	-1.36	0.175
L-DOPA	-0.49	2.39	161.43	-0.21	0.838
Timepoint	3.98	2.40	162.73	1.65	0.100
Amisulpride:timepoint	2.77	3.52	169.53	0.79	0.432
L-DOPA:timepoint	-2.02	3.52	169.53	-0.58	0.566

Table S5 Linear mixed effect model for the pharmacological effects on diastolic blood pressure. Table depicts the β-weights, *SEM*, degrees of freedom, *t*-value and *p*-value for the fixed effects. These included main effects for the intercept, the two drugs (amisulpride and L-DOPA) compared to placebo and the two measuring timepoints (prior to the first drug administration and after the study). Additionally, fixed effects included interactions of the drugs with the measuring timepoint. Asterisks represent significant effects based on $p < 0.05$. The diastolic blood pressure significantly differs from zero (significant intercept) and there is no significant drug effect. The marginal $R^2_{GLMM} = 0.005$.

	***β*-weight**	***SEM***	**df**	***t*-value**	***p*-value**
Intercept	83.51	1.97	107.07	42.35	< 2e-16 *
Amisulpride	-1.39	2.28	159.03	-0.61	0.542
L-DOPA	-2.16	2.28	159.03	-0.95	0.344
Timepoint	-0.11	2.29	160.03	-0.05	0.961
Amisulpride:timepoint	0.59	3.37	165.81	0.18	0.861
L-DOPA:timepoint	1.62	3.37	165.81	0.48	0.632

Table S6 Pharmacological effects on mood measured with the BL-VAS and visual attention measured with the TMT. Depicted are the *mean(sd)* of the three factors of the BL-VAS and TMT scores in seconds for each drug condition. Significant deviations from placebo are marked with an asterisks based on $p < 0.05$. L-DOPA significantly increases the factor calmness.

	Placebo	**Amisulpride**	**L-DOPA**
Alertness	7.41(1.64)	7.23(1.73)	7.24(1.68)
Contentedness	7.93(1.57)	7.92(1.53)	8.11(1.42)
Calmness	7.51(1.62)	7.63(2.05)	8.00(1.63) *
TMT	17.19(5.31)	17.50(7.25)	16.40(4.41)

Table S7 General linear mixed effects model controlling for the significant effect of L-DOPA on calmness. Table depicts the β-weights, *SEM*, *z*-value and *p*-value for the fixed effects. These included main effects for the intercept (side bias), drugs, z-scaled differences scores (Δ) between the two options for expected value (EV; constituting of mean-centered values for reward magnitude and reward probability), reward magnitude (M) and probability (M), a repetition bias and the calmness scores. Additionally, fixed effects included interactions of the drug with the EV difference, reward magnitude difference, reward probability difference, the repetition bias and the calmness scores. The dependent variable was choice (right-side choice). The marginal R^2_{GLMM} = 0.674. Asterisks represent significant effects based on $p < 0.05$.

	***β*-weight**	***SEM***	***z*-value**	***p*-value**
Intercept	0.00	0.07	0.06	0.953
Amisulpride	0.04	0.06	0.74	0.457
L-DOPA	-0.05	0.07	-0.78	0.435
ΔEV	0.91	0.13	7.26	< 0.001 *
ΔM	2.51	0.25	10.15	< 2e-16 *
ΔP	3.81	0.27	14.20	< 2e-16 *
Repetition	-0.10	0.05	-1.83	0.068
Calmness	0.02	0.05	0.42	0.671
Amisulpride:ΔEV	-0.03	0.04	-0.60	0.551
L-DOPA:ΔEV	0.02	0.05	0.35	0.730
Amisulpride:ΔM	-0.12	0.05	-2.26	0.024 *
L-DOPA:ΔM	0.17	0.06	2.94	0.003 *
Amisulpride:ΔP	-0.23	0.07	-3.38	< 0.001 *
L-DOPA:ΔP	0.21	0.07	2.86	0.004 *
Amisulpride:repetition	-0.12	0.07	-1.65	0.099
L-DOPA:repetition	0.08	0.08	1.00	0.318
Amisulpride:calmness	0.01	0.05	0.24	0.813
L-DOPA:calmness	-0.04	0.05	-0.69	0.491

Table S8 General linear mixed effects model: session order effects. Table depicts the β-weights, *SEM*, *z*-value and *p*-value for the fixed effects. These included main effects for the intercept (side bias), drugs, z-scaled differences scores (Δ) between the two options for expected value (EV; constituting of mean-centered values for reward magnitude and reward probability), reward magnitude (M) and probability (P) and a repetition bias. Additionally, fixed effects included interactions of the drugs and the session order with the EV difference, reward magnitude difference, reward probability difference and the repetition bias. The dependent variable was choice (right-side choice). The marginal R^2_{GLMM} = 0.676. Asterisks represent significant effects based on $p < 0.05$.

	β-weight	***SEM***	***z*-value**	***p*-value**
Intercept	0.00	0.07	0.00	0.997
Amisulpride	0.05	0.06	0.85	0.395
L-DOPA	-0.05	0.07	-0.80	0.424
ΔEV	0.91	0.13	7.25	< 0.001 *
ΔM	2.50	0.25	10.04	< 2e-16 *
ΔP	3.81	0.27	14.11	< 2e-16 *
Repetition	-0.10	0.05	-1.78	0.076
Amisulpride:ΔEV	-0.02	0.04	-0.48	0.634
L-DOPA:ΔEV	0.01	0.05	0.28	0.783
Amisulpride:ΔM	-0.08	0.06	-1.53	0.127
L-DOPA:ΔM	0.20	0.06	3.37	< 0.001 *
Amisulpride:ΔP	-0.17	0.07	-2.40	0.017 *
L-DOPA:ΔP	0.23	0.07	3.10	0.002 *
Amisulpride:repetition	-0.13	0.08	-1.73	0.083
L-DOPA:repetition	0.08	0.08	1.02	0.308
Session:ΔEV	0.03	0.02	1.41	0.159
Session:ΔM	0.00	0.02	-0.12	0.903
Session:ΔP	0.22	0.03	7.67	< 0.001 *
Session: repetition	0.00	0.02	0.20	0.843

Table S9 General linear mixed effects model: session order effects independent of drug. Table depicts the β-weights, *SEM*, *z*-value and *p*-value for the fixed effects. These included main effects for the intercept (side bias), z-scaled differences scores (Δ) between the two options for expected value (EV; constituting of mean-centered values for reward magnitude and reward probability), reward magnitude (M) and probability (P) and a repetition bias. Additionally, fixed effects included interactions of the session order with the EV difference, reward magnitude difference, reward probability difference and the repetition bias. The dependent variable was choice (right-side choice). The marginal R^2_{GLMM} = 0.675. Asterisks represent significant effects based on $p < 0.05$.

	β-weight	***SEM***	***z*-value**	***p*-value**
Intercept	-0.01	0.05	-0.14	0.888
ΔEV	0.91	0.12	7.40	< 0.001 *
ΔM	2.53	0.25	10.28	< 2e-16 *
ΔP	3.82	0.27	14.37	< 2e-16 *
Repetition	-0.10	0.04	-2.51	0.012 *
Session:ΔEV	0.03	0.02	1.56	0.120
Session:ΔM	0.01	0.02	0.30	0.762
Session:ΔP	0.24	0.03	8.26	< 2e-16 *
Session:repetition	0.01	0.02	0.30	0.765

Table S10 Model fits for the different computational models per session. Bayes Information Criterion (BIC) was used to compare model fits. Lower BIC indicates better fit. The hybrid model without a bias is the best fitting model in each session. Values present *mean (SE)*.

Session 1	**BIC**
Hybrid model	341.80 (19.44)
Hybrid model with repetition bias	346.23 (19.08)
Additive model	362.29 (17.78)
Multiplicate model	403.18 (17.05)
Prospect Theory with magnitude distortion	344.60 (19.22)
Prospect Theory with probability distortion	375.63 (17.63)
Prospect theory with magnitude and probability distortion	344.20 (19.34)
Session 2	**BIC**
Hybrid model	298.24 (16.91)
Hybrid model with repetition bias	303.31 (16.79)
Additive model	319.37 (16.35)
Multiplicate model	404.03 (19.80)
Prospect Theory with magnitude distortion	304.28 (18.11)
Prospect Theory with probability distortion	363.80 (18.37)
Prospect theory with magnitude and probability distortion	300.40 (16.91)
Session 3	**BIC**
Hybrid model	303.98 (16.06)
Hybrid model with repetition bias	309.14 (16.17)
Additive model	327.79 (14.51)
Multiplicate model	395.64 (18.02)
Prospect Theory with magnitude distortion	309.86 (16.21)
Prospect Theory with probability distortion	355.35 (17.25)
Prospect theory with magnitude and probability distortion	308.46 (15.85)

Table S11 Parameter collinearity. Correlation between the model parameters based on the subject-level posterior distributions.

	ω_{mult}	ω_p	τ
ω_{mult}	1.00	-0.05	0.50
ω_p	-0.05	1.00	-0.06
τ	0.50	-0.06	1.00

Supplementary figures

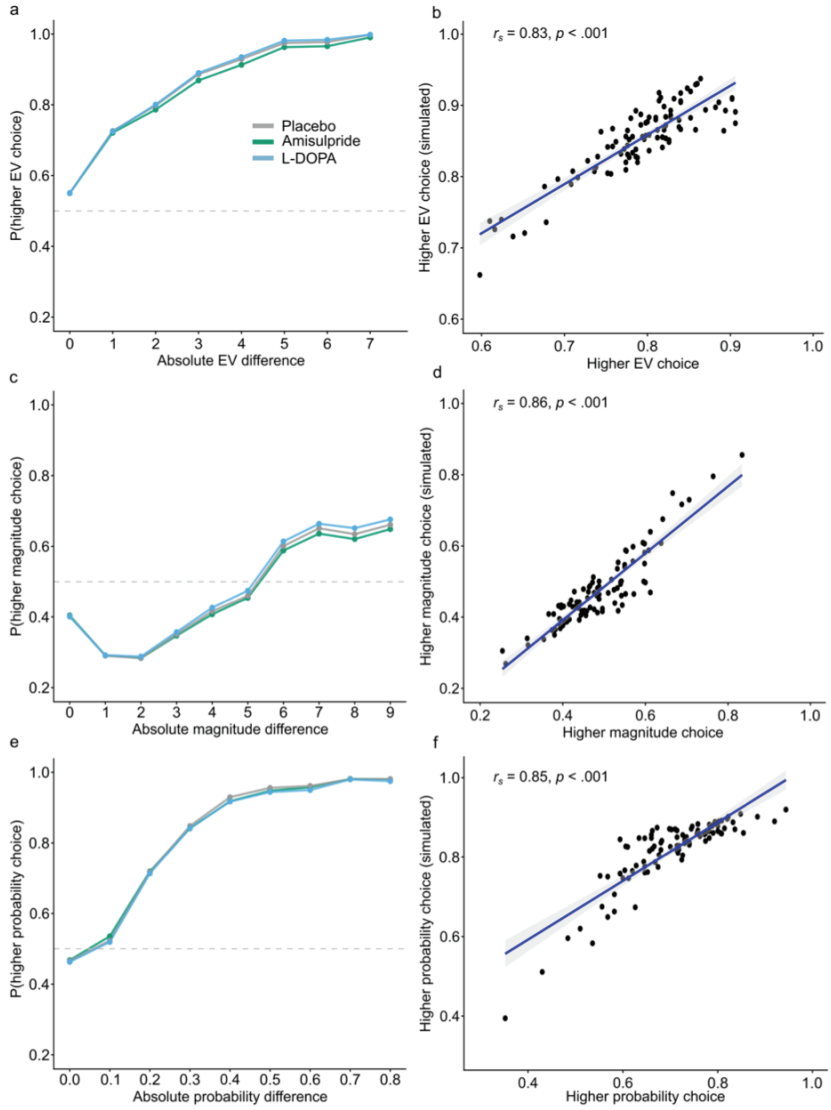

Fig. S1 Posterior predictive checks. To evaluate the hybrid model's ability to capture the data accurately, we generated 500 simulated datasets based on the posterior distributions of subject-level parameters from the Bayesian hierarchical model. The simulated data is plotted (a, c, e) and correlated (b, d, f) with key features of the real data. In a, c and e drug conditions are color coded. Shaded areas around the graphs depict the *SEM*. (a), Probability of choosing the choice option with a

higher EV depending on the absolute EV difference between choice options. (b), Correlation between real and simulated choices with higher EVs (c), Probability of choosing the choice option with a higher reward magnitude depending on the absolute magnitude difference between choice options. (d), Correlation between real and simulated choices with higher reward magnitudes (e), Probability of choosing the choice option with a higher reward probability depending on the absolute probability difference between choice options. (f), Correlation between real and simulated choices with higher reward probabilities.

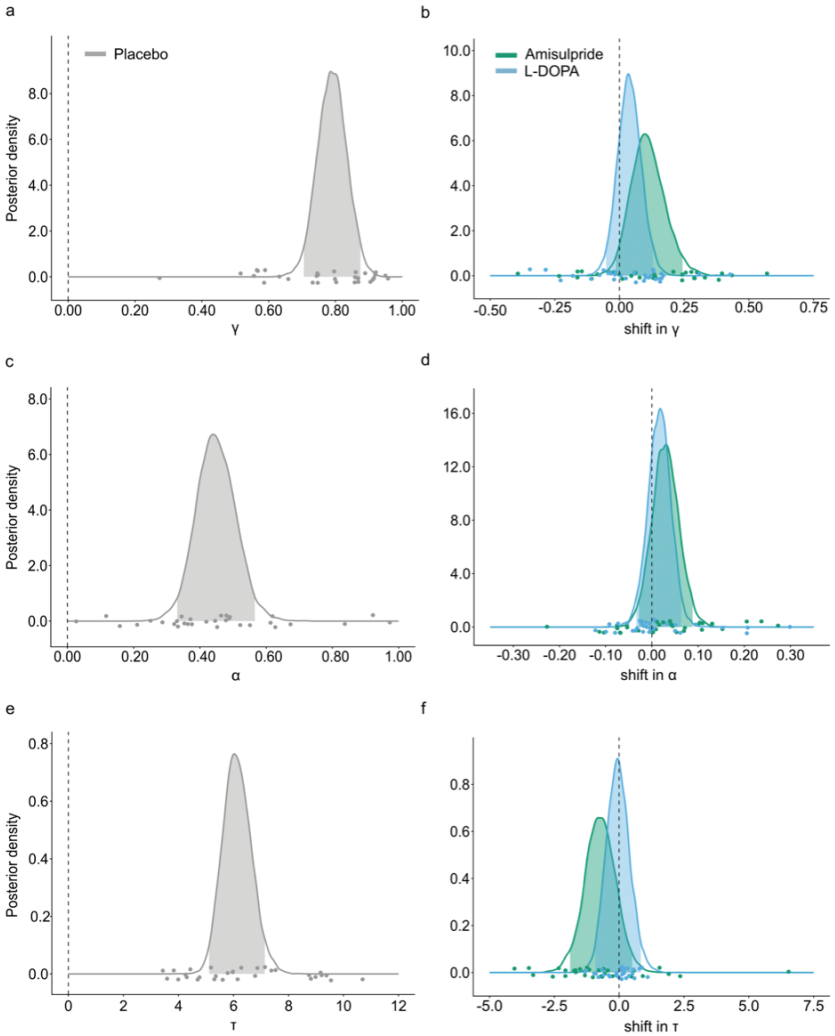

Fig. S2 Posterior distributions of the group level estimate of the parameters from the Bayesian hierarchical Prospect Theory model. Panels on the left (a, c, e) are the posterior distributions of the three model parameters, the probability distortion γ, the magnitude distortion α and the softmax inverse temperature τ. Panels on the right (b, d, f) are the posterior distributions of the shift parameters, color-coded for each drug. Shaded areas in the distributions are the 95%-CI. Dots represent single-subject estimates. (a) As shown by median γ = 0.79 (95%- HDI: 0.71 – 0.87), participants distort reward probabilities. (b), This probability distortion is not significantly shifted by amisulpride (*Mdn* = 0.11, 95%- HDI: -0.01 – 0.24) or L-DOPA (*Mdn* = 0.04, 95%- HDI: -0.05 – 0.13) since the 95%-CI overlap with zero. Nevertheless, there is a trend effect where amisulpride increases γ since 91,1% of the posterior distribution does not overlap with zero. The increase in γ leads to a reduced probability distortion under amisulpride (c), Reward magnitudes are distorted as shown by median α = 0.45 (95%- HDI: 0.33 – 0.57). (d), This magnitude distortion is not significantly shifted by amisulpride (*Mdn* = 0.03, 95%- HDI: -0.03 – 0.09) or L-DOPA (*Mdn* = 0.02, 95%- HDI: -0.03 – 0.06) since the 95%-CI overlap with zero. (e), The

median of the inverse softmax temperature τ is estimated *Mdn* = 6.12 (95%- HDI: 5.11 – 7.14). (f)**,** The inverse softmax temperature is not significantly shifted by amisulpride (*Mdn* = -0.73, 95%- HDI: -1.90 – 0.50) or L-DOPA (*Mdn* = -0.05, 95%- HDI: -0.92 – 0.84) since the 95%-CI overlap with zero.

Study 3: Cholinergic and noradrenergic modulation of perceptual decision making and learning

Reproduced from

Dias Maile AA, Andronova E, Ball F, Aravitska D, Dannenberg LK, Schnitzler A, O'Reilly JX, Jocham G (2026). Cholinergic and noradrenergic modulation of perceptual decision making and learning. bioRxiv. https://doi.org/10.64898/2026.06.22.732890

Cholinergic and noradrenergic modulation of perceptual decision making and learning

Ana Antonia Dias Maile[1], Evelina Andronova[1], Felix Ball[1], Dzhamilia Aravitska[2], Lisa K Dannenberg[3], Alfons Schnitzler[2], Jill X O'Reilly[4], Gerhard Jocham[1]

[1]Biological Psychology of Decision Making, Institute of Experimental Psychology, Heinrich Heine University Düsseldorf, 40225 Düsseldorf, Germany

[2]Institute of Clinical Neuroscience and Medical Psychology, Medical Faculty, Heinrich Heine University Düsseldorf, 40225 Düsseldorf, Germany

[3]Clinic of Cardiology, Pulmonology & Angiology, University Hospital Düsseldorf, 40225 Düsseldorf, Germany

[4]Department of Experimental Psychology, University of Oxford, Oxford, UK

Author contributions

- Study conception and design (AADM, FB, JXOR, GJ), data acquisition (AADM, EA, FB, DA, LKD), data analysis (AADM, JXOR, GJ), interpretation of data for the work (AADM, JXOR, GJ)
- Drafting the article (AADM, JXOR, GJ), revising it for intellectual content (all authors)
- Approving the final version of the manuscript (all authors)

Correspondence: Ana Antonia Dias Maile
ana.dias.maile@uni-duesseldorf.de

Acknowledgements

We thank Tomke Bartels, Hayden Bera, Johanna Dappen, Iremnaz Ercan, Julia Hoffmann, Janne Knipp, Lukas Leib, Sophie Öhlschläger and Nils Schäfer for their support during data acquisition. Computational infrastructure and support were provided by the Centre for Information and Media Technology at Heinrich Heine University Düsseldorf.

Funding

This work was supported by an ERC Consolidator Grant from the European Research Council (ERC-CoG 771432) to GJ.

Competing Interests

On behalf of all authors, the corresponding author states that there is no conflict of interest.

Abstract

Decision making often requires the integration of noisy bottom-up sensory evidence with top-down prior expectations learned from past experiences. Acetylcholine and noradrenaline have been proposed to shape these computations, yet it remains unclear whether they directly influence the weighting of sensory evidence and prior expectations during decision making or instead shape the learning process that gives rise to these expectations. To disentangle this, healthy participants (n = 62) completed a perceptual decision-making task under the influence of either the muscarinic acetylcholine receptor antagonist biperiden, the β-adrenoceptor antagonist propranolol, or placebo, in a within-subject crossover design. The task required the integration of sensory evidence with learned expectations. The reliability of these two sources of information varied independently. We show that both drugs led to a faster updating of current beliefs in response to new evidence. Under propranolol, these effects were specific to reward outcomes, whereas under biperiden, faster updating in response to both reward and non-reward outcomes resulted in less stable beliefs. Notably, neither drug affected the degree to which choices were governed by the strength of the sensory evidence. Together, these findings suggest that acetylcholine and noradrenaline guide perceptual decision making by modulating the updating of top-down prior expectations in response to new bottom-up evidence during learning.

Introduction

Perception often relies on noisy and uncertain sensory input. For example, when someone waves at you in foggy weather, limited visibility may make it difficult to identify the person. However, past experience allows learning that certain people are more likely to be encountered in particular contexts. Being on a university campus, for instance, increases the expectation that the person is a fellow student or colleague. Perception and decision making therefore depend on the continuous integration of bottom-up sensory evidence with top-down prior expectations learned from past experiences.

Given the importance of this integration, previous research has been investigating its underlying neurochemical mechanisms. In particular, acetylcholine and noradrenaline have been proposed to play a key role in learning from past outcomes and, consequently, in the formation of top-down expectations. Consistent with this, muscarinic acetylcholine receptor antagonist has been shown to affect reward-guided decision making only when learning is required. Specifically, muscarinic receptor blockade reduces the stability of learned beliefs by accelerating their updating in volatile environments (Kurtenbach et al., 2026). Muscarinic acetylcholine receptor antagonist has further been shown to impair error-related behavioral and cortical adjustments (Danielmeier et al., 2015). Correspondingly, cholinergic responses in the basal forebrain have been shown to provide a precise reinforcement signal that scales with outcome expectancy (Hangya et al., 2015). Noradrenaline has been proposed to play an opposite role to this. Tonic noradrenergic activity facilitates attention-shifting to contextual changes, thereby promoting exploration and responses to new task-relevant stimuli (Aston-Jones & Cohen, 2005; Devauges & Sara, 1990). Additionally, a large body of evidence shows that noradrenaline plays a key role in synaptic plasticity, learning and memory consolidation (Jami et al., 2023; Larsen et al., 2023; Sara et al.,

1999). In line with this, β-adrenoceptor antagonism has been shown to slow bottom-up updating of reward-contingencies in volatile environments (Lawson et al., 2021).

An alternative account proposes that acetylcholine and noradrenaline influence decision making by modulating how top-down expectations are integrated with bottom-up sensory evidence (Yu & Dayan, 2005). Within this framework, the effects of noradrenaline and acetylcholine on learning may arise from a differential weighting of the reliability of new bottom-up information relative to that of the current top-down belief. Both neuromodulators have been shown to play an important role in sharpening sensory neuronal representations (Eggermann et al., 2014; Hasselmo et al., 1997; Herrero et al., 2017; Kossl & Vater, 1989). Consequently, noradrenaline and acetylcholine would determine the extent to which incoming evidence updates current expectations. However, it remains unclear whether this integration is primarily linked to learning. Alternatively, acetylcholine and noradrenaline may govern the weighting of bottom-up information and top-down knowledge independently of learning at the time of decision making.

To disentangle pharmacological effects on evidence weighting from learning itself, we implemented a perceptual decision-making paradigm in which the reliability of bottom-up sensory evidence and top-down learned expectations within each decision was manipulated orthogonally. Because the weighting of each information source during decision making should depend on its reliability (de Lange et al., 2018; Hanks et al., 2011), this design allowed us to quantify their independent contributions to choice behavior. Additionally, learning of the top-down prior was independent of the strength of sensory evidence, as veridical feedback was given after each decision. This allowed us to measure effects on learning independently of perception and its integration. Participants completed the task across three pharmacological sessions in which they received the muscarinic acetylcholine receptor antagonist biperiden and

the β-adrenoceptor antagonist propranolol in a randomized within-subject, placebo-controlled design. We investigated whether the drugs directly altered the weighting of sensory evidence and prior expectations during decision making or instead influenced reward-based learning. We expected biperiden to increase the learning rate causing a faster updating of prior beliefs, whereas propranolol was expected to reduce the learning rate leading to slower updating. Additionally, previous research has implicated both noradrenaline and acetylcholine in regulating spontaneous activity and evoked responses in sensory cortices. We therefore expected both drugs to reduce participants' perceptual discrimination performance (Eggermann et al., 2014; Hasselmo et al., 1997; Herrero et al., 2017; Jimenez-Martin et al., 2021; Kasamatsu & Heggelund, 1982; Kossl & Vater, 1989; Kuchibhotla et al., 2017; McLean & Waterhouse, 1994; Meir et al., 2018; Waterhouse et al., 1998).

In brief, we find that both biperiden and propranolol increased learning rates, resulting in faster updating of prior beliefs. This accelerated updating was specific to reward outcomes under propranolol, whereas under biperiden it led to a maladaptive adjustment of prior beliefs across both reward and non-reward outcomes. Notably, neither drug affected the sensitivity to sensory evidence nor the integration of sensory evidence and prior expectations independently of learning at the time of choice.

Results

To investigate the distinct contributions of acetylcholine and noradrenaline in perception, learning and their integration into a decision, 62 healthy participants performed a modified version of the random dot motion task (RDM). Participants were asked to indicate, on each trial, the mean movement direction of a noisy display of moving dots. We manipulated the quality of the sensory evidence by varying motion coherence (from 0 to 48%), the proportion of dots moving coherently to the left or right (Figure 1b). In addition, the task consisted of periods in which both movement

directions were equally likely and periods in which either a left- or rightward motion was more probable (prior probability, Figure 1c). Changes between these periods were not signaled to participants but needed to be learned. Therefore, decisions could be based on both the available sensory evidence and the learned prior expectation (see Figure 1b-c; similar to Froböse & Ort, 2022; Marshall et al., 2024). We reasoned that statistical knowledge based on prior experience would be particularly beneficial on trials with low strength of sensory evidence. Participants performed the task on three separate sessions, where they received either a single oral dose of the M_1-preferring muscarinic receptor antagonist biperiden (4mg), the β-adrenoceptor antagonist propranolol (40mg), or a placebo in a randomized, within-subject design (Figure 1a).

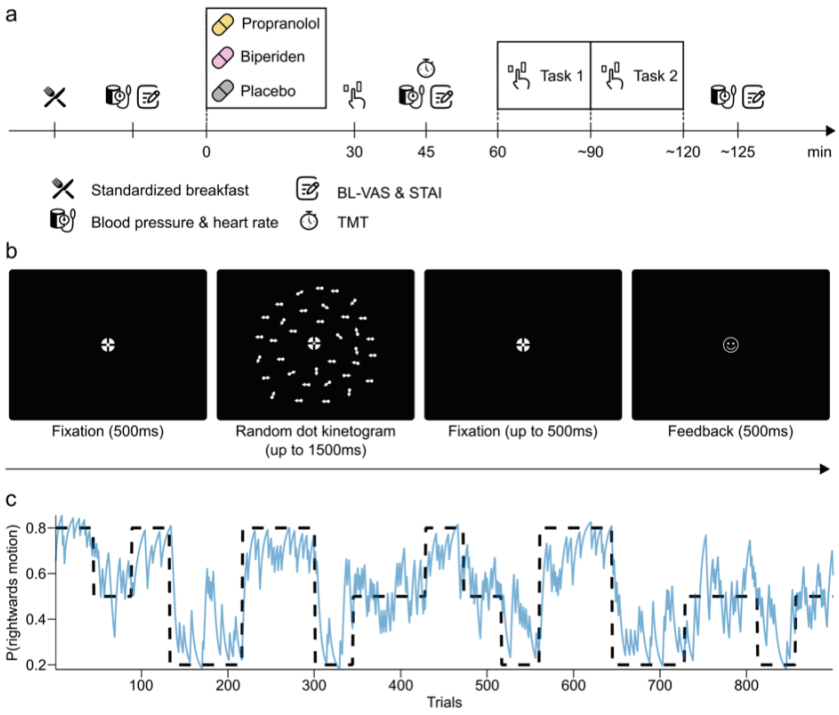

Figure 1: Study procedure and experimental task. (a) Timeline of experimental procedures (kept constant across sessions). Each testing day began with a standardized breakfast. Participants ingested the pill 1 h before performing the experimental tasks. Task order was constant within participants but counterbalanced across participants. Heart

rate and blood pressure were monitored at three different time points, during which participants also completed the Bond & Lader visual analogue scales (BL-VAS) and the State-Trait Anxiety Inventory (STAI). Immediately prior to the first task, participants additionally performed the Trail-Making Test (TMT). These measures were used for control analyses (Supplement 2) **(b)** In the random dot motion task, participants were asked to indicate the mean movement direction of the random dot kinematogram. For this, they could use two sources of information: the coherent motion and a prior probability of a left- or rightward movement, which could be inferred based on the outcomes of previous trials. Participants were allowed to respond until up to 500 ms after the offset of the kinematogram (2000 ms response deadline altogether) **(c)** Example of the time-varying prior probability of movement direction, which switched every 44 or 84 trials. The dashed line represents the true prior and the solid blue line is the estimated prior from a Bayesian optimal learner.

Choice behavior is affected both by motion coherence and prior expectations

We first confirmed that participants' decisions were indeed consistently influenced by both the level of motion coherence and the learned prior belief. A shift in decision making to favor the motion direction of the prior was evident in the raw task behavior (Figure 2a). This was confirmed using a general linear mixed-effects model (GLMM) investigating the influence of motion coherence and prior on choice (left vs. right) across drug conditions. Since the prior was not explicitly signaled to participants, here, we estimated it using a Bayesian optimal learner, which captured what participants could ideally know. Participants' estimates of prior left- or rightward motion probability may well deviate from these normative estimates, a point that we will investigate in further detail in subsequent sections. Model results corroborated that coherence level and the estimated prior had a significant main effect on choice behavior (coherence level: $\beta = 2.08$, $SEM = 0.11$, $z(166673) = 18.42$, $p < 0.001$; prior: $\beta = 0.59$, $SEM = 0.04$, $z(166673) = 16.19$, $p < 0.001$; marginal $R^2_{GLMM} = 0.593$; Figure 2c and Table S1). With increasing coherence and prior strength, participants were more likely to choose the corresponding motion direction (Figure 2a). Furthermore, participants appeared to put more weight on the perceptual information (i.e., the coherent motion) as on the learned prior, as indicated by the higher regression weight (Figure 2c). Furthermore, participants flexibly integrated the coherent motion and the learned prior when making decisions. Choice behavior (Figure 2a) clearly indicated that, under lower levels of perceptual reliability (i.e., at low motion coherence), participants relied more on the

learned prior probability. To quantify this relationship, we set up a GLMM in which we asked whether the increase in the probability of making a correct choice as a function of (unsigned) motion coherence differed between congruent and incongruent trials (i.e., trials in which the prior indicated the same vs. the opposite choice as the direction of coherent motion). This analysis confirmed that the difference in the percentage of correct choices between congruent and incongruent trials decreased with increasing motion coherence (β = -0.66, *SEM* = 0.05, $t(185) = -13.73$, $p < 0.001$; marginal R^2_{GLMM} = 0.235; Figure 2a-b and Table S2).

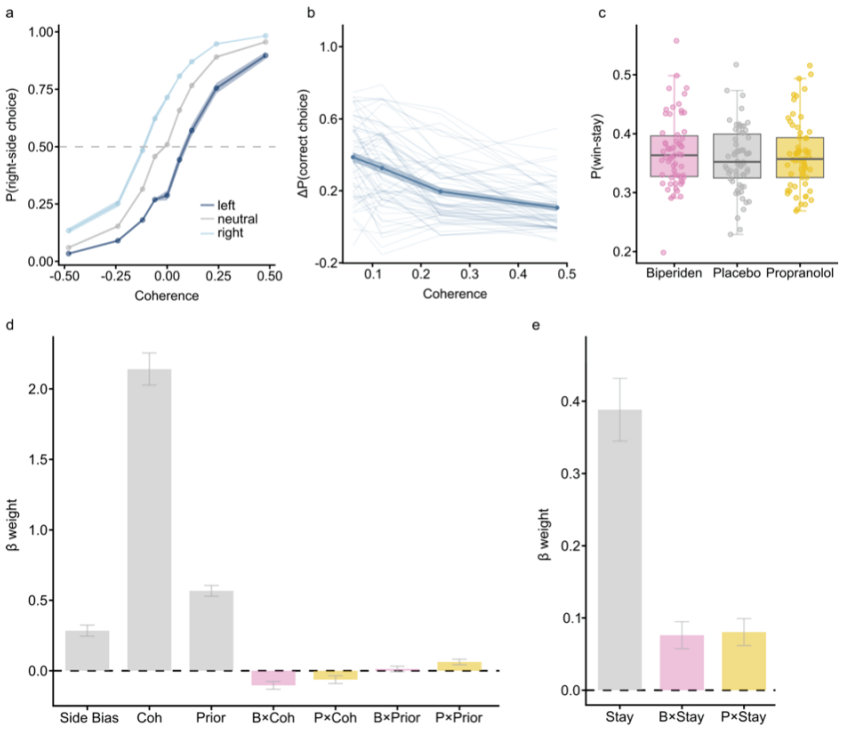

Figure 2: Drug effects on choice behavior. (a) Raw task behavior, averaged across drug condition: Probability for a right-side choice as a function of motion coherence and prior probability (shades of blue, Bayes-optimal prior favoring a left or right choice, or neutral prior where both directions are equally likely on average). Negative coherence levels correspond to leftward motion. Shades depict the standard error. **(b)** Raw prior influence, averaged across drug condition: Difference in the probability of a correct choice between trials in which Bayes-optimal prior was aligned with versus opposed to motion coherence. Light blue lines represent individual participant. The thick blue line indicates the group mean and the shaded area reflects the standard error. **(c)** Raw win-stay behavior, separated by drug condition. The probability of a win-stay choice for each drug condition, with individual participants

represented as dots and distributions summarized by boxplots. Win-stay behavior was increased under both propranolol and biperiden relative to placebo. **(d)** GLMM of participants choice behavior (right-side choices). Bars represent regression coefficients (β) with standard errors. Choices are influenced by both motion coherence (Coh) and prior belief (Prior), with a stronger effect of motion coherence. The effect of coherence on choice behavior was reduced under propranolol (P) and biperiden (B) relative to placebo, as indicated by the significant negative interaction terms. In contrast, the influence of prior was increased under propranolol, as reflected by a significant positive interaction. **(e)** GLMM of win-stay behavior. Bars represent regression coefficients (β) with standard errors. Following reward outcomes, participants tended to repeat the same choice (stay), which was further increased under propranolol (P) and biperiden (B) as indicated by the significant positive interaction terms.

Biperiden and propranolol both appear to affect the balance between sensory evidence and prior belief

Turning to interactions between coherence, prior and drug condition in the same GLMM, we found that both biperiden and propranolol reduced the degree to which choices were governed by sensory evidence (effect of coherent motion, β = -0.10, *SEM* = 0.03, $z(166658) = -3.76$, $p < 0.001$; β = -0.01, *SEM* = 0.03, $z(166658) = -2.26$, $p = 0.024$; for the interaction of biperiden and propranolol with coherence level, respectively, marginal $R^2_{GLMM} = 0.594$; Figure 2c and Table S3). This seems to suggest that both drugs reduce participants' sensitivity to the strength of the sensory evidence. However, we will show below that this apparent effect on perceptual sensitivity may instead reflect an underlying effect on learning. In addition, propranolol increased the effect of the learned prior on choices (β = 0.06, *SEM* = 0.02, $z(166658) = 3.23$, $p = 0.001$; marginal $R^2_{GLMM} = 0.594$; Figure 2c and Table S3). This may indicate a stronger influence of learned prior expectations on participants' choices under propranolol, in line with our predictions.

Biperiden and propranolol may affect learning, rather than weighting, of the prior

Previous work showed that biperiden affects reward-guided decision making by modifying the learning rate, rather than affecting decisions themselves (Kurtenbach et al., 2026). Similarly, noradrenergic transmission is involved in learning under conditions of changing contingencies (Glennon et al., 2019; Jepma et al., 2016) Therefore, an alternative explanation for the apparent downweighting of sensory

evidence compared to the prior (Figure 2) is that the prior is inaccurately learned in the drug condition. The estimates of prior probability used above were based on a Bayesian optimal learner, which captured what participants could ideally know (Behrens et al., 2007). Hence, this drug effect on prior probability may either reflect a change in the use of this information or a change in learning i.e., how closely participants' estimates of prior probability aligned with the Bayesian optimal learner.

We therefore used, in a first step, a model-agnostic approach to determine whether the degree to which past outcomes were used to guide future choices was affected by drug condition, namely a win-stay/lose-switch analysis. Faster updating of the prior belief is reflected in an increased likelihood of repeating a previously rewarded choice on the next trial (win-stay), whereas previously non-rewarded choices are related to a higher probability of switching (lose-switch; Estes, 1957). Conversely, slower updating is characterized by reduced win-stay/lose-switch behavior. Drug effects were analyzed separately for trials following rewarded and non-rewarded outcomes to assess potential differences. We observe increased win-stay behavior under both biperiden and propranolol (β = 0.09, *SEM* = 0.02, $z(133447) = 4.07$, $p < 0.001$; β = 0.08, *SEM* = 0.02, $z(133447) = 4.30$, $p < 0.001$; for the interaction of biperiden and propranolol with stay bias, respectively, marginal $R^2_{GLMM} = 0.622$; Figure 2b,d and Table S4). This pattern suggested faster updating of prior beliefs in response to reward outcomes. While this finding was consistent with the hypothesis for biperiden, it contradicted the prediction for propranolol where we expected a slower updating of the prior. In contrast, neither drug significantly modulated lose-switch behavior (β = -0.04, *SEM* = 0.04, $z(32971) = -1.02$, $p = 0.309$; β = 0.02, *SEM* = 0.04, $z(32971) = 0.49$, $p = 0.627$; for the interaction of biperiden and propranolol with stay bias, respectively, marginal $R^2_{GLMM} = 0.568$; Table S5). The effect therefore did not extend to non-reward

outcomes, where a faster updating would be expected to reduce stay behavior after errors.

Notably, the apparent drug modulation of motion coherence was reduced in this win-stay/lose-switch analysis, where we approximated learning by accounting for how past outcomes guide current choices, supporting the interpretation that the apparent effect of drug on weighting of the sensory evidence in fact reflects misestimation of the prior. Only biperiden significantly modulated the influence of motion coherence on choice behavior by decreasing the degree to which choices were governed by sensory evidence in response to reward outcomes (interaction of biperiden with coherence in trials following reward: β = -0.12, *SEM* = 0.03, $z(133447) = -3.72$, $p < 0.001$; for all other drug interactions with coherence following rewarded or unrewarded trials: $\beta \geq -0.07$, *SEM* ≥ 0.03, $z \geq -1.34$, $p \geq 0.182$).

Participants additionally exhibited a bias toward rightward motion, as indicated by a significant intercept across all models (Figure 2c, intercept from the choice model including all trials: $\beta = 0.28$, *SEM* = 0.04, $z(166658) = 7.24$, $p < 0.001$; marginal $R^2_{GLMM} = 0.594$; Figure 2c and Table S3). However, this bias was not modulated by either of the drugs ($\beta = 0.03$, *SEM* = 0.04, $z(166658) = 0.69$, $p = 0.492$; $\beta = -0.03$, *SEM* = 0.04, $z(166658) = -0.71$, $p = 0.481$; for the main effect of biperiden and propranolol in the choice model including all trials, respectively, marginal $R^2_{GLMM} = 0.594$). Nevertheless, given its pronounced influence on choice behavior, the side bias was taken into account in the subsequent computational modeling.

We additionally confirmed that drug effects were independent of the following potential confounds: All cholinergic and noradrenergic effects on participants' choices were independent of drug effects on mood, state anxiety, visuomotor processes, heart rate, blood pressure and session order (see Supplement 2 for control analyses). Further, the drugs did not significantly influence participants' reaction times (Table S6).

In sum, participants appear to update their prior expectations faster in response to rewards under both drugs compared to placebo. Therefore, both drugs seem to modulate learning, rather than weighting, of the prior.

Computational learning model confirms that biperiden and propranolol affect learning rate rather than evidence weighting

While our win-stay analyses provided model-agnostic evidence for drug effects on learning, they only captured effects of the outcome from the immediately preceding trial. To fully account for how participants inferred beliefs about prior probability across multiple trials and how this was integrated with sensory evidence, we implemented computational models. This allowed us to determine whether the observed drug effects reflect changes in learning and/or in the flexible weighting of the two information sources (motion coherence and learned prior). The preregistered model implemented a Q-learning with a delta update rule governed by a learning rate (see methods, equation 1). Given the reward-specific effects of both drugs in the model-free win-stay analyses above, we additionally tested a model variant with separate learning rates for rewarded and unrewarded trials. However, a joint learning rate provided a better fit to the data (BIC = 730.39 and BIC = 732.04 for median Bayes Information Criterions (BIC) of the models with one learning or separate learning rates, respectively). Consistent with the flexible influence of the prior depending on perceptual reliability observed in participants' behavior (Figure 2a-b), the model assumed an additive value construction. In particular, the evidence in favor of either a left or right choice was jointly governed by (signed) motion coherence and prior belief, with their relative contribution being determined by the weighting parameter θ (values closer to 0 indicated a stronger reliance on the prior and values closer to 1 indicated a stronger reliance on sensory evidence). Choices were generated using a softmax choice rule with an inverse

temperature τ capturing choice stochasticity and a side bias parameter b capturing left- or right-choice biases.

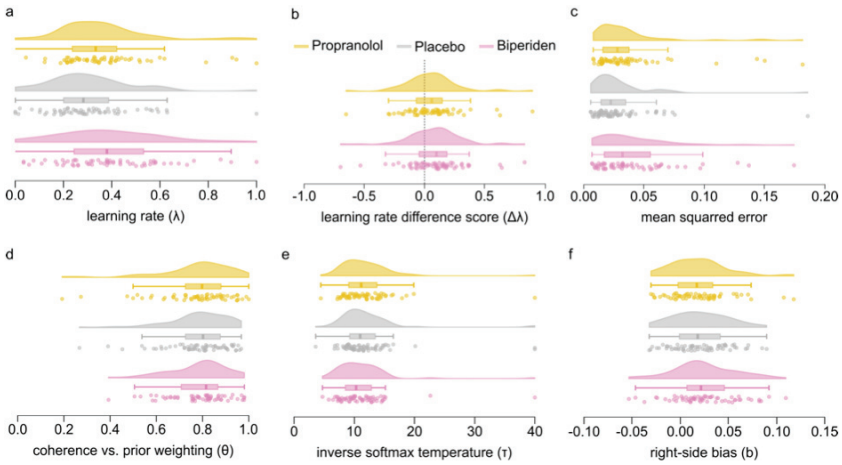

Figure 3: Parameter estimates per participant and drug conditions. Raincloud plots in **a**, **d**, **e**, **f** illustrate the distribution of the four model parameters across drug conditions: **(a)** learning rate (λ), **(d)** relative weighting (θ), **(e)** inverse softmax temperature (τ) and **(f)** right-side bias (b). Panel **b** shows difference scores for the learning rate (Δλ; drug-placebo), with the dotted line marking zero (no difference). Panel **c** displays the distribution of mean squared error (MSE) across drug conditions. Half-violins and boxplots summarize the distribution of single-subject values (dots) for each drug condition. **(a,b)** Learning rates were significantly higher under biperiden and propranolol compared to placebo. **(c)** This increased updating was maladaptive under biperiden, as reflected by significantly higher MSE relative to placebo. **(d)** The relative weighting of perceptual information and the prior beliefs was not significantly modulated by drug condition. **(e)** Choices tended to be more stochastic under biperiden, reflected in a trend for a lower inverse softmax temperature compared to placebo. There was no significant effect for propranolol. **(e)** Participants displayed a right-side choice bias that was not significantly modulated by drug condition.

The learning rate λ was significantly increased under both biperiden ($Mdn_{biperiden}$ = 0.38, $Mdn_{placebo}$ = 0.28, z = 3.14, p = 0.002, r = 0.40) and propranolol ($Mdn_{propranolol}$ = 0.33, z = 2.09, p = 0.037, r = 0.26; Figure 3a-b). This indicated that participants updated their prior estimate faster under both drugs, consistent with the win-stay/lose-switch analysis. To assess whether this pattern led to estimates of the prior that more closely tracked the optimal estimates, we computed the mean squared errors (MSE) of each participant's trial-wise prior estimates and compared them between placebo and drugs. Under biperiden, the MSE was significantly higher than under placebo suggesting that the increased learning rate led to worse prior estimates, making it maladaptive

($Mdn_{biperiden}$ = 0.03, $Mdn_{placebo}$ = 0.02, z = 3.17, p = 0.002, r = 0.23; Figure 3c). In contrast, there was no significant difference in the MSE between propranolol and placebo ($Mdn_{propranolol}$ = 0.03, z = 1.52, p = 0.127, r = 0.11; Figure 3c).

Differential drug effects on learning from positive and negative outcomes

Given that the effects we observed above in our model-free analyses were specific to win-stay behavior, we further examined the model with separate learning rates for rewarded and unrewarded choices. While this model did not improve the fit compared to the joint learning rate model, it allowed us to assess whether changes in learning were specific to reward or non-reward outcomes, or whether these changes occurred regardless of outcome type.

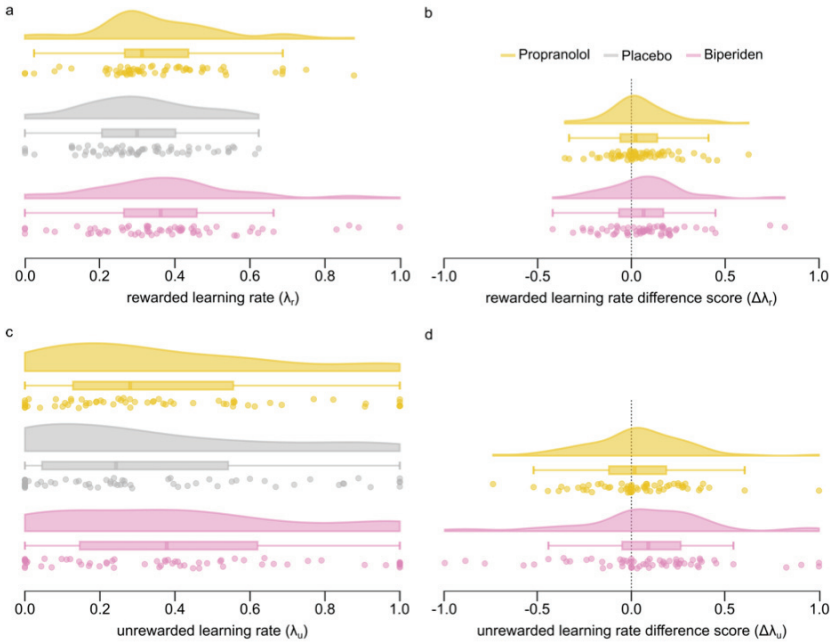

Figure 4: Different learning rates for reward and non-reward outcomes per participant and drug condition. Raincloud plots in **a** and **c** illustrate the distribution of rewarded **(a)** and unrewarded **(c)** learning rate across drug conditions. Panels **b** and **d** shows difference scores for the rewarded **(b)** and unrewarded **(d)** learning rate ($\Delta\lambda_r$ and $\Delta\lambda_u$; drug-placebo), with the dotted line marking zero (no difference). Half-violins and boxplots summarize the distribution of single-subject values (dots) for each drug condition. **(a,b)** Learning rates of rewarded trials were

significantly higher under biperiden and propranolol compared to placebo. **(c,d)** Learning rates of unrewarded trials were significantly higher under biperiden, with no significant effect under propranolol.

This model revealed that propranolol specifically increased learning rates for rewarded choices ($Mdn_{propranolol}$ = 0.31, $Mdn_{placebo}$ = 0.30, z = 1.98, p = 0.048, r = 0.25; Figure 4a-b) with no significant effect on the unrewarded learning rate ($Mdn_{propranolol}$ = 0.28, $Mdn_{placebo}$ = 0.24, z = 1.07, p = 0.285, r = 0.14; Figure 4c-d). Biperiden, in contrast, increased learning rates for both rewarded ($Mdn_{biperiden}$ = 0.36, z = 2.53, p = 0.012, r = 0.32; Figure 4a-b) and unrewarded trials ($Mdn_{biperiden}$ = 0.38, z = 2.22, p = 0.027, r = 0.28; Figure 4c-d), with larger effects for rewarded trials (see Supplement 3 for complete model description).

Once differences in learning rate are accounted for biperiden and propranolol do not affect the weighting of sensory and prior evidence

Based on the GLMM, we expected a relative shift in the weighting of coherence and prior under propranolol. However, the relative weighting was not significantly modulated by either propranolol ($Mdn_{propranolol}$ = 0.80, z = -0.87, p = 0.383, r = 0.11) or biperiden ($Mdn_{biperiden}$ = 0.82, z = -0.11, p = 0.914, r = 0.01; Figure 3d). Hence, there was no cholinergic or noradrenergic effect on the relative weight given to sensory evidence versus prior probability, contrary to our hypotheses. However, regardless of drug condition and consistent with the results from the GLMM, participants' choices were influenced more strongly by coherent motion than by the learned prior, as indicated by values of the weighting parameter θ close to 1 ($Mdn_{placebo}$ = 0.80).

The inverse softmax temperature (τ), capturing choice stochasticity, was not significantly modulated by propranolol ($Mdn_{propranolol}$ = 10.29, $Mdn_{placebo}$ = 10.96, z = 0.14, p = 0.886, r = 0.02). There was a trend toward a lower inverse temperature and thus an increased choice stochasticity under biperiden ($Mdn_{biperiden}$ = 11.13, z = -1.84,

p = 0.066, r = 0.23; Figure 3e). Participants additionally exhibited a rightward choice bias, which was not modulated by either drug ($Mdn_{placebo}$ = 0.02, biperiden: $Mdn_{biperiden}$ = 0.16, z = 1.54, p = 0.124, r = 0.20; propranolol: $Mdn_{propranolol}$ = 0.02, z = -0.47, p = 0.636, r = 0.06; Figure 3f), consistent with the GLMM.

Parameter recovery and model validation confirmed the reliability of the fitting procedure (Supplement 4). Simulated behavior successfully recovered the ground-truth parameters and reproduced key behavioral findings including the drug effects on motion coherence observed in the GLMM. Importantly, the drug modulation of coherence effects on choice observed in the GLMM could be fully explained by drug-dependent changes in the learning rate. This aligns with the win-stay/lose-switch analysis where drug modulations of coherence were also less robust. Together, this suggests that the observed drug-induced changes of coherence effects on choice we reported above using our regression-based approach do not reflect a genuine change in sensitivity to sensory inputs and instead reflects altered learning of environmental contingencies.

Taken together, propranolol and biperiden significantly altered learning dynamics, with both drugs causing a faster updating of prior beliefs. Notably, once this learning effects was accounted for, neither propranolol nor biperiden modulated the relative weighting of perceptual and learned information at the time of choice. Biperiden tended to additionally increase choice stochasticity.

Discussion

Decision making relies on learning from past experiences and integrating this prior knowledge with current perceptual evidence. Noradrenaline and acetylcholine, which modulate both perception and learning, are thought to guide this integration (Eggermann et al., 2014; Hangya et al., 2015; Kossl & Vater, 1989; Lawson et al., 2021; McLean & Waterhouse, 1994; Meir et al., 2018; Yu & Dayan, 2005). In the present

study, we investigated the role of these neurotransmitter systems in a perceptual decision-making task that required the integration of sensory evidence with prior expectations learned across past outcomes. Participants received the muscarinic acetylcholine receptor antagonist biperiden and the β-adrenoceptor antagonist propranolol in a within-subject, double-blind, placebo-controlled, crossover design. We investigated drug effects using two complementary approaches: First, GLMMs allowed us to examine how task parameters influenced behavior and how these effects were modulated by the pharmacological manipulations. Second, computational modeling allowed us to analyze drug effects on the underlying computations, including learning and the flexible integration of prior knowledge and sensory information. Our results highlight the role of noradrenaline and acetylcholine in learning and updating of top-down prior beliefs based on new bottom-up evidence. Specifically, muscarinic acetylcholine receptor antagonist under biperiden and β-antagonism under propranolol lead to a faster updating of prior beliefs as indicated by increased learning rates under both drugs compared to placebo. Therefore, biperiden and propranolol caused prior estimates to be influenced more strongly by recent outcomes compared to more distant experiences. Moreover, modulation of learning rates under biperiden led prior estimates to deviate more from the statistical optimum compared to placebo. Hence, increased learning rates under biperiden caused maladaptive adjustments in estimates of the prior. Prior estimates under propranolol did not significantly deviate relative to the statistical optimum compared to placebo possibly due a less pronounced effect on learning rates or to the selectivity for reward outcomes: Following a rewarded choice, prior estimates were adjusted faster under propranolol compared to placebo. Updates following non-rewarded choices however did not significantly differ between propranolol and placebo.

Perceptual discriminability has been shown to depend on cholinergic and noradrenergic modulation of the signal-to-noise-ratio in sensory cortices (Eggermann & Feldmeyer, 2009; Hasselmo et al., 1997; Kasamatsu & Heggelund, 1982; Meir et al., 2018). Acetylcholine is proposed to increase the response magnitude by suppressing spontaneous activity and thereby heightening sensitivity to incoming signals (Herrero et al., 2017; Minces et al., 2017; Soma et al., 2013). In turn, noradrenaline enhances the strength and selectivity of neuronal responses to sensory input, thereby sharpening perceptual tuning curves (Kossl & Vater, 1989; McLean & Waterhouse, 1994; Waterhouse et al., 1990). Accordingly, we hypothesized that propranolol and biperiden would reduce participants' perceptual acuity. A GLMM revealed a decreased influence of motion coherence on choices under both biperiden and propranolol, compared to placebo. While this suggests reduced perceptual abilities under both drugs, computational modeling results indicate that this effect does not reflect a genuine change in sensory processing. Instead, biperiden and propranolol seem to selectively modulate learning.

The GLMM relied on prior estimates from the Bayesian learner and therefore could not capture participants' true trial-by-trial updating. In contrast, win-stay/lose-switch analyses allowed a model-free approximation: faster updating of the prior belief was reflected in an increased likelihood of repeating a previously rewarded choice on the next trial (win-stay), whereas previously non-rewarded choices were associated with a higher probability of switching (lose-switch). Biperiden and propranolol significantly increased the probability to repeat a previously rewarded response compared to placebo. Choices following non-rewarded responses were not significantly modulated by either drug. Computational modeling allowed us to further disentangle these effects by capturing the latent cognitive processes. Accordingly, propranolol and biperiden increased learning rates compared to placebo causing a

faster updating, with no effects on the weighting of sensory evidence. Hence, prior estimates under both drugs were influenced more strongly by recent outcomes compared to more distant experiences. Conversely, we hypothesized that propranolol would decrease learning rates leading to a slower updating of prior beliefs. In a similar experimental paradigm, Lawson et al. (2021) found a slower updating of outcome contingencies under propranolol. The reason for the divergence of our results remains unclear but may be caused by differential modeling approaches. Lawson et al. (2021) model choice behavior using a Hierarchical Gaussian Filter framework that did not incorporate the influence of the sensory evidence. Participants' choices in our study appeared to rely strongly on perceptual information (coherent motion), as indicated by the high regression weight and values of the integration parameter θ close to 1. This suggests a greater influence of sensory relative to learned evidence. Accordingly, our computational model incorporated the sensory evidence and estimated its integration with the learned prior belief.

Consistent with the observed increase in learning rates under propranolol, noradrenaline is proposed to stabilize estimates of environmental volatility (Marshall et al., 2016; Yu & Dayan, 2005). Accordingly, noradrenergic antagonism has been shown to lead to faster updating, as unexpected outcomes are more likely to be attributed to changes in the underlying contingency (Marshall et al., 2016). This is consistent with the increased learning rate observed here. However, it is important to note that prior work targeted α_1-adrenoceptors, whereas the present study involved β-adrenoceptor antagonism. Nevertheless, it has been shown that β-adrenoceptor activity contributes to learning by supporting synaptic plasticity in the hippocampus, which is essential for memory formation (Jami et al., 2023; Larsen et al., 2023; Sara et al., 1999). We extend this finding by identifying a role of β-adrenoceptor activity in trial-by-trial learning whereby recent outcomes have a stronger influence compared to more distant

experiences. Moreover, noradrenergic effects on learning have been shown to be specific to volatile environments and to track change points (Glennon et al., 2019; Jepma et al., 2016). This is consistent with our experimental paradigm, which incorporated volatility in prior probabilities, and fits the proposed noradrenergic mechanism of stabilizing estimates of the underlying contingency. Our findings further indicate that the effects of propranolol on learning were specific to rewarded outcomes, as learning rates were selectively increased following rewarded choices. Accordingly, no significant noradrenergic modulation of learning rates was observed following non-rewarded choices.

Similar to noradrenaline, cholinergic effects on learning have been shown to be specific to volatile environments (Kurtenbach et al., 2026). Recent own work has demonstrated that biperiden increases learning rates in volatile learning environments, in line with our hypothesis and current findings (Kurtenbach et al., 2026). Consistent with this, faster updating under biperiden leads prior estimates to deviate stronger from the statistical optimum compared to placebo. Hence, increased learning rates under biperiden cause maladaptive adjustments in prior beliefs. This pattern was observed both in the present study and in Kurtenbach et al. (2026). It has been proposed that muscarinic acetylcholine receptor antagonist causes impaired adaptions to probabilistic noise. More specifically, unexpected outcomes do not lead to an adequate adjustment of beliefs regarding probabilistic outcomes. This causes unexpected outcomes to be instead attributed to contingency changes, in turn causing a faster maladaptive updating (Kurtenbach et al., 2026; Marshall et al., 2016; Piray & Daw, 2021; Yu & Dayan, 2005). This interpretation is further supported by the effects of cholinergic activity in the brain. Activity of cholinergic neurons in the basal forebrain has been identified as a precise reinforcement signal (Hangya et al., 2015). Furthermore, muscarinic acetylcholine receptor antagonist by biperiden has been

shown to decreases the prediction error signal correlate in high-beta power in the lateral prefrontal cortex (Kurtenbach et al., 2026). This in turn may lead to the impaired post-error adjustments that have been observed in sensory cortical areas (Danielmeier et al., 2015). Moreover, cholinergic effects on learning have been reported to be specific to rewarded choices, with only a trend-level effect for unrewarded learning rates (Kurtenbach et al., 2026). While we observe increased learning rates following both rewarded and unrewarded outcomes, differences in effects sizes, together with the win-stay/lose-switch analysis, suggest a similar pattern in our data: biperiden effects on the rewarded learning rates are larger than those on unrewarded learning rates, which only showed a small effect size. In addition, faster updating under biperiden was specific to win-stay and did not hold for lose-switch choices.

We did not find significant drug effects on the integration parameter θ, which defined the relative weighting of bottom-up sensory evidence versus top-down prior beliefs during decision making. Nevertheless, noradrenergic and cholinergic effects on learning provide insights into this integration: increased learning rates under both drugs suggests that prior beliefs are more uncertain and hence environmental contingencies need to be updated faster. Therefore, top-down prior expectations are suppressed in order to facilitate learning from bottom-up evidence, which is augmented (Yu & Dayan, 2005). This suggest that the balance between top-down prior information and bottom-up evidence is regulated indirectly by the dynamic updating of prior expectations based on the expected environmental uncertainty.

Lastly, theoretical models postulate a role of noradrenaline in guiding choice stochasticity (Doya, 2002). In our computational models, this was operationalized by an inverse temperature τ, with higher values indicating more deterministic choices. However, propranolol had no effect on choice stochasticity. Instead biperiden tended to decrease the inverse temperature, indicative of more stochastic choices. While we

did not hypothesize this modulation, a similar effect of biperiden on choice stochasticity has been observed in previous work (Erfanian Abdoust et al., 2024; Kurtenbach et al., 2026).

Taken together, our findings provide causal evidence that acetylcholine and noradrenaline shape learning by modulating, in distinct ways, how prior expectations are updated in response to new information. Importantly, once differences in learning were accounted for, neither biperiden nor propranolol altered the relative weighting of sensory evidence and prior expectations during choices. These findings therefore suggest that acetylcholine and noradrenaline contribute to choice behavior by shaping learning of the internal contingencies of the environment, rather than by directly modulating the integration of sensory evidence and prior knowledge at the time of decision making.

Methods

The study was approved by the medical ethics board of Heinrich Heine University Düsseldorf (study-ID: 2024-286) and is in line with the Helsinki Declaration of 1975. The described methods follow the planned procedure, which can be found at https://doi.org/10.17605/OSF.IO/AQD2R (Dias Maile et al., 2025). Analyses which diverged from this, were marked accordingly.

Participants

Participants were native-level German speakers with normal or corrected-to-normal vision. They were naïve to the purpose of the study and gave written informed consent. Compensation followed a fixed rate plus an additional performance-based bonus. Due to the pharmacological intervention, participants were screened for certain pre-existing medical conditions, including neurological and psychiatric disorders (Supplement 5). As part of this screening, they were also required to reach a predefined performance

threshold in the two experimental tasks. Participants who failed to meet this performance threshold across the three pharmacological sessions were excluded post hoc (*N* = 6). Of the 72 participants who took part in the study, four dropped out and six were excluded based on task performance resulting in a final sample of 62 participants (36 female). On average, they were *M* = 23.77 years old (*SD* = 3.88 years) and weight *M* = 70.28 kg (*SD* = 7.31 kg). Most participants were right-handed (*N* = 52).

Procedure

The study consisted of a medical screening followed by three pharmacological sessions. In the screening, participants were required to meet the medical inclusion criteria (see supplements). This included an evaluation of participants' heart rate and ECG conducted by a cardiologist to assess potential abnormalities (particularly atrioventricular block). In addition, participants filled out the Beck's Depression Inventory (BDI; Beck et al., 1996), the State-Trait Anxiety Inventory (STAI; Spielberger et al., 1983), the Barratt Impulsiveness scale (BIS-15; Meule et al., 2011; Spinella, 2007) and a modified version of the Edinburgh Handedness Inventory (Oldfield, 1971). They also completed the two experimental tasks and needed to meet pre-defined performance criteria: at least 65% correct responses in the random dot motion task (RDM) and fewer than ten missed trials in the explore-exploit-task (EET; not further analyzed in this study).

The three pharmacological sessions were conducted in the morning and were separated by at least five days to account for the drugs' half-lives (Borgstrom et al., 1981; Brocks, 1999; Grimaldi et al., 1986; Kalam et al., 2020). Each session lasted approximately three hours and followed an identical procedure, only the drug (or placebo) administered differed (Figure 1a). In a double-blind, within-subject, crossover design participants received a single oral dose of either the M_1-preferring muscarinic

receptor antagonist biperiden (4mg), the β-adrenoceptor antagonist propranolol (40mg), or a placebo. Prior to the drug administration, participants were provided a standardized breakfast. Vital signs (blood pressure and heart rate) were measured at three time points per session: before drug administration, immediately before the experimental tasks (45 min after drug administration), and after the experimental tasks (approximately 125 min after drug administration). At the same three time points, participants also filled out the Bond and Lader Visual Analogue Mood Scale (BL-VAS; Bond & Lader, 1974) and the STAI. Thirty minutes after drug administration, participants refamiliarized themselves with the experimental tasks. After 50 min they performed the Trail Making Test (TMT; part A; Rodewald et al., 2012). Participants began the experimental tasks one hour after drug intake in accordance with the average time for peak plasma concentration (Borgstrom et al., 1981; Brocks, 1999; Grimaldi et al., 1986; Kalam et al., 2020). Each task lasted approximately 25-35 min. Task order was counterbalanced across participants but remained constant within participant. At the end of the pharmacological session, participants had the opportunity to see the study physician. Following the third session, they were asked to indicate the perceived order of drug administration.

Random dot motion task

In the RDM, participants viewed a random dot kinematogram in which most dots moved randomly, while a subset moved coherently either leftward or rightward (Figure 1b,c ; similar to Froböse & Ort, 2022; Marshall et al., 2024). Participants were instructed to indicate the overall movement direction (left or right) with a button press.

Two aspects of the task were manipulated. First, motion coherence i.e., the proportion of coherently moving dots, was varied across four levels (6%, 12%, 24% and 48%). Second, a prior probability for motion direction was introduced. Specifically,

across a given phase (44 or 84 trials), there was a probability *p* that the direction of movement would be to the right, where *p* took one of three values (0.2, 0.5, 0.8). The prior probability and its switches were not explicitly cued and therefore needed to be learned by participants. To assess performance based solely on the learned prior, four trials with 0% motion coherence were included in each prior phase. Coherence and prior were counterbalanced. The task consisted of 18 blocks with 50 trials each. Participants were allowed to rest after each block. Prior to the main task, they (re-) familiarized themselves with the task by completing two blocks featuring higher coherence levels (70%, 75%, 80% and 85%) but identical prior levels and trial structure.

In detail, each trial began with the presentation of a fixation dot (radius = 0.4 degrees visual angle (dva)), which was presented centrally for 800ms prior to the presentation of the random dot kinematogram (Thaler et al., 2013). The fixation dot remained onscreen with the kinematogram, which was presented in a ring with an inner/outer radius of 1.25/5.00 dva. On average, it consisted of 250 dots, which had a size of four pixels per dot resulting in a dot density of 3.4 dots/dva^2. Dots moved at a speed of 3.6 dva/s and had a lifetime of four frames. Their positions were updated on every frame. After four frames, a dot was replaced by a new one appearing at a random location within the cloud. Dots were presented in light gray (RGB value: 236, 236, 236) against a dark gray background (RGB: 13, 13, 13). The random dot kinematogram was shown for 1500 ms. If no response was made during this period, another 500 ms response window followed without the stimulus on screen. Responses made after this were marked as too late. Early responses were defined as those given within 200 ms of stimulus onset. In cases of early or late responses, a warning was presented on the screen. Otherwise, feedback was provided in the form of a centrally presented smiley or frowny (radius = 0.67 dva) for 500 ms, indicating whether the response was correct.

At the end of each block, participants received feedback on their percentage of correct answers. They were then given the opportunity to take a self-paced break of at least 10 s before continuing. The RDM was programmed using Psychopy (version 3.1.5; Peirce, 2007) and presented on a 16 inch screen with a refresh rate of 60 Hz. Participants were situated at a screen distance of 80 cm in a dimly lit room.

Statistical analyses

General linear mixed-effects modeling

In order to evaluate drug effects on perceptual decision making and the independent weighting of perceptual evidence and prior information, behavioral data was first analyzed using GLMM. Analyses were conducted in R (version 4.2.2; R Development Core Team, 2022) using the lme4 package (version 3.1–3; Bates, Machler, et al., 2015). We chose this approach since it allowed estimating both within- and between-subject variability in accordance with our within-subject experimental design (Brown, 2021; Harrison et al., 2018; Jaeger, 2008). Using these models, we examined task and drug effects on participants' choices and reaction times. Choice behavior (left vs. right) was modeled using a GLMM with a binomial distribution. Fixed effects included the degree of coherent motion, the learned prior and the drug condition and its interaction with both coherence and prior. Since participants did not know the true prior distribution and had to instead learn it over time, the prior was estimated individually for each participant and pharmacological condition using a Bayesian optimal learner set up in MATLAB (version R2021a; The MathWorks Inc., 2021). Deviating from the original analyses plan, we implemented the Bayesian learner described in Behrens et al. (2007) since it provided the best model fit. We applied treatment contrasts and z-scored all continuous predictors to achieve standardized estimates. The random-effects structure was determined using a principal component analysis (PCA) following

the recommendation of Bates, Kliegl, et al. (2015), where random components needed to explain at least 1% variance . The choice model included both a random intercept and a random slope for the within-subject factors motion coherence, prior and drug. Exploratory analyses of learning also examined participants' win-stay/lose-switch behavior (see supplements for a complete overview of model structure). Where we observed significant drug effects on control measures (mood, state anxiety, visuomotor abilities, heart rate and blood pressure), we added them to our GLMM as fixed effects to verify that our effects of interest were not affected by these covariates. A further control analysis encompassed adding the session number as fixed effects to control for putative order effects. All *p*-values were based on asymptotic Wald tests. R^2 was reported for all models using the r.squaredGLMM procedure of the MuMIn package (version 1.48.4; Bartoń, 2024).

Computational modeling

To analyze the drug effects on the underlying cognitive processes (i.e., learning and the relative weighting of information sources) that determined participants' choice behavior, we used computational modeling. Based on an independent dataset using the same perceptual decision-making task, we identified the best-fitting model. Specifically, we compared a basic model in which the influence of motion coherence and prior information was governed by a relative weighting parameter to several other implementations of this integration process. These included a model with coherence-dependent weighting, in which the influence of prior information decreased with increasing motion coherence, as well as a variant in which this dependence was exponentially scaled. We further tested a model incorporating a coherence-dependent modulation of the learning rate. Lastly, we also compared all models to a version including a side bias, given its pronounced influence on raw choice behavior. We found

that the basic model with an added side bias provided the best fit to participants' choice behavior. We therefore preregistered this model for implementation in the present pharmacological dataset. Contrary to our planned analyses, we were unable to fit the data in a Bayesian hierarchal framework due to model complexity. Therefore, the preregistered model was implemented non-hierarchically in Matlab (MATLAB Version R2021a, Massachusetts: The Mathworks Inc.). The model assumed an additive integration of the motion coherence and the learned prior:

$$sv_{D,t} = \theta * c_{D,t} + (1-\theta) * v_{D,t} + b \quad (1)$$

where $sv_{D,t}$ was the subjective value of direction D on trial t, and $c_{D,t}$ and $v_{D,t}$ represented the coherence and the learned prior (both scaled between -1 and 1), respectively. The parameter θ determined the relative weighting of these two sources of information. Values $\theta > 0.5$ indicated that choices were more strongly influenced by the motion coherence than by the learned prior. Since GLMMs revealed a right-side bias, the model additionally included a side bias b. The learned prior was modelled using a Q-learning rule, where the current prior ($v_{D,t}$) was updated for the next trial ($v_{D,t+1}$) based on the outcome of the current trial ($r_{D,t}$) and the learning rate λ:

$$v_{D,t+1} = v_{D,t} + \lambda * (r_{D,t} - v_{D,t}) \quad (2)$$

Given the specific drug effects on participants' win-stay behavior, an exploratory model further incorporated differential learning rates based on if participants were rewarded (λ_r) or not (λ_u) on the current trial:

$$v_{D,t+1} = v_{D,t} + \lambda_{r,u} * (r_{D,t} - v_{D,t}) \quad (3)$$

Choices were modelled using a softmax choice rule including an inverse temperature τ to capture choice stochasticity. Therefore, the probability to choose direction D was generated as:

$$p_{D,t} = \frac{1}{1+e^{-(\Delta sv_t \tau)}} \quad (4)$$

Where ∆sv denoted the subjective value difference (left minus right for direction *D* = left). Because the distribution of parameter estimates deviated from normality, drug effects were assessed using Wilcoxon-signed rank tests. We additionally performed a parameter recovery and model validation to evaluate model integrity. For this purpose, we simulated 500 datasets per participant and pharmacological session. For model validation, the data was average across simulation using the mode, thereby preserving the binomial structure of the behavioral data and key behavioral findings were replicated. Parameter recovery involved refitting the model on the simulated datasets and verifying successful recovery of the ground-truth parameters.

Code and data availability

All data and codes will be made available on OSF.

References

Aston-Jones, G., & Cohen, J. D. (2005). An integrative theory of locus coeruleus-norepinephrine function: adaptive gain and optimal performance. *Annu Rev Neurosci*, *28*, 403–450. https://doi.org/10.1146/annurev.neuro.28.061604.135709

Bartoń, K. (2024). MuMIn: multi-model inference. R package version 1.48. 4. In.

Bates, D., Kliegl, R., Vasishth, S., & Baayen, H. (2015). Parsimonious mixed models. https://arxiv.org/abs/1506.04967

Bates, D., Machler, M., Bolker, B. M., & Walker, S. C. (2015). Fitting Linear Mixed-Effects Models Using lme4. *Journal of Statistical Software*, *67*(1), 1–48. https://doi.org/DOI 10.18637/jss.v067.i01

Beck, A. T., Steer, R. A., & Brown, G. K. (1996). *Manual for the Beck Depression Inventory–II*. Psychological Corporation.

Behrens, T. E., Woolrich, M. W., Walton, M. E., & Rushworth, M. F. (2007). Learning the value of information in an uncertain world. *Nat Neurosci*, *10*(9), 1214–1221. https://doi.org/10.1038/nn1954

Bond, A., & Lader, M. (1974). The use of analogue scales in rating subjective feelings. *British Journal of Medical Psychology*.

Borgstrom, L., Johansson, C. G., Larsson, H., & Lenander, R. (1981). Pharmacokinetics of propranolol. *J Pharmacokinet Biopharm*, *9*(4), 419–429. https://doi.org/10.1007/BF01060886

Brocks, D. R. (1999). Anticholinergic drugs used in Parkinson's disease: An overlooked class of drugs from a pharmacokinetic perspective. *J Pharm Pharm Sci*, *2*(2), 39–46.

Brown, V. A. (2021). An Introduction to Linear Mixed-Effects Modeling in R. *Advances in Methods and Practices in Psychological Science*, *4*(1). https://doi.org/10.1177/2515245920960351

Danielmeier, C., Allen, E. A., Jocham, G., Onur, O. A., Eichele, T., & Ullsperger, M. (2015). Acetylcholine mediates behavioral and neural post-error control. *Curr Biol*, *25*(11), 1461–1468. https://doi.org/10.1016/j.cub.2015.04.022

de Lange, F. P., Heilbron, M., & Kok, P. (2018). How Do Expectations Shape Perception? *Trends in Cognitive Sciences*, *22*(9), 764–779. https://doi.org/10.1016/j.tics.2018.06.002

Devauges, V., & Sara, S. J. (1990). Activation of the noradrenergic system facilitates an attentional shift in the rat. *Behav Brain Res*, *39*(1), 19–28. https://doi.org/10.1016/0166-4328(90)90118-x

Dias Maile, A. A., Andronova, E., O'Reilly, J., & Jocham, G. (2025). *Cholinergic and noradrenergic modulation of perceptual decision making and learning*. https://osf.io/aqd2r/overview

Doya, K. (2002). Metalearning and neuromodulation. *Neural Netw*, *15*(4-6), 495–506. https://doi.org/10.1016/s0893-6080(02)00044-8

Eggermann, E., & Feldmeyer, D. (2009). Cholinergic filtering in the recurrent excitatory microcircuit of cortical layer 4. *Proc Natl Acad Sci U S A*, *106*(28), 11753–11758. https://doi.org/10.1073/pnas.0810062106

Eggermann, E., Kremer, Y., Crochet, S., & Petersen, C. C. H. (2014). Cholinergic signals in mouse barrel cortex during active whisker sensing. *Cell Rep*, *9*(5), 1654–1660. https://doi.org/10.1016/j.celrep.2014.11.005

Erfanian Abdoust, M., Frobose, M. I., Schnitzler, A., Schreivogel, E., & Jocham, G. (2024). Dopamine and acetylcholine have distinct roles in delay- and effort-based decision-making in humans. *PLoS Biol*, *22*(7), e3002714. https://doi.org/10.1371/journal.pbio.3002714

Estes, W. K. (1957). Theory of Learning with Constant, Variable, or Contingent Probabilities of Reinforcement. *Psychometrika*, *22*(2), 113–132. https://doi.org/Doi 10.1007/Bf02289048

Froböse, M. I., & Ort, E. (2022). *Glutamatergic And GABAergic Effects On Learning And Decision Making: A Pharmacological MEG Study With Lorazepam, D-Cycloserine And Placebo*. https://osf.io/cmyh2/overview

Glennon, E., Carcea, I., Martins, A. R. O., Multani, J., Shehu, I., Svirsky, M. A., & Froemke, R. C. (2019). Locus coeruleus activation accelerates perceptual learning. *Brain Res*, *1709*, 39–49. https://doi.org/10.1016/j.brainres.2018.05.048

Grimaldi, R., Perucca, E., Ruberto, G., Gelmi, C., Trimarchi, F., Hollmann, M., & Crema, A. (1986). Pharmacokinetic and pharmacodynamic studies following the intravenous and oral administration of the antiparkinsonian drug biperiden to normal subjects. *Eur J Clin Pharmacol*, *29*(6), 735–737. https://doi.org/10.1007/BF00615970

Hangya, B., Ranade, S. P., Lorenc, M., & Kepecs, A. (2015). Central Cholinergic Neurons Are Rapidly Recruited by Reinforcement Feedback. *Cell*, *162*(5), 1155–1168. https://doi.org/10.1016/j.cell.2015.07.057

Hanks, T. D., Mazurek, M. E., Kiani, R., Hopp, E., & Shadlen, M. N. (2011). Elapsed decision time affects the weighting of prior probability in a perceptual decision task. *J Neurosci*, *31*(17), 6339–6352. https://doi.org/10.1523/JNEUROSCI.5613-10.2011

Harrison, X. A., Donaldson, L., Correa-Cano, M. E., Evans, J., Fisher, D. N., Goodwin, C. E. D., Robinson, B. S., Hodgson, D. J., & Inger, R. (2018). A brief introduction to mixed effects modelling and multi-model inference in ecology. *PeerJ*, *6*, e4794. https://doi.org/10.7717/peerj.4794

Hasselmo, M. E., Linster, C., Patil, M., Ma, D., & Cekic, M. (1997). Noradrenergic suppression of synaptic transmission may influence cortical signal-to-noise ratio. *J Neurophysiol*, *77*(6), 3326–3339. https://doi.org/10.1152/jn.1997.77.6.3326

Herrero, J. L., Gieselmann, M. A., & Thiele, A. (2017). Muscarinic and Nicotinic Contribution to Contrast Sensitivity of Macaque Area V1 Neurons. *Front Neural Circuits*, *11*, 106. https://doi.org/10.3389/fncir.2017.00106

Jaeger, T. F. (2008). Categorical Data Analysis: Away from ANOVAs (transformation or not) and towards Logit Mixed Models. *J Mem Lang*, *59*(4), 434–446. https://doi.org/10.1016/j.jml.2007.11.007

Jami, S. A., Wilkinson, B. J., Guglietta, R., Hartel, N., Babiec, W. E., Graham, N. A., Coba, M. P., & O'Dell, T. J. (2023). Functional and phosphoproteomic analysis

of beta-adrenergic receptor signaling at excitatory synapses in the CA1 region of the ventral hippocampus. *Sci Rep*, *13*(1), 7493. https://doi.org/10.1038/s41598-023-34401-7

Jepma, M., Murphy, P. R., Nassar, M. R., Rangel-Gomez, M., Meeter, M., & Nieuwenhuis, S. (2016). Catecholaminergic Regulation of Learning Rate in a Dynamic Environment. *Plos Computational Biology*, *12*(10), e1005171. https://doi.org/10.1371/journal.pcbi.1005171

Jimenez-Martin, J., Potapov, D., Potapov, K., Knopfel, T., & Empson, R. M. (2021). Cholinergic modulation of sensory processing in awake mouse cortex. *Sci Rep*, *11*(1), 17525. https://doi.org/10.1038/s41598-021-96696-8

Kalam, M. N., Rasool, M. F., Rehman, A. U., & Ahmed, N. (2020). Clinical Pharmacokinetics of Propranolol Hydrochloride: A Review. *Curr Drug Metab*, *21*(2), 89–105. https://doi.org/10.2174/1389200221666200414094644

Kasamatsu, T., & Heggelund, P. (1982). Single cell responses in cat visual cortex to visual stimulation during iontophoresis of noradrenaline. *Exp Brain Res*, *45*(3), 317–327. https://doi.org/10.1007/BF01208591

Kossl, M., & Vater, M. (1989). Noradrenaline enhances temporal auditory contrast and neuronal timing precision in the cochlear nucleus of the mustached bat. *J Neurosci*, *9*(12), 4169–4178. https://doi.org/10.1523/JNEUROSCI.09-12-04169.1989

Kuchibhotla, K. V., Gill, J. V., Lindsay, G. W., Papadoyannis, E. S., Field, R. E., Sten, T. A., Miller, K. D., & Froemke, R. C. (2017). Parallel processing by cortical inhibition enables context-dependent behavior. *Nat Neurosci*, *20*(1), 62–71. https://doi.org/10.1038/nn.4436

Kurtenbach, H., Froböse, M. I., Ort, E., Bahners, B., Butz, M., Schnitzler, A., Hirschmann, J., & Jocham, G. (2026). Cholinergic modulation of reinforcement learning and prefrontal value computations under uncertainty. *bioRxiv*, 2024.2009.2020.614105. https://doi.org/10.1101/2024.09.20.614105

Larsen, M. E., Buonarati, O. R., Qian, H., Hell, J. W., & Bayer, K. U. (2023). Stimulating beta-adrenergic receptors promotes synaptic potentiation by switching CaMKII movement from LTD to LTP mode. *J Biol Chem*, *299*(6), 104706. https://doi.org/10.1016/j.jbc.2023.104706

Lawson, R. P., Bisby, J., Nord, C. L., Burgess, N., & Rees, G. (2021). The Computational, Pharmacological, and Physiological Determinants of Sensory Learning under Uncertainty. *Curr Biol*, *31*(1), 163–172 e164. https://doi.org/10.1016/j.cub.2020.10.043

Marshall, L., Mathys, C., Ruge, D., de Berker, A. O., Dayan, P., Stephan, K. E., & Bestmann, S. (2016). Pharmacological Fingerprints of Contextual Uncertainty. *PLoS Biol*, *14*(11), e1002575. https://doi.org/10.1371/journal.pbio.1002575

Marshall, T. R., Ruesseler, M., Hunt, L. T., & O'Reilly, J. X. (2024). The representation of priors and decisions in the human parietal cortex. *PLoS Biol*, *22*(1), e3002383. https://doi.org/10.1371/journal.pbio.3002383

McLean, J., & Waterhouse, B. D. (1994). Noradrenergic modulation of cat area 17 neuronal responses to moving visual stimuli. *Brain Res*, *667*(1), 83–97. https://doi.org/10.1016/0006-8993(94)91716-7

Meir, I., Katz, Y., & Lampl, I. (2018). Membrane Potential Correlates of Network Decorrelation and Improved SNR by Cholinergic Activation in the Somatosensory Cortex. *J Neurosci*, *38*(50), 10692–10708. https://doi.org/10.1523/JNEUROSCI.1159-18.2018

Meule, A., Vögele, C., & Kübler, A. (2011). *Psychometrische Evaluation der deutschen Barratt Impulsiveness Scale – Kurzversion (BIS-15)* (Vol. 57). Hogrefe Verlag. https://doi.org/10.1026/0012-1924/a000042

Minces, V., Pinto, L., Dan, Y., & Chiba, A. A. (2017). Cholinergic shaping of neural correlations. *Proc Natl Acad Sci U S A*, *114*(22), 5725–5730. https://doi.org/10.1073/pnas.1621493114

Oldfield, R. C. (1971). The assessment and analysis of handedness: the Edinburgh inventory. *Neuropsychologia*, *9*(1), 97–113. https://doi.org/10.1016/0028-3932(71)90067-4

Peirce, J. W. (2007). PsychoPy--Psychophysics software in Python. *J Neurosci Methods*, *162*(1-2), 8–13. https://doi.org/10.1016/j.jneumeth.2006.11.017

Piray, P., & Daw, N. D. (2021). A model for learning based on the joint estimation of stochasticity and volatility. *Nat Commun*, *12*(1), 6587. https://doi.org/10.1038/s41467-021-26731-9

R Development Core Team. (2022). *R: A Language and Environment for Statistical Computing*. In (Version 4.2.2) R Foundation for Statistical Computing.

Rodewald, K., Bartolovic, M., Debelak, R., Aschenbrenner, S., Weisbrod, M., & Roesch-Ely, D. (2012). Eine Normierungsstudie eines modifizierten Trail Making Tests im deutschsprachigen Raum. *Zeitschrift für Neuropsychologie*, *23*(1), 37–48. https://doi.org/10.1024/1016-264X/a000060

Sara, S. J., Roullet, P., & Przybyslawski, J. (1999). Consolidation of memory for odor-reward association: beta-adrenergic receptor involvement in the late phase. *Learn Mem*, *6*(2), 88–96.

Soma, S., Shimegi, S., Suematsu, N., & Sato, H. (2013). Cholinergic modulation of response gain in the rat primary visual cortex. *Sci Rep*, *3*, 1138. https://doi.org/10.1038/srep01138

Spielberger, C. D., Gorsuch, R. L., Lushene, R., Vagg, P. R., & Jacobs, G. A. (1983). *Manual for the State-Trait Anxiety Inventory (Form Y)*. Consulting Psychologists Press.

Spinella, M. (2007). NORMATIVE DATA AND A SHORT FORM OF THE BARRATT IMPULSIVENESS SCALE. *International Journal of Neuroscience*, *117*(3), 359–368. https://doi.org/10.1080/00207450600588881

Thaler, L., Schütz, A. C., Goodale, M. A., & Gegenfurtner, K. R. (2013). What is the best fixation target? The effect of target shape on stability of fixational eye movements. *Vision Research*, *76*, 31–42. https://doi.org/10.1016/j.visres.2012.10.012

The MathWorks Inc. (2021). *MATLAB*. In (Version R2021a) The MathWorks Inc. https://www.mathworks.com

Waterhouse, B. D., Azizi, S. A., Burne, R. A., & Woodward, D. J. (1990). Modulation of rat cortical area 17 neuronal responses to moving visual stimuli during

norepinephrine and serotonin microiontophoresis. *Brain Res*, *514*(2), 276–292. https://doi.org/10.1016/0006-8993(90)91422-d

Waterhouse, B. D., Moises, H. C., & Woodward, D. J. (1998). Phasic activation of the locus coeruleus enhances responses of primary sensory cortical neurons to peripheral receptive field stimulation. *Brain Res*, *790*(1-2), 33–44. https://doi.org/10.1016/s0006-8993(98)00117-6

Yu, A. J., & Dayan, P. (2005). Uncertainty, neuromodulation, and attention. *Neuron*, *46*(4), 681–692. https://doi.org/10.1016/j.neuron.2005.04.026

Supplement 1: Complete mixed model fits

Tables depicts the complete mixed model fits including a description of the fixed and random effect structure. Columns show the β-weights, SEM, z-value (t-values for linear mixed models) and p-value for the fixed effects. Linear mixed effects further include a column showing the df. Stars represent significant effects based on $p < 0.05$.

Table S1 General linear mixed effects model: task effects. Fixed effects included main effects for the intercept (side bias), z-scaled coherence and z-scaled prior (based on the Bayes optimal learner). The model included a full random-effect structure. The dependent variable was choice (right-side choice). Marginal $R^2_{GLMM} = 0.593$.

	β-weight	***SEM***	***z*-value**	***p*-value**
Intercept	0.28	0.03	8.76	< 2e-16 *
Coherence	2.08	0.11	18.42	< 2e-16 *
Prior	0.59	0.04	16.19	< 2e-16 *

Table S2 Linear mixed effects model: task effects on prior. Fixed effects included main effects for the intercept and z-scaled coherence. The model included a random intercept. The dependent variable was the difference in the probability of a correct choice between trials in which priors were aligned with versus opposed to motion coherence. Marginal $R^2_{GLMM} = 0.235$.

	β-weight	***SEM***	**df**	**t-value**	***p*-value**
Intercept	0.40	0.03	97.82	17.49	< 2e-16 *
Coherence	-0.66	0.05	185.00	-13.73	< 2e-16 *

Table S3 General linear mixed effects model: drug effects. Fixed effects included main effects for the intercept (side bias), drugs, z-scaled coherence and z-scaled prior (based on the Bayes optimal learner). Additionally, fixed effects included interactions of the drugs with the z-scaled coherence and z-scaled prior. The random effects included a random intercept and slope for the main effects of z-scaled coherence, z-scaled prior and the drugs. The dependent variable was choice (right-side choice). Marginal $R^2_{GLMM} = 0.594$.

	β-weight	***SEM***	***z*-value**	***p*-value**
Intercept	0.28	0.04	7.24	< 0.001 *
Biperiden	0.03	0.04	0.69	0.492
Propranolol	-0.03	0.04	-0.71	0.481
Coherence	2.14	0.11	18.74	< 2e-16 *
Prior	0.57	0.04	14.83	< 2e-16 *
Biperiden:coherence	-0.10	0.03	-3.76	< 0.001 *
Propranolol:coherence	-0.06	0.03	-2.26	0.024 *
Biperiden:prior	0.01	0.02	0.68	0.497
Propranolol:prior	0.06	0.02	3.23	0.001 *

Table S4 General linear mixed effects model: win-stay. Fixed effects included main effects for the intercept (side bias), drugs, z-scaled coherence and z-scaled stay bias. Additionally, fixed effects included interactions of the drugs with the z-scaled coherence and z-scaled stay bias. The random

effects included a random intercept and slope for the main effects of z-scaled coherence, z-scaled prior and the drugs. The dependent variable was choice (right-side choice). The model only included trials following a correct choice. The number of iterations was set to 100000. Marginal $R^2_{GLMM} = 0.622$.

	β-weight	*SEM*	*z*-value	*p*-value
Intercept	0.30	0.04	7.78	< 0.001 *
Biperiden	0.05	0.04	1.32	0.186
Propranolol	-0.01	0.04	-0.28	0.782
Coherence	2.55	0.11	23.03	< 2e-16 *
Stay	0.39	0.04	8.93	< 2e-16 *
Biperiden:coherence	-0.12	0.03	-3.72	< 0.001 *
Propranolol:coherence	-0.03	0.03	-0.97	0.333
Biperiden:stay	0.08	0.02	4.07	< 0.001 *
Propranolol:stay	0.08	0.02	4.39	< 0.001 *

Table S5 General linear mixed effects model: lose-switch. Fixed effects included main effects for the intercept (side bias), drugs, z-scaled coherence and z-scaled stay bias. Additionally, fixed effects included interactions of the drugs with the z-scaled coherence and z-scaled stay bias. Random effects included a random intercept and slope for the main effects of z-scaled coherence, z-scaled stay bias and drugs. The dependent variable was choice (right-side choice). The model only included trials following an incorrect choice. Marginal $R^2_{GLMM} = 0.568$.

	β-weight	*SEM*	*z*-value	*p*-value
Intercept	0.23	0.05	4.69	< 0.001 *
Biperiden	-0.04	0.05	-0.73	0.466
Propranolol	-0.06	0.05	-1.13	0.257
Coherence	2.37	0.11	20.64	< 2e-16 *
Stay	-0.25	0.05	-4.58	< 0.001 *
Biperiden:coherence	-0.07	0.05	-1.34	0.182
Propranolol:coherence	-0.07	0.05	-1.30	0.194
Biperiden:stay	-0.04	0.04	-1.02	0.309
Propranolol:stay	0.02	0.04	0.49	0.627

Table S6 Linear mixed effects model: reaction times. Fixed effects included main effects for the intercept, drugs, z-scaled absolute coherence and z-scaled congruency (coding if the Bayes optimal prior is congruent with the coherent motion). Additionally, fixed effects included interactions of the drugs with the z-scaled coherence and z-scaled congruency. Random effects included a random intercept and slope for the main effects of the drugs. The dependent variable was log-transformed reaction times. Marginal $R^2_{GLMM} = 0.077$.

	β-weight	*SEM*	*df*	t-value	*p*-value
Intercept	-0.41	0.03	61.01	-13.52	< 2e-16 *
Biperiden	-0.01	0.02	61.00	-0.36	0.721

Propranolol	-0.02	0.02	61.01	-1.16	0.249
Coherence	-0.10	0.00	155400.00	-80.92	< 2e-16 *
Congruency	-0.02	0.00	155400.00	-16.27	< 2e-16 *
Biperiden:coherence	0.00	0.00	155400.00	-0.05	0.959
Propranolol:coherence	0.00	0.00	155400.00	-1.00	0.317
Biperiden:congruency	0.00	0.00	155400.00	0.90	0.369
Propranolol:congruency	0.00	0.00	155400.00	-0.79	0.431

Supplement 2: Control analyses

Control analyses included capturing drug effects on participants' mood (measured with the Bond and Lader Visual Analogue Mood Scale; BL-VAS; Bond & Lader, 1974), state anxiety (measured with the State-Trait Anxiety Inventory; STAI; Spielberger et al., 1983), visuomotor abilities (measured with the Trail Making Test; TMT; Rodewald et al., 2012), blood pressure and heart rate. Mood, state anxiety and vital parameters were measured at three different time points per pharmacological session: before drug administration (baseline), 45 min after drug administration (timepoint 2) and approximately 2 h after drug administration (timepoint 3). Visuomotor abilities are tested 50 min after drug administration. Linear mixed models are implemented to test the drug effects on these measures. Significantly modulated measures are added as fixed effects to the models investigating drug effects in the experimental task to verify that our effects of interest are not affected by these covariates. Additionally, we add the session number as fixed effect to ensure that that our effects of interest are not affected by training effects. Tables depicts the complete mixed model fits including a description of the fixed and random effect structure. Columns show the β-weights, SEM, t-value (z-values for general linear mixed models) and p-value for the fixed effects. Linear mixed effects further include a column showing the df. Stars represent significant effects based on $p < 0.05$.

Table S7 Linear mixed effects model: alertness. Fixed effects included main effects for the intercept, measurement timepoint and drugs. Additionally, fixed effects included interactions of the drugs with the measurement timepoint. Random effects include a random intercept. The dependent variable was alertness (measured with the BL-VAS). Biperiden significantly reduces participants' alertness at measurement timepoint 3. Propranolol has no significant effect.

	β-weight	***SEM***	***df***	***t*-value**	***p*-value**
Intercept	7.84	0.26	177.30	29.73	< 2e-16 *
Biperiden	0.23	0.26	488.00	0.88	0.382
Propranolol	-0.03	0.26	488.00	-0.10	0.918
Timepoint 2	-0.27	0.26	488.00	-1.04	0.298
Timepoint 3	-1.38	0.26	488.00	-5.29	< 0.001 *
Biperiden:Timepoint 2	-0.59	0.37	488.00	-1.60	0.111
Propranolol:Timepoint 2	0.09	0.37	488.00	0.25	0.806
Biperiden:Timepoint 3	-1.52	0.37	488.00	-4.12	< 0.001 *
Propranolol:Timepoint 3	-0.30	0.37	488.00	-0.81	0.419

Table S8 Linear mixed effects model: calmness. Fixed effects included main effects for the intercept, measurement timepoint and drugs. Additionally, fixed effects included interactions of the drugs with the measurement timepoint. Random effects include a random intercept. The dependent variable was calmness (measured with the BL-VAS). The drugs have no significant effect on participants' calmness.

	β-weight	***SEM***	***df***	***t*-value**	***p*-value**
Intercept	8.34	0.20	191.35	41.51	< 2e-16 *
Biperiden	0.03	0.20	488.00	0.16	0.875
Propranolol	0.09	0.20	488.00	0.42	0.676

Timepoint 2	0.20	0.20	488.00	1.00	0.318
Timepoint 3	0.50	0.20	488.00	2.46	0.014 *
Biperiden:Timepoint 2	0.05	0.29	488.00	0.17	0.868
Propranolol:Timepoint 2	0.04	0.29	488.00	0.09	0.927
Biperiden:Timepoint 3	-0.54	0.29	488.00	-1.86	0.064
Propranolol:Timepoint 3	-0.13	0.29	488.00	-0.46	0.647

Table S9 Linear mixed effects model: contentedness. Fixed effects included main effects for the intercept, measurement timepoint and drugs. Additionally, fixed effects included interactions of the drugs with the measurement timepoint. Random effects include a random intercept. The dependent variable was contentedness (measured with the BL-VAS). The drugs have no effect on participants' contentedness

	***β*-weight**	***SEM***	***df***	***t*-value**	***p*-value**
Intercept	4.75	0.29	256.20	16.48	< 2e-16 *
Biperiden	0.68	0.32	488.00	2.11	0.035 *
Propranolol	0.02	0.32	488.00	0.06	0.955
Timepoint 2	0.02	0.32	488.00	0.06	0.951
Timepoint 3	-0.02	0.32	488.00	-0.08	0.940
Biperiden:Timepoint 2	-0.69	0.45	488.00	-1.52	0.129
Propranolol:Timepoint 2	-0.01	0.45	488.00	-0.01	0.989
Biperiden:Timepoint 3	-0.78	0.45	488.00	-1.72	0.085
Propranolol:Timepoint 3	0.00	0.45	488.00	0.00	0.999

Table S10 Linear mixed effects model: state anxiety. Fixed effects included main effects for the intercept, measurement timepoint and drugs. Additionally, fixed effects included interactions of the drugs with the measurement timepoint. Random effects include a random intercept. The dependent variable was state anxiety (measured with the STAI). The drugs have no significant effect on participants' state anxiety

	***β*-weight**	***SEM***	***df***	***t*-value**	***p*-value**
Intercept	29.39	0.78	110.33	37.71	< 2e-16 *
Biperiden	1.35	0.60	488.00	2.26	0.024 *
Propranolol	0.65	0.60	488.00	1.08	0.282
Timepoint 2	-0.05	0.60	488.00	-0.08	0.936
Timepoint 3	1.03	0.60	488.00	1.72	0.085
Biperiden:Timepoint 2	-0.08	0.85	488.00	-0.10	0.924
Propranolol:Timepoint 2	-0.65	0.85	488.00	-0.76	0.446
Biperiden:Timepoint 3	1.48	0.85	488.00	1.75	0.080
Propranolol:Timepoint 3	-0.47	0.85	488.00	-0.55	0.581

Table S11 Linear mixed effects model: visuomotor abilities. Fixed effects included main effects for the intercept and drugs. Random effects include a random intercept. The dependent variable was visuomotor abilities (measured with the TMT). The drugs have no significant effect on participants' visuomotor abilities.

	β-weight	*SEM*	*df*	*t*-value	*p*-value
Intercept	25.34	1.23	108.52	20.67	< 2e-16 *
Biperiden	0.87	1.12	122.00	0.78	0.436
Propranolol	0.89	1.12	122.00	0.79	0.429

Table S12 Linear mixed effects model: systolic blood pressure. Fixed effects included main effects for the intercept, measurement timepoint and drugs. Additionally, fixed effects included interactions of the drugs with the measurement timepoint. Random effects include a random intercept. The dependent variable was the systolic blood pressure. Biperiden significantly reduces participants' systolic blood pressure at measurement timepoint 2. Propranolol significantly reduces participants' systolic blood pressure at measurement timepoint 2 and 3.

	β-weight	*SEM*	*df*	*t*-value	*p*-value
Intercept	98.29	2.83	70.72	34.70	< 2e-16 *
Biperiden	0.10	1.14	487.00	0.09	0.932
Propranolol	1.65	1.14	487.00	1.45	0.149
Timepoint 2	-1.23	1.14	487.00	-1.08	0.282
Timepoint 3	-0.99	1.14	487.01	-0.87	0.386
Biperiden:Timepoint 2	-3.31	1.61	487.00	-2.06	0.040 *
Propranolol:Timepoint 2	-3.35	1.61	487.00	-2.09	0.038 *
Biperiden:Timepoint 3	-2.25	1.61	487.01	-1.40	0.163
Propranolol:Timepoint 3	-8.69	1.61	487.01	-5.39	< 0.001 *

Table S13 Linear mixed effects model: diastolic blood pressure. Fixed effects included main effects for the intercept, measurement timepoint and drugs. Additionally, fixed effects included interactions of the drugs with the measurement timepoint. Random effects include a random intercept. The dependent variable was the diastolic blood pressure. Biperiden significantly reduces participants' diastolic blood pressure at measurement timepoint 2. Propranolol significantly reduces participants' diastolic blood pressure at measurement timepoint 3.

	β-weight	*SEM*	*df*	*t*-value	*p*-value
Intercept	91.26	2.84	69.83	32.11	< 2e-16 *
Biperiden	1.40	1.09	487.00	1.28	0.200
Propranolol	1.45	1.09	487.00	1.33	0.185
Timepoint 2	-1.63	1.09	487.00	-1.49	0.137
Timepoint 3	-2.67	1.10	487.01	-2.43	0.015 *
Biperiden:Timepoint 2	-4.15	1.55	487.00	-2.68	0.008 *
Propranolol:Timepoint 2	-2.86	1.55	487.00	-1.85	0.065

Biperiden:Timepoint 3	-1.75	1.55	487.01	-1.13	0.259
Propranolol:Timepoint 3	-6.25	1.55	487.01	-4.04	< 0.001 *

Table S14 Linear mixed effects model: heart rate. Fixed effects included main effects for the intercept, measurement timepoint and drugs. Additionally, fixed effects included interactions of the drugs with the measurement timepoint. Random effects include a random intercept. The dependent variable was the heart rate. Biperiden significantly reduces participants' heart rate at measurement timepoint 2 and 3. Propranolol significantly reduces participants' heart rate at measurement timepoint 3.

	***β*-weight**	***SEM***	***df***	***t*-value**	***p*-value**
Intercept	74.60	1.25	146.09	59.80	< 2e-16 *
Biperiden	2.13	1.14	486.72	1.88	0.061
Propranolol	0.81	1.14	486.72	0.71	0.478
Timepoint 2	0.21	1.14	486.72	0.19	0.854
Timepoint 3	-3.37	1.14	486.80	-2.95	0.003 *
Biperiden:Timepoint 2	-8.23	1.61	486.72	-5.12	< 0.001 *
Propranolol:Timepoint 2	-5.47	1.61	486.72	-3.40	0.001
Biperiden:Timepoint 3	-10.99	1.61	486.76	-6.83	< 0.001 *
Propranolol:Timepoint 3	-9.91	1.61	486.76	-6.15	< 0.001 *

Table S15 General linear mixed effects model: drug effects controlling for session order. Fixed effects included main effects for the intercept (side bias), drugs, z-scaled coherence and z-scaled prior (based on the Bayes optimal learner). Additionally, fixed effects included interactions of the drugs and z-scaled session order with the z-scaled coherence and z-scaled prior. The random effects included a random intercept and slope for the main effects of z-scaled coherence, z-scaled prior and the drugs. The dependent variable was choice (right-side choice). Drug effects in our experimental task are not affected by the session order.

	***β*-weight**	***SEM***	***z*-value**	***p*-value**
Intercept	0.28	0.04	7.23	< 0.001 *
Biperiden	0.03	0.04	0.71	0.480
Propranolol	-0.03	0.04	-0.71	0.480
Coherence	2.14	0.11	18.74	< 2e-16 *
Prior	0.57	0.04	14.81	< 2e-16 *
Biperiden:coherence	-0.11	0.03	-3.88	< 0.001 *
Propranolol:coherence	-0.07	0.03	-2.34	0.019 *
Biperiden:prior	0.02	0.02	0.81	0.418
Propranolol:prior	0.06	0.02	3.32	< 0.001 *
Session:coherence	-0.03	0.01	-2.76	0.006 *
Session:prior	0.06	0.01	7.89	< 0.001 *

Table S16 General linear mixed effects model: drug effects controlling for alertness. Fixed effects included main effects for the intercept (side bias), drugs, z-scaled coherence, z-scaled prior (based on the Bayes optimal learner) and z-scaled alertness (difference score timepoint 1 – timepoint 3). Additionally, fixed effects included interactions of the drugs and the z-scaled coherence, z-scaled prior and z-scaled alertness. The random effects included a random intercept and slope for the main effects of z-scaled coherence, z-scaled prior and the drugs. The dependent variable was choice (right-side choice). Drug effects in our experimental task are not affected by drug effects on participants' alertness.

	***β*-weight**	***SEM***	***z*-value**	***p*-value**
Intercept	0.27	0.04	6.60	< 0.001 *
Biperiden	0.04	0.04	1.08	0.279
Propranolol	-0.01	0.04	-0.37	0.712
Coherence	2.14	0.11	18.74	< 2e-16 *
Prior	0.57	0.04	14.83	< 2e-16 *
Alertness	-0.05	0.05	-0.92	0.360
Biperiden:coherence	-0.10	0.03	-3.76	< 0.001 *
Propranolol:coherence	-0.06	0.03	-2.26	0.024 *
Biperiden:prior	0.01	0.02	0.69	0.493
Propranolol:prior	0.06	0.02	3.23	0.001 *
Biperiden:alertness	0.03	0.06	0.56	0.576
Propranolol:alertness	0.05	0.06	0.84	0.401

Table S17 General linear mixed effects model: drug effects controlling for systolic blood pressure at timepoint 2. Fixed effects included main effects for the intercept (side bias), drugs, z-scaled coherence, z-scaled prior (based on the Bayes optimal learner) and z-scaled systolic blood pressure (difference score timepoint 1 – timepoint 2). Additionally, fixed effects included interactions of the drugs with the z-scaled coherence, z-scaled prior and z-scaled systolic blood pressure. The random effects included a random intercept and slope for the main effects of z-scaled coherence, z-scaled prior and the drugs. The dependent variable was choice (right-side choice). Drug effects in our experimental task are not affected by drug effects on participants' systolic blood pressure at timepoint 2.

	***β*-weight**	***SEM***	***z*-value**	***p*-value**
Intercept	0.27	0.04	6.96	< 0.001 *
Biperiden	0.04	0.04	1.03	0.303
Propranolol	-0.01	0.04	-0.31	0.754
Coherence	2.14	0.11	18.77	< 2e-16 *
Prior	0.57	0.04	14.85	< 2e-16 *
systole	-0.04	0.03	-1.37	0.171
Biperiden:coherence	-0.10	0.03	-3.76	< 0.001 *
Propranolol:coherence	-0.06	0.03	-2.26	0.024 *
Biperiden:prior	0.01	0.02	0.68	0.498
Propranolol:prior	0.06	0.02	3.22	0.001 *

Biperiden:systole	0.02	0.04	0.55	0.585
Propranolol:systole	0.02	0.05	0.35	0.723

Table S18 General linear mixed effects model: drug effects controlling for systolic blood pressure at timepoint 3. Fixed effects included main effects for the intercept (side bias), drugs, z-scaled coherence, z-scaled prior (based on the Bayes optimal learner) and z-scaled systolic blood pressure (difference score timepoint 1 – timepoint 3). Additionally, fixed effects included interactions of the drugs with the z-scaled coherence, z-scaled prior and z-scaled systolic blood pressure. The random effects included a random intercept and slope for the main effects of z-scaled coherence, z-scaled prior and the drugs. The dependent variable was choice (right-side choice). Drug effects in our experimental task are not affected by drug effects on participants' systolic blood pressure at timepoint 3.

	***β*-weight**	***SEM***	***z*-value**	***p*-value**
Intercept	0.26	0.04	6.32	< 0.001 *
Biperiden	0.05	0.04	1.30	0.195
Propranolol	0.00	0.04	0.07	0.947
Coherence	2.14	0.11	18.71	< 2e-16 *
Prior	0.57	0.04	14.77	< 2e-16 *
systole	-0.03	0.04	-0.83	0.406
Biperiden:coherence	-0.10	0.03	-3.73	< 0.001 *
Propranolol:coherence	-0.06	0.03	-2.25	0.025 *
Biperiden:prior	0.01	0.02	0.71	0.481
Propranolol:prior	0.06	0.02	3.25	0.001 *
Biperiden:systole	0.06	0.04	1.36	0.174
Propranolol:systole	0.01	0.05	0.25	0.804

Table S19 General linear mixed effects model: drug effects controlling for diastolic blood pressure at timepoint 2. Fixed effects included main effects for the intercept (side bias), drugs, z-scaled coherence, z-scaled prior (based on the Bayes optimal learner) and z-scaled diastolic blood pressure (difference score timepoint 1 – timepoint 2). Additionally, fixed effects included interactions of the drugs with the z-scaled coherence, z-scaled prior and z-scaled diastolic blood pressure. The random effects included a random intercept and slope for the main effects of z-scaled coherence, z-scaled prior and the drugs. The dependent variable was choice (right-side choice). Drug effects in our experimental task are not affected by drug effects on participants' diastolic blood pressure at timepoint 2.

	***β*-weight**	***SEM***	***z*-value**	***p*-value**
Intercept	0.27	0.04	6.66	< 0.001 *
Biperiden	0.05	0.04	1.21	0.225
Propranolol	-0.01	0.04	-0.26	0.798
Coherence	2.14	0.11	18.75	< 2e-16 *
Prior	0.57	0.04	14.84	< 2e-16 *
diastole	-0.05	0.04	-1.29	0.199
Biperiden:coherence	-0.10	0.03	-3.76	< 0.001 *

Propranolol:coherence	-0.06	0.03	-2.27	0.024 *
Biperiden:prior	0.01	0.02	0.68	0.496
Propranolol:prior	0.06	0.02	3.22	0.001 *
Biperiden:diastole	0.02	0.04	0.36	0.721
Propranolol:diastole	0.01	0.04	0.20	0.845

Table S20 General linear mixed effects model: drug effects controlling for diastolic blood pressure at timepoint 3. Fixed effects included main effects for the intercept (side bias), drugs, z-scaled coherence, z-scaled prior (based on the Bayes optimal learner) and z-scaled diastolic blood pressure (difference score timepoint 1 – timepoint 3). Additionally, fixed effects included interactions of the drugs with the z-scaled coherence, z-scaled prior and z-scaled diastolic blood pressure. The random effects included a random intercept and slope for the main effects of z-scaled coherence, z-scaled prior and the drugs. The dependent variable was choice (right-side choice). Drug effects in our experimental task are not affected by drug effects on participants' diastolic blood pressure at timepoint 3.

	***β*-weight**	***SEM***	***z*-value**	***p*-value**
Intercept	0.26	0.04	6.41	< 0.001 *
Biperiden	0.04	0.04	1.12	0.261
Propranolol	0.00	0.04	-0.05	0.959
Coherence	2.14	0.11	18.74	< 2e-16 *
Prior	0.57	0.04	14.78	< 2e-16 *
diastole	-0.04	0.04	-1.03	0.302
Biperiden:coherence	-0.10	0.03	-3.74	< 0.001 *
Propranolol:coherence	-0.06	0.03	-2.25	0.025 *
Biperiden:prior	0.01	0.02	0.70	0.483
Propranolol:prior	0.06	0.02	3.25	0.001 *
Biperiden:diastole	0.00	0.05	-0.05	0.964
Propranolol:diastole	0.04	0.05	0.73	0.464

Table S21 General linear mixed effects model: drug effects controlling for heart rate at timepoint 2. Fixed effects included main effects for the intercept (side bias), drugs, z-scaled coherence, z-scaled prior (based on the Bayes optimal learner) and z-scaled heart rate (difference score timepoint 1 – timepoint 2). Additionally, fixed effects included interactions of the drugs with the z-scaled coherence, z-scaled prior and z-scaled heart rate. The random effects included a random intercept and slope for the main effects of z-scaled coherence, z-scaled prior and the drugs. The dependent variable was choice (right-side choice). Drug effects in our experimental task are not affected by drug effects on participants' heart rate at timepoint 2.

	***β*-weight**	***SEM***	***z*-value**	***p*-value**
Intercept	0.25	0.05	5.40	< 0.001 *
Biperiden	0.07	0.05	1.51	0.131
Propranolol	0.01	0.05	0.24	0.810
Coherence	2.14	0.11	18.78	< 2e-16 *

Prior	0.57	0.04	14.84	< 2e-16 *
diastole	-0.07	0.04	-1.59	0.112
Biperiden:coherence	-0.10	0.03	-3.76	< 0.001 *
Propranolol:coherence	-0.06	0.03	-2.27	0.023 *
Biperiden:prior	0.01	0.02	0.68	0.496
Propranolol:prior	0.06	0.02	3.23	0.001 *
Biperiden:heart rate	0.06	0.05	1.11	0.266
Propranolol:heart rate	0.07	0.05	1.27	0.204

Table S22 General linear mixed effects model: drug effects controlling for heart rate at timepoint 3. Fixed effects included main effects for the intercept (side bias), drugs, z-scaled coherence, z-scaled prior (based on the Bayes optimal learner) and z-scaled heart rate (difference score timepoint 1 – timepoint 3). Additionally, fixed effects included interactions of the drugs with the z-scaled coherence, z-scaled prior and z-scaled heart rate. The random effects included a random intercept and slope for the main effects of z-scaled coherence, z-scaled prior and the drugs. The dependent variable was choice (right-side choice). Drug effects in our experimental task are not affected by drug effects on participants' heart rate at timepoint 3.

	***β*-weight**	***SEM***	***z*-value**	***p*-value**
Intercept	0.21	0.05	4.12	< 0.001 *
Biperiden	0.10	0.05	1.88	0.060
Propranolol	0.05	0.05	0.99	0.325
Coherence	2.14	0.11	18.72	< 2e-16 *
Prior	0.57	0.04	14.77	< 2e-16 *
diastole	-0.09	0.05	-1.92	0.055
Biperiden:coherence	-0.10	0.03	-3.74	< 0.001 *
Propranolol:coherence	-0.06	0.03	-2.25	0.024 *
Biperiden:prior	0.01	0.02	0.71	0.478
Propranolol:prior	0.06	0.02	3.25	0.001 *
Biperiden:heart rate	0.10	0.06	1.64	0.100
Propranolol:heart rate	0.08	0.05	1.45	0.146

Table S23 General linear mixed effects model: win-stay controlling for session order. Fixed effects included main effects for the intercept (side bias), drugs, z-scaled coherence and z-scaled stay bias. Additionally, fixed effects included interactions of the drugs and z-scaled session order with the z-scaled coherence and z-scaled stay bias. The random effects included a random intercept and slope for the main effects of z-scaled coherence, z-scaled stay bias and the drugs. The dependent variable was choice (right-side choice). The model only included trials following a correct choice. Drug effects on win-stay behavior are not affected by the session order.

	***β*-weight**	***SEM***	***z*-value**	***p*-value**
Intercept	0.30	0.04	7.76	< 0.001 *

Biperiden	0.05	0.04	1.32	0.188
Propranolol	-0.01	0.04	-0.28	0.782
Coherence	2.55	0.11	23.08	< 2e-16 *
Stay	0.39	0.04	8.90	< 2e-16 *
Biperiden:coherence	-0.12	0.03	-3.88	< 0.001 *
Propranolol:coherence	-0.03	0.03	-1.07	0.286
Biperiden:stay	0.08	0.02	4.26	< 0.001 *
Propranolol:stay	0.08	0.02	4.38	< 0.001 *
Session:coherence	-0.01	0.01	-1.27	0.206
Session:stay	0.06	0.01	8.08	< 0.001 *

Table S24 General linear mixed effects model: win-stay controlling for alertness. Fixed effects included main effects for the intercept (side bias), drugs, z-scaled coherence, z-scaled stay bias and z-scaled alertness (difference score timepoint 1 – timepoint 3). Additionally, fixed effects included interactions of the drugs with the z-scaled coherence, z-scaled stay bias and z-scaled alertness. The random effects included a random intercept and slope for the main effects of z-scaled coherence, z-scaled prior and the drugs. The dependent variable was choice (right-side choice). The model only included trials following a correct choice. Drug effects on win-stay behavior are not affected by drug effects on participants' alertness.

	***β*-weight**	***SEM***	***z*-value**	***p*-value**
Intercept	0.28	0.04	7.09	< 0.001 *
Biperiden	0.07	0.04	1.86	0.062
Propranolol	0.00	0.04	0.09	0.925
Coherence	2.55	0.11	23.05	< 2e-16 *
Stay	0.39	0.04	8.95	< 2e-16 *
Alertness	-0.06	0.05	-1.31	0.192
Biperiden:coherence	-0.12	0.03	-3.72	< 0.001 *
Propranolol:coherence	-0.03	0.03	-0.97	0.333
Biperiden:stay	0.08	0.02	4.08	< 0.001 *
Propranolol:stay	0.08	0.02	4.30	< 0.001 *
Biperiden:alertness	0.04	0.05	0.79	0.430
Propranolol:alertness	0.06	0.06	0.95	0.345

Table S25 General linear mixed effects model: win-stay controlling for systolic blood pressure at timepoint 2. Fixed effects included main effects for the intercept (side bias), drugs, z-scaled coherence, z-scaled stay bias and z-scaled systolic blood pressure (difference score timepoint 1 – timepoint 2). Additionally, fixed effects included interactions of the drugs with the z-scaled coherence, z-scaled stay bias and z-scaled systolic blood pressure. The random effects included a random intercept and slope for the main effects of z-scaled coherence, z-scaled stay bias and the drugs. The dependent variable was choice (right-side choice). The model only included trials following a correct choice. Drug

effects on win-stay behavior are not affected by drug effects on participants' systolic blood pressure at timepoint 2.

	β-weight	*SEM*	*z*-value	*p*-value
Intercept	0.29	0.04	7.50	< 0.001 *
Biperiden	0.06	0.04	1.59	0.111
Propranolol	0.00	0.04	0.12	0.908
Coherence	2.55	0.11	22.96	< 2e-16 *
Stay	0.39	0.04	8.92	< 2e-16 *
Systole	-0.04	0.03	-1.23	0.217
Biperiden:coherence	-0.12	0.03	-3.73	< 0.001 *
Propranolol:coherence	-0.03	0.03	-0.97	0.333
Biperiden:stay	0.08	0.02	4.07	< 0.001 *
Propranolol:stay	0.08	0.02	4.29	< 0.001 *
Biperiden:systole	0.02	0.04	0.61	0.544
Propranolol:systole	0.00	0.04	-0.05	0.964

Table S26 General linear mixed effects model: win-stay controlling for systolic blood pressure at timepoint 3. Fixed effects included main effects for the intercept (side bias), drugs, z-scaled coherence, z-scaled stay bias and z-scaled systolic blood pressure (difference score timepoint 1 – timepoint 3). Additionally, fixed effects included interactions of the drugs with the z-scaled coherence, z-scaled stay bias and systolic blood pressure. The random effects included a random intercept and slope for the main effects of z-scaled coherence, z-scaled stay bias and the drugs. The dependent variable was choice (right-side choice). The model only included trials following a correct choice. Drug effects on win-stay behavior are not affected by drug effects on participants' systolic blood pressure at timepoint 3.

	β-weight	*SEM*	*z*-value	*p*-value
Intercept	0.28	0.04	6.87	< 0.001 *
Biperiden	0.07	0.04	1.85	0.064
Propranolol	0.01	0.04	0.34	0.738
Coherence	2.54	0.11	22.91	< 2e-16 *
Stay	0.39	0.04	8.96	< 2e-16 *
Systole	-0.03	0.04	-0.75	0.452
Biperiden:coherence	-0.11	0.03	-3.69	< 0.001 *
Propranolol:coherence	-0.03	0.03	-0.95	0.343
Biperiden:stay	0.07	0.02	3.98	< 0.001 *
Propranolol:stay	0.08	0.02	4.20	< 0.001 *
Biperiden:systole	0.05	0.04	1.22	0.223
Propranolol:systole	0.01	0.05	0.28	0.782

Table S27 General linear mixed effects model: win-stay controlling for diastolic blood pressure at timepoint 2. Fixed effects included main effects for the intercept (side bias), drugs, z-scaled coherence, z-scaled stay bias and z-scaled diastolic blood pressure (difference score timepoint 1 – timepoint 2). Additionally, fixed effects included interactions of the drugs with the z-scaled coherence, z-scaled stay bias and z-scaled diastolic blood pressure. The random effects included a random intercept and slope for the main effects of z-scaled coherence, z-scaled stay bias and the drugs. The dependent variable was choice (right-side choice). The model only included trials following a correct choice. Drug effects on win-stay behavior are not affected by drug effects on participants' diastolic blood pressure at timepoint 2.

	***β*-weight**	***SEM***	***z*-value**	***p*-value**
Intercept	0.28	0.04	7.19	< 0.001 *
Biperiden	0.07	0.04	1.79	0.073
Propranolol	0.01	0.04	0.18	0.861
Coherence	2.55	0.11	23.13	< 2e-16 *
Stay	0.39	0.04	8.95	< 2e-16 *
Diastole	-0.05	0.04	-1.31	0.190
Biperiden:coherence	-0.12	0.03	-3.73	< 0.001 *
Propranolol:coherence	-0.03	0.03	-0.97	0.331
Biperiden:stay	0.08	0.02	4.07	< 0.001 *
Propranolol:stay	0.08	0.02	4.29	< 0.001 *
Biperiden:diastole	0.02	0.04	0.49	0.625
Propranolol:diastole	0.00	0.04	-0.07	0.945

Table S28 General linear mixed effects model: win-stay controlling for diastolic blood pressure at timepoint 3. Fixed effects included main effects for the intercept (side bias), drugs, z-scaled coherence, z-scaled stay bias and z-scaled diastolic blood pressure (difference score timepoint 1 – timepoint 3). Additionally, fixed effects included interactions of the drugs with the z-scaled coherence, z-scaled stay bias and z-scaled diastolic blood pressure. The random effects included a random intercept and slope for the main effects of z-scaled coherence, z-scaled stay bias and the drugs. The dependent variable was choice (right-side choice). The model only included trials following a correct choice. Drug effects on win-stay behavior are not affected by drug effects on participants' diastolic blood pressure at timepoint 3.

	***β*-weight**	***SEM***	***z*-value**	***p*-value**
Intercept	0.27	0.04	6.95	< 0.001 *
Biperiden	0.07	0.04	1.82	0.068
Propranolol	0.01	0.04	0.30	0.762
Coherence	2.54	0.11	23.05	< 2e-16 *
Stay	0.39	0.04	8.98	< 2e-16 *
Diastole	-0.05	0.04	-1.31	0.189
Biperiden:coherence	-0.12	0.03	-3.70	< 0.001 *
Propranolol:coherence	-0.03	0.03	-0.95	0.343

Biperiden:stay	0.07	0.02	3.97	< 0.001 *
Propranolol:stay	0.08	0.02	4.20	< 0.001 *
Biperiden:diastole	0.02	0.05	0.36	0.721
Propranolol:diastole	0.06	0.05	1.15	0.248

Table S29 General linear mixed effects model: win-stay controlling for heart rate at timepoint 2. Fixed effects included main effects for the intercept (side bias), drugs, z-scaled coherence, z-scaled stay bias and z-scaled heart rate (difference score timepoint 1 – timepoint 2). Additionally, fixed effects included interactions of the drugs with the z-scaled coherence, z-scaled stay bias and heart rate. The random effects included a random intercept and slope for the main effects of z-scaled coherence, z-scaled stay bias and the drugs. The dependent variable was choice (right-side choice). The model only included trials following a correct choice. Drug effects on win-stay behavior are not affected by drug effects on participants' heart rate at timepoint 2.

	***β*-weight**	***SEM***	***z*-value**	***p*-value**
Intercept	0.23	0.05	4.54	< 0.001 *
Biperiden	0.11	0.05	2.24	0.025
Propranolol	0.06	0.05	1.28	0.200
Coherence	2.54	0.11	23.05	< 2e-16 *
Stay	0.39	0.04	8.97	< 2e-16 *
Diastole	-0.09	0.05	-1.92	0.055
Biperiden:coherence	-0.12	0.03	-3.71	< 0.001 *
Propranolol:coherence	-0.03	0.03	-0.95	0.340
Biperiden:stay	0.07	0.02	3.97	< 0.001 *
Propranolol:stay	0.08	0.02	4.20	< 0.001 *
Biperiden:heart rate	0.11	0.06	1.84	0.066
Propranolol:heart rate	0.08	0.05	1.44	0.149

Table S30 General linear mixed effects model: win-stay controlling for heart rate at timepoint 3. Fixed effects included main effects for the intercept (side bias), drugs, z-scaled coherence, z-scaled stay bias and z-scaled heart rate (difference score timepoint 1 – timepoint 3). Additionally, fixed effects included interactions of the drugs with the z-scaled coherence, z-scaled stay bias and z-scaled heart rate. The random effects included a random intercept and slope for the main effects of z-scaled coherence, z-scaled stay bias and the drugs. The dependent variable was choice (right-side choice). The model only included trials following a correct choice. Drug effects on win-stay behavior are not affected by drug effects on participants' heart rate at timepoint 3.

	***β*-weight**	***SEM***	***z*-value**	***p*-value**
Intercept	0.23	0.05	4.54	< 0.001 *
Biperiden	0.11	0.05	2.24	0.025
Propranolol	0.06	0.05	1.28	0.200
Coherence	2.54	0.11	23.05	< 2e-16 *
Stay	0.39	0.04	8.97	< 2e-16 *

Diastole	-0.09	0.05	-1.92	0.055
Biperiden:coherence	-0.12	0.03	-3.71	< 0.001 *
Propranolol:coherence	-0.03	0.03	-0.95	0.340
Biperiden:stay	0.07	0.02	3.97	< 0.001 *
Propranolol:stay	0.08	0.02	4.20	< 0.001 *
Biperiden:heart rate	0.11	0.06	1.84	0.066
Propranolol:heart rate	0.08	0.05	1.44	0.149

Supplement 3: Complete model fits of computational model with separate learning rates

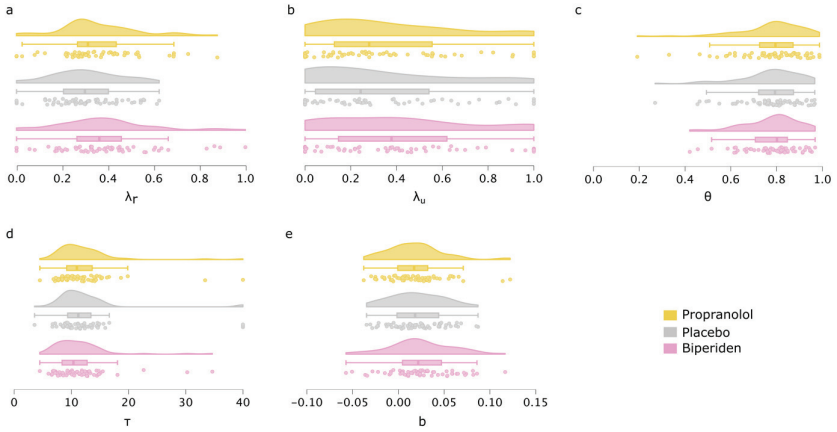

Figure S1: Model fit of computational model with separate learning rate for rewarded and unrewarded trials. Raincloud plots in **a**, **d**, **c**, **d**, **e** illustrate the distribution of the five model parameters across drug conditions: **(a)** learning rate for rewarded trials (λ_r), **(d)** learning rate for unrewarded trials (λ_u), **(c)** relative weighting (θ), **(d)** inverse softmax temperature (τ) and **(e)** right-side bias (b).

Supplement 4: Model validation and parameter recovery

We performed a model validation and parameter recovery for both computational models (one learning rate vs. two separate learning rates) to ensure the reliability of the fitting procedure. Based on the parameter fits of the computational models, 500 dataset per participant and pharmacological session were simulated. Model validation included reproducing key behavioral findings based on the simulated data. Parameter recovery entailed fitting the computational models on the simulated data and recovering the ground-truth parameters.

Best fitting Model with one learning rate

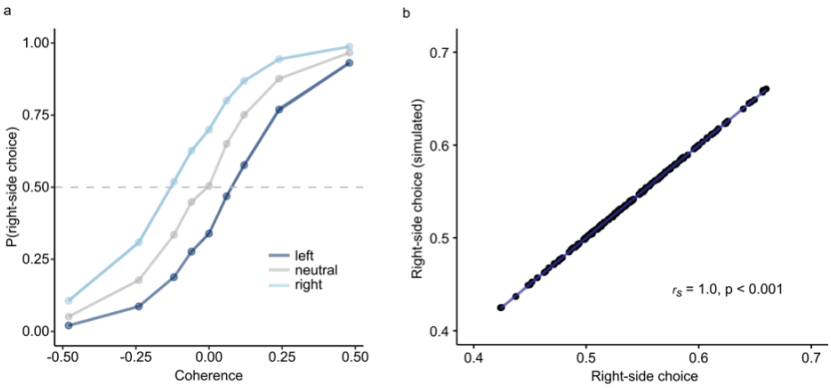

Figure S2: Model validation. Simulated data can reproduce the behavioral pattern. **(a)** simulated behavior average across pharmacological condition. Plotted is the probability for a right-side choice as a function of motion coherence (x-axis) and prior belief (shades of blue). Negative coherence levels correspond to leftward motion. As right-side motion increases, participants are more likely to choose the right side. Further, participants show a higher probability of right-side choice when expecting right-side motion (right prior). Shades around the graphs represent the standard error. **(b)** Spearman correlation between the probability of a right-side choice for simulated and participants' data.

Table S31 General linear mixed effects model: simulated data. The model was run on the simulated data whereby the mode was used to average across simulations (to keep the binary data structure). Fixed effects included main effects for the intercept (side bias), drugs, z-scaled coherence and z-scaled prior (based on the Bayes optimal learner). Additionally, fixed effects included interactions of the drugs with the z-scaled coherence and z-scaled prior. The random effects included a random intercept and slope for the main effects of z-scaled coherence, z-scaled prior and the drugs. The dependent variable was choice (right-side choice). In order to enable model convergence with the same random effects structure as in the original model (TableS2), we needed to use the "bobyqa" optimizer. However, results did not differentiate compared to the default optimizer. We can successfully reproduce key behavioral findings including the negative interaction of both drugs with coherence.

	β-weight	***SEM***	***z*-value**	***p*-value**
Intercept	0.95	0.15	6.30	< 0.001 *
Biperiden	0.12	0.14	0.89	0.373
Propranolol	-0.17	0.14	-1.22	0.223
Coherence	6.17	0.08	80.23	< 2e-16 *
Prior	2.49	0.04	67.77	< 2e-16 *

Biperiden:coherence	-0.44	0.10	-4.19	< 0.001 *
Propranolol:coherence	-1.03	0.10	-10.40	< 2e-16 *
Biperiden:prior	0.06	0.05	-1.25	0.212
Propranolol:prior	-0.05	0.05	-1.08	0.281

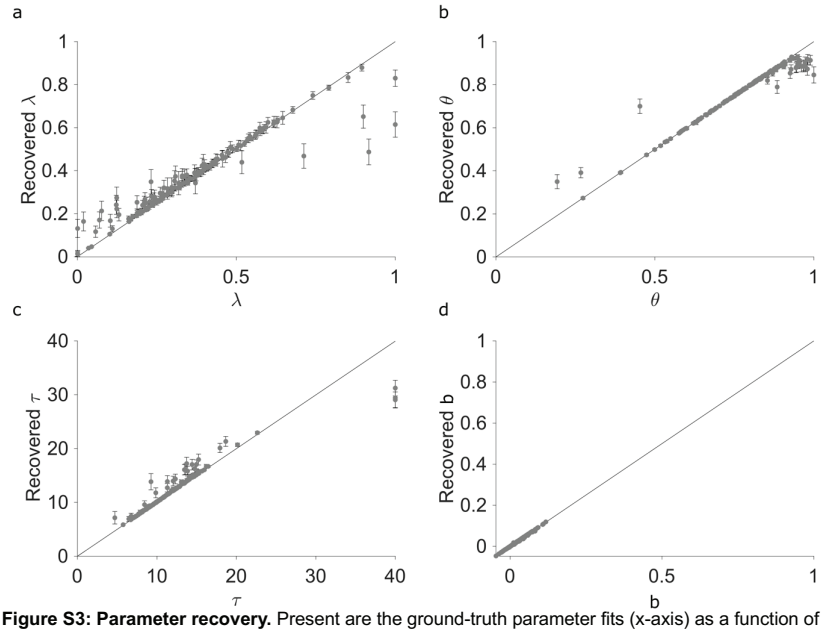

Figure S3: Parameter recovery. Present are the ground-truth parameter fits (x-axis) as a function of the recovered parameter fits (y-axis) for the four model parameters: λ **(a)**, θ **(b)**, τ **(c)**, b **(d)**. Parameter fits based on the simulated data can recover the ground truth parameters.

Model with separate learning rates

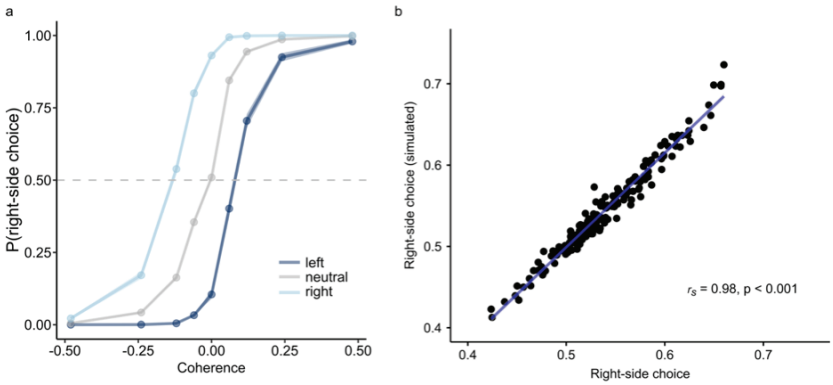

Figure S4: Model validation. Simulated data can reproduce the behavioral pattern. **(a)** simulated behavior average across pharmacological condition. Plotted is the probability for a right-side choice as a function of motion coherence (x-axis) and prior belief (shades of blue). Negative coherence levels correspond to leftward motion. As right-side motion increases, participants are more likely to choose the right side. Further, participants show a higher probability of right-side choice when expecting right-side motion (right prior). Shades around the graphs represent the standard error. **(b)** Spearman correlation between the probability of a right-side choice for simulated and participants' data.

Table S32 General linear mixed effects model: simulated data. The model was run on the simulated data whereby the mode was used to average across simulations (to keep the binary data structure). Fixed effects included main effects for the intercept (side bias), drugs, z-scaled coherence and z-scaled prior (based on the Bayes optimal learner). Additionally, fixed effects included interactions of the drugs with the z-scaled coherence and z-scaled prior. The random effects included a random intercept and slope for the main effects of z-scaled coherence, z-scaled prior and the drugs. The dependent variable was choice (right-side choice). In order to enable model convergence with the same random effects structure as in the original model (TableS2), we needed to use the "bobyqa" optimizer. However, results did not differentiate compared to the default optimizer. We can successfully reproduce key behavioral findings including the negative interaction of both drugs with coherence.

	***β*-weight**	***SEM***	***z*-value**	***p*-value**
Intercept	1.20	0.24	5.04	< 0.001 *
Biperiden	0.23	0.20	1.16	0.245
Propranolol	-0.10	0.20	-0.53	0.595
Coherence	10.70	0.99	10.82	< 2e-16 *
Prior	2.74	0.12	22.80	< 2e-16 *
Biperiden:coherence	-0.20	0.09	-2.34	0.020 *
Propranolol:coherence	-0.64	0.08	-7.89	< 0.001 *
Biperiden:prior	0.04	0.06	0.69	0.491
Propranolol:prior	0.07	0.05	1.21	0.226

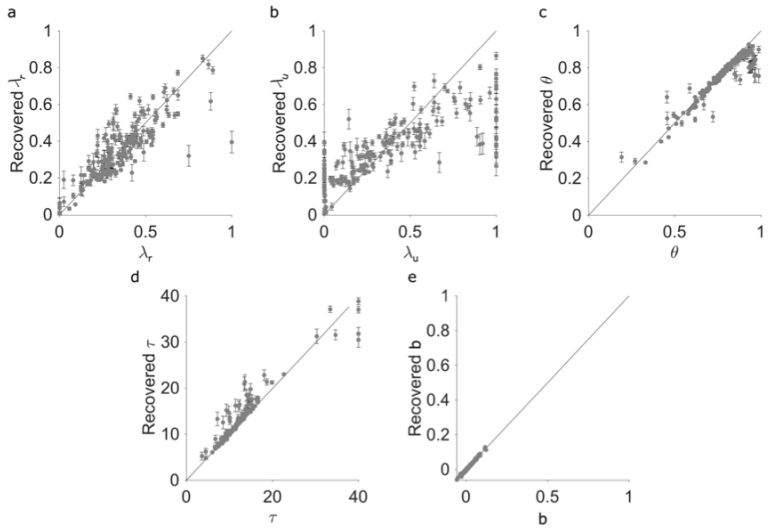

Figure S5: Parameter recovery. Present are the ground-truth parameter fits (x-axis) as a function of the recovered parameter fits (y-axis) for the five model parameters: λ_r **(a)**, λ_u **(b)**, θ **(c)**, τ **(d)**, b **(e)**. Parameter fits based on the simulated data can recover the ground truth parameters.

Supplement 5: Exclusion criteria

- German skills below B2 level
- Age < 18 years or > 35 years
- Weight < 50 kg or > 90
- BMI < 18.5 or > 28.0
- Lactose intolerance
- Possibility of pregnancy or current pregnancy
- Breastfeeding
- Hypersensitivity to the active ingredients or other components of biperiden, propranolol, or other beta-receptor blockers
- Heart rate < 60 bpm
- Smoking > 6 cigarettes per day
- Consumption of >13 units of alcohol (man)/ > 10 units of alcohol (women)
- Significant history of substance abuse (cannabis, amphetamines, cocaine, ecstasy, barbiturates, tranquilizers, opiates, psychedelics, etc.)
    - "Significant" is defined as
        - Consumption of any of the above substances within the last month
        - More than occasional consumption (> 5 times in a lifetime) of any of the above substances with the exception of cannabis
        - Regular (more than once a month on average) use of cannabis
- Significant heart conditions in (grand)parents and siblings (e.g., heart attack or bradycardic cardiac arrhythmia before the age of 70)
- Cardiovascular diseases (hypertension, hypotension, cardiac arrhythmias, hemophilia, heart failure, heart block, acidosis, Late stages of peripheral circulatory disorders, pulmonary obstructions, conditions that can lead to tachycardia, etc.)
- Current or previous treatment for psychiatric or neurological disorders
- Unexplained loss of consciousness in the past
- Head injury in the past
- Epilepsy
- Diabetes
- Asthma
- Bronchial spasms
- Thyroid dysfunction
- Glaucoma or angle-closure glaucoma
- Ileus
- Megacolon
- Stenosis of gastrointestinal tract
- Stomach or duodenal ulcer
- (History of) Bleeding in the gastrointestinal tract
- Organ dysfunction (e.g., renal dysfunction or liver failure)
- Prostate adenoma with residual urine formation
- Shock
- Performance-based exclusion:

- RDM: performance < 65% both in the screening and across the three pharmacological sessions
- EET: > 10 missed trials in the screening

References

Bond, A., & Lader, M. (1974). The use of analogue scales in rating subjective feelings. *British Journal of Medical Psychology*.

Rodewald, K., Bartolovic, M., Debelak, R., Aschenbrenner, S., Weisbrod, M., & Roesch-Ely, D. (2012). Eine Normierungsstudie eines modifizierten Trail Making Tests im deutschsprachigen Raum. *Zeitschrift für Neuropsychologie*, *23*(1), 37–48. https://doi.org/10.1024/1016-264X/a000060

Spielberger, C. D., Gorsuch, R. L., Lushene, R., Vagg, P. R., & Jacobs, G. A. (1983). *Manual for the State-Trait Anxiety Inventory (Form Y)*. Consulting Psychologists Press.

Danksagung

Ich kann es kaum glauben, aber ich habe es geschafft. Diese Dissertation wäre aber nicht möglich gewesen ohne die Unterstützung vieler Menschen bei denen ich mich an dieser Stelle bedanken möchte.

Zunächst möchte ich mich bei Gerhard Jocham für seine Betreuung während meiner Promotion bedanken. Egal wie viele Aufgaben du gerade zu bewältigen hattest, hast du dir immer die Zeit genommen um mit mir - meist sehr spontan - über meine neusten Ideen nachzudenken oder frische Ergebnisse zu interpretieren. Du hast meine wissenschaftliche Arbeitsweise stark geprägt und mich immer wieder dazu ermutigt, weiter nachzustochern und die zugrunde liegenden Mechanismen kritisch zu hinterfragen.

Außerdem möchte ich mich bei Monja Froböse bedanken. Du hast meine Entwicklung als Wissenschaftlerin unglaublich gefördert. Dabei hast du mich immer wieder motiviert und ermutigt, mich aber auch auf den Boden der Tatsachen zurückgeholt, wenn ich mal wieder etwas zu cool war. Außerdem warst du der beste Office Mate, den man sich hätte wünschen können. Dank unseres täglichen Rumalberns, inklusive singen, tanzen und Schnapswitzen, bin ich jeden Tag mit einem breiten Grinsen nach Hause gefahren.

Vielen Dank auch an Hannah Kurtenbach. Unser Austausch hat mir immer sehr geholfen, einschließlich der gelegentlichen Beschlagnahmung deines White Boards. Aber auch außerhalb von dem fachlichen Arbeiten, hatte ich immer sehr viel Spaß mit dir. Sei es sich über Monjas Langbein-Suppe lustig zu machen oder die besten Jumpstyle Videos herauszusuchen.

Weiter bedanke ich mich bei Mani Erfanian Abdoust und Evelina Andronova dafür, dass wir Teile unsere Doktorandenzeit gemeinsam durchlaufen durften und uns dabei

stets unterstützt haben. Thank you also to my colleagues Eduard Ort, Anna Marzecová and Lina Skora for the motivated work environment and lively lunch breaks. Ich bedanke mich zudem bei Christiane Heil für ihre Unterstützung in jeglichen administrativen Aufgaben und sehr vielen lustigen Geschichten beim Mittagessen. I also want to thank our cooperation partners including Jill O'Reilly, Oliver Kohl, Esther Florin, Alfons Schnitzler, Markus Butz, Dzhamilia Aravitska, Lisa Dannenberg and Elisabeth Schreivogel. The scientific exchanges with you shaped this dissertation. Vielen Dank auch an alle wissenschaftlichen Hilfskräfte für ihre Unterstützung, vor allem in der Datenerhebung. Die Datenerhebung wäre zudem nicht möglich gewesen ohne die Menschen, die sich die Zeit genommen haben, um an unseren Studien teilzunehmen. Vielen Dank!

Zuletzt möchte ich mich bei meiner Familie und meinen Freunden bedanken, die mich in allen Phasen meiner Promotion sehr unterstützt haben. Obrigada Mama, pelos telefonemas e o apoio todos os dias – muitas vezes mais do que uma vez por dia. Vielen Dank Papa, dafür dass du mich immer an unsere Wahrscheinlichkeitsregel erinnert hast. Vielen Dank auch an meine Freunde und ganz besonders Stella, die es immer wieder geschafft haben, mich auf andere Gedanken zu bringen und mir wertvolle Pausen vom Promotionsalltag zu schenken. Zuletzt möchte ich mich bei Noah bedanken. Du hast mich in meiner gesamten Promotion mit deiner Ruhe, Geduld und Zuversicht sehr unterstützt. Dabei warst du genauso enthusiastisch für meine Forschung wie ich und hast jeden Erfolg – egal wie klein – mit mir gefeiert.

Eidesstattliche Versicherung

Ich versichere an Eides Statt, dass die Dissertation von mir selbständig und ohne unzulässige fremde Hilfe unter Beachtung der „Grundsätze zur Sicherung guter wissenschaftlicher Praxis an der Heinrich-Heine-Universität Düsseldorf“ erstellt worden ist.

Düsseldorf, _____ _____